NATIONAL TECHNICAL UNIVERSITY OF ATHENS
SCHOOL OF CIVIL ENGINEERING
DEPARTMENT OF STRUCTURAL ENGINEERING
INSTITUTE OF STRUCTURAL ANALYSIS & ANTISEISMIC RESEARCH

Generation of structural systems based on topology optimization

A Dissertation Presented

by

Stefanos G. Sotiropoulos

Submitted to the School of Civil Engineering of the
National Technical University of Athens
for the degree of

DOCTOR OF PHILOSOPHY

June 2021

ΕΘΝΙΚΟ ΜΕΤΣΟΒΙΟ ΠΟΛΥΤΕΧΝΕΙΟ
ΣΧΟΛΗ ΠΟΛΙΤΙΚΩΝ ΜΗΧΑΝΙΚΩΝ
ΤΟΜΕΑΣ ΔΟΜΟΣΤΑΤΙΚΗΣ
ΕΡΓΑΣΤΗΡΙΟ ΣΤΑΤΙΚΗΣ & ΑΝΤΙΣΕΙΣΜΙΚΩΝ ΕΡΕΥΝΩΝ

Γένεση δομικών συστημάτων βάσει βελτιστοποίησης τοπολογίας

Διδακτορική Διατριβή

Στέφανος Γ. Σωτηρόπουλος

Υποβληθείσα στη Σχολή Πολιτικών Μηχανικών του
Εθνικού Μετσόβιου Πολυτεχνείου
για τον τίτλο του

Διδάκτορα

Ιούνιος 2021

Ευρωπαϊκή Ένωση
European Social Fund

Operational Programme
Human Resources Development,
Education and Lifelong Learning

Co-financed by Greece and the European Union

ΕΣΠΑ
2014-2020
ανάπτυξη - εργασία - αλληλεγγύη

Committee:

_____
1. Nikos D. Lagaros
Professor, Department of Structural Engineering,
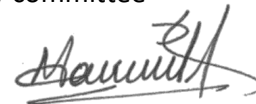School of Civil Engineering, N.T.U.A., Supervisor

_____
2. Vlasis Koumousis
Emeritus Professor, Department of Structural Engineering,
School of Civil Engineering, N.T.U.A., Member of the advisory committee

_____
3. Charalampos Gantes
Professor, Department of Structural Engineering,
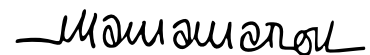School of Civil Engineering, N.T.U.A., Member of the advisory committee

_____
4. Marios Phocas
Professor, Department of Architecture,
University of Cyprus

_____
5. Vagelis Plevris
Associate Professor, Department of Civil and Architectural Engineering,
Qatar University

_____
6. Maria Matheou
Junior Professor, Faculty of Civil and Environmental Design,
University of Stuttgart

_____
7. Savvas Triantafyllou
Assistant Professor, Department of Structural Engineering,
School of Civil Engineering, N.T.U.A.

To my mother.

Declaration

I hereby declare that except where specific reference is made to the work of others, the contents of this dissertation are original and have not been submitted in whole or in part for consideration for any other degree or qualification in this, or any other university. This dissertation is my own work and contains nothing which is the outcome of work done in collaboration with others, except as specified in the text and Acknowledgments.

<div align="right">

Stefanos G. Sotiropoulos

June 2021

</div>

Acknowledgments

First and foremost, I would like to express my most sincere gratitude to my supervisor, Professor Nikolaos Lagaros, whose expertise was invaluable in formulating the research questions and methodologies. His insightful feedback along with the countless hours of constructive collaboration, pushed me to sharpen my thinking and brought my work to a higher level.

I would also like to express my gratitude towards Professor Vlasis Koumousis and Professor Charalampos Gantes for sharing their expertise and experience, as members of my advisory committee. My sincere gratitude also goes to Prof. Marios Phocas, Prof. Vagelis Plevris, Prof. Maria Matheou and Prof. Savvas Triantafyllou for serving on my examination committee and their valuable comments and suggestions.

I would also like to thank the members of Prof. Nikolaos Lagaros' research group, Dr. Nikolaos Kallioras, Dr. Stavros Chatzieleftheriou and PhD candidates George Kazakis, Spyros Damikoukas and Pantelis Tsakalis for a harmonic and productive collaboration.

Εκτενής Περίληψη

1. Εισαγωγή

Η βελτίωση της αποδοτικότητας των κατασκευών όσον αφορά την ασφάλεια, την οικονομία και τη βιωσιμότητά τους, αποτελεί αντικείμενο διαρκούς έρευνας των πολιτικών μηχανικών. Η πρόοδος στον κατασκευαστικό κλάδο επιτυγχάνεται μέσω της διαμόρφωσης νέων διαδικασιών σχεδιασμού και αξιολόγησης σε σχέση με τις δομικές, ενεργειακές και περιβαλλοντικές επιδόσεις των κατασκευών, που συνήθως απαιτούν αυξημένη υπολογιστική ισχύ. Η ανάπτυξη της ανάλυσης και του σχεδιασμού των κατασκευών έχει συσχετιστεί αμετάβλητα με τη διατύπωση δαπανηρών υπολογιστικών προβλημάτων, καθώς οι μηχανικοί μπορούν πάντα να διατυπώσουν ένα πρόβλημα που θα παρέχει μια καλύτερη λύση, όμως ταυτόχρονα απαιτεί περισσότερη από τη διαθέσιμη υπολογιστική ισχύ. Η αξιοποίηση της συνεχώς αυξανόμενης υπολογιστικής ισχύς απαιτεί την ανάπτυξη αριθμητικών τεχνικών και εργαλείων, τα οποία τελικά επιτρέπουν την προσομοίωση σύνθετων φυσικών φαινομένων, χρησιμοποιώντας προσεγγίσεις που δεν ήταν δυνατόν να εφαρμοστούν μέχρι σήμερα.

Η βελτιστοποίηση τοπολογίας (Topology Optimization - TO) είναι μια μαθηματική μέθοδος εύρεσης μορφής, που ωρίμασε τα τελευταία χρόνια, από ένα ακαδημαϊκό αντικείμενο σε ένα πρακτικό εργαλείο σχεδιασμού των κατασκευών. Μέχρι στιγμής, το ΤΟ έχει εφαρμοστεί σε πραγματικές εφαρμογές στον κλάδο της αυτοκινητοβιομηχανίας, της αεροδιαστημικής και άλλων μηχανολογικών βιομηχανιών. Αντίθετα, η εφαρμογή του σε κατασκευές πολιτικού μηχανικού, περιορίζεται στο αρχικό στάδιο του εννοιολογικού σχεδιασμού (conceptual design) μιας κατασκευής. Το βασικό αντικείμενο της παρούσας διδακτορικής διατριβής, είναι η εγκαθίδρυση ορισμένων μαθηματικών διατυπώσεων του προβλήματος του ΤΟ για την υποστήριξη του σχεδιασμού δομικών συστημάτων υψηλών κτιρίων αλλά και κελυφωτών κατασκευών, από την αρχική φάση του εννοιολογικού σχεδιασμού έως την τελική κατασκευαστική φάση. Η αναπαράσταση και η κατασκευασιμότητα της τελικής μορφής η οποία προκύπτει από τη διαδικασία του ΤΟ,

είναι δύο κρίσιμα ζητήματα που λαμβάνονται υπόψιν σε όλη τη διατριβή. Η δημιουργία δομικών συστημάτων που αποτελούνται από διακριτά μέλη, είναι επίσης βασικός στόχος της παρούσας διατριβής.

Για την επίτευξη των στόχων, θα επιβληθούν κατασκευαστικοί περιορισμοί στη συμβατική διατύπωση της γενικευμένης βελτιστοποίησης σχήματος (Generalized Shape Optimization - GSO), προκειμένου να παραχθούν κατασκευές τύπου δικτυώματος. Θα συνδυαστούν διαφορετικοί τύποι πεπερασμένων στοιχείων, προκειμένου να προσδιοριστεί η επίδρασή τους στην γένεση της βέλτιστης μορφής. Θα διερευνηθούν τεχνικές επεξεργασίας εικόνας για την αυτοματοποιημένη αναπαράσταση των βελτιστοποιημένων δομικών συστημάτων. Επιπλέον, προκατασκευασμένα δομικά στοιχεία θα χρησιμοποιηθούν για την αντικατάσταση των τυπικών ορθογωνικών πεπερασμένων στοιχείων και θα μελετηθούν τεχνικές παραμετρικού σχεδιασμού για την τελική ενσωμάτωση των βελτιστοποιημένων κατασκευών σε CAD (Computer-Aided Design) περιβάλλον. Επιπροσθέτως, τυποποιημένες διατομές δομικού χάλυβα θα εφαρμοστούν στο πρόβλημα της βελτιστοποίησης τοπολογίας δοκών (Frame Structural Topology Optimization - FSTO) ενώ θα επιβληθούν περιορισμοί ελέγχου των διατομών σύμφωνα με τους κανονισμούς του Ευρωκώδικα. Για τη διαδικασία ανάλυσης και σχεδιασμού των κατασκευών, θα χρησιμοποιηθούν εμπορικά πακέτα λογισμικού τύπου CAE (Computer-Aided Engineering). Τέλος, θα μελετηθεί η επίδραση της θεώρησης δυναμικών συνθηκών στη διαδικασία του FSTO κατά τη γένεση δομικών συστημάτων.

Η παρούσα διατριβή αποτελείται από 9 κεφάλαια, συμπεριλαμβανομένου και του εισαγωγικού κεφαλαίου. Στο δεύτερο κεφάλαιο παρουσιάζεται η μαθηματική διατύπωση του προβλήματος της βελτιστοποίησης κατασκευών, ενώ γίνεται εκτενής αναφορά για τις διάφορες μεθοδολογίες που εφαρμόζονται στο ΤΟ. Στο κεφάλαιο 3, εισάγεται ο ορισμός του δομικού συστήματος και παρουσιάζονται διάφορα δομικά συστήματα για την υποστήριξη υψηλών κτιρίων και κελυφωτών κατασκευών, στα οποία εφαρμόζονται όλες οι προτεινόμενες μεθοδολογίες της παρούσας διατριβής. Στο τέταρτο κεφάλαιο η προσέγγιση της GSO υλοποιείται σε εφαρμογές πολιτικού μηχανικού, στο αρχικό στάδιο του εννοιολογικού σχεδιασμού. Επιβάλλονται

περιορισμοί κατασκευασιμότητας προκειμένου να παραχθούν δομικά συστήματα υψηλών κτιρίων που αποτελούνται από διαγώνια στοιχεία, ενώ παρουσιάζεται μια αυτοματοποιημένη μέθοδος για την άμεση αναπαράσταση της βέλτιστης κατασκευής σε CAD περιβάλλον. Στο κεφάλαιο 5, παρουσιάζεται μια καινοτόμα μεθοδολογία για τη δημιουργία δομικών συστημάτων βάσει ΤΟ, σύμφωνα με την οποία δημιουργούνται ορθογωνικά υπερστοιχεία βασισμένα σε προκαθορισμένα δομικά στοιχεία. Χρησιμοποιώντας την προτεινόμενη μεθοδολογία, επιβάλλονται αισθητικοί και κατασκευαστικοί περιορισμοί στη μαθηματική διατύπωση του προβλήματος και αναπτύσσονται καινοτόμα δομικά συστήματα που δεν μπορούν να επιτευχθούν μέσω συμβατικών προσεγγίσεων. Στο έκτο κεφάλαιο, παρουσιάζεται η μαθηματική διατύπωση του FSTO προβλήματος και περιγράφεται αναλυτικά η υλοποίησή του στο εμπορικό πρόγραμμα SAP2000. Στο κεφάλαιο 7, προτείνεται μια πρωτότυπη μεθοδολογία βασισμένη στη διατύπωση και διαδοχική επίλυση δύο διαφορετικών προβλημάτων βελτιστοποίησης κατασκευών, του ΤΟ και της βελτιστοποίησης μεγέθους (Structural Sizing Optimization - SSO). Για την εφαρμογή της μεθόδου λαμβάνονται υπόψιν ρεαλιστικές συνθήκες σχεδιασμού και τυποποιημένες μεταλλικές διατομές, ενώ εφαρμόζονται περιορισμοί που προκύπτουν από τους κανόνες σχεδιασμού του Ευρωκώδικα. Στο όγδοο κεφάλαιο, εξετάζονται τρεις συνθήκες δυναμικής απόκρισης κατά την εφαρμογή της FSTO στη διαδικασία γένεσης δομικών συστημάτων υψηλών κτιρίων. Τα δομικά συστήματα εξετάζονται σε συνθήκες ελεύθερης και εξαναγκασμένης ταλάντωσης, ενώ για την επίλυση των δυναμικών φορτίσεων χρησιμοποιούνται μεθοδολογίες άμεσης και έμμεσης ολοκλήρωσης του χρόνου. Στο τελευταίο κεφάλαιο, συζητούνται τα συμπεράσματα της παρούσας διατριβής και προτείνονται ιδέες για περαιτέρω έρευνα.

2. Βελτιστοποίηση Κατασκευών

Η βελτιστοποίηση κατασκευών είναι η διαδικασία παραγωγής μιας κατασκευής η οποία αντέχει τα επιβαλλόμενα φορτία με τον καλύτερο δυνατό τρόπο. Κρίσιμο σημείο είναι

το πως ορίζεται ο όρος «καλύτερο». Για παράδειγμα ένας στόχος των μηχανικών είναι η μείωση της ποσότητας του υλικού της κατασκευής όσο το δυνατόν περισσότερο. Ταυτόχρονα όμως, η ενίσχυση μιας κατασκευής έναντι αστάθειας και φαινομένων λυγισμού είναι επίσης πολύ σημαντική. Ωστόσο, ελαχιστοποιήσεις και μεγιστοποιήσεις τέτοιων μεγεθών δεν μπορούν να πραγματοποιηθούν χωρίς την επιβολή ορισμένων περιορισμών. Τυπικές ποσότητες που χρησιμοποιούνται τόσο ως στόχοι βελτιστοποίησης όσο και ως περιορισμοί, είναι οι τάσεις, μετατοπίσεις, γεωμετρία κτλ.

Σε οποιαδήποτε διατύπωση ενός προβλήματος βελτιστοποίησης κατασκευών οι ακόλουθες ποσότητες είναι προαπαιτούμενες:

- *Αντικειμενική συνάρτηση* (f): Πρόκειται για μια μαθηματική εξίσωση, η οποία επιστρέφει μία μόνο τιμή, η οποία αντιπροσωπεύει το πόσο καλή είναι μια κατασκευή όσον αφορά ένα συγκεκριμένο χαρακτηριστικό. Συνήθως, η f είναι μια συνάρτηση που θέλουμε να ελαχιστοποιηθεί, αλλά, σε ορισμένες περιπτώσεις, απαιτείται η μεγιστοποίηση μιας αντικειμενικής συνάρτησης.

- *Μεταβλητή σχεδιασμού* (x): Είναι ένα διάνυσμα αριθμητικών τιμών, που αλλάζουν εντός ενός προκαθορισμένου εύρους κατά τη διάρκεια της διαδικασίας βελτιστοποίησης, προκειμένου να καθοριστεί ο σχεδιασμός της κατασκευής. Μεταβλητές σχεδιασμού που χρησιμοποιούνται συχνά είναι, το εμβαδόν διατομής μιας δοκού, το πάχος μιας πλάκας ή ο τύπος του υλικού της κατασκευής.

- *Μεταβλητή κατάστασης* (y): Το y είναι μια συνάρτηση ή ένα διάνυσμα που μετρά την απόκριση της κατασκευής, για μια δεδομένη μεταβλητή σχεδιασμού, η οποία μπορεί να οριστεί με όρους μετατοπίσεων, τάσεων ή δυνάμεων της κατασκευής.

Επομένως, μια γενική διατύπωση ενός προβλήματος βελτιστοποίησης κατασκευών (Structural Optimization - SO) εκφράζεται ως εξής:

$$(SO) \begin{cases} ελαχιστοποίηση\ f(x,y)\ βάσει\ των\ x\ και\ y \\ όπου \begin{cases} περιορισμοί\ συμπεριφοράς\ στο\ y \\ περιορισμοί\ σχεδιασμού\ στο\ x \\ εξίσωση\ ισορροπίας \end{cases} \end{cases} \qquad (1)$$

Υποθέτοντας ότι, $u(x)$ είναι το διάνυσμα μετατοπίσεων μιας κατασκευής και ότι όλοι οι περιορισμοί μπορούν να εκφραστούν σε μία συνάρτηση, η μαθηματική διατύπωση ενός προβλήματος SO είναι:

$$(SO)\begin{cases} \min\limits_{x} & f\big(x, u(x)\big) \\ s.t. & g\big(x, u(x)\big) \leq 0 \end{cases} \qquad (2)$$

όπου το s.t. υποδηλώνει την έκφραση "subject to".

Είναι κοινώς αποδεκτό ότι το SO χωρίζεται σε τρεις κύριες ευρείες κατηγορίες:

- Βελτιστοποίηση μεγέθους (sizing optimization): Αυτός είναι ο πιο συνηθισμένος τύπος βελτιστοποίησης σε όλους τους τομείς της μηχανικής, καθώς το μαθηματικό πρόβλημα ορίζεται εύκολα και η προτεινόμενη λύση δεν χρειάζεται ιδιαίτερη επεξεργασία για την εφαρμογή της.

- Βελτιστοποίηση σχήματος (shape optimization): Σε αυτόν τον τύπο βελτιστοποίησης, τα όρια της κατασκευής αλλάζουν δίνοντας νέα μορφή στη βελτιστοποιημένη λύση.

- Βελτιστοποίηση τοπολογίας (Topology Optimization - TO): Αυτός είναι ο πιο ολιστικός τύπος βελτιστοποίησης, καθώς δεν αλλάζουν μόνο οι διαστάσεις της κατασκευής, αλλά επίσης αναπτύσσεται μια νέα μορφή και τοπολογία.

Στη παρούσα διατριβή χρησιμοποιούνται κυρίως τεχνικές TO. Το TO διακρίνεται σε δύο κατηγορίες: (i) βελτιστοποίηση διάταξης (Layout Optimization - LO) και (ii) γενικευμένη βελτιστοποίηση σχήματος (Generalized Shape Optimization - GSO). Η LO εφαρμόζεται τόσο σε μονοδιάστατες (One Dimensional - 1D) όσο και σε δισδιάστατες (Two Dimensional - 2D) κατασκευές. Η αρχική κατασκευή αποτελείται συνήθως από το συνδυασμό όλων των πιθανών μελών, διαμορφώνοντας το λεγόμενο Ground Structure (GS). Η GSO εφαρμόζεται σε 2D και τρισδιάστατα (Three Dimensional - 3D) προβλήματα με τη θεώρηση του συνεχούς μέσου. Σε αυτόν τον τύπο TO, η αρχική κατασκευή διακριτοποιείται με πεπερασμένα στοιχεία ενώ το πάχος ή η πυκνότητα ενός στοιχείου αποτελούν τη μεταβλητή σχεδιασμού, η οποία λαμβάνει τιμές από 1 έως 0 υποδηλώνοντας την ύπαρξη ή μη ενός στοιχείου.

3. Δομικά συστήματα

Στον κλάδο της δομοστατικής μηχανικής, ο όρος δομικό σύστημα αναφέρεται συνήθως σε ένα υποσύστημα μιας κατασκευής. Ο σκοπός ενός δομικού συστήματος είναι η συναρμολόγηση των δομικών στοιχείων με τέτοιο τρόπο, έτσι ώστε τα φορτία που εφαρμόζονται στην κατασκευή, να μεταδίδονται με ασφάλεια από τη κατασκευή στο έδαφος, χωρίς τα μέλη του να υπερβαίνουν συγκεκριμένες μηχανικές απαιτήσεις. Η συντριπτική πλειονότητα των παραδειγμάτων στα οποία εφαρμόζονται οι προτεινόμενες μεθοδολογίες της τρέχουσας διατριβής, αναφέρεται σε δομικά συστήματα ψηλών κτιρίων ή κελυφωτών κατασκευών.

Η επιλογή του δομικού συστήματος ενός υψηλού κτιρίου, εξαρτάται κυρίως από τους σκοπούς λειτουργικότητας, τις αρχιτεκτονικές απαιτήσεις και τα γεωμετρικά χαρακτηριστικά του κτιρίου. Στη βιομηχανία των κατασκευών, υπάρχουν πολλοί τύποι συστημάτων πλευρικής αντίστασης, των οποίων ο σκοπός είναι η αντοχή έναντι πλευρικών φορτίων όπως π.χ. σεισμικές φορτίσεις, φορτία ανέμου κτλ. Τα δομικά συστήματα υψηλών κτιρίων μπορούν να χωριστούν σε τέσσερις κατηγορίες:

- Διατμητικά τοιχία (Shear walls)
- Καμπτόμενα πλαίσια (Moment Resisting Frames - MRFs)
- Συστήματα με ζυγοστάτες (Outrigger systems)
- Ενισχυμένα πλαίσια (Braced Frames - BFs)

Στα δομικά συστήματα BFs, χρησιμοποιούνται διαγώνια μεταλλικά μέλη προκειμένου να αυξηθεί η ακαμψία του κτιρίου. Τα συστήματα αυτά, έχουν τη δυνατότητα να μεταφέρουν αξονικές δυνάμεις και να μειώνουν τις απαιτήσεις των δοκαριών και των υποστυλωμάτων έναντι κάμψης. Τα διαγώνια μέλη μπορούν να τοποθετηθούν είτε στις όψεις ή είτε στον πυρήνα της κατασκευής. Σε σύγκριση με το MRF, το σύστημα στήριξης BF είναι πολύ πιο οικονομικό, ειδικά όταν πρόκειται για ψηλά κτίρια. Υπάρχουν διάφορες διατάξεις των διαγώνιων μελών που μπορούν να εφαρμοστούν και κατηγοριοποιούνται σε δύο κύρια δομικά συστήματα, το ομόκεντρο ενισχυμένο πλαίσιο

(Concentric Braced Frame - CBF) και το έκκεντρο ενισχυμένο πλαίσιο (Eccentric Braced Frame - EBF).

Οι κελυφωτές κατασκευές είναι από τα πιο δύσκολα και ενδιαφέροντα δομικά συστήματα στον κλάδο της αρχιτεκτονικής και του πολιτικού μηχανικού. Το βασικό χαρακτηριστικό αυτών των κατασκευών, είναι η σχεδιαστική ελευθερία που παρέχουν στον αρχιτέκτονα να παράγει εντυπωσιακές μορφές μεγάλων ανοιγμάτων και ταυτόχρονα να αντιστέκονται ιδιαιτέρως αποτελεσματικά στις εξωτερικές φορτίσεις. Η μορφή τους δημιουργείται απευθείας από τη ροή των δυνάμεων και καθορίζει τη συμπεριφορά της κατασκευής έναντι των φορτίσεων. Συγκεκριμένα, οι κελυφωτές κατασκευές ορίζονται από 3D καμπυλωτές επιφάνειες, στις οποίες η κάθετη προς την επιφάνεια διάσταση, είναι πολύ μικρότερη σε σύγκριση με τις άλλες δύο. Όσον αφορά το σχήμα τους, τα κελύφη μπορούν να είναι διπλής ή μονής καμπυλότητας. Σε μια «ιδανική» κελυφωτή κατασκευή, τα εξωτερικά φορτία μεταφέρονται στα στηρίγματα αναπτύσσοντας μόνο αξονικές δυνάμεις. Ένα κέλυφος μπορεί να κατασκευαστεί, είτε ως μονολιθική κατασκευή, συνεχής επιφάνεια, είτε ως συναρμολόγηση διακριτών στοιχείων, το λεγόμενο πλέγμα (gridshell).

4 Παραγωγή δομικών συστημάτων βάσει της GSO

Την τελευταία δεκαετία, η μέθοδος ΤΟ άρχισε να εφαρμόζεται σε εφαρμογές πολιτικού μηχανικού, κυρίως σε ερευνητικό επίπεδο. Στη βιβλιογραφία, οι μελέτες που υλοποιούν την ΤΟ λαμβάνοντας υπόψιν κριτήρια που επιβάλλονται από αρχιτέκτονες και πολιτικούς μηχανικούς, είναι περιορισμένες. Στο παρόν κεφάλαιο, παρουσιάζεται η θεμελιώδης θεωρία του GSO προβλήματος, χρησιμοποιώντας τη μέθοδο Simplified Isotropic Material with Penalization (SIMP). Επιπλέον, επιβάλλονται τρεις κατασκευαστικοί περιορισμοί για τη δημιουργία δομικών συστημάτων BF, ενώ αναπτύσσεται μια αυτόματη διαδικασία, η οποία μετατρέπει το αποτέλεσμα των εικόνων του προβλήματος ΤΟ σε αρχεία CAD.

Ο στόχος σε ένα πρόβλημα GSO, είναι η εύρεση της βέλτιστης τοπολογίας των εσωτερικών ορίων και του σχήματος, τόσο των εσωτερικών όσο και των εξωτερικών ορίων ενός διάτρητου ή σύνθετου συνεχούς σώματος. Συγκεκριμένα, οι προϋποθέσεις για τη διατύπωση του προβλήματος GSO είναι ο καθορισμός του αρχικού χωρίου σχεδιασμού Ω, όπου θα δημιουργηθεί η βελτιστοποιημένη κατασκευή, το κλάσμα όγκου της βελτιστοποιημένης κατασκευής, οι συνοριακές συνθήκες και οι συνθήκες φόρτισης. Η μέθοδος SIMP, είναι μια μέθοδος κατανομής υλικού για την εύρεση της βέλτιστης διάταξης ενός δομικού συστήματος, που αποτελείται από γραμμικά ελαστικό ισότροπο υλικό. Επομένως, το ερώτημα που πρέπει να απαντηθεί, είναι πώς να κατανεμηθεί ο όγκος του υλικού στον τομέα Ω, προκειμένου να ελαχιστοποιηθεί ένα συγκεκριμένο κριτήριο. Η τυπική μαθηματική διατύπωση του προβλήματος TO με αντικειμενική συνάρτηση την ενδοτικότητα της κατασκευής εκφράζεται ως εξής:

$$\min_{x} C(x) = F^T u(x) \qquad (3α)$$

$$s.t.$$

$$K(x)u(x) = F \qquad (3β)$$

$$\frac{V(x)}{V_0} = f_{VolFrac} \qquad (3γ)$$

$$0 < x_{min} < x_e < 1, \quad e = 1,2,\dots,N_{ele} \qquad (3δ)$$

όπου $C(x)$ είναι η ενδοτικότητα της κατασκευής για συγκεκριμένες πυκνότητες, το F υποδηλώνει το διάνυσμα φόρτισης, $u(x)$ είναι οι μετατοπίσεις που προκύπτουν από την επίλυση των εξισώσεων ισορροπίας, το $V(x)$ αντιπροσωπεύει τον όγκο του τρέχοντος σχεδιασμού, το V_o αναφέρεται στον αρχικό όγκο, το $f_{VolFrac}$ είναι το κλάσμα του τελικού όγκου που επιβάλλεται στο πρόβλημα, το $K(x)$ είναι το καθολικό μητρώο ακαμψίας, το x αντιπροσωπεύει το διάνυσμα της μεταβλητής σχεδιασμού, το x_e είναι η πυκνότητα κάθε πεπερασμένου στοιχείου και το N_{ele} είναι ο συνολικός αριθμός των πεπερασμένων στοιχείων που χρησιμοποιούνται για τη διακριτοποίηση του χωρίου.

Για την επίλυση αυτού του προβλήματος βελτιστοποίησης, με τη μέθοδο των πεπερασμένων στοιχείων, η παράμετρος που εισάγεται είναι η πυκνότητα κάθε πεπερασμένου στοιχείου. Η μεταβλητή σχεδιασμού x_e, κυμαίνεται στο εύρος $[x_{min}, 1]$, όπου το x_{min} είναι μια μικρή τιμή κοντά στο μηδέν, προκειμένου να αποφευχθούν αριθμητικές αστάθειες. Τα στοιχεία που έχουν πυκνότητες κοντά στα x_{min} πρέπει να αφαιρεθούν από το χωρίο σχεδιασμού και τα στοιχεία με πυκνότητες κοντά στο 1 θα αποτελούν μέρος της τελικής κατασκευής. Όσον αφορά τις ενδιάμεσες τιμές μεταξύ x_{min} και 1, εφαρμόζονται συγκεκριμένες τεχνικές ώστε τέτοιες τιμές να αποφεύγονται.

Σύμφωνα με τη μέθοδο SIMP, οι πυκνότητες των πεπερασμένων στοιχείων συσχετίζονται με το μέτρο ελαστικότητας, ως εξής:

$$E_e(x_e) = x_e^p E_e^0 \Leftrightarrow k_e(x_e) = x_e^p k_e^0 \tag{4}$$

όπου η παράμετρος p είναι ένας σταθερός ακέραιος αριθμός, ο οποίος τις περισσότερες φορές λαμβάνει την τιμή 3. Λαμβάνοντας υπόψιν την παραπάνω εξίσωση η ενδοτικότητα της κατασκευής παίρνει την εξής μορφή:

$$C(x) = \sum_{e=1}^{N_{ele}} (x_e)^p u_e^T k_e^0 u_e \tag{5}$$

Το πρόβλημα της μαθηματικής βελτιστοποίησης που διατυπώθηκε, μπορεί να επιλυθεί χρησιμοποιώντας διάφορους μαθηματικούς αλγόριθμους που απαιτούν τον υπολογισμό της παραγώγου, όπως ο Optimality Criteria (OC), η Method of Moving Asymptotes (MMA) και ο Sequential Linear Programming (SLP). Επιπλέον, λόγω του προβλήματος της σκακιέρας (checkerboard problem), μια κοινή πρακτική είναι η εφαρμογή φίλτρων κατά τη διαδικασία βελτιστοποίησης, όπως τα φίλτρα πυκνότητας και ευαισθησίας. Στη παρούσα διατριβή εφαρμόζεται ο αλγόριθμος OC, ενώ η παράγωγος της ενδοτικότητας υπολογίζεται ως εξής:

$$\frac{\partial C(x)}{\partial x_e} = -u_e(x)^T \frac{\partial k_e(x)}{\partial x_e} u_e(x) \tag{6}$$

Στο Σχήμα 1 βλέπουμε την όψη ενός υψηλού κτιρίου καθώς και τη διακριτοποίησή της με πεπερασμένα στοιχεία, που χρησιμοποιείται για την εφαρμογή των προτεινόμενων κατασκευαστικών περιορισμών. Η διακριτοποίηση του πλέγματος αποτελείται από 80

(α)   (β)
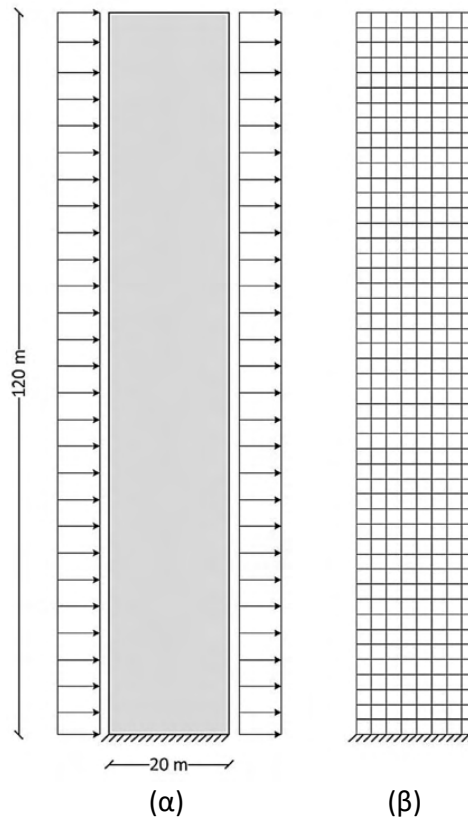
Σχήμα 1 Σχεδιασμός BF συστήματος υψηλού κτιρίου: (α) αρχικό χωρίο και (β) διακριτοποίηση του πλέγματος.

στοιχεία στην οριζόντια κατεύθυνση και 480 στοιχεία στην κατακόρυφη κατεύθυνση, καταλήγοντας σε συνολικά 38.400 ορθογωνικά πεπερασμένα στοιχεία επίπεδης έντασης (bilinear quadrilateral elements – Q4). Στο κάτω άκρο της κατασκευής θεωρείται πάκτωση ενώ εξετάζονται τρεις διατυπώσεις του προβλήματος: (α) περιορισμός συμμετρίας, (β) περίπτωση μη βελτιστοποιήσιμων περιοχών και (γ) συνδυασμός των Q4 στοιχείων με πεπερασμένα στοιχεία δοκού. Σε κάθε περίπτωση εξετάζονται δύο διαφορετικοί τύποι φορτίσεων (κατανεμημένες φορτίσεις και κομβικές δυνάμεις).

Για την εφαρμογή της συμμετρίας δεν χρειάζονται ιδιαίτερες τροποποιήσεις στην διαμόρφωση του προβλήματος ΤΟ. Πιο συγκεκριμένα, εφαρμόζοντας αντισυμμετρικές φορτίσεις, η τελική κατασκευή καταλήγει σε έναν συμμετρικό φορέα. Στη συνέχεια, για

την καλύτερη διαμόρφωση των υποστυλωμάτων και των διαγώνιων του δομικού μας συστήματος, εφαρμόζεται η τεχνική των μη βελτιστοποιήσιμων περιοχών. Σε αυτήν την προσέγγιση, επιλέγονται οι περιοχές που επιθυμούμε να έχουν πάντα υλικό ή να μην έχουν και επιβάλλονται η μέγιστη και η ελάχιστη, αντίστοιχα, τιμή της πυκνότητας. Έτσι, οι πυκνότητες αυτές δεν είναι πλέον άγνωστες μεταβλητές και για το λόγο αυτό οι περιοχές αυτές αποκαλούνται μη βελτιστοποιήσιμες (non-optimizable).

Ακολούθως, μια καινοτόμα μέθοδος υλοποιείται, στην οποία το υπάρχον πλέγμα που αποτελείται από Q4 στοιχεία, ενισχύεται στις κατακόρυφες πλευρές με πεπερασμένα στοιχεία δοκού. Ο αριθμός των στοιχείων δοκού που προστίθενται εξαρτάται από τις συνθήκες φόρτισης που επιβάλλονται. Στην περίπτωση των κατανεμημένων φορτίων, σε κάθε πλευρά προσθέτουμε 480 στοιχεία, ενώ στη περίπτωση των σημειακών φορτίσεων 6 στοιχεία δοκού προστίθενται σε κάθε πλευρά. Τα στοιχεία δοκού αποτελούνται από δύο βαθμούς ελευθερίας μετατόπισης και έναν στροφικό ενώ τα Q4 στοιχεία από δύο μεταφορικούς βαθμούς ελευθερίας. Επομένως κατά την συρραφή των διαφορετικών τύπου πεπερασμένων στοιχείων, γίνεται υπέρθεση των μεταφορικών βαθμών ελευθερίας ενώ ο στροφικός βαθμός ελευθερίας προστίθεται, επεκτείνοντας το μητρώο ακαμψίας. Στο Σχήμα 2, παρουσιάζονται διάφορα BF δομικά συστήματα που προκύπτουν εφαρμόζοντας τους διάφορους περιορισμούς που περιγράφηκαν.

Όπως βλέπουμε στο Σχήμα 2, στην περίπτωση που έχουμε εφαρμόσει απλά τον συμμετρικό περιορισμό, το περισσότερο υλικό συγκεντρώνεται στην βάση του δομικού συστήματος μην αφήνοντας αρκετό υλικό για την ανάπτυξη διαγώνιων μελών και υποστυλωμάτων στο πάνω μέρος της κατασκευής. Εφαρμόζοντας την τεχνική των μη βελτιστοποιήσιμων περιοχών, τα υποστυλώματα εκτείνονται μέχρι την κορυφή των BF, όμως στη βάση τους είναι μεγαλύτερα ενώ και πάλι τα διαγώνια μέλη δεν έχουν σχηματιστεί ολοκληρωμένα. Με την μέθοδο της συρραφής των επιπλέον στοιχείων δοκού, το μέγεθος των υποστυλωμάτων παραμένει σταθερό καθ' όλο το ύψος του δομικού συστήματος, ενώ και στις δύο συνθήκες φόρτισης σχηματίζονται πλήρη διαγώνια μέλη. Επομένως, αυτή η μεθοδολογία μπορεί να εφαρμοστεί στη διαδικασία γένεσης των δομικών συστημάτων BF κατά τη σχεδίαση ενός υψηλού κτιρίου.

Το αποτέλεσμα της μεθοδολογίας GSO, όπως φαίνεται και στο Σχήμα 2, είναι μια εικόνα ενός συνεχούς μέσου, το οποίο πρέπει με κάποιο τρόπο να μετατραπεί σε ένα σύνολο δομικών στοιχείων που χρησιμοποιούνται στις εφαρμογές του πολιτικού μηχανικού.
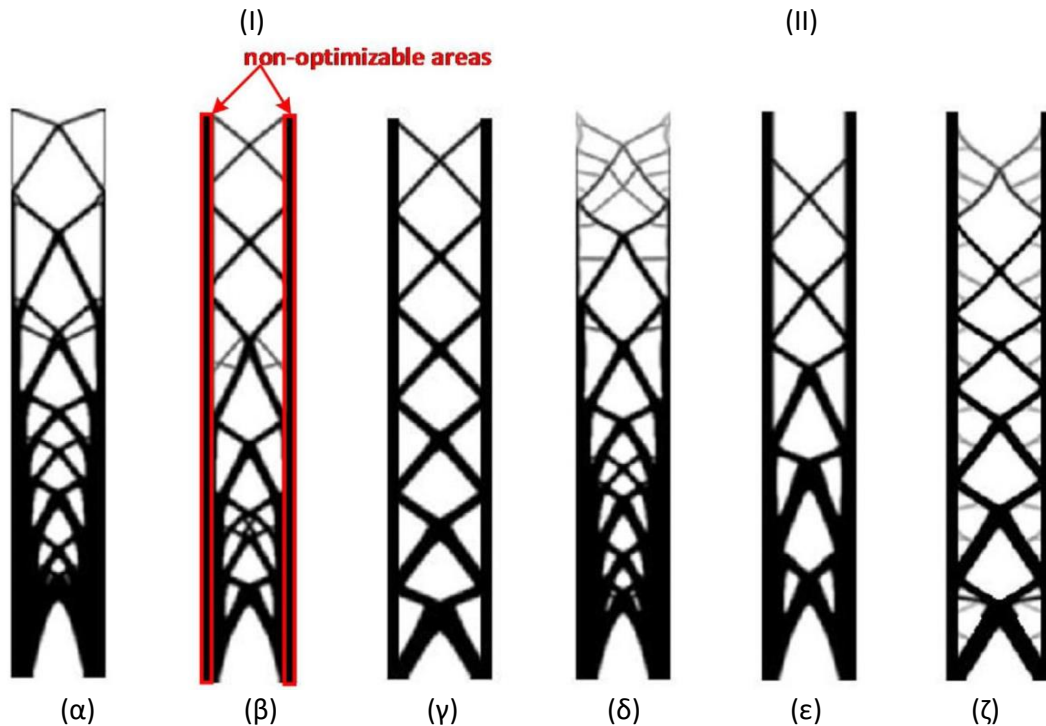
Σχήμα 2 BF σύστημα ενός υψηλού κτιρίου: Βελτιστοποιημένη κατασκευή ($f_{VolFrac} =$ 50%): I. Συγκεντρωμένα σημειακά φορτία: (α) βασική περίπτωση, (β) μη βελτιστοποιήσιμες περιοχές (με κόκκινο χρώμα) και (γ) στοιχεία δοκού. II. Κατανεμημένη φόρτιση στις δύο πλευρές: (δ) βασική περίπτωση (ε) μη βελτιστοποιήσιμες περιοχές (όπως στο β) και (ζ) στοιχεία δοκού.

Στο παρόν κεφάλαιο, παρουσιάζεται μια πλήρως αυτοματοποιημένη διαδικασία μετατροπής του αποτελέσματος της GSO σε αρχείο CAD. Το πρώτο βήμα είναι η μετατροπή του τελικού αποτελέσματος σε μια ασπρόμαυρη (bitmap) εικόνα καθώς και ο προσδιορισμός των ορίων της. Το επόμενο βήμα είναι ο διαχωρισμός των σημείων των σχημάτων που συνδέονται με «φανταστικές» γραμμές σε ξεχωριστά μητρώα και πραγματοποιείται με τη διαδικασία «connected-component labelling». Μέχρι στιγμής, τα σημεία κατά μήκος των ορίων ταξινομούνται σε ομάδες ανάλογα με το εσωτερικό σχήμα που ανήκουν, ωστόσο δεν είναι τοποθετημένα στη σωστή σειρά ώστε να σχηματίζουν μια ενιαία γραμμή. Για το σκοπό αυτό, εφαρμόζεται μια διαδικασία

ταξινόμησης (sorting) για να σχηματιστούν οι σωστές γραμμές και συγκεκριμένα η μέθοδος του πλανόδιου πωλητή. Στη συνέχεια, αναπτύσσεται μια διαδικασία, με στόχο τον διαχωρισμό των σημείων που ενώνονται σχηματίζοντας ευθείες γραμμές και αυτών που σχηματίζουν καμπύλες γραμμές (splines). Στις γραμμές οι οποίες θα αποτελέσουν τις splines, εφαρμόζεται μια διαδικασία λείανσης (smoothing) και στη συνέχεια εφαρμόζεται το μαθηματικό μοντέλο Non-Uniform Rational B-Splines (NURBS). Τέλος, όλες οι προαναφερθείσες λειτουργίες, γράφονται αυτόματα σε ένα αρχείο τύπου IGES, το οποίο είναι συμβατό με πλήθος εμπορικών προγραμμάτων τύπου CAD. Στο Σχήμα 3, παρουσιάζονται τρία BF δομικά συστήματα που αναπαρήχθησαν με την αυτοματοποιημένη διαδικασία. Παρατηρείται, ότι η τελική κατασκευή είναι αρκετά ακριβής και αποτελεί ένα σχήμα το οποίο θα μπορούσε να είχε προκύψει από χειροκίνητο σχεδιασμό.

(α)   (β)   (γ)
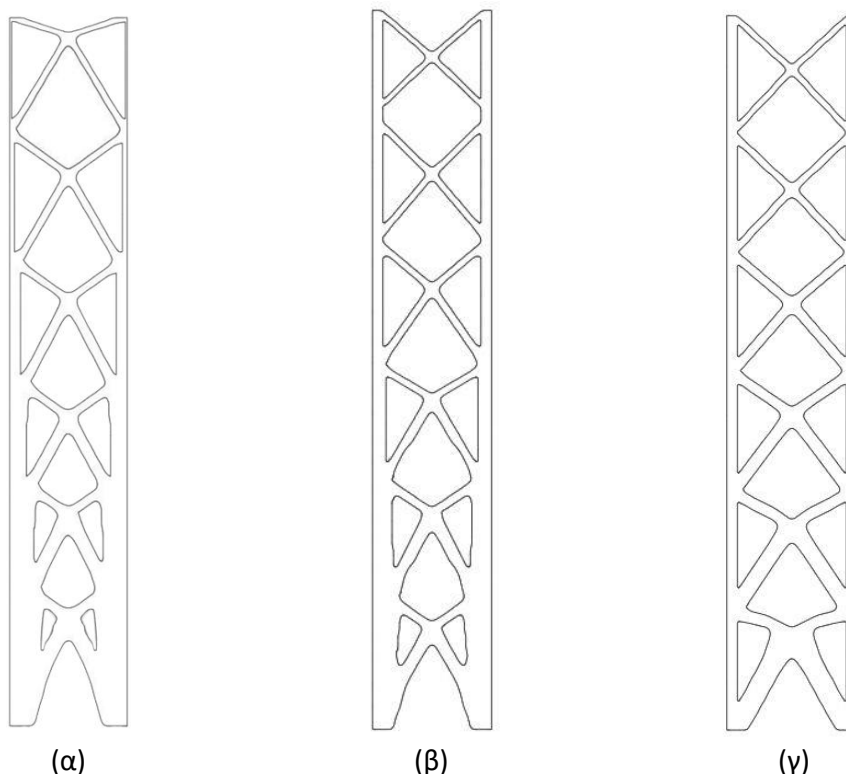
Σχήμα 3 Αυτοματοποιημένη αναπαράσταση βελτιστοποιημένων κατασκευών ($f_{VolFrac} = 40\%$) για σημειακές φορτίσεις: (α) βασική περίπτωση, (β) μη βελτιστοποιήσιμες περιοχές και (γ) στοιχεία δοκού.

5 Εννοιολογικός σχεδιασμός δομικών συστημάτων βάσει ΤΟ και προκατασκευασμένων δομικών στοιχείων

Σε αυτό το κεφάλαιο, εισάγεται μια καινοτόμα μεθοδολογία με βάση το ΤΟ η οποία βρίσκει εφαρμογή στη δημιουργία πρωτότυπων δομικών συστημάτων που αποτελούνται από προκαθορισμένα δομικά στοιχεία (Shaped Units based Topology Optimization - SUTO). Η προτεινόμενη μέθοδος, εκμεταλλευόμενη τεχνικές και εργαλεία παραμετρικού σχεδιασμού, αποτελεί ένα ισχυρό εργαλείο για τη διαδικασία του εννοιολογικού σχεδιασμού, όταν τα δομικά στοιχεία επιλέγονται από μια προκαθορισμένη ομάδα πιθανών στοιχείων. Η καινοτομία της προτεινόμενης μεθοδολογίας, επικεντρώνεται στη κατανομή ενός διακριτού συνόλου προκαθορισμένων δομικών στοιχείων τα οποία είναι εγγεγραμμένα σε ορθογωνικά πεπερασμένα στοιχεία. Το κομμάτι της μεθόδου που αναφέρεται στη βελτιστοποίηση και την ανάλυση πεπερασμένων στοιχείων αναπτύχθηκε σε προσωπικό υπολογιστικό κώδικα MATLAB ενώ το τμήμα της αναπαράστασης της τελικής κατασκευής στο παραμετρικό περιβάλλον του Grasshopper. Η σύνδεση των δύο προγραμμάτων πραγματοποιείται μέσω ενός προσωπικού υπολογιστικού κώδικα που αναπτύχθηκε σε γλώσσα C#.

Η βασική διαφοροποίηση της προτεινόμενης μεθοδολογίας σε σχέση με την SIMP μέθοδο, είναι ότι αντί να κατανέμεται το υλικό ανάλογα με την πυκνότητα του κάθε πεπερασμένου στοιχείου, κατανέμεται ένας αριθμός από προκαθορισμένα σχήματα. Το σχήμα των πιθανών προκατασκευασμένων στοιχείων επιλέγεται από τον αρχιτέκτονα ή τον πολιτικό μηχανικό, δίνοντας έτσι τη δυνατότητα παραγωγής διάφορων σετ προκαθορισμένων στοιχείων. Με τον τρόπο αυτό, μπορούν να προκύψουν ενδιαφέρουσες αρχιτεκτονικές μορφές, που δεν μπορούν να επιτευχθούν μέσω συμβατικών μεθόδων σχεδιασμού. Τα κριτήρια για την επιλογή των πιθανών δομικών στοιχείων μπορεί να είναι είτε αισθητικά είτε πρακτικά, όπως για παράδειγμα η επιρροή τους στην σκίαση κατά τη δημιουργία ενός στεγάστρου ή ενός τοιχίου. Στη συνέχεια παρουσιάζονται οι θεμελιώδεις τροποποιήσεις στη διαμόρφωση του ΤΟ προβλήματος, η οποία βασίζεται στο γεγονός ότι το αρχικό σχεδιαστικό χωρίο διακριτοποιείται με Q4

ή 3D πεπερασμένα στοιχεία και στη συνέχεια οι προκαθορισμένες δομές αντικαθιστούν τα πεπερασμένα στοιχεία. Αναλυτικά η μαθηματική διατύπωση του προβλήματος είναι η ακόλουθη:

$$\min_{sh_e} C(sh_e) = F^T u(sh_e) = u(sh_e)^T K(sh_e) u(sh_e) \tag{7α}$$

$$s.t.$$

$$K(sh_e) u(sh_e) = F \tag{7β}$$

$$\frac{V(sh_e)}{V_0} = f_{VolFrac} \tag{7γ}$$

$$\sum_{e=1}^{N_{ele}} a_e \leq V_0 \tag{7δ}$$

$$sh_e \in A_{SH} = \{SH_i, i = 1,2,\dots,m\} \tag{7ε}$$

Όπου $C(sh_e)$ είναι η ενδοτικότητα της κατασκευής ενώ οι εξισώσεις (7β) και (7γ) είναι ανάλογες με τις εξισώσεις (3β),(3γ). Η βασική διαφοροποίηση της μαθηματικής διατύπωσης στην εξίσωση 7 έγκειται στη μεταβλητή σχεδιασμού, όπου στην προτεινόμενη διατύπωση αντί για την πυκνότητα κάθε πεπερασμένου στοιχείου, η μεταβλητή σχεδιασμού είναι το εμβαδόν των διαφόρων σχημάτων από τα οποία θα αποτελείται η τελική κατασκευή. Συγκεκριμένα, επιλέγεται από ένα διακριτό σετ A_{SH} που αποτελείται από m προκατασκευασμένα δομικά στοιχεία SH_i, που αντιστοιχούν σε διαφορετικά εμβαδά a_i.

Το πρώτο στάδιο της προτεινόμενης μεθοδολογίας είναι η δημιουργία του διακριτού σχεδιαστικού σετ. Στην εφαρμογή της μεθόδου στο παρόν κεφάλαιο, χρησιμοποιούνται προκατασκευασμένα δομικά στοιχεία τα οποία είναι εγγεγραμμένα σε προκαθορισμένα ορθογώνια που έχουν επιλεχθεί στην αρχή της διαδικασίας. Αυτό οφείλεται στο γεγονός ότι το αρχικό χωρίο διαχωρίζεται με ένα δομημένο πλέγμα πεπερασμένων στοιχείων που βασίζεται σε ορθογωνικά πεπερασμένα στοιχεία συγκεκριμένου μεγέθους ανάλογα με την πυκνότητα του πλέγματος. Επομένως, τα πιθανά σχήματα οφείλουν να έχουν 4

κόμβους στις άκρες τους που να συμπίπτουν με αυτές των Q4 στοιχείων. Στη παρούσα μελέτη, το διακριτό σετ σχεδιασμού αποτελείται από $m = 10$ διαφορετικά σχήματα που προέκυψαν από παραμετρική μελέτη μειώνοντας σταδιακά το εμβαδόν τους, όπως φαίνεται στο Σχήμα 4. Η μεταβλητή σχεδιασμού παίρνει τέτοιες τιμές ώστε η μικρότερή της τιμή να μην οδηγεί σε κενό σχήμα, ενώ η μεγαλύτερη να μην είναι τετράγωνο. Συγκεκριμένα, το εμβαδόν του πλήρους τετραγώνου είναι $a_{rec} = 1$, ενώ οι οριακές τιμές είναι $a_{min} = Area(SH_{m=10}) = 0.1$ και $a_{max} = Area(SH_1) = 0.9$.
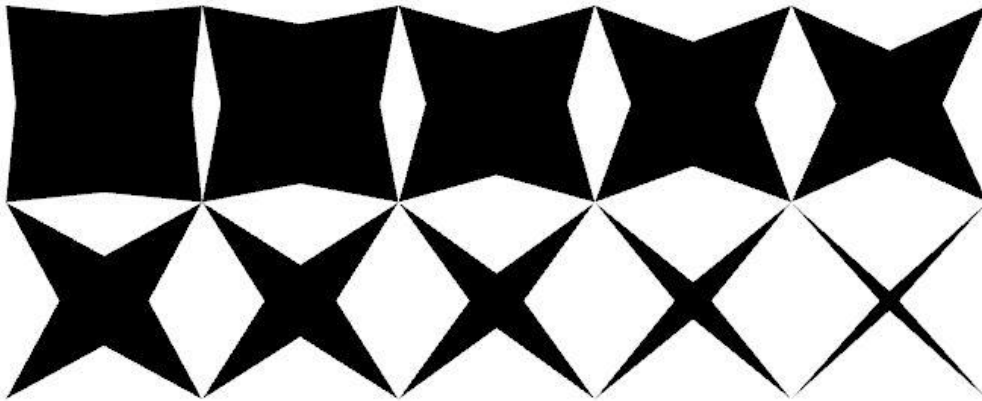
Σχήμα 4 Παραμετρική μελέτη για δέκα προκαθορισμένα σχήματα.

Έχοντας δημιουργήσει το διακριτό σύνολο σχεδιασμού, το επόμενο βήμα της μεθοδολογίας είναι η δημιουργία του κάθε υπερστοιχείου. Η εφαρμογή της προτεινόμενης μεθοδολογίας βασίζεται σε ισοδύναμα Q4 στοιχεία, των οποίων το μητρώο ακαμψίας είναι ένας πίνακας μεγέθους 8×8:

$$K_e^{Q4} = \begin{bmatrix} k_{11}^{Q4} & \cdots & k_{18}^{Q4} \\ \vdots & \ddots & \vdots \\ k_{81}^{Q4} & \cdots & k_{88}^{Q4} \end{bmatrix} \qquad (8)$$

Για τη διακριτοποίηση των προκαθορισμένων σχημάτων, χρησιμοποιήθηκαν τριγωνικά πεπερασμένα στοιχεία τριών κόμβων. Ο αριθμός των βαθμών ελευθερίας κάθε σχήματος εξαρτάται από την ποιότητα του πλέγματος. Τα μητρώα ακαμψίας των υπερστοιχείων προκύπτουν από τη μέθοδο της στατικής συμπύκνωσης. Υποθέτουμε ότι οι βαθμοί ελευθερίας που πρόκειται να εξαλειφθούν επισημαίνονται ως e και αυτοί που πρέπει να συμπυκνωθούν ως c. Σύμφωνα με αυτόν το συμβολισμό, οι εξισώσεις ισορροπίας για κάθε προκαθορισμένο σχήμα γράφονται ως εξής:

$$\begin{Bmatrix} F_e \\ F_c \end{Bmatrix} = \begin{bmatrix} K_{ee} & K_{ec} \\ K_{ce} & K_{cc} \end{bmatrix} \begin{Bmatrix} u_e \\ u_c \end{Bmatrix} \qquad (9)$$

Μετά από ορισμένες αντικαταστάσεις το συμπυκνωμένο μητρώο γράφεται ως εξής:

$$\overline{K} = K_{cc} - K_{ce}K_{ee}^{-1}K_{ec} \qquad (10)$$

Έτσι οι κόμβοι των ισοδύναμων ορθογωνικών στοιχείων συμπίπτουν με τους 4 συμπυκνωμένους κόμβους των προκαθορισμένων σχημάτων.

$$K_{sh}^i = \begin{bmatrix} k_{11}^i & \cdots & k_{1n}^i \\ \vdots & \ddots & \vdots \\ k_{n1}^i & \cdots & k_{nn}^i \end{bmatrix} \rightarrow \overline{K}_{sh}^i = \begin{bmatrix} \overline{k}_{11}^i & \cdots & \overline{k}_{18}^i \\ \vdots & \ddots & \vdots \\ \overline{k}_{81}^i & \cdots & \overline{k}_{88}^i \end{bmatrix} \qquad (11)$$

$$n = depending \ on \ mesh \ quality, \qquad i = 1,2, \dots, m$$

Η εξίσωση 11, δείχνει τη διαδικασία μετασχηματισμού του καθολικού μητρώου ακαμψίας K_{sh}^i του προκαθορισμένου σχήματος που έχει n βαθμούς ελευθερίας στο ισοδύναμο μητρώο μεγέθους 8×8, για κάθε ένα από τα m σχήματα.

Για την επίλυση του ΤΟ προβλήματος απαιτείται ο υπολογισμός του καθολικού μητρώου ακαμψίας που προκύπτει από το αρχικό σχεδιαστικό χωρίο, βάσει της μεταβλητής σχεδιασμού σε κάθε εσωτερική επανάληψη του αλγόριθμου. Επομένως, στο σημείο αυτό πρέπει να συσχετιστεί η τιμή της μεταβλητής σχεδιασμού που προκύπτει από τον εκάστοτε αλγόριθμο (OC ή MMA) με τα προκαθορισμένα σχήματα. Αρχικά πραγματοποιείται μια ανάλυση παλινδρόμησης και το ακόλουθο πολυώνυμο τετάρτου βαθμού εφαρμόζεται:

$$f_{ij}^e(a_e) = a_{ij}a_e^4 + b_{ij}a_e^3 + c_{ij}a_e^2 + d_{ij}a_e + e_{ij} \qquad (12)$$

$$\tilde{k}_{ij}^e = f_{ij}^e(a_e) \qquad (13)$$

όπου $a_{ij}, b_{ij}, c_{ij}, d_{ij}, e_{ij}$ είναι οι συντελεστές της πολυωνυμικής καμπύλης και a_e είναι το εμβαδόν του e^{th} στοιχείου. Η ανάλυση παλινδρόμησης πραγματοποιείται για την εύρεση του κάθε ανεξάρτητου στοιχείου του μητρώου ακαμψίας, εκμεταλλευόμενοι την συμμετρία. Στο Σχήμα 5, παρουσιάζεται η προσεγγιστική καμπύλη για τον υπολογισμό του $\tilde{k}_{11}^e$ στοιχείου του μητρώου ακαμψίας. Στην εξίσωση 14 βλέπουμε ότι για τον

υπολογισμό του μητρώου ακαμψίας ενός στοιχείου του αρχικού σχεδιαστικού χωρίου, απαιτούνται 8 αναλύσεις παλινδρόμησης.

Σχήμα 5 Ανάλυση παλινδρόμησης για το $\tilde{k}_{11}^e$

Επιπλέον στην εξίσωση 15 παρουσιάζεται και ο υπολογισμός της παραγώγου που απαιτείται για τον μαθηματικό αλγόριθμο.

$$\widetilde{K}_e^{sh} = \begin{bmatrix} \tilde{k}_{11}(a_e) & \cdots & \tilde{k}_{18}(a_e) \\ \vdots & \ddots & \vdots \\ \tilde{k}_{81}(a_e) & \cdots & \tilde{k}_{88}(a_e) \end{bmatrix} =$$

$$= \begin{bmatrix} \tilde{k}_1(a_e) & & & & & & & \\ \tilde{k}_2(a_e) & \tilde{k}_3(a_e) & & & & SYM & & \\ \tilde{k}_4(a_e) & \tilde{k}_5(a_e) & \tilde{k}_1(a_e) & & & & & \\ -\tilde{k}_5(a_e) & \tilde{k}_6(a_e) & -\tilde{k}_2(a_e) & \tilde{k}_3(a_e) & & & & \\ -\tilde{k}_1(a_e)/2 & -\tilde{k}_2(a_e) & \tilde{k}_7(a_e) & \tilde{k}_5(a_e) & \tilde{k}_1(a_e) & & & \\ -\tilde{k}_2(a_e) & -\tilde{k}_3(a_e)/2 & -\tilde{k}_5(a_e) & \tilde{k}_8(a_e) & \tilde{k}_2(a_e) & \tilde{k}_3(a_e) & & \\ \tilde{k}_7(a_e) & -\tilde{k}_5(a_e) & -\tilde{k}_1(a_e)/2 & \tilde{k}_2(a_e) & \tilde{k}_4(a_e) & \tilde{k}_5(a_e) & \tilde{k}_1(a_e) & \\ \tilde{k}_5(a_e) & \tilde{k}_8(a_e) & \tilde{k}_2(a_e) & -\tilde{k}_3(a_e)/2 & -\tilde{k}_5(a_e) & \tilde{k}_6(a_e) & -\tilde{k}_2(a_e) & \tilde{k}_3(a_e) \end{bmatrix} \quad (14)$$

$$a_e \in A, \qquad A = [a_{min}, a_{max}]$$

$$\frac{d\tilde{k}_{ij}^e}{da_e} = \frac{df_{ij}(a_e)}{da_e} = 4a_{ij}a_e^3 + 3b_{ij}a_e^2 + 2c_{ij}a_e + d_{ij} \qquad (15)$$

Για την εφαρμογή της προτεινόμενης μεθοδολογίας, αναπτύχθηκε προσωπικός υπολογιστικός κώδικας στη MATLAB. Πιο συγκεκριμένα, όλες οι προαναφερθείσες διαδικασίες συγκεντρώθηκαν σε μια συνάρτηση $[K_e, dK_e] = Fshapes(a_e)$, η οποία ουσιαστικά αντικαθιστά την συνάρτηση της SIMP, η οποία δημιουργεί τα μητρώα ακαμψίας. Μετά τη σύγκλιση του προβλήματος, οι μεταβλητές σχεδιασμού λαμβάνουν συνεχείς τιμές, επομένως πρέπει να προστεθεί μια διαδικασία για την μετατροπή των τιμών αυτών, σε τιμές που αντιστοιχούν στα πραγματικά σχήματα. Αυτό πραγματοποιείται σύμφωνα με την ακόλουθη έκφραση:

$$sh_e = SH_j : dist_j = min(dist = |a_e - a_i|), \qquad i = 1,2,\dots m \qquad (16)$$

Στο Σχήμα 6 παρουσιάζεται η αναπαράσταση της τελικής κατασκευής μέσω της MATLAB, όπου κάθε προκαθορισμένο δομικό στοιχείο αντιστοιχεί σε διαφορετικό χρώμα. Στο Σχήμα 7, παρουσιάζεται το διάγραμμα ροής της μεθοδολογίας και συγκρίνεται με αυτό της SIMP.
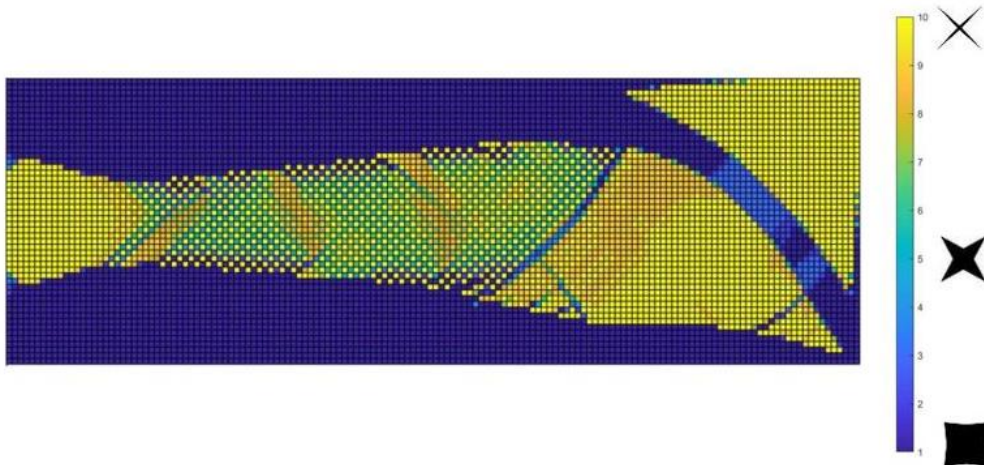
Σχήμα 6 Απεικόνιση στη MATLAB. Με κίτρινο χρώμα το μικρότερο σχήμα και με μπλε το μεγαλύτερο
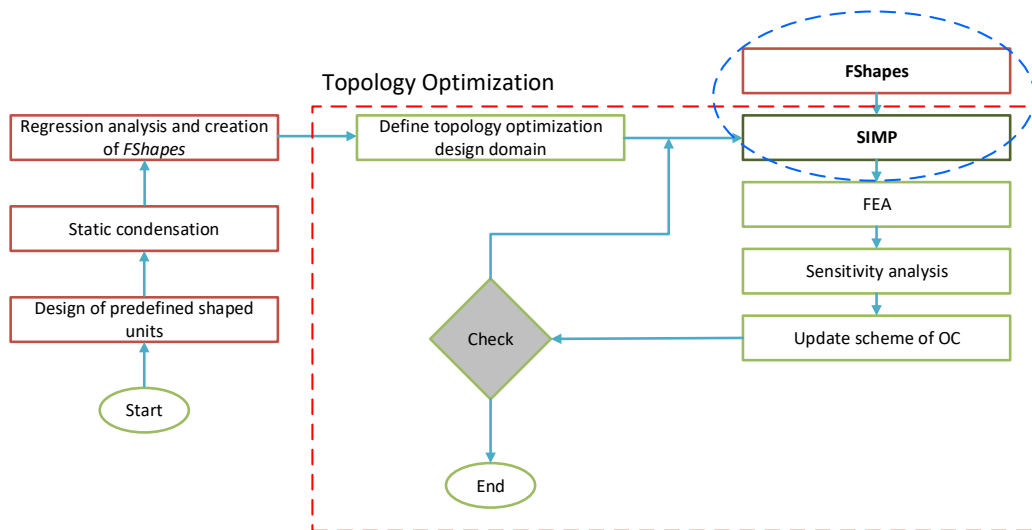
Σχήμα 7 Διάγραμμα ροής της SIMP και της SUTO

Η αναπαράσταση της τελικής κατασκευής σε ένα πρόγραμμα τύπου CAD, είναι βασικό αντικείμενο καθ' όλη τη παρούσα διατριβή. Στο παρόν κεφάλαιο, αναπτύχθηκε ένας κώδικας σε γλώσσα C# σε συνδυασμό με το πρόγραμμα παραμετρικού σχεδιασμού Grasshopper, προκειμένου το τελικό αποτέλεσμα να αναπαραχθεί στο σχεδιαστικό πρόγραμμα Rhino3D. Στο Σχήμα 8, παρουσιάζεται το βελτιστοποιημένο αποτέλεσμα του προβλήματος *"BBeam test example"*, που αποτελείται από 150 στοιχεία στη Χ διεύθυνση και 50 στη Υ. Η αριστερή πλευρά θεωρείται πακτωμένη ενώ επιβάλλεται ένα σημειακό φορτίο κάτω δεξιά.
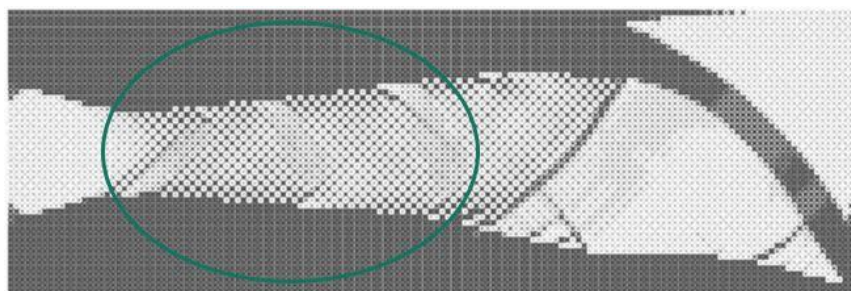
(α)
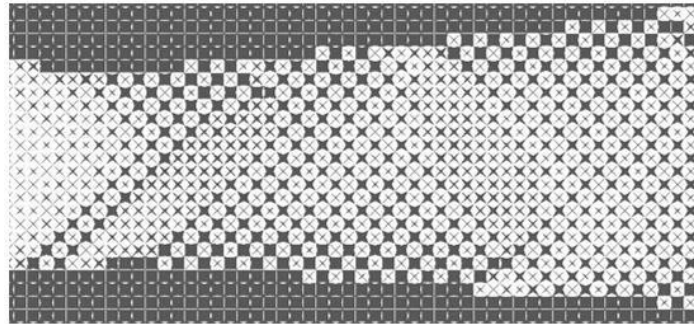
(β)

Σχήμα 8 BBeam παράδειγμα: (α) αναπαράσταση στο Rhino3D, (β) μεγεθυμένη περιοχή

Στη συνέχεια η μεθοδολογία SUTO εφαρμόζεται σε μια επίπεδη πλάκα η οποία με την κατάλληλη επεξεργασία μπορεί να τροποποιηθεί σε καμπύλο κέλυφος μονής καμπυλότητας. Το πλέγμα της αρχικής κατασκευής αποτελείται από 200 στοιχεία σε κάθε διεύθυνση, στις 4 άκρες την πλάκας τοποθετούνται πακτώσεις ενώ 5 σημειακά φορτία εφαρμόζονται. Στο Σχήμα 9 παρουσιάζεται μια πρωτότυπη κελυφωτή κατασκευή που θα μπορούσε να είναι ένα εκθεσιακό περίπτερο ή ένα στέγαστρο.

(α)

(β)

(γ)
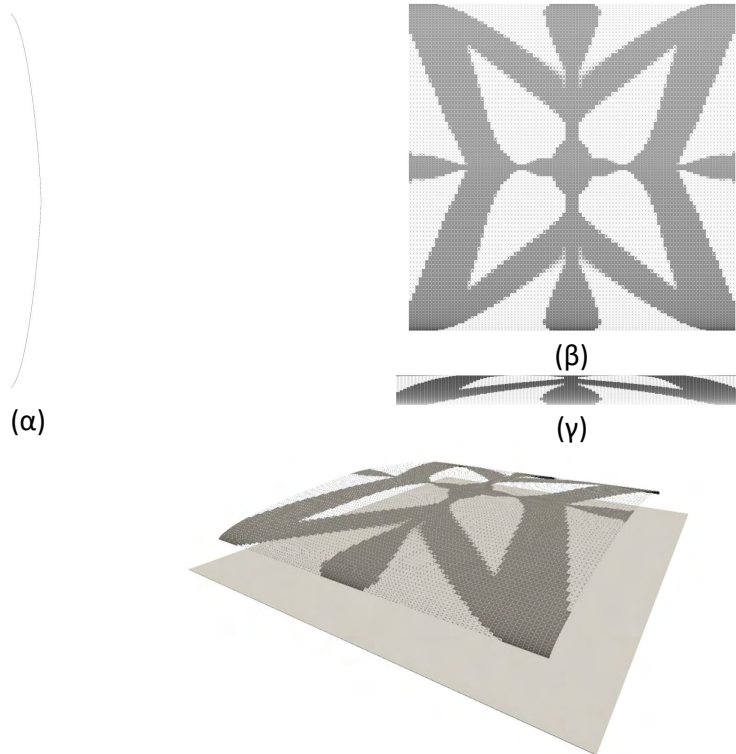
(δ)

Σχήμα 9 Στέγαστρο: (α) όψη, (β) κάτοψη, (γ) πλάγια όψη και (δ) προοπτική όψη.

6 Υλοποίηση της FSTO μεθόδου στο SAP2000

Μέχρι στιγμής, οι προτεινόμενες μεθοδολογίες γένεσης δομικών συστημάτων για εφαρμογές πολιτικού μηχανικού, βασίζονται στη GSO προσέγγιση. Στο κεφάλαιο αυτό εισάγεται η διατύπωση του FSTO προβλήματος το οποίο ανήκει στην κατηγορία προβλημάτων LO. Στη διεθνή βιβλιογραφία, οι περισσότερες εργασίες που πραγματεύονται με τα LO προβλήματα χρησιμοποιούν την Truss Structural Topology Optimization (TSTO) διατύπωση, στην οποία μετέχουν μέλη που αναπτύσσουν μόνο αξονικές τάσεις. Ωστόσο, η συμμετοχή μελών που λαμβάνουν τόσο αξονικές όσο και καμπτικές τάσεις είναι μια ενδιαφέρουσα και καινοτόμα πτυχή του πεδίου του TO. Στο παρόν κεφάλαιο, παρουσιάζεται η συμβατική διατύπωση του FSTO προβλήματος έχοντας σαν αντικειμενική συνάρτηση την ελαχιστοποίηση της ενδοτικότητας. Παρουσιάζονται επίσης δύο τεχνικές δημιουργίας του αρχικού GS, μια μέσω του προγράμματος παραμετρικού σχεδιασμού Grasshopper και μια με ανάπτυξη κώδικα στη MATLAB. Η ανάλυση πεπερασμένων στοιχείων του προβλήματος πραγματοποιείται στο εμπορικό πρόγραμμα SAP2000, ενώ όλη η διαδικασία της βελτιστοποίησης υλοποιείται μέσω προσωπικού υπολογιστικού κώδικα στη C#.

Η δημιουργία του αρχικού σχεδιαστικού χωρίου είναι από τα πιο σημαντικά στοιχεία της διαμόρφωσης ενός LO προβλήματος αφού καθορίζει το ποσοστό σχεδιαστικής ελευθερίας που δίνεται στον αλγόριθμο. Στη διεθνή βιβλιογραφία, όλες οι προτεινόμενες τεχνικές δημιουργίας του GS, βασίζονται σε ανάπτυξη υπολογιστικού κώδικα, περιορίζοντας με αυτό τον τρόπο τη σχεδιαστική ελευθερία του μηχανικού. Στα πλαίσια της παρούσας διατριβής, αναπτύχθηκε μια μέθοδος στο πρόγραμμα Grasshopper για τη δημιουργία του GS, η οποία δίνει τη δυνατότητα της εφαρμογής του FSTO προβλήματος σε πιο πολύπλοκες κατασκευές, όπως φαίνεται και στο παράδειγμα του gridshell στο τέλος του κεφαλαίου. Ανάλογα με τις απαιτήσεις του προβλήματος μπορούν να δημιουργηθούν διάφορα στάδια συνδεσιμότητας. Όταν η αρχική γεωμετρία του προβλήματος είναι σχετικά απλή, στην περίπτωση που πρέπει να εφαρμοστούν ορισμένοι κατασκευαστικοί περιορισμοί ή περισσότερα στάδια συνδεσιμότητας, η δημιουργία του GS είναι απλούστερη μέσω υπολογιστικού κώδικα. Στο Σχήμα 10

παρουσιάζονται τρία στάδια συνδεσιμότητας μιας απλής 2D κατασκευής, που δημιουργήθηκαν μέσω του MATLAB κώδικα.
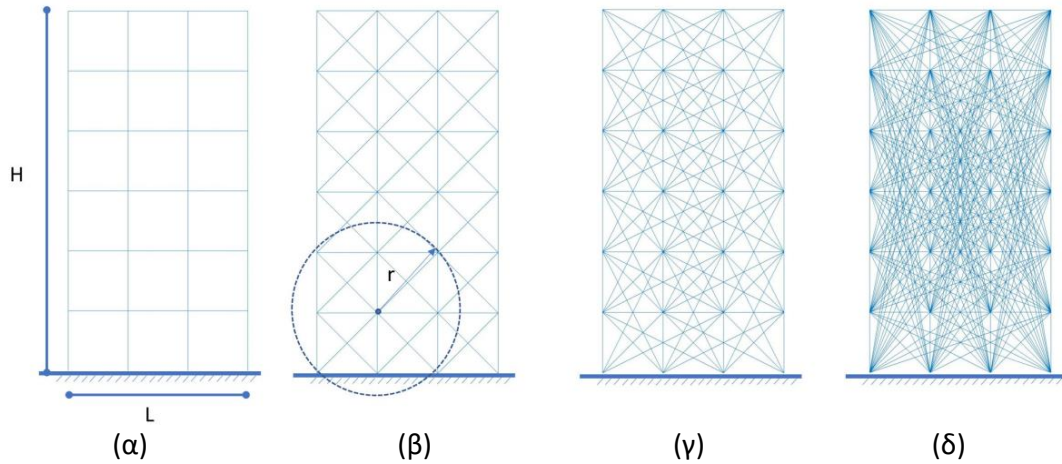
Σχήμα 10 (α) Κατασκευή μόνο με κολώνες και δοκάρια $L = 3m$, $H = 6m$ και διαφορετικά GS για (β) $r = 1.41m$, (γ) $r = 3.0m$ και (δ) $r = 6.71m$

Η μαθηματική διατύπωση του FSTO προβλήματος με αντικειμενική συνάρτηση την ελαχιστοποίηση της ενδοτικότητας περιγράφεται ως εξής:

$$\min_{a} C(a) = F^T d(a) \tag{17α}$$

$$s.t.$$

$$K(a)d(a) = F \tag{17β}$$

$$a^T \cdot L \leq V_{lim} \tag{17γ}$$

$$a_{min,e} \leq a_e \leq a_{max,e}, \quad e = 1,2,\dots,N_{ele} \tag{17δ}$$

όπου C είναι η ενδοτικότητα της κατασκευής, F και d είναι τα διανύσματα φορτίσεων και μετατοπίσεων αντίστοιχα, το K είναι το καθολικό μητρώο ακαμψίας, το L είναι το διάνυσμα με τα μήκη των πεπερασμένων στοιχείων και το V_{lim} είναι ο όγκος της τελικής κατασκευής. Οι μεταβλητές σχεδιασμού του προβλήματος είναι το εμβαδόν των διατομών των στοιχείων δοκού που χρησιμοποιούνται και συμβολίζονται με το a. Στη μαθηματική διατύπωση, το a_{min} υποδηλώνει έναν πολύ μικρό αριθμό για την αποφυγή μαθηματικής αστάθειας ενώ το a_{max} είναι η μέγιστη τιμή εμβαδού που μπορεί να πάρει

ένα στοιχείο. Σε αντίθεση με την GSO μέθοδο, η μεταβλητή σχεδιασμού δεν μπορεί να βγει κοινός παράγοντας από το μητρώο ακαμψίας έτσι ώστε να υπολογιστεί η παράγωγος. Προκειμένου το μητρώο ακαμψίας να γίνει διαφορίσιμο, πρέπει η ροπή αδράνειας να εκφραστεί συναρτήσει του εμβαδού. Για διατομές με απλή γεωμετρία, είναι διαθέσιμη η αναλυτική έκφραση της σχέσης μεταξύ $\left(a_e - I_y\right)$, π.χ. για τετραγωνική διατομή $\left(I_y = \frac{1}{12} \cdot a_e^2\right)$ και για κυκλική $\left(I_y = \frac{\pi}{4} \cdot a_e^2\right)$. Η παράγωγος της ενδοτικότητας υπολογίζεται από τη σχέση:

$$\frac{\partial C}{\partial a_e} = -d_e^T \frac{\partial K_e}{\partial a_e} d_e \qquad (18)$$

Για την επίλυση του FSTO προβλήματος αναπτύχθηκε κώδικας στη C#, ο οποίος ενσωματώθηκε στην υπολογιστική πλατφόρμα High-Performance Topology Optimization Computing Platform (HP-TOCP). Η συγκεκριμένη διαδικασία χωρίζεται σε δύο μέρη, την προ-επεξεργασία και την επαναληπτική διαδικασία. Και στα δύο μέρη υπάρχουν δύο ανεξάρτητες διαδικασίες που πραγματοποιούνται. Αρχικά, ανακτώνται όλες οι απαραίτητες πληροφορίες από το στατικό πρόγραμμα SAP2000. Αυτό επιτυγχάνεται με τη δημιουργία κατάλληλων συναρτήσεων μέσω του API του SAP2000, με τις οποίες λαμβάνονται μόνο οι απαραίτητες, για την επίλυση του προβλήματος, πληροφορίες. Στη συνέχεια, ο υπολογιστικός πυρήνας του HP-TOCP εκτελεί όλους τους απαραίτητους υπολογισμούς. Στην επαναληπτική διαδικασία δημιουργήθηκε μια συνάρτηση wrapper, η οποία καλεί τη συνάρτηση fmincon, της σουίτας βελτιστοποίησης της MATLAB, υλοποιώντας τη διαδικασία χωρίς να χρειάζεται να ανοίξει καν το πρόγραμμα της MATLAB. Κατά τη διάρκεια της επαναληπτικής διαδικασίας υπάρχει πάντα αλληλεπίδραση μεταξύ του στατικού προγράμματος και του υπολογιστικού πυρήνα του HP-TOCP, επειδή απαιτούνται τα αποτελέσματα μετά από κάθε στατική ανάλυση.

Στο στάδιο της προ-επεξεργασίας, μετά την εισαγωγή του GS στο SAP2000, πρέπει να καθοριστούν εντός του προγράμματος οι συνοριακές συνθήκες καθώς και οι φορτίσεις. Στη συνέχεια επιλέγεται το είδος τις διατομής των στοιχείων δοκού του προβλήματος. Όπως αναφέρθηκε και προηγουμένως, το εμβαδόν των διατομών είναι η μεταβλητή σχεδιασμού του FSTO προβλήματος. Όμως προκειμένου να οριστούν οι διατομές στο

εμπορικό πρόγραμμα απαιτούνται οι ακριβής διαστάσεις των διατομών. Χρησιμοποιώντας τις κυκλικές ή τετραγωνικές διατομές, η συγκεκριμένη πληροφορία προκύπτει αυτόματα ξέροντας μόνο το εμβαδόν της διατομής. Το πρώτο βήμα της πλατφόρμας HP-TOCP, είναι η ανάκτηση όλων των πληροφοριών της γεωμετρίας της κατασκευής. Δημιουργούνται ορισμένες βιβλιοθήκες με τα ονόματα των πεπερασμένων στοιχείων, τα ονόματα και τις συντεταγμένες των κόμβων και τα ονόματα των συνδυασμών φόρτισης. Το επόμενο βήμα είναι η συσχέτιση των μεταβλητών σχεδιασμού με την κατασκευή. Για το σκοπό αυτό, δημιουργούνται τόσες διατομές όσα είναι και τα στοιχεία δοκού, επομένως κάθε μέλος έχεις ξεχωριστή διατομή.

Στο επαναληπτικό στάδιο, το πρώτο βήμα της κάθε επανάληψης είναι η ενημέρωση του μοντέλου του στατικού προγράμματος με τις καινούργιες διαστάσεις που προτείνει ο μαθηματικός αλγόριθμος. Στη συνέχεια πραγματοποιείται η στατική ανάλυση και ανακτώνται οι δυνάμεις και οι μετατοπίσεις κάθε κόμβου. Με την πληροφορία αυτή υπολογίζεται η ενδοτικότητα και ο συνολικός όγκος της κατασκευής. Χρησιμοποιώντας την συνάρτηση που εφαρμόζει τον αλγόριθμο της MATLAB, ανανεώνονται οι μεταβλητές σχεδιασμού. Μετά την σύγκλιση του αλγορίθμου, οι μεταβλητές σχεδιασμού λαμβάνουν τιμές από a_{min} έως a_{max}. Όμως, όπως αναφέρθηκε προηγουμένως, το a_{min} είναι μια πολύ μικρή τιμή για την αποφυγή του φαινομένου της μοναδικότητας. Επομένως, πρέπει να οριστεί ένα επιπλέον όριο, το οποίο θα υποδηλώνει ότι οποιαδήποτε διατομή λαμβάνει τιμή μικρότερη από αυτό το μέλος, στην πραγματικότητα δεν υπάρχει. Στο Σχήμα 11 παρουσιάζεται το διάγραμμα ροής της προαναφερθείσας διαδικασίας.

Στο Σχήμα 12 παρουσιάζονται δύο GS, προκειμένου να τονιστεί η σημασία της συνδεσιμότητας στο FSTO πρόβλημα, για την προσομοίωση μια γέφυρας μήκους $24m$ και ύψους $H = 6m$. Στο αριστερό και δεξί άκρο έχουν εφαρμοστεί πακτώσεις ενώ στην κάτω πλευρά εφαρμόζονται σημειακά φορτία σε κάθε κόμβο $P = 100KN$. Χρησιμοποιούνται κυκλικές διατομές με $a_{max} = 4 \cdot 10^{-2} m^2$, $a_{min} = 2 \cdot 10^{-4} m^2$ ενώ τίθεται ο περιορισμός $V_{lim} = 1.2 m^3$.
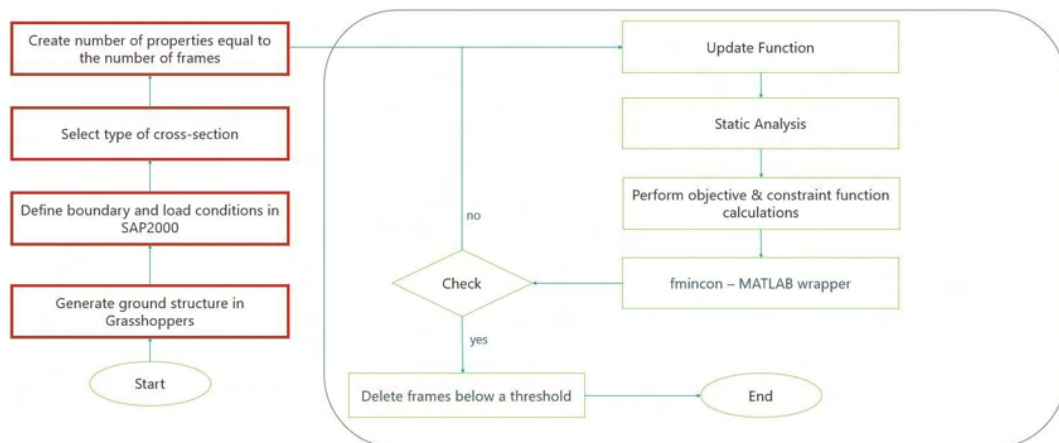
Σχήμα 11 Διάγραμμα ροής της FSTO με την υλοποίηση της πλατφόρμας HP-TOCP

Στο Σχήμα 13 παρουσιάζονται οι προτεινόμενες λύσεις. Στη περίπτωση που χρησιμοποιείται το απλό GS η ενδοτικότητα της βέλτιστης κατασκευής είναι ίση με $C = 1.31 \cdot 10^3 \, Nm$, ενώ στην περίπτωση που χρησιμοποιείται το πλήρες GS είναι $C = 1.06 \cdot 10^3 \, Nm$. Παρατηρείται δηλαδή μείωση της αντικειμενικής συνάρτησης 19.1%.

(α)

(β)
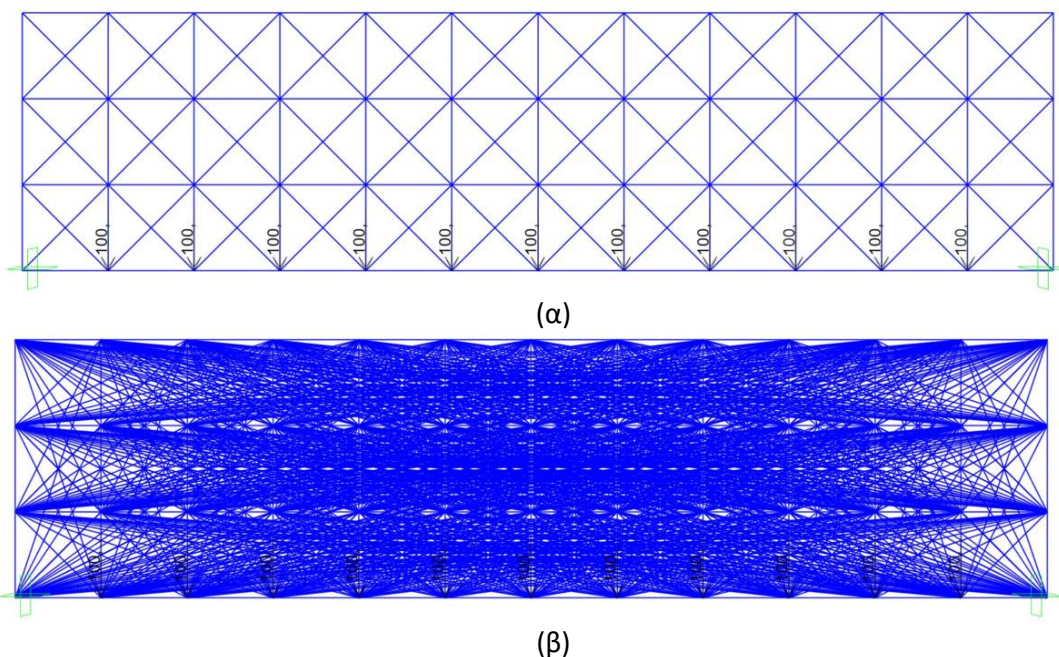
Σχήμα 12 Αρχικό σχεδιαστικό χωρίο γέφυρας για GS (α) απλής και (β) πλήρους συνδεσιμότητας.
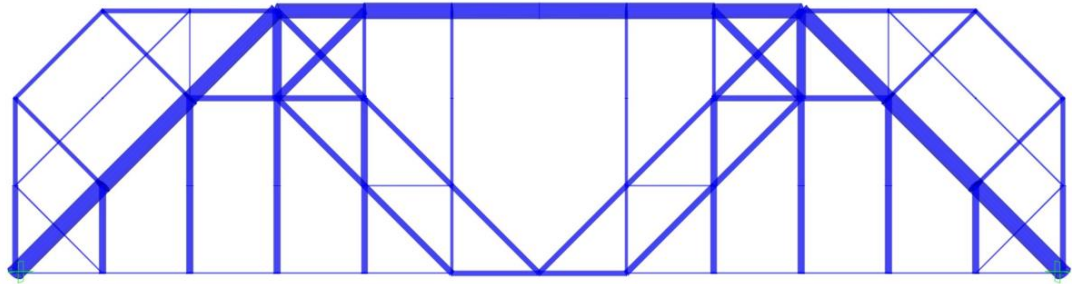
(α)
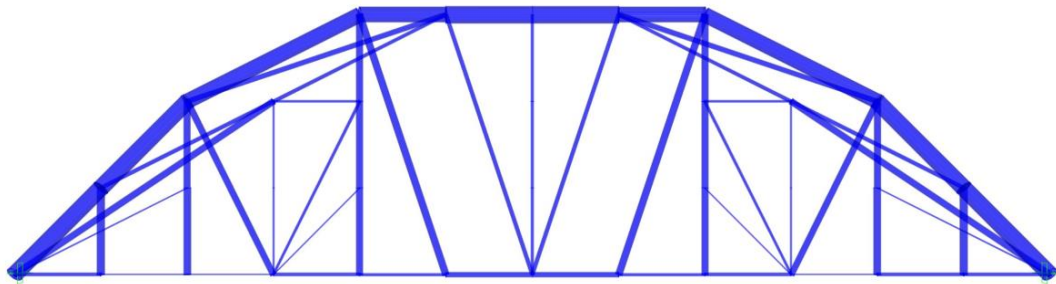
(β)

Σχήμα 13 Γέφυρα: Βελτιστοποιημένη κατασκευή για $V_{lim} = 1.2m^3$ για GS (α) απλής και (β) πλήρους συνδεσιμότητας.

Στα Σχήματα 14 και 15 παρουσιάζονται δύο προτάσεις για τη δημιουργία ενός gridshell το οποίο θα μπορούσε να είναι στέγαστρο ή εκθεσιακό περίπτερο (pavilion). Και στις δύο περιπτώσεις παρατηρείται ότι το FSTO είναι ένα δυνατό υπολογιστικό εργαλείο, για τη δημιουργία καινοτόμων και πρωτότυπων δομικών συστημάτων που δεν μπορούν να παραχθούν με συμβατικές μεθόδους.
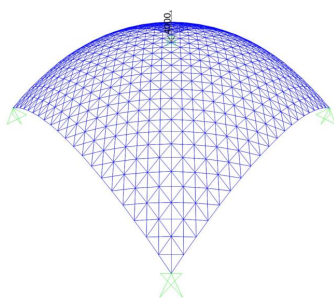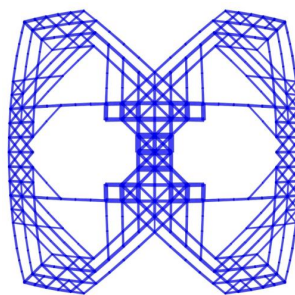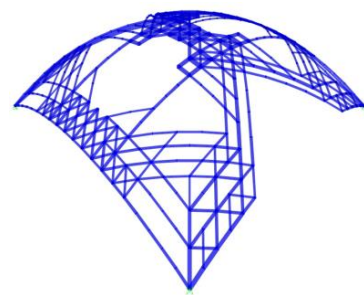
(α)   (β)   (γ)

Σχήμα 14 GS1: (α) Αρχική κατασκευή για απλής συνδεσιμότητας GS, (β) κάτοψη και (γ) προοπτική όψη βέλτιστιτοποιημένης κατασκευής για $V_{lim} = 60m^3$
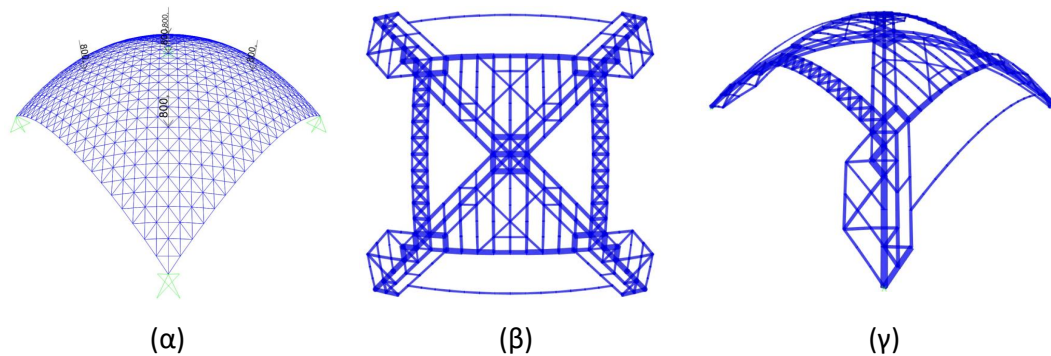
Σχήμα 15 GS2: (α) Αρχική κατασκευή για απλής συνδεσιμότητας GS, (β) κάτοψη και (γ) προοπτική όψη βέλτιστιτοποιημένης κατασκευής για $V_{lim} = 80m^3$

7 Συνδυασμός SSO και FSTO προβλήματος για το σχεδιασμό δομικών συστημάτων

Στις συμβατικές διατυπώσεις των STO προβλημάτων, η αντικειμενική συνάρτηση είναι συνήθως η ενδοσιμότητα ενώ βασικός περιορισμός είναι ο τελικός όγκος της κατασκευής. Ωστόσο, στα έργα του πολιτικού μηχανικού, μια μαθηματική διατύπωση η οποία μειώνει το κόστος υλικού της κατασκευής είναι σαφώς πιο ενδιαφέρουσα. Ωστόσο στη διεθνή βιβλιογραφία, οι μελέτες οι οποίες εφαρμόζουν μια τέτοια διατύπωση σε FSTO είναι ιδιαιτέρως περιορισμένες. Στο κεφάλαιο αυτό συνδυάζονται δύο διαφορετικά είδη βελτιστοποίησης κατασκευών, για την υποστήριξη των έργων πολιτικού μηχανικού τόσο στο αρχικό στάδιο όσο και στο τελικό στάδιο σχεδιασμού. Ειδικότερα, διατυπώνονται προβλήματα βελτιστοποίηση τοπολογίας και μεγέθους και επιλύονται διαδοχικά. Λαμβάνονται υπόψιν ρεαλιστικές συνθήκες φόρτισης, εφαρμόζονται τυποποιημένες μεταλλικές διατομές ενώ ως περιορισμοί τίθενται κανονισμοί του Ευρωκώδικα.

Στις πραγματικές κατασκευές, τα στοιχεία δοκού αποτελούνται από διάφορα είδη διατομών, όπως π.χ. διατομές "Η" για τις κολώνες, "I" για τα δοκάρια και κοίλες (κυκλικές ή ορθογωνικές) για τα διαγώνια μέλη. Στο παρόν κεφάλαιο, χρησιμοποιούνται τυπικές διατομές βάσει του Ευρωκώδικα 3 και συγκεκριμένα διατομές ΗΕΑ, ΙΡΕ και CHS. Στη συνέχεια, το πρόβλημα βελτιστοποίησης διατυπώνεται είτε ως ένα συνεχές πρόβλημα είτε ως διακριτό. Για την περίπτωση που το πρόβλημα έχει συνεχή μεταβλητή

σχεδιασμού, προκειμένου να υπολογιστεί και η παράγωγος του μητρώου ακαμψίας των στοιχείων δοκού, θα πρέπει το εμβαδόν της διατομής να συσχετιστεί με άλλες ιδιότητες των διατομών. Μέσω μεθόδων ανάλυσης παλινδρόμησης, η μεταβλητή σχεδιασμού συσχετίζεται με τις υπόλοιπες ιδιότητες οι οποίες απαιτούνται για την ανάλυση των πεπερασμένων στοιχείων αλλά και τη διαστασιολόγηση των μελών. Στην παρούσα διατριβή, χρησιμοποιείται η ακόλουθη σχέση η οποία γυρίζει πάντα θετικό αριθμό:

$$f_{CSP}(a) = (b_1 a^3 + b_2 a^2 + b_3 a)^2 \tag{19}$$

Όπου $f_{CSP}(a)$ είναι η συνάρτηση για συγκεκριμένη ιδιότητα για κάθε τυποποιημένη διατομή και b_i είναι οι συντελεστές της εξίσωσης. Στο Σχήμα 16 παρουσιάζεται η προσεγγιστική καμπύλη που δίνει τη σχέση εμβαδού διατομής και ροπής αδράνειας. Παρατηρείται ότι επιτυγχάνεται πολύ ακριβής προσέγγιση και για τα τρία είδη διατομών.
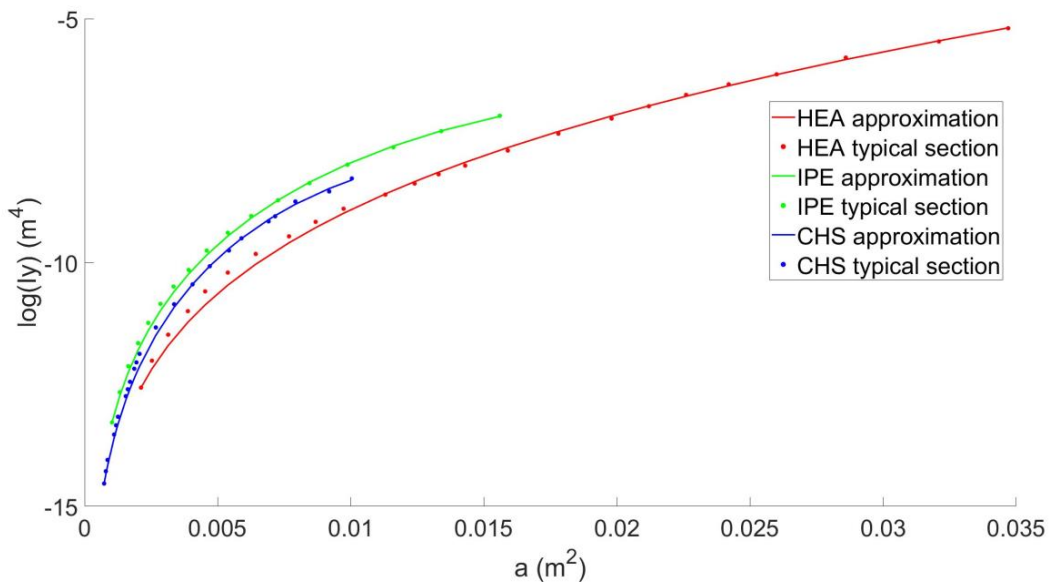
Σχήμα 16 Προσεγγιστική καμπύλη μετά από ανάλυση παλινδρόμησης για τη ροπή αδράνειας (I_y) για τις διατομές HEA, IPE και CHS

Με την παραγώγιση της εξίσωσης 19, υπολογίζεται και η παράγωγος του τοπικού μητρώο ακαμψίας κάθε πεπερασμένου στοιχείου:

$$\frac{dK_e(a_e)}{da_e} = \frac{E}{L_e}\begin{bmatrix} 1 & 0 & 0 & -1 & 0 & 0 \\ 0 & \dfrac{12\dfrac{df_I(a_e)}{da_e}}{L_e^2} & \dfrac{6\dfrac{df_I(a_e)}{da_e}}{L_e} & 0 & -\dfrac{12\dfrac{df_I(a_e)}{da_e}}{L_e^2} & \dfrac{6\dfrac{df_I(a_e)}{da_e}}{L_e} \\ 0 & \dfrac{6\dfrac{df_I(a_e)}{da_e}}{L_e} & 4\dfrac{df_I(a_e)}{da_e} & 0 & -\dfrac{6\dfrac{df_I(a_e)}{da_e}}{L_e} & 2\dfrac{df_I(a_e)}{da_e} \\ -1 & 0 & 0 & 1 & 0 & 0 \\ 0 & -\dfrac{12\dfrac{df_I(a_e)}{da_e}}{L_e^2} & -\dfrac{6\dfrac{df_I(a_e)}{da_e}}{L_e} & 0 & \dfrac{12\dfrac{df_I(a_e)}{da_e}}{L_e^2} & -\dfrac{6\dfrac{df_I(a_e)}{da_e}}{L_e} \\ 0 & \dfrac{6\dfrac{df_I(a_e)}{da_e}}{L_e} & 2\dfrac{df_I(a_e)}{da_e} & 0 & -\dfrac{6\dfrac{df_I(a_e)}{da_e}}{L_e} & 4\dfrac{df_I(a_e)}{da_e} \end{bmatrix} \quad (20)$$

Σύμφωνα με τον Ευρωκώδικα, η μέγιστη οριζόντια επιτρεπτή μετατόπιση για ένα μονώροφο κτίριο είναι $d_{allow} = \frac{H}{150}$, όπου H είναι το ύψος του κτιρίου ενώ δεν υπάρχει κάποια συγκεκριμένη οδηγία για πολυώροφα. Στη διεθνή βιβλιογραφία, παρατηρείται ότι στην περίπτωση των ψηλών κτιρίων συνήθως έχουν σχεδιαστεί με εύρος από $\frac{H}{200}$ έως $\frac{H}{600}$, ενώ η πλειοψηφία τους έχει μέγιστη μετατόπιση $\frac{H}{400}$. Στο παρόν κεφάλαιο χρησιμοποιούνται κυρίως τιμές από $\frac{H}{200}$ έως $\frac{H}{600}$. Επιπλέον, για τον ελαστικό ή πλαστικό έλεγχο μια διατομής, χρησιμοποιείται η συντηρητική προσέγγιση της γραμμικής αλληλεπίδρασης που εκφράζεται ως εξής:

$$DC_c = \frac{N_{Ed}}{N_{Rd}} + \frac{M_{y,Ed}}{M_{y,Rd}} + \frac{M_{z,Ed}}{M_{z,Rd}} \leq 1 \quad (21)$$

$$N_{Rd,t} = \frac{Af_y}{\gamma_{M0}}, N_{Rd,c} = \frac{\chi Af_y}{\gamma_{M1}}, M_{Rd} = \frac{Wf_y}{\gamma_{M0}} \quad (22)$$

Όπου DC_C είναι ο έλεγχος σχεδιασμού, N_{Ed}, M_{Ed} είναι οι εσωτερικές δυνάμεις και N_{Rd}, M_{Rd} είναι οι τιμές σχεδιασμού της αντοχής.

Προκειμένου να ικανοποιηθούν οι οριακές καταστάσεις λειτουργικότητας, πρέπει να εφαρμοστεί ένα άνω όριο μεγίστης μετατόπισης. Επειδή όμως δεν υπάρχει αναλυτική έκφραση της παραγώγου της μετατόπισης, χρησιμοποιείται η ενδοτικότητα της κατασκευής. Επιπλέον, αφού δεν υπάρχει αναλυτική έκφραση της παραγώγου του DC_C,

υπολογίζεται με αριθμητικές μεθόδους. Η διατύπωση του προβλήματος αρχικά διατυπώθηκε ως εξής:

$$\min_{a} V(a) = a^T L \tag{23α}$$

$$s.t.$$

$$K(a)d(a) = F \tag{23β}$$

$$C(a) \leq F^T d(a) \tag{23γ}$$

$$DC_c(a) \leq 1 \tag{23δ}$$

$$a_{min,e} \leq a_e \leq a_{max,e}, \quad e = 1,2,\dots,N_{ele} \tag{23ε}$$

Για την επίλυση του προαναφερθέντος προβλήματος, χρησιμοποιήθηκε ο αλγόριθμος interior point, ενώ για την αρχική τιμή των μεταβλητών σχεδιασμού εφαρμόστηκε ομοιόμορφη κατανομή υλικού σε κάθε πεπερασμένο στοιχείο. Σε αυτό το σημείο, πρέπει να τονιστούν δύο σημαντικά χαρακτηριστικά της συμπεριφοράς της παραπάνω διατύπωσης του προβλήματος. Στις περιπτώσεις που η βελτιστοποιημένη κατασκευή ικανοποιούσε τον περιορισμό για το DC_C, η κατανομή του υλικού καθοδηγούνταν από τον περιορισμό της ενδοτικότητας, καταλήγοντας στο ίδιο σχήμα με τη διαμόρφωση του προβλήματος που εφαρμοζόταν μόνο η ανισότητα (23γ). Στην αντίθετη περίπτωση, όπου ο περιορισμός DC_C δεν ικανοποιούνταν, η διάταξη του αρχικού GS δεν άλλαξε καθόλου, καταλήγοντας σε ένα SSO πρόβλημα. Επομένως σύμφωνα με την πρώτη διερεύνηση, μπορεί να εξαχθεί το συμπέρασμα ότι οι περιορισμοί (23γ) και (23δ) είναι αλληλοσυγκρουόμενοι και η σύγκλιση σε μια βελτιστοποιημένη λύση είναι ανέφικτη. Για το λόγο αυτό στη συνέχεια εξετάστηκε μια διατύπωση προβλημάτων βελτιστοποίησης κατασκευών σε δύο στάδια. Στο πρώτο στάδιο επιλύεται ένα FSTO πρόβλημα ελαχιστοποίησης του συνολικού όγκου της κατασκευής με περιορισμούς τους (23β), (23γ), (23ε) και στο δεύτερο στάδιο ένα SSO πρόβλημα ελαχιστοποίησης του συνολικού όγκου της κατασκευής με περιορισμούς τους (23β), (23δ), (23ε). Στο FSTO στάδιο η παράμετρος a_{min} λαμβάνει μια μικρή τιμή για την αποφυγή του προβλήματος της

μοναδικότητας ενώ στο SSO στάδιο η τιμή αυτή αντιστοιχεί στο μικρότερο εμβαδόν διατομής που προκύπτει από την λίστα των τυποποιημένων διατομών. Όσον αφορά την επιλογή του αλγορίθμου, διαπιστώθηκε ότι ο interior point ήταν αποτελεσματικός στο FSTO στάδιο, όμως στο SSO στάδιο επιλέχθηκε ο Sequential Quadratic Programming (SQP). Επιπλέον, όσον αφορά την επιλογή του αρχικού σχεδιασμού, στο SSO στάδιο διαπιστώθηκε ότι επηρεάζει αρκετά την βέλτιστη λύση που θα συγκλίνει ο αλγόριθμος σε αντίθεση με το FSTO στάδιο στο οποίο ο αλγόριθμος συνέκλινε πάντα στην ίδια λύση. Για το λόγο αυτό, στο SSO στάδιο χρησιμοποιήθηκε η εξίσωση Global Search της MATLAB.

Στη συνέχεια, παρουσιάζονται ορισμένα παραδείγματα για δομικά συστήματα Moment Resisting Braced Frame (MRBF) υψηλών κτιρίων. Στο Σχήμα 17, παρουσιάζεται το MRBF1 εφαρμόζοντας τρία διαφορετικά GS. Το μήκος του είναι $L = 9m$, το ύψος $H = 18m$ ενώ το φορτίο είναι ίσο με $P = 4MN$. Στο συγκεκριμένο παράδειγμα χρησιμοποιούνται μόνο HEA διατομές, με μεγαλύτερη την HEA1000 ($a_{max} = 347cm^2$) ενώ η κρίσιμη τιμή εμβαδού ορίστηκε η $a_{crit} = 10cm^2$. Για κάθε διαφορετικό GS, διερευνήθηκαν δύο διαφορετικά επιτρεπόμενα όρια μετατόπισης, $d_{allow,1} = \frac{H}{200}$ και $d_{allow,2} = \frac{H}{400}$. Στον Πίνακα 1 παρουσιάζονται τα αποτελέσματα του FSTO σταδίου, στον οποίο παρατηρείται ότι το σφάλμα κατά την μετατροπή των συνεχών μεταβλητών σχεδιασμού στις πρότυπες διατομές είναι αρκετά μικρό, για την ενδοτικότητα κυμαίνεται από 0.20% έως 2.78% ενώ για τον όγκο της κατασκευής από 0.04% έως 2.36%. Επίσης, διαπιστώνεται ότι σε όλες τις κατασκευές που ξεκίνησαν από πυκνότερα GS, η τελική κατασκευή ήταν πάντα πιο ελαφριά σε σχέση με αυτές που ξεκίνησαν από πιο αραιότερα GS. Στα Σχήματα 18 και 19 παρουσιάζονται οι βέλτιστες κατασκευές που προέκυψαν από το $d_{allow,1} = \frac{H}{200}$ και $d_{allow,2} = \frac{H}{400}$ αντίστοιχα. Στον Πίνακα 2 παρουσιάζονται τα αποτελέσματα του SSO σταδίου, όπου διαπιστώνονται εξίσου καλά αποτελέσματα όσον αφορά την προσέγγιση των πρότυπων διατομών. Ωστόσο, το κρίσιμο συμπέρασμα που απορρέει από τον Πίνακα 2 είναι ότι , ανεξάρτητα από το GS, η τιμή της ενδοτικότητας είτε μειώνεται είτε αυξάνεται μετά το FSTO στάδιο, προκειμένου να ελαχιστοποιηθεί ο όγκος και να ικανοποιηθεί το DC_C. Αποδεικνύεται με αυτό τον τρόπο ότι οι περιορισμοί της

ενδοτικότητας και του ελέγχου σχεδιασμού είναι αλληλοσυγκρουόμενοι. Για το σύνολο των διαφορετικών GS, συμπεραίνεται ότι η ενδοτικότητα των βέλτιστων κατασκευών κυμαίνεται από 0.268MNm έως 0.294MNm ή σε όρους μετατόπισης από $\frac{H}{268}$ έως $\frac{H}{246}$.

*($\times 10^5$)

Test case	Continuous approach		Standardized cross-sectional properties (HEA)		Error		Number of frames
	C* (Nm)	V (m^3)	C* (Nm)	V (m^3)	C (%)	V (%)	N_e
MRBF1Sd1		1.0944	3.6656	1.1006	1.82	0.57	18
MRBF1Md1	3.6	0.9924	3.7000	0.9920	2.78	0.04	22
MRBF1Fd1		0.9869	3.6879	0.9636	2.44	2.36	20
MRBF1Sd2		2.3508	1.7964	2.3600	0.20	0.39	39
MRBF1Md2	1.8	1.9830	1.8208	1.9660	1.15	0.86	25
MRBF1Fd2		1.9670	1.8259	1.9415	1.44	1.30	20

Πίνακας 1 MRBF1#d#-FSTO στάδιο: Σύγκριση μεταξύ συνεχούς θεώρησης και τυποποιημένων διατομών

*($\times 10^5$)

| Test case	Continuous approach		Standardized cross-sectional properties (HEA)			Error	
	C* (Nm)	V (m^3)	C* (Nm)	V (m^3)	DC	C (%)	V (%)
MRBF1Sd1	2.9439	1.5635	2.9344	1.5682	1.003	0.32	0.30
MRBF1Md1	2.6896	1.5202	2.6597	1.5382	1.033	1.11	1.17
MRBF1Fd1	2.8634	1.4120	2.8723	1.4093	1.025	0.31	0.19
MRBF1Sd2	2.7992	1.6203	2.8254	1.6076	1.056	0.94	0.79
MRBF1Md2	2.7310	1,5007	2.7353	1.5037	1.021	0.16	0.20
MRBF1Fd2	2.8877	1,3970	2.8692	1.4060	1.029	0.64	0.64

Πίνακας 2 MRBF1#d#-SSO στάδιο: Σύγκριση μεταξύ συνεχούς θεώρησης και τυποποιημένων διατομών
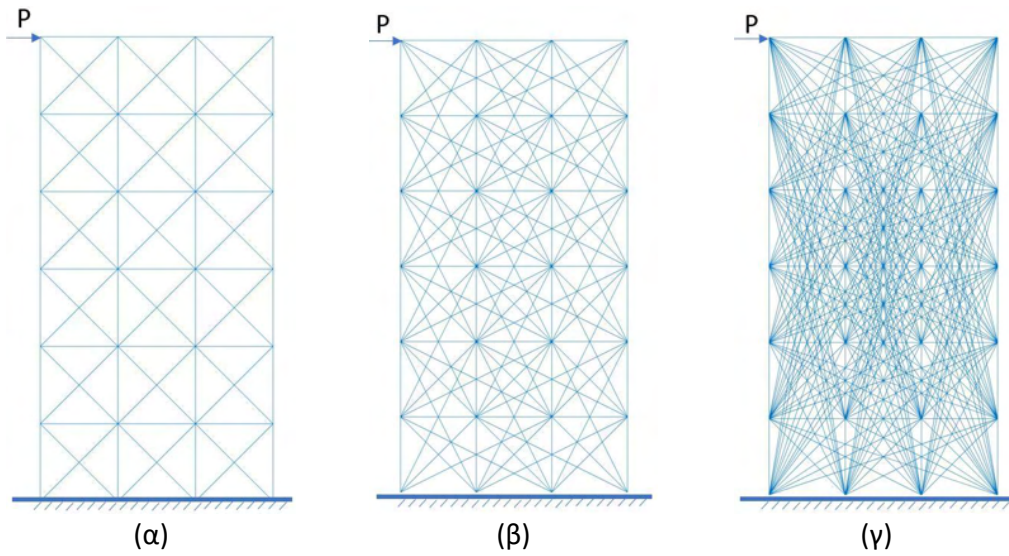
Σχήμα 17 MRBF1: Αρχικό χωρίο σχεδιασμού για (α) απλής (MRBF1Sd#), (β) μεσαίας (MRBF1Md#) και (γ) πλήρης (MRBF1Fd#) συνδεσιμότητας GS.
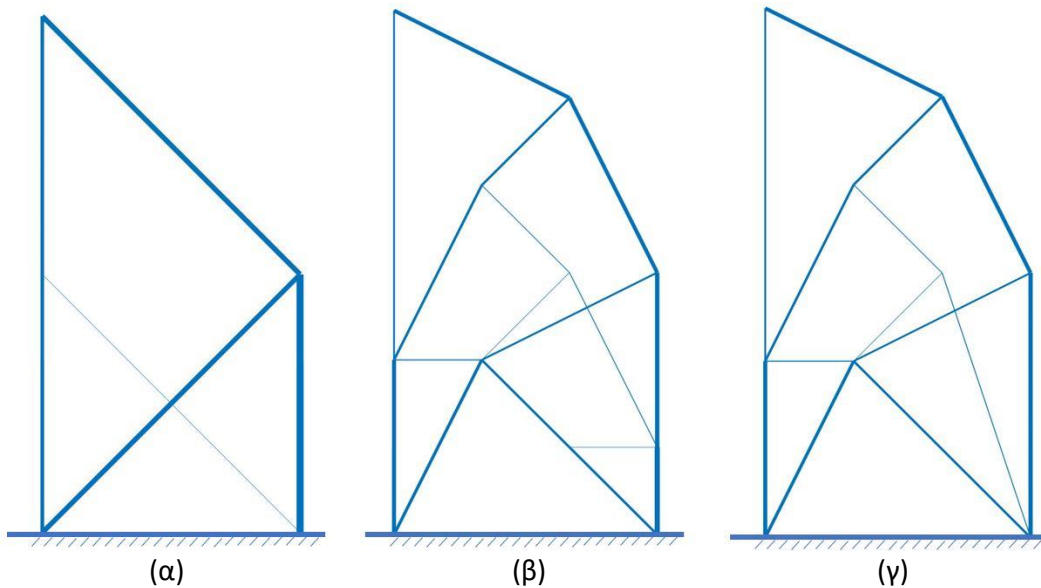
Σχήμα 18 MRBF1#d1: βελτιστοποιημένα δομικά συστήματα (α) MRBF1Sd1, (β) MRBF1Md1 και (γ) MRBF1Fd1.
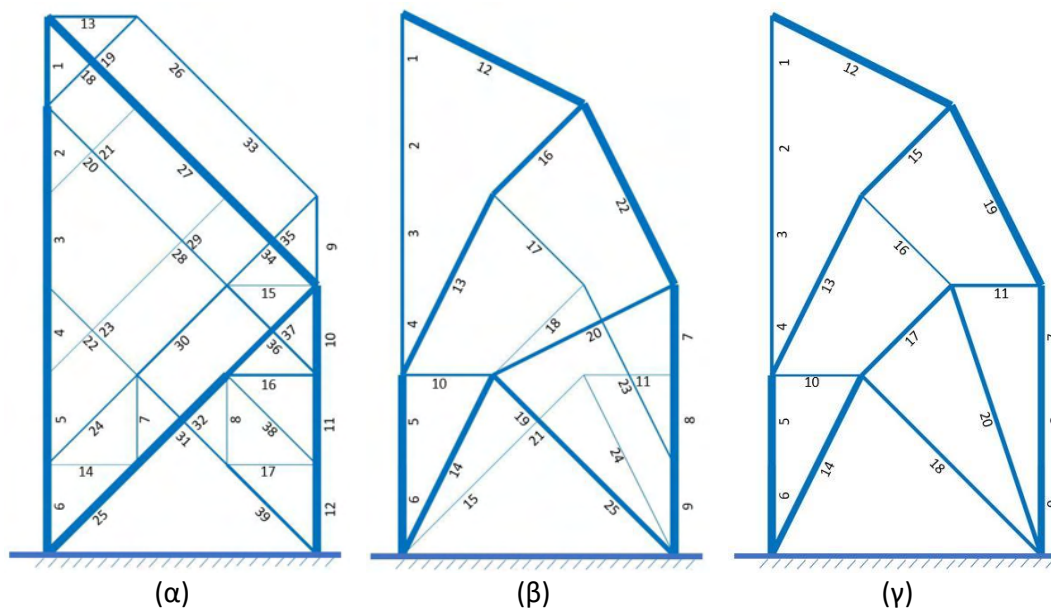
Σχήμα 19 MRBF1#d2: βελτιστοποιημένα δομικά συστήματα (α) MRBF1Sd2, (β) MRBF1Md2 και (γ) MRBF1Fd2

Στη συνέχεια το SSO στάδιο της προτεινόμενης μεθοδολογίας, εφαρμόζεται σε ένα εμπορικό πρόγραμμα προκειμένου η τελική κατασκευή να είναι πιο κοντά σε μια ρεαλιστική κατασκευή στην οποία εφαρμόζονται όλοι οι κανονισμοί. Συγκεκριμένα χρησιμοποιήθηκε η πλατφόρμα HP-OCP σε συνδυασμό με το ETABS v18.1.1. Οι κατασκευές που προέκυψαν από το SSO στάδιο στην προηγούμενη διερεύνηση με τον προσωπικό υπολογιστικό κώδικα δεν ικανοποιούσαν όλους τους ελέγχους του εμπορικού προγράμματος. Όμως το HP-OCP, για καλύτερη αποδοτικότητα απαιτεί η πρώτη λύση να είναι εφικτή. Για τον λόγο αυτό εφαρμόζεται μια διαδικασία διόρθωσης στην οποία επιλέγονται ορισμένες μεγαλύτερες διατομές από τη λίστα. Για την καλύτερη κατανόηση των δυνατοτήτων της προτεινόμενης μεθοδολογίας συγκρίνονται τέσσερις κατασκευές. Συγκεκριμένα, ένα δομικό σύστημα που αποτελείται από χιαστί σε όλους τους ορόφους και τα δομικά συστήματα που προέκυψαν από τον περιορισμό $d_{allow,2} = \frac{H}{400}$. Όπως παρατηρείται στον Πίνακα 4, το HP-OCP μείωσε σε όλες τις περιπτώσεις την τροποποιημένη κατασκευή που προέκυψε από τη διαδικασία διόρθωσης. Στο Σχήμα 20 παρατηρείται ότι ορισμένα μέλη φτάνουν πολύ κοντά στην πλήρη εκμετάλλευση της διατομής τους. Σημαντικό συμπέρασμα είναι η μείωση που επιτυγχάνεται καθώς

πυκνώνουμε το αρχικό GS. Αρχικά παρατηρείται ότι το MRBF1Sd2 έχει 13.54% υλικό σε σχέση με το MRBF1X. Αυτό μπορεί να τεκμηριωθεί από το γεγονός ότι η MRBF1X κατασκευή διατηρεί αρκετά περιττά μέλη. Συγκρίνοντας το MRBF1Sd2 με το MRBF1Md2 παρατηρείται επιπλέον 10.32% μείωση. Δίνοντας δηλαδή περισσότερη σχεδιαστική ελευθερία επιτυγχάνεται αξιοσημείωτη μείωση υλικού. Συγκρίνοντας το MRBF1Md2 με το MRBF1Fd2 παρατηρείται επιπλέον 1.98% μείωση. Παρατηρείται δηλαδή, ότι παρότι σχεδόν διπλασιάστηκε η σχεδιαστική ελευθερία, ή μείωση του υλικού δεν είναι αντίστοιχη. Αυτό είναι κρίσιμο συμπέρασμα στην περίπτωση εφαρμογής της προτεινόμενης μεθόδου σε μεγαλύτερα δομικά συστήματα, όπου το υπολογιστικό κόστος είναι πολύ μεγαλύτερο.

Note: [1]MRBF1Sd2 vs MRBF1X, [2]MRBF1Md2 vs MRBF1Sd2, [3]MRBF1Fd2 vs MRBF1Md2.

Test case	Reference (Modified) Design		Optimized Design		Volume Reduction (%)	
	V (m^3)	DC	V (m^3)	DC	by HP-OCP	by test case
MRBF1X	2.3057	0.978	2.2587	0.982	2.04	-
MRBF1Sd2	2.0015(1.6076)	0.967	1.9528	0.974	2.43	13.54[1]
MRBF1Md2	1.7721(1.5037)	0.972	1.7512	0.984	1.18	10.32[2]
MRBF1Fd2	1.7314(1.4060)	0.977	1.7165	0.987	0.86	1.98[3]

Πίνακας 4 HP-OCP εφαρμογή και σύγκριση διαφορετικών GS για MRBF1
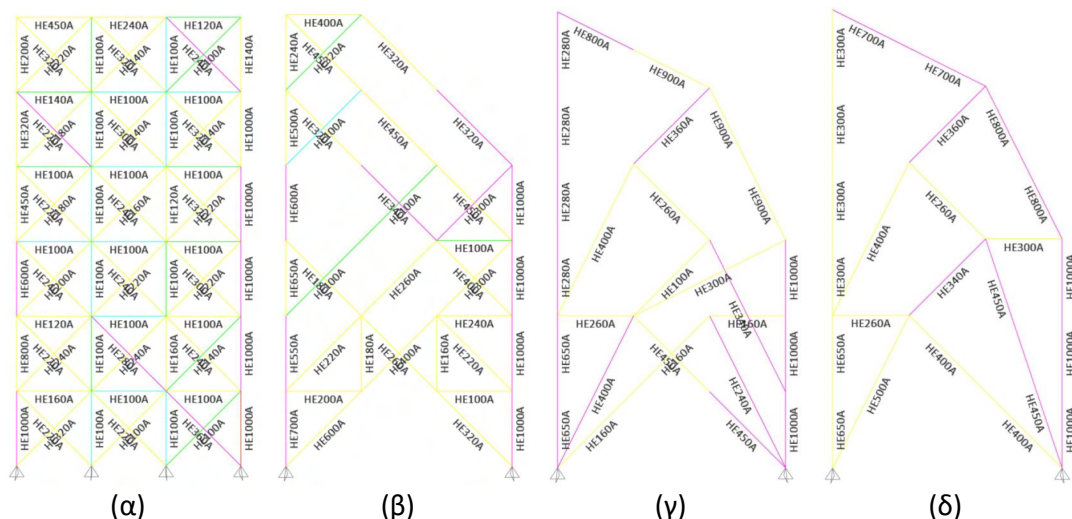
Σχήμα 20 Έλεγχος σχεδιασμου για (α) X-braced, (β) MRBF1Sd2, (γ) MRBF1Md2 και (δ) MRBF1Fd2

8 FSTO βάσει δυναμικής ανάλυσης

Μέχρις στιγμής, όλες οι μεθοδολογίες που παρουσιάζονται στην παρούσα διατριβή βασίζονται στη θεώρηση στατικών φορτίσεων. Επίσης, στην συντριπτική πλειοψηφία της βιβλιογραφίας που εστιάζουν σε STO προβλήματα, οι συνθήκες φόρτισης θεωρούνται στατικές και ντετερμινιστικές. Ωστόσο, η συνεκτίμηση της δυναμικής απόκρισης της κατασκευής, είναι σαφώς πιο απαιτητική και ενδιαφέρουσα και, σε αρκετές περιπτώσεις, πιο κοντά στην πραγματικότητα. Στις μελέτες δυναμικών προβλημάτων STO, οι προσεγγίσεις που υιοθετούνται αφορούν το πρόβλημα της ελεύθερης ή εξαναγκασμένης ταλάντωσης, εφαρμόζοντας άμεση ολοκλήρωση του χρόνου, τεχνικές ιδιομορφικής υπέρθεσης (modal superposition) και τη μέθοδο της της ανάλυσης φάσματος απόκρισης (Response Spectrum Modal Analysis - RSMA). Ωστόσο, οι περισσότερες εργασίες στη διεθνή βιβλιογραφία που ασχολούνται με τις προαναφερθείσες δυναμικές συνθήκες, εφαρμόζουν τις διατυπώσεις θεωρώντας τη GSO προσέγγιση.

Κύριος στόχος αυτού του κεφαλαίου είναι η γένεση δομικών συστημάτων πλευρικής στήριξης για ψηλά κτίρια, λαμβάνοντας υπόψιν τη δυναμική απόκριση των κατασκευών. Αρχικά λαμβάνονται υπόψιν συνθήκες ελεύθερης ταλάντωσης και ως αντικειμενική συνάρτηση του FSTO προβλήματος ορίζεται η μεγιστοποίηση συγκεκριμένων ιδιοσυχνοτήτων των δομικών συστημάτων. Στη συνέχεια, αντιμετωπίζεται το πρόβλημα δυναμικής φόρτισης, θεωρώντας είτε αρμονική φόρτιση είτε δεδομένα πραγματικού σεισμού, ενώ επιλύεται με ανάλυση χρονοϊστορίας. Ως αντικειμενική συνάρτηση ορίζεται είτε η δυναμική ενδοσιμότητα είτε η ρίζα του αθροίσματος των τετραγώνων των μετατοπίσεων (Square Root of the Sum of the Squares - SRSS). Τέλος, εφαρμόζεται η RSMA προκειμένου να μειωθεί το υπολογιστικό κόστος, το σεισμικό φορτίο υπολογίζεται από τον Ευρωκώδικα ενώ αντικειμενική συνάρτηση επιλέγεται το άθροισμα των μορφικών ενδοσιμοτήτων (modal compliances).

Οι εξισώσεις κίνησης ενός συστήματος που υπόκεινται σε δυναμική φόρτιση εκφράζονται ως εξής:

$$M(a)\ddot{u}_t + C(a)\dot{u}_t + K(a)u_t = R_t \tag{24}$$

όπου $M(a)$, $C(a)$ και $K(a)$ είναι τα μητρώα μάζας, απόσβεσης και ακαμψίας αντίστοιχα, συναρτήσει της μεταβλητής σχεδιασμού a. Το R_t είναι το διάνυσμα φόρτισης, τα u, $\dot{u}$ και $\ddot{u}$ είναι τα διανύσματα μετατοπίσεων, ταχυτήτων και επιταχύνσεων. Στο σημείο αυτό πρέπει να γίνει η εισαγωγή του ορισμού του μητρώου μάζας. Στο παρόν κεφάλαιο εξετάζονται διάφοροι σχηματισμοί για MRBF δομικά συστήματα υψηλών κτιρίων, επομένως το καθολικό μητρώο μάζας απαρτίζεται από τη μάζα των δομικών και μη δομικών στοιχείων του δομικού συστήματος. Η μάζα των δομικών στοιχείων αποτελείται από τη μάζα του GS, ενώ το τοπικό μητρώο μάζας ενός πεπερασμένο στοιχείο δοκού ορίζεται ως εξής:

$$M_e^d = \frac{\rho a_e L_e}{6} \begin{bmatrix} 2 & 0 & 0 & 1 & 0 & 0 \\ 0 & 0 & 0 & 0 & 0 & 0 \\ 0 & 0 & 0 & 0 & 0 & 0 \\ 1 & 0 & 0 & 2 & 0 & 0 \\ 0 & 0 & 0 & 0 & 0 & 0 \\ 0 & 0 & 0 & 0 & 0 & 0 \end{bmatrix} + \frac{\rho a_e L_e}{420} \begin{bmatrix} 0 & 0 & 0 & 0 & 0 & 0 \\ 0 & 156 & 22L_e & 0 & 54 & -13L_e \\ 0 & 22L_e & 4L_e^2 & 0 & 13L_e & -3L_e^2 \\ 0 & 0 & 0 & 0 & 0 & 0 \\ 0 & 54 & 13L_e & 0 & 156 & -22L_e \\ 0 & -13L_e & -3L_e^2 & 0 & -22L_e & 4L_e^2 \end{bmatrix} \tag{25}$$

όπου ρ είναι η πυκνότητα του υλικού, a_e είναι το εμβαδόν της διατομής και L_e είναι το μήκος του πεπερασμένου στοιχείου. Για την περίπτωση των μη δομικών στοιχείων της κατασκευής θεωρήθηκε μια συγκεντρωμένη μάζα στο κέντρο του κάθε ορόφου:

$$M^l = \begin{bmatrix} m_1 & \cdots & 0 \\ \vdots & \ddots & \vdots \\ 0 & \cdots & m_{N_f} \end{bmatrix} \tag{26}$$

όπου m_i είναι η μάζα του κάθε ορόφου και N_f ο συνολικός αριθμός των ορόφων. Παρά το γεγονός ότι η μάζα των δομικών στοιχείων είναι συγκριτικά μικρότερη από τη μάζα των μη δομικών στοιχείων, θα ήταν ανακριβές να την παραλείψουμε. Επιπλέον επειδή η μάζα των μη δομικών στοιχείων είναι ανεξάρτητη της μεταβλητής σχεδιασμού, ($\nabla_a M^l = 0$), η παράληψη τη μάζας των δομικών στοιχείων οδηγεί τον αλγόριθμο σε αριθμητική αστάθεια. Επομένως στο καθολικό σύστημα ισχύει:

$$M(a) = M_g^l + M_g^d(a) \tag{27}$$

Για την περίπτωση του FSTO προβλήματος όπου θεωρείται ελεύθερη ταλάντωση και αντικειμενική συνάρτηση είναι η μεγιστοποίηση μιας ιδιοτιμής, η διατύπωση του προβλήματος είναι η εξής:

$$\min_{a}[-\lambda_k(a)] \tag{28α}$$

$$s.t.$$

$$\left(K(a) - \omega_k^2(a)M(a)\right)\varphi_k(a) = 0, \quad k = 1, \dots, N_{DOF} \tag{28β}$$

$$\varphi_j^T(a)M(a)\varphi_k(a) = \delta_{jk}, \quad j, k = 1, \dots, N_{DOF} \tag{28γ}$$

$$a^T \cdot L \leq V_{lim} \tag{28δ}$$

$$a_{min,e} \leq a_e \leq a_{max,e}, \quad e = 1, 2, \dots, N_{ele} \tag{28ε}$$

όπου $\lambda_k(a)$ και $\omega_k(a)$ είναι η ιδιοτιμή και η ιδιοσυχνότητα ενώ το $\varphi_k(a)$ είναι το αντίστοιχο ιδιοδιάνυσμα. Για την επίλυση του προβλήματος απαιτείται ο υπολογισμός της παραγώγου της ιδιοτιμής και πραγματοποιείται με χρήση του adjoint μοντέλου. Παραγωγίζοντας την εξίσωση (28β) βάσει του a_e, λαμβάνοντας υπόψιν τις εξισώσεις (28β), (28γ) και τη συμμετρία των μητρώων K και M, η παράγωγος υπολογίζεται:

$$\frac{\partial \lambda_k}{\partial a_e} = \varphi_k^T\left(\frac{\partial K}{\partial a_e} - \lambda_k \frac{\partial M}{\partial a_e}\right)\varphi_k \tag{29}$$

όπου η παράγωγος $\frac{\partial K}{\partial a_e}$ έχει αναλυθεί σε προηγούμενα κεφάλαια ενώ το $\frac{\partial M}{\partial a_e}$ υπολογίζεται με ευθεία παραγώγιση της εξίσωσης 25.

Στην περίπτωση της εξαναγκασμένης ταλάντωσης, εξετάζονται δύο συνθήκες φόρτισης. Για την αρμονική ταλάντωση ισχύει:

$$F_t = Psin(\omega t) \tag{30}$$

ενώ στην περίπτωση του πραγματικού σεισμού:

$$F_t = -Mr\ddot{u}_g(t) \tag{31}$$

όπου r είναι το διάνυσμα επιρροής και $\ddot{u}_g(t)$ είναι η επιτάχυνση εδάφους. Στο σημείο αυτό εισάγεται και το μητρώο απόσβεσης το οποίο υπολογίζετε:

$$C = a_r M + \beta_r K \tag{32}$$

όπου οι συντελεστές απόσβεσης a_r, β_r εξαρτώνται από το ποσοστό απόσβεσης και την ιδιοσυχνότητα. Στην παρούσα εργασία το ποσοστό απόσβεσης λαμβάνει την τιμή $\zeta = 0.05$. Για την επίλυση του προβλήματος της εξίσωσης κίνησης χρησιμοποιείται η αριθμητική μέθοδος Newmark Beta. Για την περίπτωση της αρμονικής φόρτισης, αντικειμενική συνάρτηση του FSTO προβλήματος επιλέγεται η δυναμική ενδοσιμότητα ενώ επιβάλλεται φόρτιση μισού κύκλου. Αναλυτικά η διατύπωση του προβλήματος είναι:

$$min \, f = \sum_{j=t_i}^{t_N} \sum_{i=1}^{N_{dof}} u_i^T F_j \Delta t \tag{33α}$$

$$s.t.$$

$$M(a)\ddot{u}_t + C(a)\dot{u}_t + K(a)u_t = F_t \tag{33β}$$

$$a^T \cdot L \leq V_{lim} \tag{33γ}$$

$$a_{min,e} \leq a_e \leq a_{max,e}, \quad e = 1,2,\ldots,N_{ele} \tag{33δ}$$

όπου $t_i = 0$ και Δt είναι ένα μικρό χρονικό βήμα εξαρτώμενο από τη συχνότητα της εξωτερικής φόρτισης. Για την περίπτωση του πραγματικού σεισμού αντικειμενική συνάρτηση επιλέγεται το SRSS των μετατοπίσεων της κορυφής της κατασκευής, επειδή η δυναμική ενδοσιμότητα λαμβάνει αρνητική τιμή κατά τη διάρκεια της ταλάντωσης:

$$f = \|l^T u_t\|_2 = \sqrt{\sum_{t=0}^{t_N} (l^T u_t)^2} \tag{34}$$

Για την επίλυση του προβλήματος απαιτείται ο υπολογισμός των παραγώγων τόσο των μετατοπίσεων όσο και της αντικειμενικής συνάρτησης. Χρησιμοποιώντας την μέθοδο άμεσης ολοκλήρωσης η εξίσωση κίνησης μετατρέπεται σε:

$$M \frac{d^2}{dt^2}\left(\frac{du}{da_e}\right) + C \frac{d}{dt}\left(\frac{du}{da_e}\right) + K \frac{du}{da_e} = \frac{\partial F_t}{\partial a_e} - \frac{\partial M}{\partial a_e}\ddot{u} - \frac{\partial C}{\partial a_e}\dot{u} - \frac{\partial K}{\partial a_e}u \qquad (35)$$

Η εξίσωση 35 λύνεται με τη μέθοδο Newmark Beta, ενώ όσον αφορά την παράγωγο των αντικειμενικών συναρτήσεων, για τη δυναμική ενδοσιμότητα ισχύει:

$$\frac{\partial}{\partial a_e}(u_n^T F_n) = \frac{\partial u_n^T}{\partial a_e}M\ddot{u}_n + \frac{\partial u_n^T}{\partial a_e}C\dot{u}_n + \frac{\partial u_n^T}{\partial a_e}Ku_n \qquad (36)$$

ενώ για το SRSS των μετατοπίσεων:

$$\frac{\partial f}{\partial a_e} = 0.5\left(\sum_{t=0}^{t_N}(l^T u_t)^2\right)^{-1/2}\sum_{t=0}^{t_N}2l^T u_t \frac{\partial u_n}{\partial a_e} \qquad (37)$$

Η μέθοδος RSMA είναι μια απλοποίηση της προσέγγισης της υπέρθεσης των ιδιομορφών έτσι ώστε να αποφευχθεί η υπολογιστικά κοστοβόρος ανάλυση της χρονοϊστορίας της δυναμικής εξίσωσης. Συγκεκριμένα οι μετατοπίσεις του δομικού συστήματος υπολογίζονται με τον εξής τρόπο:

$$u_t = \sum_{j=1}^{n} \varGamma_j \phi_j SD_j \qquad (38)$$

όπου n είναι ο μέγιστος αριθμός των συμβαλλόμενων ιδιομορφών, ϕ_j είναι η ιδιομορφή SD_j είναι η φασματική μετακίνηση και $\varGamma_j$ είναι ο συντελεστής συμμετοχής της ιδιομορφής j, όπου υπολογίζεται ως εξής:

$$\varGamma_j = \frac{\phi_j^T M r}{\phi_j^T M \phi_j} \qquad (39)$$

Στην περίπτωση του σεισμού, οι εξωτερικές φορτίσεις προκύπτουν από αδρανειακές δυνάμεις και εξαρτώνται από τη μεταβλητή σχεδιασμού. Προκειμένου να υπάρξει μια χαλάρωση του μαθηματικού προβλήματος, μόνο για τον υπολογισμό των σεισμικών

φορτίων χρησιμοποιείται το μητρώο μάζας M_g^l. Με τον τρόπο αυτό, το διάνυσμα των μέγιστων μετατοπίσεων U_j υπολογίζεται:

$$U_j = K^{-1}F_j \tag{40}$$

$$F_j = \Gamma_j M_g^l \phi_j SA(T_j) \tag{41}$$

όπου F_j είναι το διάνυσμα των σεισμικών φορτίων και $SA(T_j)$ είναι η ελαστική φασματική επιτάχυνση. Για την επιλογή του αριθμού n, εφαρμόστηκε η απαίτηση του Ευρωκώδικα ότι το άθροισμα των ενεργών ιδιομορφικών μαζών πρέπει να είναι τουλάχιστον ίσο με το 90% της συνολικής μάζας που αντιστοιχεί στην υπό εξέταση διεύθυνση:

$$m_{en,i} = \frac{\left(\phi_j^T M r\right)^2}{\phi_j^T M \phi_j} \tag{42}$$

Η μαθηματική διατύπωση του προβλήματος FSTO, θεωρώντας ως αντικειμενική συνάρτηση το άθροισμα των ιδιομορφικών ενδοσιμοτήτων είναι:

$$min\ f = \sum_{j=1}^{n} F_j^T(a)U_j(a) \tag{43α}$$

$$s.t.$$

$$\left(K(a) - \omega_j^2 M(a)\right)\phi_j = 0 \tag{43β}$$

$$a^T \cdot L \leq V_{lim} \tag{43γ}$$

$$a_{min,e} \leq a_e \leq a_{max,e}, \quad e = 1,2,\dots,N_{ele} \tag{43δ}$$

Η παράγωγος της αντικειμενικής συνάρτησης, υπολογίζεται με παρόμοιο τρόπο με την περίπτωση της στατικής ενδοσιμότητας, για κατασκευή που υπόκειται σε πολλαπλές φορτίσεις εξαρτώμενες από τη μεταβλητή σχεδιασμού:

xlviii

$$\frac{df}{da_e} = \sum_{j=1}^{n} -U_j^T \frac{\partial K}{\partial a_e} U_j \qquad (44)$$

Στη συνέχεια διάφορα MRBF χρησιμοποιήθηκαν για την υλοποίηση των προτεινόμενων μεθοδολογιών. Στο Σχήμα 21, παρουσιάζεται το αρχικό GS ενός MRBF όπου φαίνεται η κατανομή των μαζών. Όσον αφορά της διατομές των στοιχείων δοκού, χρησιμοποιήθηκαν HEA για τις κολώνες, IPE για τα δοκάρια και CHS για τις διαγώνιες, βασιζόμενοι στο Κεφάλαιο 7.
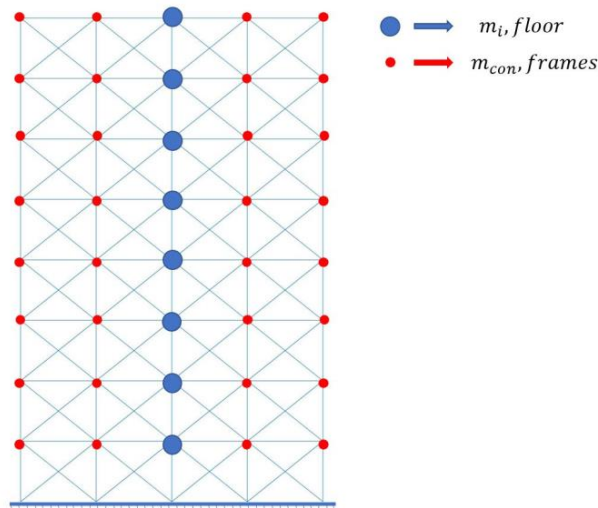
Σχήμα 21 Κατανομή μάζας στο αρχικό δομικό σύστημα, με μπλε χρώμα η μάζα του ορόφου και με κόκκινο η μάζα των δομικών στοιχείων

Για την περίπτωση της ελεύθερης ταλάντωσης, η μεθοδολογία εφαρμόζεται σε ένα MRBF ενός κτιρίου συνολικού ύψους $64m$ ενώ χρησιμοποιούνται δύο είδη GS, απλής και μεσαίας συνδεσιμότητας (HRBS και HRBM αντίστοιχα). Η FSTO υλοποιήθηκε για τις πρώτες πέντε ιδιομορφές, στον Πίνακα 5 παρουσιάζονται τα αριθμητικά αποτελέσματα ενώ στα Σχήματα 22 και 23 παρουσιάζονται οι προτεινόμενες κατασκευές. Όσον αφορά την τοπολογία των κατασκευών, η πρώτη παρατήρηση είναι ότι η μεγιστοποίηση της πρώτης ιδιομορφής, οδηγεί σε παρόμοια σχήματα με αυτά που προκύπτουν από το στατικό πρόβλημα. Αυτό είναι λογικό, αφού οι διατυπώσεις των δυο προβλημάτων έχουν παρόμοιο στόχο που είναι η μεγιστοποίηση της ακαμψίας. Μια δεύτερη παρατήρηση

είναι ότι σε κάθε προτεινόμενη κατασκευή υπάρχουν περιοχές που δημιουργούνται λιγότερες διαγώνιοι οι οποίες βρίσκονται στα άκρα του σχήματος των ιδιομορφών.

*(rad/s)

Eigenfreq.	$w_1{}^*$		$w_2{}^*$		$w_3{}^*$		$w_4{}^*$		$w_5{}^*$	
Test Case	HRBS	HRBM	HRBS	HRBM	HRBS	HRBM	HRBS	HRBM	HRBS	HRBM
Opt. w_1	**0.99**	**1.09**	2.86	2.71	4.93	4.27	6.56	4.87	7.77	5.71
Opt. w_2	0.59	0.54	3.71	**4.10**	4.53	4.10	7.77	5.99	8.68	6.43
Opt. w_3	0.54	0.55	2.44	2.26	**7.41**	**7.47**	7.41	7.47	8.59	7.81
Opt. w_4	0.54	0.54	2.66	2.00	4.98	4.71	**10.60**	**10.82**	10.60	10.82
Opt. w_5	0.47	0.54	1.56	2.07	4.51	4.73	6.51	6.42	**13.48**	**12.86**

Πίνακας 5 HRBS και HRBM – μεγιστοποίηση των 5 πρώτων ιδιοσυχνοτήτων

(α) (β) (γ) (δ) (ε)
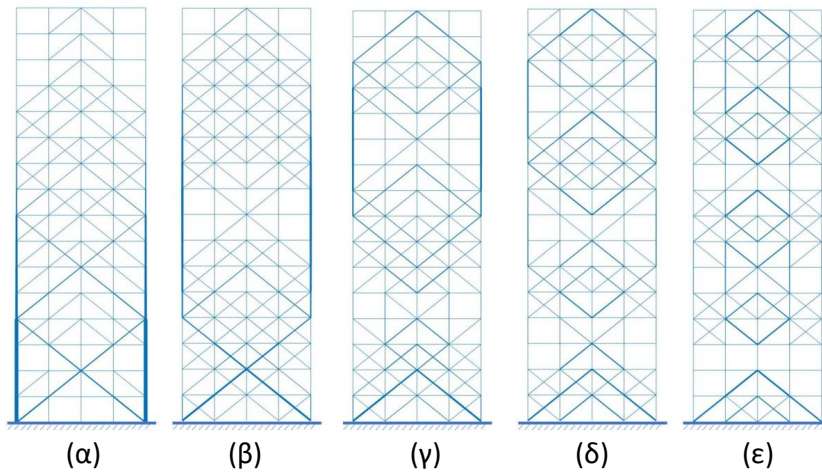
Σχήμα 22 HRBS (64m ύψος), βελτιστοποιημένα δομικά συστήματα για μεγιστοποίηση των 5 πρώτων ιδιοσυχνοτήτων (α)-(ε)

(α) (β) (γ) (δ) (ε)
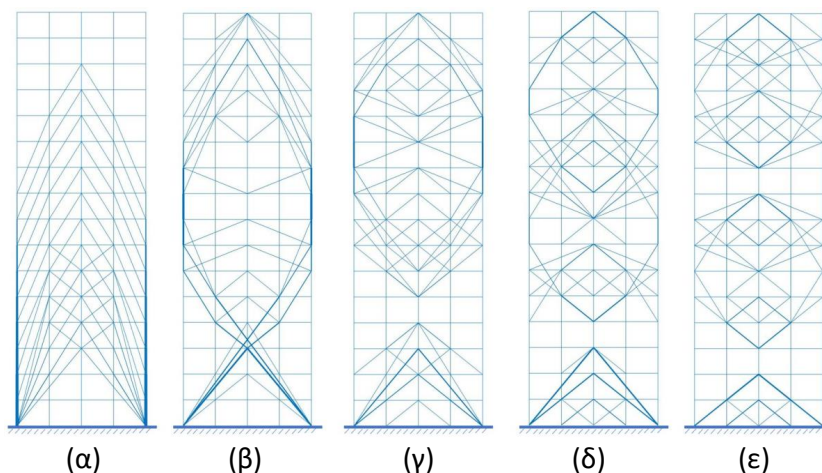
Σχήμα 23 HRBM, βελτιστοποιημένα δομικά συστήματα για μεγιστοποίηση των 5 πρώτων ιδιοσυχνοτήτων (α)-(ε)

1

Επίσης στην περίπτωση που παρέχεται μεγαλύτερη σχεδιαστική ελευθερία επιπλέον ελλειψοειδή σχήματα σχηματίζονται, μειώνοντας έτσι την παρουσία των χιαστί. Όσον αφορά τα αριθμητικά αποτελέσματα στην περίπτωση του HRBM, η αντικειμενική συνάρτηση είναι μεγαλύτερη σε σχέση με το HRBS όμως οι διαφορές μεταξύ των ιδιομορφών του ίδιου σχεδιασμού είναι μικρότερες ενώ παρουσιάζονται και επαναλαμβανόμενες ιδιοσυχνότητες. Επομένως ενώ η αντικειμενική συνάρτηση είναι καλύτερη η γενικότερη δυναμική συμπεριφορά της κατασκευής δεν είναι απαραίτητα καλύτερη, τονίζοντας με αυτό τον τρόπο τις δυσκολίες αλλά και την πρόκληση της ανάπτυξη μεθοδολογιών βελτιστοποίησης πολλαπλών ιδιοσυχνοτήτων.

Στη συνέχεια, μια ημιτονοειδής φόρτιση μισού κύκλου εφαρμόζεται στην κορυφή ενός δομικού συστήματος κτιρίου ύψους $32m$ ενώ χρησιμοποιούνται δύο είδη GS, απλής και μεσαίας συνδεσιμότητας (MRBS και MRBM αντίστοιχα). Για την κατανόηση της συμπεριφοράς του FSTO προβλήματος, επιλέγονται τρεις φορτίσεις με διαφορετικές συχνότητες, $\omega_1 = 1\frac{rad}{s}$, $\omega_2 = 4\frac{rad}{s}$ και $\omega_3 = 8\frac{rad}{s}$, ενώ παρουσιάζονται τα αποτελέσματα και της στατικής φόρτισης. Στα Σχήματα 24 και 25, παρουσιάζονται οι βελτιστοποιημένες κατασκευές των MRBS και MRBM προβλημάτων.
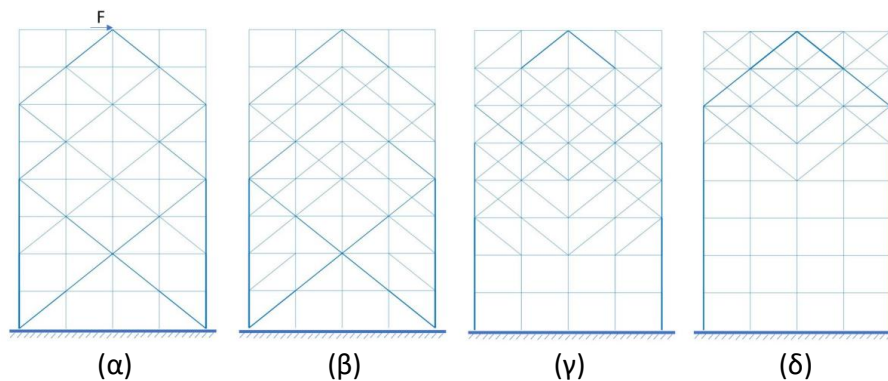
Σχήμα 24 MRBS (32m ύψος) Δομικό σύστημα για (α) στατική φόρτιση και (β)-(δ) ω_1, ω_2, ω_3.
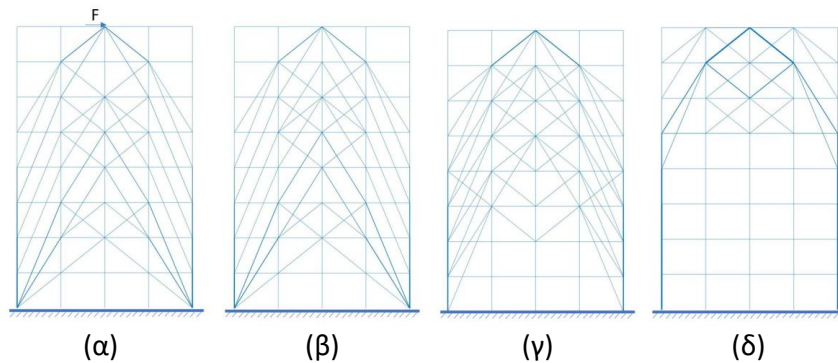
Σχήμα 25 MRBM Δομικό σύστημα για (α) στατική φόρτιση και (β)-(δ) ω_1, ω_2, ω_3.

Όσον αφορά την περίπτωση της χαμηλής συχνότητας, παρατηρείται ότι η τελική διάταξη του δομικού συστήματος είναι παρόμοια με αυτή που προκύπτει από την περίπτωση στατικής φόρτισης. Αυτό είναι λογικό δεδομένου ότι η συχνότητα διέγερσης είναι αρκετά μικρότερη της θεμελιώδους ιδιοσυχνότητας. Για την περίπτωση της συχνότητας ω_2 παρατηρείται ότι περισσότερα χιαστί και διαγώνιες προστίθενται στον πυρήνα του δομικού συστήματος ενώ περισσότερο υλικό προστίθεται στο άνω τμήμα της κατασκευής. Αυτό είναι λογικό δεδομένου ότι η συχνότητα της διέγερσης βρίσκεται μεταξύ της δεύτερης και της τρίτης ιδιοσυχνότητας, επομένως αναμένεται διαφορετική κατανομή της τάσης στα δομικά στοιχεία του συστήματος. Στην περίπτωση που η συχνότητα είναι ακόμα μεγαλύτερη (ω_3), η τοπολογία του δομικού συστήματος είναι εντελώς διαφορετική, αφού το υλικό συγκεντρώνεται μόνο στο πάνω τμήμα της κατασκευής.

9 Συμπεράσματα και Συνεισφορά

Η παρούσα διατριβή συμβάλλει στις GSO και FSTO προσεγγίσεις, στοχεύοντας την ανάπτυξη μεθόδων για τη γένεση δομικών συστημάτων πολιτικού μηχανικού. Όσον αφορά την GSO, η πρώτη συνεισφορά εντοπίζεται στην επιβολή κατασκευαστικών και αισθητικών περιορισμών μαθηματική διατύπωση του προβλήματος, οδηγώντας στην ανάπτυξη καινοτόμων δομικών συστημάτων που δεν μπορούν να επιτευχθούν μέσω συμβατικών προσεγγίσεων. Επιπλέον, εισήχθη μια νέα μεθοδολογία, με σκοπό τη

βοήθεια του μηχανικού στον εννοιολογικό σχεδιασμό δομικών συστημάτων μεγαλύτερης κλίμακας, χρησιμοποιώντας προκατασκευασμένα δομικά στοιχεία. Σημαντική συνεισφορά που σχετίζεται με τη GSO προσέγγιση, είναι η αυτοματοποιημένη μετατροπή των βελτιστοποιημένων κατασκευών σε αρχεία τύπου CAD.

Η πρώτη συμβολή στην FSTO διατύπωση του προβλήματος, είναι η ανάπτυξη μιας διαδικασίας για την εφαρμογή της συμβατικής μαθηματικής διατύπωσης σε εμπορικά λογισμικά CAD και CAE. Η δεύτερη συμβολή στο FSTO, ήταν η ανάπτυξη μιας συνδυαστικής μεθόδου βελτιστοποίησης τοπολογίας και μεγέθους, για την υποστήριξη των διαφόρων φάσεων σχεδιασμού των δομικών συστημάτων, από τη φάση του εννοιολογικού σχεδιασμού έως την τελική κατασκευαστική φάση. Η τρίτη συνεισφορά στο FSTO, περιλαμβάνει την ένταξη της δυναμικής απόκρισης των δομικών συστημάτων στη διαδικασία της βελτιστοποίησης τοπολογίας.

Abstract

The scope of this research is to establish a holistic framework for the conceptual design phase of civil engineering structures in terms of Structural Topology Optimization (STO). In the literature, the application of STO in the field of Civil Engineering, is quite limited. Basic limitations existing works, are the difficulties on the representation of the optimized layouts and the fact that in most cases idealized structural conditions are considered. The confrontation of these two issues is the overarching aim of this PhD research.

Manufacturing constraints are applied in continuum-based Topology Optimization (TO) in order to provide solutions for Civil Engineering applications. The proposed methodologies, guided the algorithm to create discrete structures, that consist of truss-like or predefined structural components. Highlight of these procedures is the automation of the optimized structures' integration in a Computer-Aided Design (CAD) environment. For this purpose, image processing approaches and parametric design techniques are applied. Innovative structural systems for tall buildings and shell structures, that cannot be produced by conventional design techniques, are presented.

Additionally, Frame Structural Topology Optimization (FSTO) is addressed and the performance of the structural systems is examined under static and dynamic loadings. The conventional formulation of the compliance's minimization is applied in the commercial software SAP2000. The dual problem of the volume minimization is performed in an in-house software, developed within the remits of this research and standardized steel members are implemented through regression analysis. Constraints imposed by design code regulations are applied, resulting to optimized layouts that are very close to real-world structures. Some of the proposed structural systems are designed also by commercial software, pointing out the importance of FSTO in the construction industry. Furthermore, an extended survey of topology optimized structures under dynamic excitations and real-world earthquake conditions is conducted. The crucial procedure of the sensitivity analysis evaluation is described thoroughly and innovative structural systems for tall buildings are presented.

Table of contents

List of tables

List of figures

lxiii

Nomenclature

1D	One-Dimensional
2D	Two-Dimensional
3D	Three-Dimensional
AEC	Architectural, Engineering and Construction
AM	Additive Manufacturing
ASCII	American Standard Code for Information Interchange
AVM	Adjoint Variable Method
BESO	Bi-directional Evolutionary Structural Optimization
BF	Braced Frame
CAD	Computer-Aided Design
CAE	Computer-Aided Engineering
CAM	Computer-Aided Manufacturing
CBF	Concentric Braced Frame
DDM	Direct Differentiation Method
DOF	Degree Of Freedom
EBF	Eccentric Braced Frame
EC3	Eurocode 3
EC8	Eurocode 8
ESO	Evolutionary Structural Optimization
FE	Finite Element
FEA	Finite Element Analysis
FEM	Finite Element Method
FSTO	Frame Structural Topology Optimization
GS	Ground Structure
GSO	Generalized Shape Optimization
HP-OCP	High-Performance Optimization Computing Platform
HP-TOCP	High-Performance Topology Optimization Computing Platform

IGES	Initial Graphics Exchange Specification
LO	Layout Optimization
MMA	Method of Moving Asymptotes
MRBF	Moment Resisting Braced Frame
MRF	Moment Resisting Frame
NURBS	Non-Uniform Rational B-Splines
OAPI	Open Application Programming Interface
OC	Optimality Criteria
Q4	4-node bilinear Quadrilateral
RAMP	Rational Approximation of Material Properties
RC	Reinforced Concrete
RSMA	Response Spectrum Modal Analysis
SIMP	Simplified Isotropic Material with Penalization
SLP	Sequential Linear Programming
SO	Structural Optimization
SQP	Sequential Quadratic Programming
SRSS	Square Root of the Sum of the Squares
SSO	Structural Sizing Optimization
STO	Structural Topology Optimization
SUTO	Shaped Units based Topology Optimization
TO	Topology Optimization
TOP	Topology Optimization Problem
TSTO	Truss Structural Topology Optimization
XML	Extensible Markup Language

Chapter 1

Introduction

1.1 Motivation

Over the years, engineers continuously strive to improve the efficiency of constructions concerning safety, economy and recently sustainability during service life. Among others, the progress in building engineering is achieved through formulation of new design and assessment procedures with respect to structural, energy and environmental performance that usually require increased computing power. Development in analysis and design of structures has been invariantly associated with the formulation of more computationally expensive problems, since engineers can always formulate a problem that will provide a better solution but requires more than the available computing power. Computational mechanics has played a key role in this process. Exploitation of the ever-increasing computing power requires the development of numerical techniques and tools, which has eventually allowed the simulation of complex multi-physics phenomena using in-depth approaches that have not been possible to be applied until today. Advanced computational methods for designing safe and economic structures have benefited from multidisciplinary approaches between computational mechanics and other fields.

The Architectural, Engineering and Construction (AEC) industry has a major impact on the environment that people spend most of their life. Therefore, it is important that the outcome of architectural intuition performs well and complies with the design demands. Aesthetic and conceptual design are highly complex processes, that intend to satisfy design goals comprising of strict, engineering constraints, together with less strict, cognitive and perceptual ones. Due to the complexity of the architectural design process, the architect's intuition alone is often insufficient to ensure proper outcomes. Computational design optimization methods can assist in confidently achieving at highly

performing architectural design solutions, as well as provide valuable inspiration during the design task. STO is a characterization of design optimization formulations that allow for predicting the layout of a structural system. In this manner, the material demands are decreased but at the same time, the material available is distributed among the structural elements of the structural system in the best possible way. As a result, the implementation of STO leads to safer and more environmentally sustainable structures.

1.2 Aim and objectives

STO is a mathematical form finding problem formulation, that the last years matured, from an academic subject to an applied sciences' practical design tool. So far, STO is implemented in real-world applications of the automotive, aerospace and other fields of the mechanical engineering industry. Its contribution to the AEC industry is limited to applications that rely only on the conceptual design process. The main scope of this research is to establish some mathematical STO formulations for supporting the design phases of large-scale civil engineering structural systems from the conceptual design phase to the final one. The interpretation and constructability of the final layout of the STO procedure, is a specific issue that is considered throughout this research. The generation of structural systems composed of discrete members is also an aim of the presented study.

Initially, manufacturing constraint are imposed in the conventional Generalized Shape Optimization (GSO) formulation in order to produce truss-like structures. Different types of Finite Elements (FEs) will be combined, to determine their impact in the layout generation. Image processing techniques will be investigated for the automatic interpretation of the optimized structural systems. Additionally, prefabricated structural components will replace the typical rectangle FEs and parametric design techniques will be studied for the final integration of the optimized structures in CAD environment. Furthermore, standardized steel profiles will be implemented in the FSTO and design code check constraints will be imposed. Commercial Computer-Aided Engineering (CAE) software that are used from civil engineers will be employed for the analysis and design

phase of the structures. Finally, the effect of the consideration of dynamic conditions in the FSTO procedure, when generating structural systems, will be studied.

1.3 Outline of the dissertation

The current thesis consists of 9 chapters. In the second Chapter of the dissertation, the fundamental theory of Structural Optimization (SO) is presented. The mathematical formulation of the generic SO problem is introduced and basic terms are defined. Consequently, the three main categories of SO problems are presented, namely sizing, shape and topology optimization. Finally, more details on STO methodologies, which are used in the largest part of the dissertation, are discussed. In Chapter 3, the term structural system is introduced and a categorization, depending on the type of the main stresses that are developed, is presented. During the current dissertation, all the civil engineering structures, that the proposed methodologies are applied, refer to structural systems of tall buildings and shell structures. Thus, a variety of structural systems for the above structures is presented.

In Chapter 4, the GSO is integrated in the conceptual design of civil engineering structures. Particularly, a variety of layouts for Braced Frames (BFs) that are applied in high-rise buildings are proposed. Manufacturability constraints, such as symmetry and non-optimizable areas, are imposed and a hybrid mesh that consists of plane stress FE and Two-Dimensional (2D) frame elements is proposed. Furthermore, an automatic process for CAD interpretation of the optimized structural systems is discussed. Image processing techniques and the Non-Uniform Rational B-Splines (NURBS) are applied to extract the final geometry, while the Initial Graphics Exchange Specification (IGES) translator is used for transferring the geometry to a CAD file. In Chapter 5, a novel methodology that relies on TO and aims to support the civil engineers in the conceptual design phase of a structural system, is presented. According to the proposed methodology, equivalent rectangular FEs are generated based on multiple specifically shaped prefabricated units, which are treated by TO as periodic unit cells. Using this methodology, aesthetic and manufacturing concerns are imposed into the mathematical formulation of the problem

and innovative structural systems are developed, that cannot be achieved through conventional approaches. The applicability of the proposed methodology is tested in 2D plane stress analysis problems and results for TO problems are shown. Three-Dimensional (3D) test cases are also examined where hangar and high-rise building type of structures are considered, simulated with 8-node hexahedron FEs. Finally, the developed methodology is integrated with the Grasshopper parametric design application, in order to interpret the optimized structures into the Rhino3D CAD software.

In Chapter 6 the FSTO is introduced. Some basic issues on the generation of the initial design domain, i.e. Ground Structure (GS) generation, are discussed and two applications are presented. The mathematical formulation of the compliance-based FSTO problem is presented and its implementation in the SAP2000 is discussed thoroughly. Numerical results in basic cantilever structures are presented, while real-world test cases of a bridge and a gridshell are examined too. In Chapter 7, two different SO problems are combined in order to support engineers not only in the conceptual design phase but also in the final design one; in particular STO and Structural Sizing Optimization (SSO) problems are formulated and solved into a sequential manner. For implementation purposes of the two problems' solution process, regression analysis techniques are applied and the two problems are formulated as minimum material volume problems subjected to design code restrictions. Additionally, real-world design characteristics (loading conditions, material properties etc.) and standardized cross-sectional properties are considered, while in the second stage of the methodology, the Eurocode design regulations are applied, thus, resulting into more realistic structures. The proposed methodology is applied in a wide variety of Moment Resisting Braced Frames (MRBFs) for mid- and high-rise buildings.

In Chapter 8, three cases of the dynamic performance of MRBFs are studied, aiming to derive their structural system. According to the first case, the structural system of MRBFs is derived by maximizing specific eigenfrequencies when MRBFs is subjected to free vibration conditions. In the second one, the structural system is obtained when its dynamic performance is evaluated considering linear time history analyses. Two loading

conditions are examined, harmonic load and earthquake ground motion records. The third case, refers to the use of Response Spectrum Modal Analysis (RSMA), that is used in order to reduce the computational effort. According to the latter case, the seismic loading is implemented according to Eurocode 8 (EC8). For each dynamic STO problem formulation described in this work, the corresponding features of the numerical implementation are discussed along with the sensitivity analysis procedures required. Several test cases are examined, where MRBFs are derived through the above-mentioned formulations aiming to generate optimized lateral bracing structural systems, the results obtained demonstrate the importance of considering the dynamic response of the structural systems. In Chapter 9, the concluding remarks of the current dissertation are discussed and ideas for future research are proposed.

1.4 Scientific outputs

During my PhD course, I have contributed in the completion of 7 publications [54,69,101,105,106,108,109] in scientific refereed journals and 4 presentations [102,103,104,107] in international conferences.

CHAPTER 2

Structural optimization

2.1 Introduction

The definition of a structure in mechanics can be given as, "any assemblage of materials which is intended to sustain loads" [27]. The term optimization refers to the selection of the best decision, considering some specific criteria, from a set of available options. Combining the two terms, it can be stated that SO, is the procedure of producing an assemblage of materials that sustain loads in the best manner. The most essential attribute that must be defined now, is the term best. A common engineering objective is to reduce the amount of the structure's material as much as possible. On the other hand, the strengthening of the structure's performance against specific instabilities or buckling phenomena, is also very important. However, minimizations and maximizations of these kind of objectives, cannot be performed without restrictions. Typical attributes that are used as constraints in SO problems are stresses, displacements, geometry etc. At this point, it is important to highlight, that most of these quantities can be used both as the objective to optimize, but also as the restrictions that the final structure must satisfy.

To understand better the concept of SO in relation with the attributes that are referred above, the main steps of the structural design process are introduced as follows [56]:

1. *Functional requirements*: This is the first step of the design process. It is very common for these requirements to be defined even before the engineer starts with the design procedure, e.g., the required number of driving lanes on a bridge or the required area of a building.

2. *Conceptual design*: In this phase, the wit and the experience of the engineer is critical, since the general planning of the structure must be performed in such way, so to satisfy the functional requirements. For example, in the procedure of

designing a bridge, the choice of whether it will be a truss or an arch bridge, is made in this stage.

3. *Optimization*: During this procedure, the best design, between many possible solutions, that satisfy the above requirements, is selected. In the past, trial and error techniques were applied, but over the last years, due to the tremendous technological development in the computer engineering field, automated procedures are implemented. An example of this phase is the selection of the cross-sectional area of a truss when designing a truss bridge.

4. *Details*: In the last stage, the final structure is checked, considering market, social or aesthetic factors. Again, the experience and the judgement of the engineer are critical, e.g., when the color of a building's facet must be decided.

The field of study of the current dissertation, is the formulation of automatic procedures, using mathematical design optimization. So, the first issue is to transpose the factors that are studied to mathematical terms. For some factors, e.g., mechanical, this transformation is straightforward while for some others, e.g., aesthetic, it is quite difficult. One of the scopes of this thesis, is to encapsulate different types of factors in the optimization procedure.

2.2 Mathematical formulation of a generic structural optimization problem

In any SO formulation, the following function and variables are prerequisites:

- *Objective function* (f): This is a mathematical equation, that returns a single value, which represents the goodness of the structure's design. Commonly, f is a value that it is desired to be minimized but, in some cases, the maximization of an objective function is also demanded. Typical quantities for f, are the weight, displacement, stresses and construction cost of a structure.

- *Design variable* (x): This is a vector of numerical values, that are changing within a predefined range during the optimization procedure, in order to define the

design of the structure. Frequently used design variables are, the cross-sectional area of a frame, the thickness of a plate or the type of the structure's material.

- *State variable* (y): For a given design variable, y is a function or a vector that measures the structure's response, which can be defined in terms of displacements, stresses or forces of the structure.

Consequently, a general formulation of an SO problem is expressed as follows:

$$(SO) \begin{cases} minimize\ f(x,y)\ with\ respect\ to\ x\ and\ y \\ subject\ to\ \begin{cases} behavioral\ constraints\ on\ y \\ box\ constraints\ on\ x \\ equilibrium\ constraint \end{cases} \end{cases} \tag{2.1}$$

Regarding the above formulation, it is possible for a problem to have more than one objective functions, i.e. the so-called multi-objective optimization. In this case, the first line of the formulation, for n objective functions, is changing to:

$$minimize\ \big(f_1(x,y), f_2(x,y), \dots, f_n(x,y)\big) \tag{2.2}$$

However, this type of optimization is beyond the scope of this research, so more details can be found in the literature [19].

Considering the constraints, three types are indicated in the above formulation. At first, the behavioral constraints are referred on the state variable. They can be written in the form of $g(y) \leq 0$, where g is a function that represents a specific response of the structure. Secondly, the box constraints are the possible values that the design variable can take. Finally, the equilibrium constraint depends on the physical phenomena that is studied. In most of the cases, this is a partial differential equation e.g. for a static problem it is the simple linear elasticity equilibrium while for a dynamic study, the dynamic equilibrium must be applied. Supposing that, $u(x)$ is the displacement vector of a structure and all the constraints can be expressed in one function, the mathematical formulation of an SO problem is:

$$(SO) \begin{cases} \min_{x} & f\big(x, u(x)\big) \\ s.t. & g\big(x, u(x)\big) \leq 0 \end{cases} \tag{2.3}$$

where s.t. denotes "subject to".

2.3 Types of structural optimization problems

It is widely accepted that SO is divided in three main broad categories:

- Sizing Optimization: This is the most common type of optimization in all of the engineering fields, since the mathematical problem is easily defined and the proposed solution needs relatively small effort in the post-process stage. The design variable can be a geometrical feature, e.g. the cross-section's dimensions of a frame profile or a material feature, e.g. different steel grades. In Figures 2.1(b1) and 2.1(b2), two examples of sizing optimization problems, for discrete and continuum structures, are illustrated.

- Shape Optimization: In this case, a part of the structure's boundary is changing and new form of the structure is produced. For example, considering a truss structure, the location of the nodes are the design variables. Important to notice at this point, that the topology of the structure remains the same. In Figures 2.1(c1) and 2.1(c2), two examples of shape optimization problems, for discrete and continuum structures, are illustrated.

- Topology Optimization (TO): This is the most holistic type of optimization, because not only the dimensions of the structure are changing, but also a new form and topology are developed. For the purposes of the current dissertation, STO methods are mainly implemented, so a more detail description is provided in the next section. In Figures 2.1(d1) and 2.1(d2), two optimized layouts of Topology Optimization Problems (TOPs), for discrete and continuum structures, are illustrated.
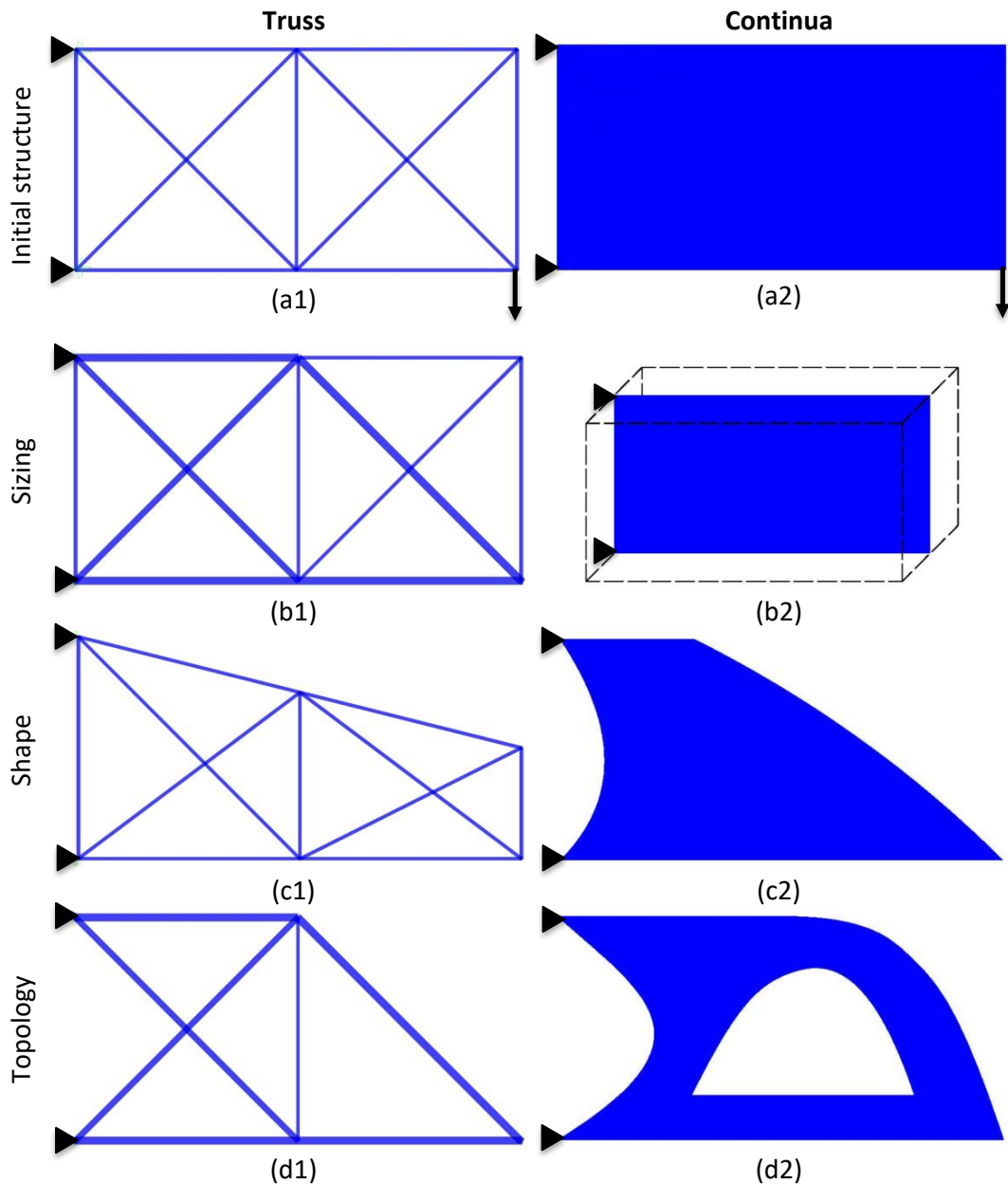
Figure 2.1 Types of SO for discrete and continuum structures

2.4 Structural topology optimization

STO is separated into two main broad classes of approaches; the Layout Optimization (LO) and the Generalized Shape Optimization (GSO) [93]. LO is implemented in One-Dimensional (1D) and 2D structures. The main geometric characteristic of 1D structures is that the cross-section's dimensions are relatively smaller compared to its length.

Assuming that in the deformed condition the cross-sections remain plane, all the internal forces and the points of the 1D structures are specified by the deformed shape of the centroidal axis. The union of the intersection of 1D structures is defined as grid, the point of the intersection is called joint, while the segment between two joints is determined as member. Some examples of 1D grids are the trusses, grillages, gridshells and cable-nets. In the Finite Element Method (FEM) [9,136], such structures are simulated with truss (bar), frame (beam) and cable FE. Regarding the application of LO in 2D structures that have similar geometrical properties, considering the dimensions' analogies, with the 1D structures, the FE that are used are the plate or shell elements. These elements can be unified in such way and create a structure, that is called honeycomb. Important characteristic of LO, is its holistic approach, since most of the times, the topology (members' connectivity), the shape (nodes' location) and the size (cross-section's dimensions) of the structure, are optimized simultaneously. Usually in LO, the initial design domain of the structure consists of all the possible members of the final structure, forming in this way the GS [30]. In some of the most well-known works [55,122,84], the redundant members of a highly connected GS are removed and the joints location are fixed.

GSO is applied in 2D and 3D structures, considering the continua approach. In the most popular form of this type of STO, the structures consist of isotropic solid or empty elements [92]. In this approach, the initial design domain is discretized with FEs and the thickness or density of each element is the design variable, that can take values 1 or 0 denoting the existence or not of an element, respectively. A common generalization of GSO is the multi-material optimization, in which the algorithm chooses a specific material, from a given set of different materials, for each element or no material at all. Bendsoe and Kikuchi [13], introduced a framework for dealing with GSO by applying a homogenization method. Particularly, composite microstructures are introduced to the design domain, homogenized equivalent materials take place of the composite ones and the optimization problem is becoming continuous and more relaxed. Extended work and

different approaches on homogenization methods can be found in the literature [115,44,45,34].

Right after the introduction of the homogenization methods, the material interpolation schemes are proposed to deal with TOP. By applying these methods, the density of each FE can take any values between 0 and 1. In order to reduce the complexity of the homogenization methods, Bendsoe [12] introduced the power-law approach, namely the Simplified Isotropic Material with Penalization (SIMP) method. In the SIMP process, the density of the FE is related with the Young Modulus using a penalty factor. In this way, the intermediate densities are penalized and the final structure tends to converge in clean 0-1 solutions. Later works [134,71] contribute to the development of SIMP, while Bendsoe and Sigmund [14] established the optimum number for penalty factor (equal to 3). Similar to the SIMP method, Stolpe and Svanberg [112] proposed another interpolation scheme called Rational Approximation of Material Properties (RAMP). Comparative studies for different material interpolation schemes can be found in literature [14,98].

As it is stated before, in the first approaches of GSO problems, the design variables can take only the values 0 or 1. Consequently, some discrete optimization approaches were developed, based on evolutionary methods [66,125]. Initially, the Evolutionary Structural Optimization (ESO) techniques, followed hard-kill approaches, where the redundant material is eliminated from the design domain in each iteration loop. In this way, during the optimization procedure the material cannot be added again in the structure. To deal with this issue, bi-directional schemes are implemented [129], where elements can reappear during the iterative process, introducing the Bi-directional Evolutionary Structural Optimization (BESO) methods. However, the most recent developments in ESO and BESO approaches, have lots of common concepts with the density method. For this reason, in literature [98] it is debatable if the above techniques should be considered as different methods or just as a subfield of the SIMP approach. Additionally, these methods sustained some criticism regarding the intuitive nature of their process and their limited applicability [94,135].

A common handicap of the above methods, is the difficulty to represent the geometry of the optimized structure with smooth curves and surfaces. To overcome this obstacle, in more recent developments of TOP, the level set approach for GSO is introduced [4,5,123]. In this method, the boundaries are defined from the contour of the level set function. Particularly, in the areas that the function is lower than a specific constant value, it is considered that there is no material, while the solid regions are defined from the areas, in which the function is bigger than this constant number. The most popular manner to update the level set function, is by solving the Hamilton-Jacobi equation. In order to gain more control in the shape of the level set function and generate new holes in the structure, the original form of the Hamilton-Jacobi equation is expanded with reactive and diffusive terms [98].

CHAPTER 3

Structural systems

3.1 Introduction

In the structural engineering field, the term structural system is referring to a load bearing subsystem of buildings or nonbuilding structures. The scope of a structural system is to assemble structural elements in such way, so that the applied loads are transmitted safely from the structure to the ground, without exceeding specific mechanical requirements in its members. Depending on the type of the main stresses that appear in the structural members, the structural systems are classified in five basic categories. Nevertheless, two or more of the following fundamental structural types can be combined and produce a unified structure e.g. a building, a bridge or a shell roof.

- Tensile structures: The structural members of these structures are carrying only tension. Considering that the tensile stresses are uniformly distributed over the cross-section of each member, the material of these structures is used in the most efficient way.

- Compressive structures: In this type of structures, compressive stresses are mainly developed. Compressive structures are sensitive to buckling or instability, therefore sometimes, additional bracing must be provided in order to avoid such failures.

- Trusses: These structures consist of straight elements, that are connected to each other with hinge connections and produce a rigid structure. Due to their low self-weight and their high strength, truss structures are between the most widely applied type of structures.

- Shear structures: Shear structures are referred mostly to reinforced concrete or wooden shear walls and are used mainly to tall buildings as a lateral resisting

system. These structures develop mostly in-plane shear stresses and relatively small bending stresses.

- Bending structures: In this type of structures, bending stresses are mostly developed, while sometimes the shear stresses that are produced from the changes in bending moments are significant too.

The vast majority of the case studies of the current dissertation are referring to structural systems of tall buildings or shell structures. Therefore, more details considering this type of structural systems, are discussed in the following.

3.2 Tall buildings

The choice of a high-rise building's structural system depends mainly on the functionality purposes, architectural requirements and the geometrical characteristics of the building. In the building construction industry, there are many types of lateral resisting systems, whose purpose is to sustain lateral loads e.g. earthquake excitations, wind loads etc. Nevertheless, these systems can be categorized into three main groups: shear wall systems, frame systems and dual systems (a combination of the other two) [120]. To understand the importance of the lateral resisting system for a tall building, it is stated that for a building that consists of approximately more than 50 floors, the cost of the material for the lateral resisting system becomes bigger comparing to the vertical load resisting system [117]. In the following, four basic structural systems for high-rise buildings are discussed.

3.2.1 Shear walls

Tall buildings with shear walls are usually stiffer than buildings with frame lateral system. This type of structural system has high in-plane resistance, thus it can sustain shear and overturning moments, that are developed from wind or seismic loads. These structural elements can be applied in several manners. Taking under consideration that a simple system which consists of columns and slabs can support 10 stories, if this system is strengthened with shear walls, the effective height can be extended up to more or less

20 stories [43]. A simple shear walls system is illustrated in Figure 3.1(a), while in Figure 3.1(b) a coupled shear walls system, that is produced by connecting single shear walls, is presented.

(a)

(b)
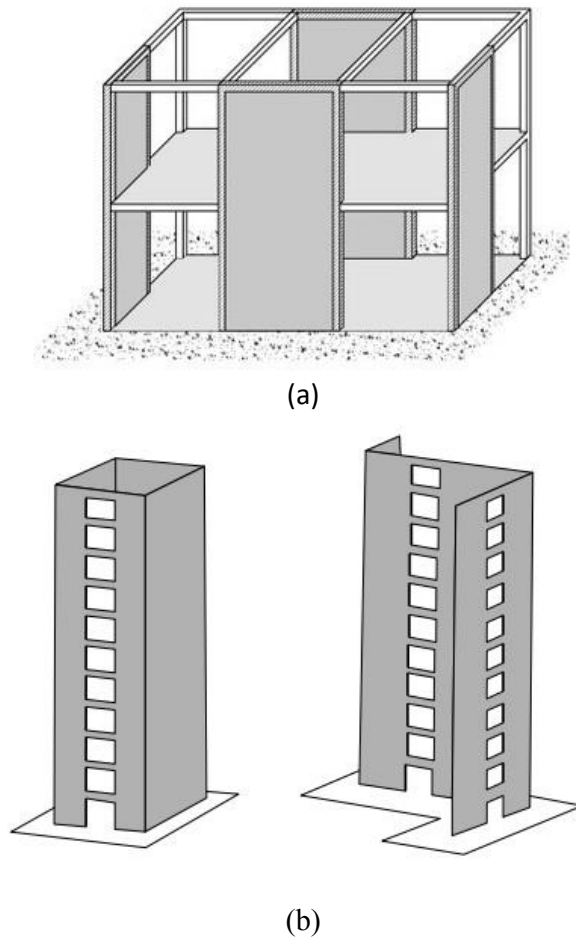
Figure 3.1 Illustration of (a) shear walls and (b) coupled shear walls system [117]

3.2.2 Moment resisting frames

This type consists of an assemblage of beams and columns, rigidly connected with each other. This configuration allows the building to resist against lateral forces, due to the bending rigidity and shear strength of the frame members and joints. For utilizing a Moment Resisting Frame (MRF), both steel and concrete can be used. A reasonable height for a steel MRF is approximately 30 stories, while for a concrete one, about 20 stories. When it comes to buildings with more than 30 stories, the connections between the

beams and the columns become too expensive and inefficient [43]. In Figure 3.2 a typical MRF system is shown.
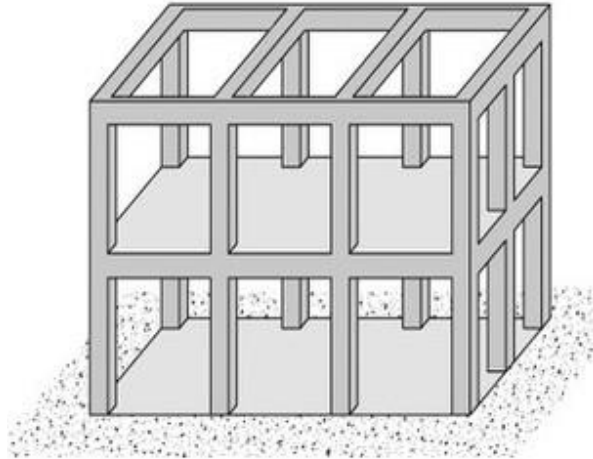
Figure 3.2 Illustration of an MRF system [49]

3.2.3 Outrigger systems

Outrigger systems are dual systems that combine braced frame and shear walls systems and are utilized in steel and composite structures. The concept of this system is to join the perimeter with the internal structure, as a unified system, to resist the lateral loads. This is succeeded by constructing a central core, which can consist of BFs or shear walls, and connecting it to the external columns with horizontal trusses or girders [47]. Usually, exterior belt girders are used too, in order to interconnect the external columns, as it shown in Figure 3.3.

3.2.4 Braced frames

In this structural system, diagonal steel frames are used, in order to strengthen the stiffness of a building. The BFs have the ability to carry the axial forces and reduce the bending demands of the beams and the columns. The diagonals members can be applied to the facets or to the core of the structure. Comparing with the MRF, the braced system is considerable more economical, especially when it comes to tall buildings. However,

some disadvantages are the decreased flexibility in floor plan layout, space planning and electrical installations [117]. There is a wide variety of different brace configurations that
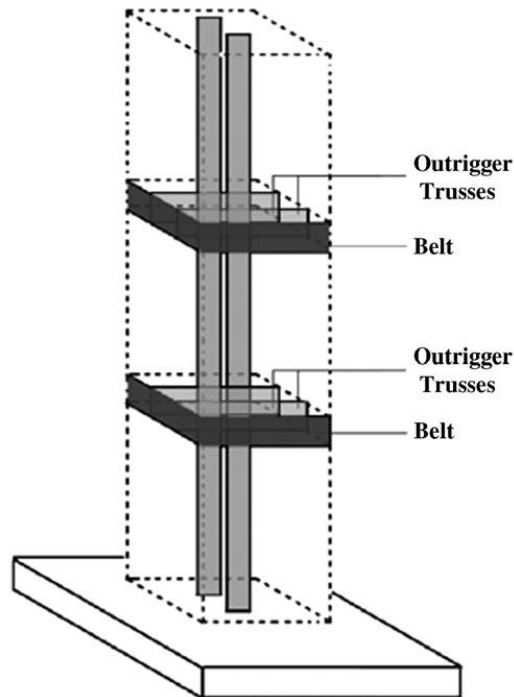
Figure 3.3 Illustration of an outrigger system [43]

can be applied and they are categorized in two main structural systems, the Concentric Braced Frames (CBFs) and the Eccentric Braced Frames (EBFs). The main geometrical characteristic of the CBFs is the fact that lots of their members are intersecting in specific nodes, oppose to the EBFs. CBF's major mechanical characteristic, is that it is very strong and stiff, making it an inappropriate solution when it comes to buildings that are constructed in high seismic zones. In these locations, EBF systems are preferred, since they combine the stiffness and the strength of a CBF, with the ability to absorb the energy dissipation of an MRF [89]. The most common configurations of CBF systems are the diagonal bracing, X-bracing, split X-bracing, chevron bracing, V-bracing and K-bracing, as it is shown in Figure 3.4. Depending on the location of the link that is produced from the braces members connection, a variety of different EBFs can be developed, as it is presented in Figure 3.5.
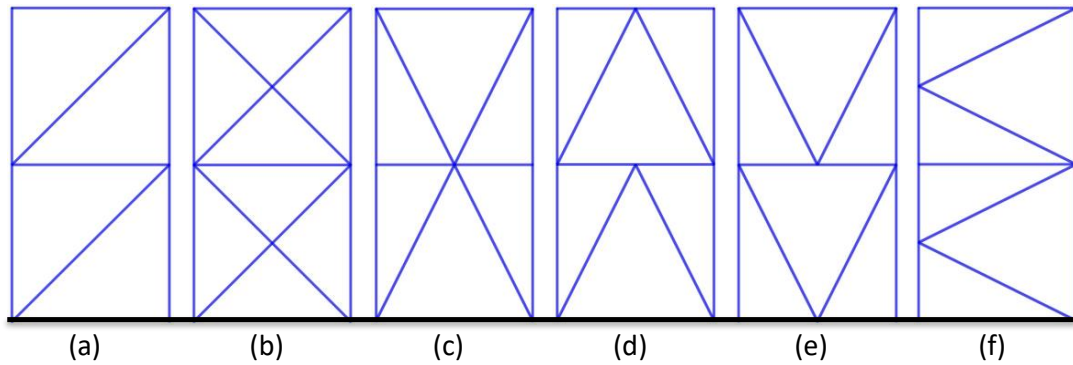
Figure 3.4 CBF configurations, (a) diagonal, (b) X, (c) split X, (d) chevron, (e) V and (f) K bracing.
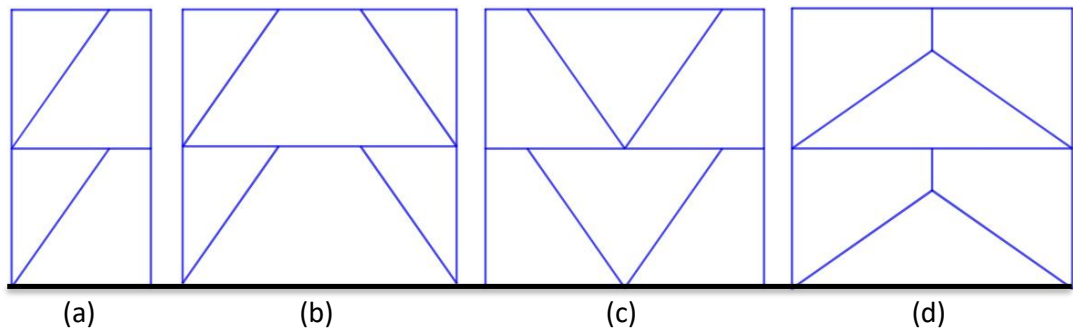
Figure 3.5 EBF configurations (a)-(d), depending on the location of link beam

3.3 Shell structures

Shell structures are one of the most challenging and interesting structural systems in the architectural and civil engineering field. The basic characteristic of these structures, is the freedom that they provide to the designer to produce eye-catching forms and at the same time to sustain loads efficiently. Their form is generated directly from the flow of the forces and determines their load bearing behavior. Particularly, shell structures are defined by 3D curved surfaces, in which the perpendicular to the surface dimension, is remarkably smaller, in comparison to the other two. Regarding their shape, shells can be curved in two dimensions or even only in one dimension. In an "ideal" shell structure, the external loads are transferred in the supports only by developing membrane forces, i.e. axial compression and tension. A shell can be constructed, either as a monolithic structure, i.e. a continuous surface, or as an assembly of discrete elements, the so-called gridshell.

Continuous shell structures can be produced from concrete, steel or masonry. The most common material that is used is the concrete and it is considered that the first concrete shell, constructed in the 2nd century [118]. In the modern era, the engineers started to construct again concrete shells in the 1920s, using mostly steel reinforced concrete without extra reinforcement [22]. Usually, these structural systems don't have interior columns or exterior buttresses and their shape can be a simple dome, ellipsoid, cylinder or even a more experimental combination of these configurations. Their main advantages are that they are robust structures, which are providing clear and big spans, resulting to open and unhindered interior. Through the '60s, this kind of structures became a trend, however the interest for concrete shells declined progressively, due to the high cost of labor and complexity of the projects formwork [118]. In Figures 3.6 and 3.7, two examples of concrete shell structures are illustrated.

The last decades, gridshells have become popular, gaining ground from traditional concrete shell structures. Gridshells, also known as lattice shells, can be classified depending on the material that they are made of, e.g., steel, aluminum, timber, and by the geometrical pattern of their grid, e.g., quadrilateral, triangle [3]. These structural systems have the shape and the strength of a double curvature shell but instead of a monolithic structure, they consist of discrete structural members [31]. The main purpose of the gridshells is to cover big spans. Particularly, they can be used to cover existing or new spaces, but also as stand-alone structures [64]. The advantages of these structural systems against the conventional ones (e.g. slabs, frame systems, continuous shells), are both aesthetical and structural. Due to the discretize topology of the gridshells, more air and light is penetrating to the structures, making them to look bigger and taller. Additionally, these structures have been proved more sustainably efficient than the conventional structural systems, due to their ability to decrease the embodied and operating energy. In Figure 3.8 an example of a steel gridshell is shown and in Figure 3.9 a timber gridshell is presented.

Figure 3.6 Palazzetto dello Sport by Pier Luigi Nervi and Annibale Vitellozi, Rome, 1958

Figure 3.7 El Oceanográfico (Valencia – Spain) by Félix Candela, Alberto Domingo and Carlos Lázaro, 2003

Figure 3.8 Steel gridshell over the courtyard of the National Maritime Museum, Amsterdam, 2011

Figure 3.9 Timber gridshell, Japanese Pavilion (Expo 2000) by Shigeru Ban and Frei Otto, Hanover, 2000

CHAPTER 4

Topology optimization aided structural design

4.1 Introduction

In the last decade, STO techniques emerged in the AEC industry. In the literature, few studies exist, where criteria, imposed by architects and engineers, are integrated into TO. Dombernowsky and Sondergaard [29] proposed some methods of using CAE software in order to explore new ways in architectural design process, aiming to take into account aesthetic criteria and engineering constraints. Stromberg et al. [113], presented a pattern gradation technique in order to achieve layouts with repetition. A new projection scheme was presented and some applications in the conceptual design of high-rise buildings are visualized. Stromberg et al. [114] introduced a new technique where beam elements and 4-node bilinear Quadrilateral (Q4) elements are combined in order to gain structures with uniform columns. Analytical study of BFs was performed and compared with the results of the TOP on high-rise buildings. Amir and Bogomonly [6] developed a computational procedure of finding the optimal material distribution of reinforced concrete structures, taking into the nonlinear behavior of the material. Besserud et al. [16] described the collaboration between architects and structural engineers in the conceptual design, leading to new architectural engineering projects. Beghini et al. [10], highlight the value of combining TO and personal aesthetics of architects. Aage et al. [1] presented a series of new TO methods that were developed specifically for conceptual architectural design of structures. Dapogny et al. [28] proposed a shape and TO framework oriented towards conceptual architectural design, where an emphasis was put on the possibility for the user to interfere on the optimization process by supplying information about his personal taste.

In this chapter, the fundamental theory of the compliance-based GSO problem formulation, using the SIMP method, is introduced. Consequently, three approaches of

imposing manufacturability constraints in the generation of BF systems are discussed. Additionally, an automatic procedure is developed, that translates the outcome of TO images into CAD files. Finally, some numerical examples are presented and the benefits of the proposed methodologies are highlighted.

4.2 GSO problem formulation with the SIMP method

The goal in a GSO problem, is to find the optimum topology of the internal boundaries and the shape of both internal and external boundaries of a perforated or composite continuum body. Particularly, the prerequisites for the formulation of the GSO problem are the initial design domain Ω, where the optimized layout will be produced, the required volume fraction of the optimized structure, the boundary and loading conditions.
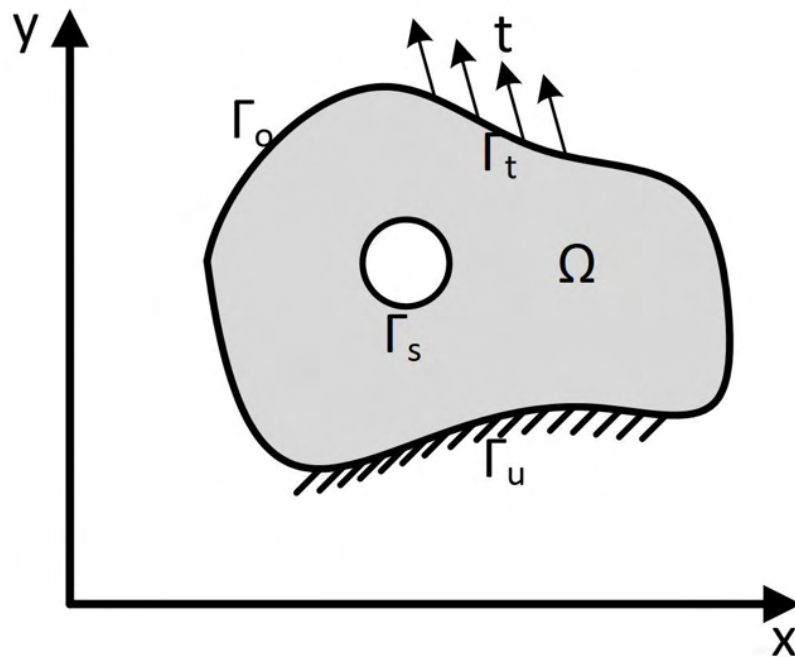
Figure 4.1 Initial design domain, boundary and loading conditions for the GSO.

As shown in Figure 4.1, the boundary Γ consist of Γ_u, Γ_o, Γ_t and Γ_s, parts where $\Gamma = \Gamma_u \cup \Gamma_o \cup \Gamma_t \cup \Gamma_s$. The loads are applied at region Γ_t, the area that doesn't participate in the optimization procedure is denoted as Γ_s, the support conditions are defined in Γ_u and Γ_o represents the geometric boundaries of Ω. As it is discussed in Section 2.4, several

approaches for dealing with GSO problems have been established. In the current dissertation, the SIMP method is applied.

The SIMP approach, is a material distribution method [111] for finding the optimum layout of a structural system, composed by linearly elastic isotropic material. Therefore, the question under investigation is how to distribute material volume into domain Ω, in order to minimize a specific criterion. The typical mathematical formulation of the compliance-based TOP can be expressed as follows:

$$\min_{x} C(x) = F^T u(x) \tag{4.1a}$$

$$s.t. $$

$$K(x)u(x) = F \tag{4.1b}$$

$$\frac{V(x)}{V_0} = f_{VolFrac} \tag{4.1c}$$

$$0 < x_{min} < x_e < 1, \quad e = 1,2,\dots,N_{ele} \tag{4.1d}$$

where $C(x)$ represents the compliance of the structure for the specific loading conditions, F denotes the load vector, $u(x)$ are the displacements resulting from the solution of the equilibrium equations, $V(x)$ represents the volume of the current design, V_o refers to the initial volume, $f_{VolFrac}$ is the volume fraction imposed by the problem, $K(x)$ is the global stiffness matrix, x represents the design vector to be optimized, x_e is the density of each FE and N_{ele} is the total number of the FEs that are used for the domain's discretization. Without limiting the applicability of the proposed methodology, in the above formulation the objective function is the minimization of the compliance under a number of constraints. The main constraint imposed, in the typical TOP formulation, concerns the limit in the area (2D) or volume (3D), with respect to the design domain. In order to solve this optimization problem by means of the FEM, the parameter that is introduced is the density of each FE. Parameter (x_e) ranges in $[x_{min}, 1]$, where x_{min} denotes a small value close to zero, in order to avoid numerical singularities. The elements having densities close to x_{min} are to be removed from the design domain and elements with densities

close to 1 will comprise part of the final form of the design domain. Regarding intermediate values between x_{min} and 1, specific technics are implemented and such values should be avoided.

According to the SIMP method, the FE density values are correlated to the corresponding Young modulus value E, through the following expression:

$$E_e(x_e) = x_e^p E_e^0 \Leftrightarrow k_e(x_e) = x_e^p k_e^0 \tag{4.2}$$

where the parameter p is a constant integer. This power law correlation is implemented in SIMP in order to achieve density values closer to the lower and upper bounds of the design variables. The value of the penalization parameter p varies depending on the problem. Common practice is that p is modified during the optimization loops or that the optimization problem is solved multiple times using different values of p [57]. However, as it is stated in Section 2.4, a common value for parameter p is equal to 3. The calculation formula of compliance can be written as follows:

$$C(x) = F^T u(x) = u(x)^T K(x) u(x) \tag{4.3}$$

By combining Eq. (4.2) and Eq. (4.3), the compliance is expressed as:

$$C(x) = \sum_{e=1}^{N_{ele}} (x_e)^p u_e^T k_e^0 u_e \tag{4.4}$$

where u_e and k_e^0 are the displacement vector and stiffness matrix respectively, for unit Young's modulus, in the elements' local coordinate system. The mathematical optimization problem that is formulated, can be solved using a variety of gradient-based algorithms such as Optimality Criteria (OC) [27], Method of Moving Asymptotes (MMA) [116] or Sequential Linear Programming (SLP) [74]. In addition, due to checkerboard problems and instabilities, a common practice is the application of filters into the optimization procedure. The most popular ones, are the density and sensitivity filters described in [18,21].

4.3 Sensitivity analysis

As it is stated in the literature [97], non-gradient algorithms are not efficient when it comes to TOP, that have huge number of design variables. Thus, the definition of the objective function's derivative, is one of the most important parts of the TOP formulation. Herein, the derivative of the compliance is evaluated. Particularly, in order to avoid the displacement's derivative calculation with respect to the design variable, a zero part is subtracted from $C(x)$:

$$C(x) = F^T u(x) - \lambda^T (K(x)u(x) - F) \tag{4.5}$$

Subsequently, the partial derivatives become:

$$\frac{\partial C(x)}{\partial x_e} = F^T \frac{\partial u_e(x)}{\partial x_e} - \lambda \frac{\partial k_e(x)}{\partial x_e} u_e(x) - \lambda k_e(x) \frac{\partial u_e(x)}{\partial x_e} =$$

$$= -\lambda \frac{\partial k_e(x)}{\partial x_e} u_e(x) + \left(F - \lambda k_e(x)\right) \frac{\partial u_e(x)}{\partial x_e} \tag{4.6}$$

Since vector λ used in the above equations is an arbitrary number, the value $\lambda = u_e(x)$ is used. Finally, the derivatives of the compliance can be expressed as follows:

$$\frac{\partial C(x)}{\partial x_e} = -u_e(x)^T \frac{\partial k_e(x)}{\partial x_e} u_e(x) \tag{4.7}$$

4.4 Optimality criteria

In the current thesis, the OC algorithm is implemented in order to solve the TOP. OC is an iterative search algorithm where the solution vector is updated in every iteration until convergence. First a linear approximation of $C(x)$ is defined close to the design variable vector x^k, as follows:

$$C(x) = C(x^k) + (y_e - y_e^k) \sum_{e=1}^{N_{ele}} \frac{\partial C(x)}{\partial y_e}\bigg|_{x=x^k} =$$

$$= C(x^k) + y_e \sum_{e=1}^{N_{ele}} \frac{\partial C(x)}{\partial y_e}\bigg|_{x=x^k} - y_e^k \sum_{e=1}^{N_{ele}} \frac{\partial C(x)}{\partial y_e}\bigg|_{x=x^k}$$

(4.8)

where $y_e = x_e^{-a}$ and the derivative of $C(x)$ with respect to y_e is calculated as follows:

$$\frac{\partial C}{\partial y_e} = \frac{\partial C}{\partial x_e}\frac{\partial x_e}{\partial y_e} = \frac{\partial C(x)}{\partial x_e}\frac{1}{\frac{\partial x_e^{-a}}{\partial x_e}} = -\frac{x_e^{1+a}}{a}\frac{\partial C(x)}{\partial x_e}$$

(4.9)

Then, $C(x)$ is expressed as:

$$C(x) = C(x^k) + \sum_{e=1}^{N_{ele}} y_e^k \left(\frac{(x_e^k)^{1+a}}{a}\frac{\partial C(x)}{\partial x_e} \right) + \sum_{e=1}^{N_{ele}} b_e^k x_e^{-a}$$

(4.10)

where b_e^k is given as:

$$b_e^k = -\frac{(x_e^k)^{1+a}}{a}\frac{\partial C(x)}{\partial x_e}\bigg|_{x=x^k}$$

(4.11)

since the derivative of the compliance can take only negative values:

$$\sum_{e=1}^{N_{ele}} y_e^k \left(\frac{(x_e^k)^{1+a}}{a}\frac{\partial C(x)}{\partial x_e^k} \right) < 0 \quad and \quad \sum_{e=1}^{N_{ele}} b_e^k x_e^{-a} > 0$$

(4.12)

Therefore, in order to maximize the subtracting part from the objective function $C(x)$, only the positive part needs to be minimized. Thus, the following subproblem is now formulated as follows:

$$\min_{x_e} C(x_e) = \sum_{e=1}^{N_{ele}} b_e^k x_e^{-a}$$

(4.13a)

$$s.t.$$

$$x_e a = V$$

(4.13b)

$$0 \leq x_e \leq 1 \tag{4.13c}$$

In order to solve this problem, the Lagrangian Duality method is applied where the corresponding Lagrangian function is expressed as follows:

$$L(x_e, \lambda) = \sum_{e=1}^{N_{ele}} b_e^k x_e^{-a} + \lambda(x_e a - V) \tag{4.14}$$

The minimum value of x_e resulted from the solution of the subproblem of Eq. (4.13) is obtained minimizing $L(x_e, \lambda)$ with respect to x_e and maximizing $L(x_e, \lambda)$ with respect to λ. The derivatives of $L(x_e, \lambda)$ with respect to x_e are:

$$\frac{\partial L}{\partial x_e} = -a b_e^k x_e^{-a-1} + \lambda a \tag{4.15}$$

and therefore, the values of x_e are obtained as follows:

$$\frac{\partial L}{\partial x_e} = 0 \Leftrightarrow x_e = \left(\frac{a b_e^k}{\lambda a_e}\right)^{\frac{1}{1+a}} \tag{4.16}$$

Since x_e takes values in the range [0,1] and large changes should be avoided, x_e is updated according to the following rules as expressed in the following equation:

$$x_e^{new} = \begin{cases} max(0, x_e - m), & if \left(\frac{a b_e^k}{\lambda a_e}\right)^{\frac{1}{1+a}} < max(0, x_e - m) \\ \left(\frac{a b_e^k}{\lambda a_e}\right)^{\frac{1}{1+a}} & if \ max(0, x_e - m) < \left(\frac{a b_e^k}{\lambda a_e}\right)^{\frac{1}{1+a}} < min(1, x_e + m) \\ min(1, x_e + m), & if \left(\frac{a b_e^k}{\lambda a_e}\right)^{\frac{1}{1+a}} > min(1, x_e + m) \end{cases} \tag{4.17}$$

m is the maximum alteration allowed for x_e. Similar to x_e, in order to calculate λ the derivatives of $L(x_e, \lambda)$ in respect to λ are defined:

$$\frac{\partial L}{\partial \lambda} = \sum_{e=1}^{N_{ele}} a_e x_e - V \tag{4.18}$$

The calculation of λ is achieved by iteratively choosing λ for each x_e until satisfying the following:

$$\frac{\partial L}{\partial \lambda} = 0 \Leftrightarrow \sum_{e=1}^{N_{ele}} a_e x_e = V \qquad (4.19)$$

A more detailed description can be found in the book by Christensen and Klarbring [27].

4.5 Imposing manufacturing constraints

In this section, TOPs are specially handled, aiming to implement TO for the conceptual design of civil engineering structural systems. In order to present the integration of TO formulations in the conceptual design of civil structures, the facet of a high-rise building, shown in Figure 4.2, is employed, where the domain and the FE mesh discretization are also depicted. In particular, problems are formulated for designing manufacturable acceptable layouts of BFs used in the design of high-rise buildings, thus TO is used as a tool for deriving multiple design alternatives. The discretization used is composed by 80 elements (in the horizontal direction) times 480 elements (in the vertical direction), resulting into 38,400 Q4 elements. The bottom edge of the domain is fixed. Three cases are examined: (a) constraint of symmetry case, (b) case of non-optimizable areas and (c) combination of continuum with beam elements case. In each case two different types of loads are considered (distribute load and nodal forces). It is important to note, that the MATLAB code written by Andreassen et al. [7] is used as a starting point, for the personal programming developments that are needed to implement the proposed manufacturing constraints.

4.5.1 Constraint of symmetry case

According to the first case, no significant modifications are implemented in the formulation of the TOP, when integrated into a conceptual design process. For this case, a lateral distributed load is applied at the left vertical edge of the domain (see Figure 4.3(a)). A typical optimized layout obtained when solving this problem is shown in Figure
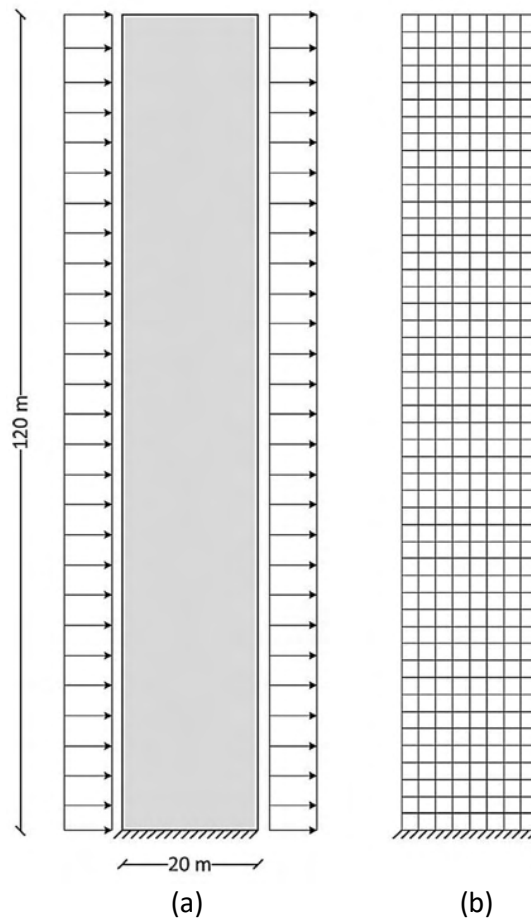
Figure 4.2 BF design of a high-rise building: (a) domain and (b) mesh discretization.

4.3(b), due to the specific loading and boundary conditions the resulted layout is not symmetric. In the problem of Figure 4.3(a), the lateral distributed load is applied at the left vertical edge only; thus, the domain demands lower density values for the elements of the right edge.

So far, no manufacturing and conceptual constraints have been taken into consideration. One basic practical and conceptual design constraint is that the final domain needs to be symmetric with respect to the vertical middle axis of the domain of Figure 4.2(a). Several formulations have been presented in the literature for dealing with these types of constraints (geometrical patterns, etc.). A rather simple approach is to make use of additional different load case, i.e. to apply two distributed loads on both vertical edges of
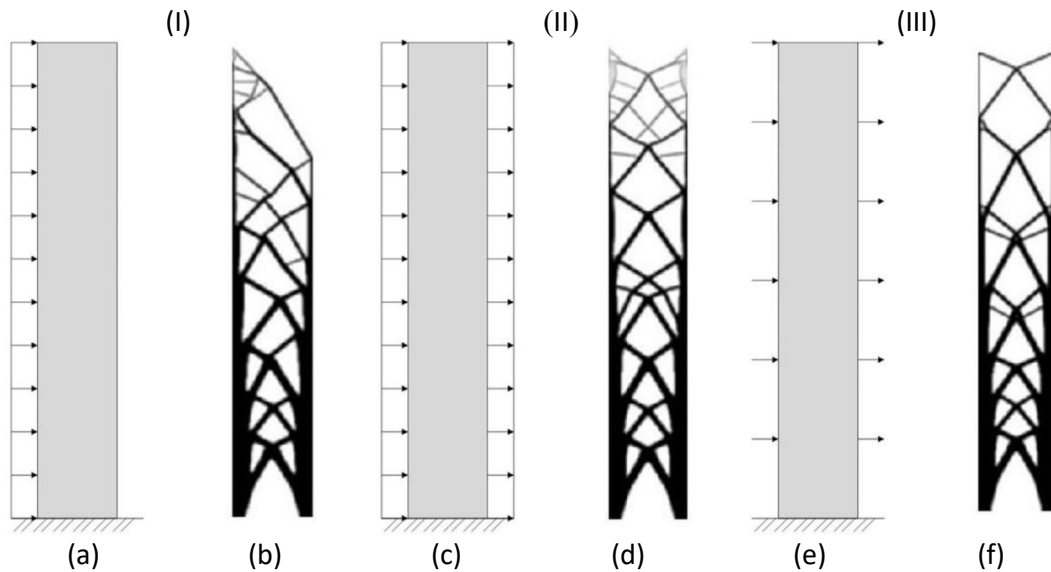
Figure 4.3 BF design of a high-rise building: I. One side distributed load-Asymmetric structure: (a) initial and (b) optimized layout. II. Both sides distributed load-Symmetric structure: (c) initial and (d) optimized layout. III. Concentrated nodal forces-Symmetric structure: (e) initial and (f) optimized layout.

the domain, facing towards the same direction (see Figure 4.3(c)). The optimized layout obtained implementing two edges distributed loads is shown in Figure 4.3(d). As it can be observed, although the layout is symmetrical with respect to the vertical middle axis, the top diagonals of the optimized design are rather incomplete. Furthermore, small truss-type forms composed by elements with low density values (grey elements) are encountered in this area. This is due to the fact that the distributed loads will not allow the formation of the diagonals and thus the optimized layout of Figure 4.3(d) remains not acceptable in terms of manufacturability constraints. Aiming to deal with this issue too, a third simple approach is implemented, by applying concentrated nodal forces. Since the height to width ratio of the domain of Figure 4.2(a) is equal to 6 by 1, it is considered that the domain is structured by 6 square blocks. The simple approach that is implemented, is to apply concentrated nodal forces at the top of each square block as shown in Figure 4.3(e) and the corresponding optimized layout is shown in Figure 4.3(f).

4.5.2 Case of non-optimizable areas

In the previous sub-section, it was observed that the optimized layouts depict increased material concentration at the edges. The reason is that near the bottom edge, increased stress concentrations are encountered, leading to increased material demands in this area. For specific volume fraction values, the approaches described in the previous section lead to designs with large material demands for the upper part of the vertical structural members, therefore, relatively low percentages of material are available for the formation of the diagonals. Aiming to deal with such issues, Bendsøe and Sigmund [15] used a specific technique, imposing geometries where void or full areas are required. In particular, the desired areas are recognized and elements composing the void or full ones are assigned to the minimum or maximum density values, respectively. These areas are also called as non-optimizable ones, since the density of their elements is not an unknown variable.

In the BF design problem, aiming to form vertical structural members next to the two vertical edges (columns) of the domain of Figure 4.2(a), the technique of Bendsøe and Sigmund [15] is used. Initially, the non-optimizable areas are chosen, i.e. number and width-height of the vertical structural members (see domains of Figure 4.4). The resulted optimized layouts are shown in Figures 4.4(b) and 4.4(e), where two non-optimizable areas are selected. It can be noticed though, that the diagonals on the top of the domain are still incomplete. This is due to the fact that the vertical structural members are enforced to have a specific width along their height, thus there is no need to develop diagonal structural members in this area. Another interesting observation obtained from Figures 4.4(b) and 4.4(e), is that the cross-section of vertical structural members varies along their height, a feature that might not be acceptable in certain cases. Varying the width of the non-optimizable areas, vertical structural members with different varying cross-sectional areas can be derived. Therefore, this approach can be used in cases where controlled varying cross-sectional areas in the vertical structural members, is preferable.
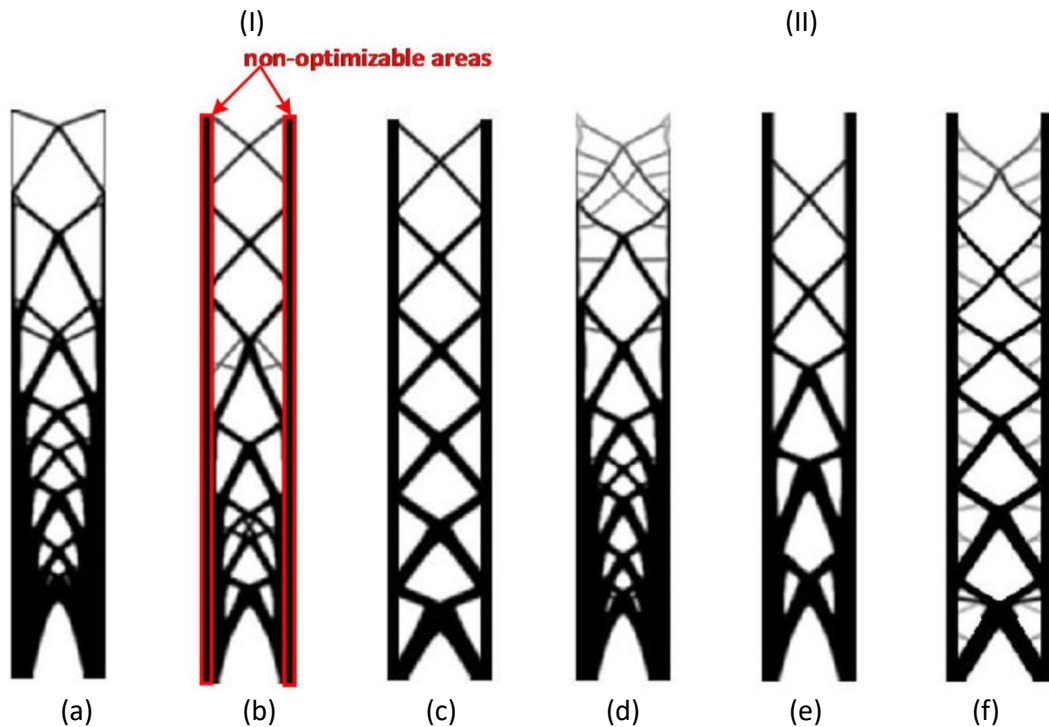
Figure 4.4 BF design of a high-rise building: Optimized layouts ($f_{VolFrac} = 50\%$): I. Concentrated nodal forces: (a) basic case, (b) non-optimizable areas (shown in red) and (c) beam elements. II. Both sides distributed load: (d) basic case (e) non-optimizable areas (as shown in b) and (f) beam elements.

4.5.3 Combination of continuum with beam elements case

So far, the optimized layouts that were derived using the above-mentioned formulations, resulted into vertical structural members with varying cross-sectional areas. The goal of the current case is to derive domains composed by distinctive structural members both vertical (with constant cross-sectional area along their height) and truss-like diagonal members. The idea, proposed by Stromberg et al. [114], rely on the introduction of hybrid mesh derived as a combination of continuum with beam elements. According to their idea, in the case of 2D domains (as the one of Figure 4.2(a)), where the mesh consists of Q4 elements (see Figure 4.2(b)), the vertical structural members are modelled with beam elements. Conventional two-node 2D beam elements are modelled with six degrees of freedom (DOFs), three per node (two translation ones horizontal-vertical and one rotational). The Q4 elements are modelled with eight DOFs (two per node, two translation

ones horizontal-vertical). Several methodologies that join discrete and continuum elements are explored in [114]. The implementation adopted in this thesis, varies with respect to the loading conditions. In the case of distributed loads, the number of beam elements used, is equal to two times the number of Q4 elements along the height of the domain (i.e. 2×480), as shown in Figure 4.5(a). In the case of concentrated nodal forces, the number of beams elements used is equal to two times the number of square blocks (i.e. 2×6), as shown in Figure 4.5(c).

As it was mentioned previously, 2D beam elements have two translational and one rotational DOFs per node and Q4 ones have only two translational DOFs per node. Therefore, combining the two types of elements is achieved by superimposing the corresponding translational DOFs and adding the rotational DOF at specific nodes of the mesh. The stiffness coefficients of the combined stiffness matrix for the DOFs of the vertical edges of the domain of Figure 4.2(b) are modified as follows:

$$k_{ij} = k_{ij}^{Q4} + k_{ij}^{beam} \tag{4.20}$$

where i and j are the domain's external DOFs of the vertical structural members. Figure 4.6 depicts the combination of beams with Q4 elements, where the 4×3 mesh of Q4 elements is combined with 6 beam elements. More specifically, for the case of the upper left beam element that is connected with the neighboring Q4 one, translational DOFs of Q4 (i.e. global DOFs 1, 2, 3 and 4) are combined with the corresponding translational DOFs of beam (i.e. local DOFs 1, 2, 4 and 5) by means of the proper transformation operation. The rotational DOFs of beam (i.e. local DOF 3 and 6), are transformed into the global system (now denoted as DOF 41 and 42, respectively). Comparing the size of the stiffness matrix composed only by Q4 elements with that of the combined Q4-beam mesh, it could be observed that the size is not altered significantly. If the size of the initial mesh is composed by $nel_x \times nel_y$ (number of elements in the *X* and *Y* direction respectively) Q4 elements and n_{beams} is the number of the beam elements integrated into the initial mesh, the number of DOFs of the initial stiffness matrix is equal to $2(nel_x + 1)(nel_y + 1)$, while those of the combined one is equal to $2(nel_x + 1)(nel_y + 1) + 2(n_{beams} + 1)$.
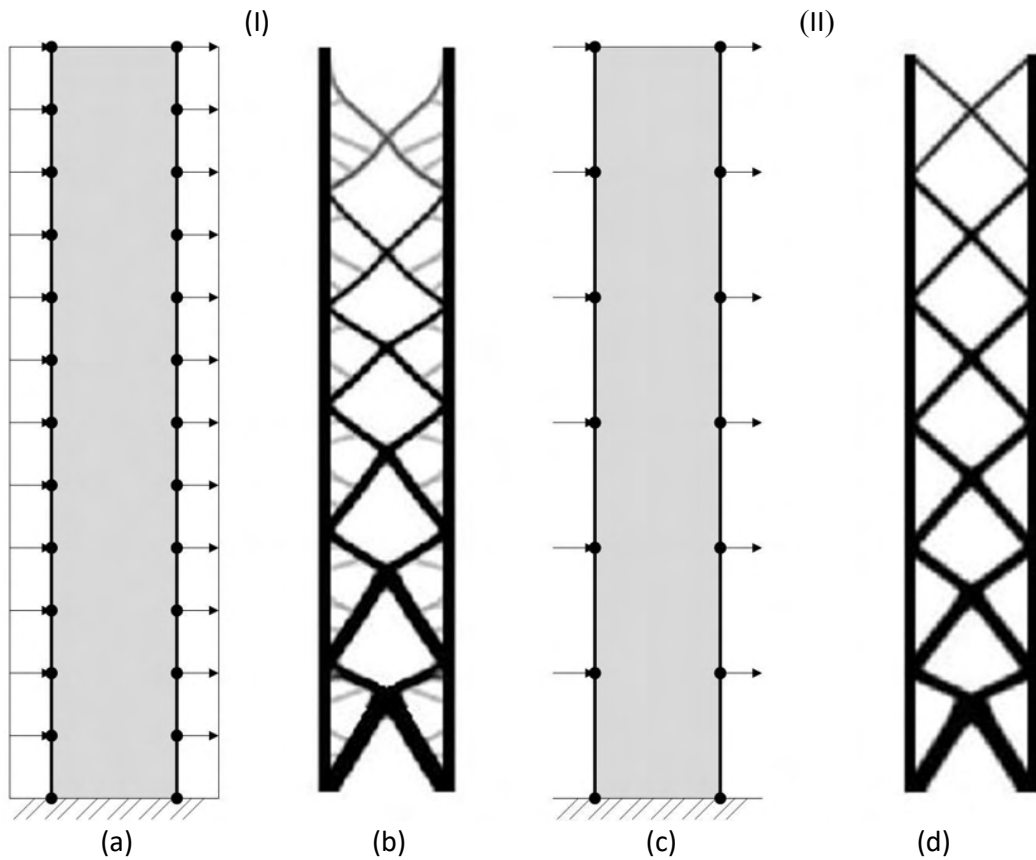
Figure 4.5 BF test example-Beam elements case: I. Both sides distributed loading: (a) initial and (b) optimized layout. II Concentrated nodal forces: (c) initial and (d) optimized layout.

Furthermore, it should be noted that the contribution of the beam elements to the volume fraction of the domain in total needs to be considered. The improvements of the optimized layouts obtained with the implementation of the continuum-beam elements case are presented in Figure 4.5, resulting into fixed width vertical structural members and development of distinct diagonal members (see for example Figures 4.5(b) and 4.5(d)). Comparing the concentrated nodal forces case (Figures 4.5(c) to 4.5(d)) with that of the distributed loads (Figures 4.5(a) to 4.5(b)), it can be observed that due to the distributed loads, multiple rather small truss-like members are developed, that connect the vertical members with the diagonal ones. On the other hand, for concentrated nodal forces the domains are much clearer (e.g. Figure 4.5(d)), fixed width vertical structural members and six distinct pairs of diagonals are generated. By decreasing the volume fraction, thinner diagonal members will be generated.
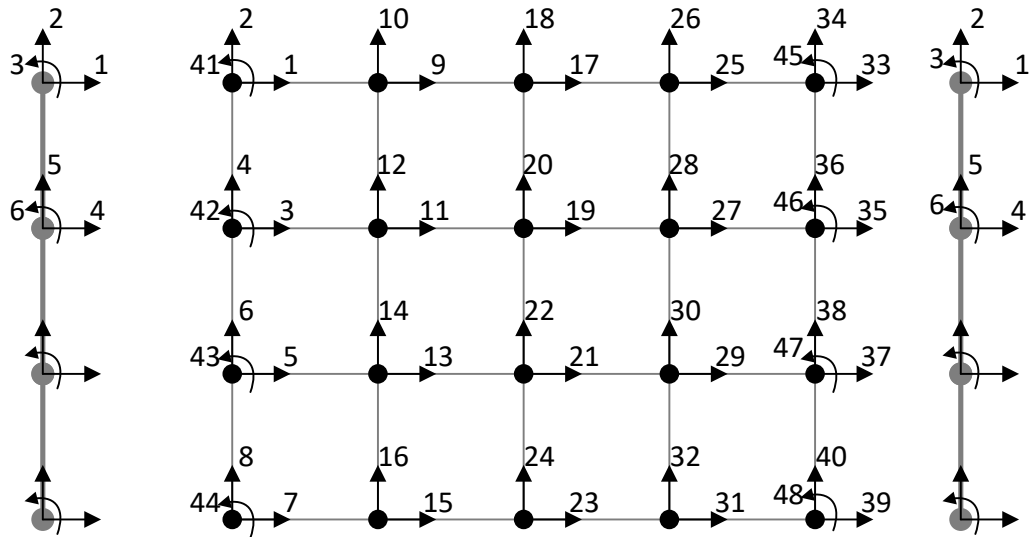
Figure 4.6 Combination of beam and continuum finite elements.

4.6 Automatic CAD interpretation of optimized designs

The results of GSO consist of massive continuous media and need to be interpreted into classical structural members used in civil engineering, such as 1D (longitudinal beams) or 2D (shells) elements. Thus, a CAD design needs to be provided to the structural engineer. In the past, Lin and Chao [60] used image-processing techniques to extract the external boundaries of the binary image and predefined shapes to design the interior holes. Tang and Chang [119] presented an integrated approach of TO for the design of structural components. The geometry of the optimized structure is translated into smoothed and parametric B-spline curves and surfaces. While, Chacon et al. [23] managed to link the topology optimized designs with CAD software using an IGES translator. One of the major difficulties in TOP is the interpretation and translation of the optimized layouts into CAD models, as shown in Figure 4.7. According to the SIMP method, density values of the FE represent the unknown parameters to be defined; thus, optimized layouts correspond to greyscale images, corresponding to the various values of the density in the range of [0,1]. However, when trying to interpret the optimized domains there are two options: either no material is allocated to a specific FE (density value equal to 0) or material is assigned to the element (density value equal to 1). In order to generate a CAD model, the first step
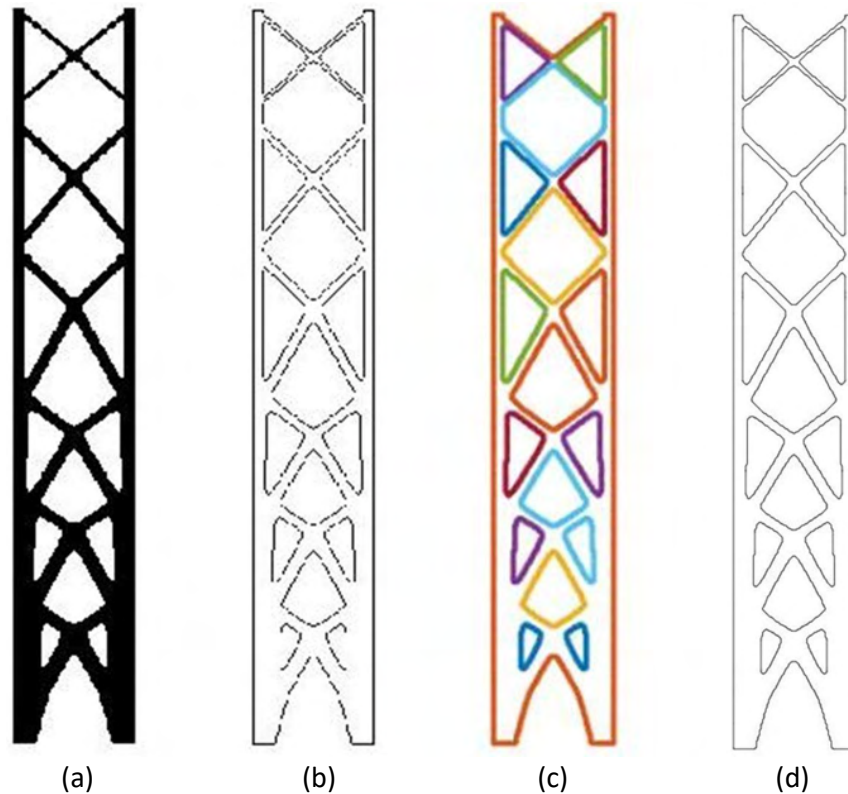
Figure 4.7 BF test example: Automatic interpretation of the optimized layout: (a) bitmap image, (b) boundary image, (c) connecting component labelling and (d) final CAD NURBS interpolated domain.

is to convert the density matrix into a bitmap image. This is performed with the use of a density threshold value, i.e. density value equal to 1 is assigned to the elements that in the optimized layout converged to density values above this threshold and density value equal to 0 is assigned to the rest ones.

In the following part of the study, a fully automated design methodology based on TOP is described, integrating also the interpretation step. Image processing methods are used in order to derive automatically the shape of the optimized layout, NURBS are used to interpolate the points (nodes of the mesh) extracted and an IGES translator is applied in order to produce a file compatible with many CAD software. The first step that needs to be taken into account, in such a fully automated design methodology, is to identify the boundaries of the bitmap image [40]. In this step, a boundary detection algorithm that identifies the coordinates of the nodes lying on the boundaries between black and white

elements is applied. The boundary of a set A, denoted by $\beta(A)$, can be obtained by eroding first A by B and then calculating the difference between A and its erosion, as expressed:

$$\beta(A) = A - (A\Theta B) \tag{4.21}$$

where B is a proper structuring element (see Figure 4.8).

The next step is to separate the points of the shapes connected to imaginary lines into distinct matrices, this is performed by the so called "connected-component labelling" [40] procedure. Extracting connected-components out of a binary image is a task of major importance in many automated image analysis applications. Let A be a set containing one or more connected-components and the array X_k (of the same size with array A), composed by 0s and 1s, is created according to the following rule: all its elements are set equal to zero (background values) except those that the corresponding elements in A belong to a connected-component, which are set equal to one (foreground values). This
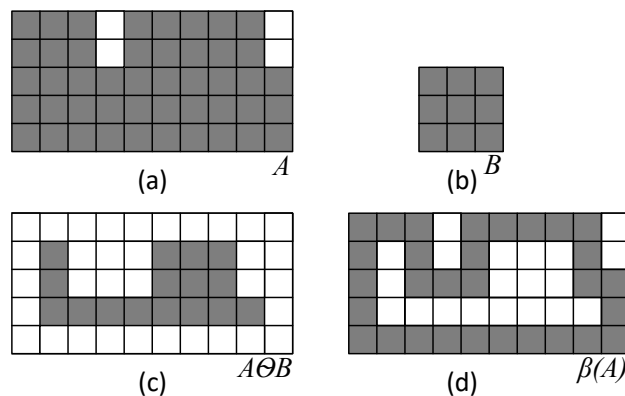
Figure 4.8 Boundary extraction: (a) Set A, (b) structuring element B, (c) A eroded by B and (d) boundary calculation as subtraction between set A and its erosion.

can be seen in see Figure 4.9, where the objective is to map the connected-components of A into the values of the elements of X_k. The following iterations describe this procedure:

$$X_k = [X_{k-1} \oplus B] \cap A, \qquad k=1,2,3,... \tag{4.22}$$

where B is a suitable structuring element. In this phase, the pixel elements of the boundary image are classified into different categories according to the region they belong to and the coordinates for the centroid of each pixel element are defined.
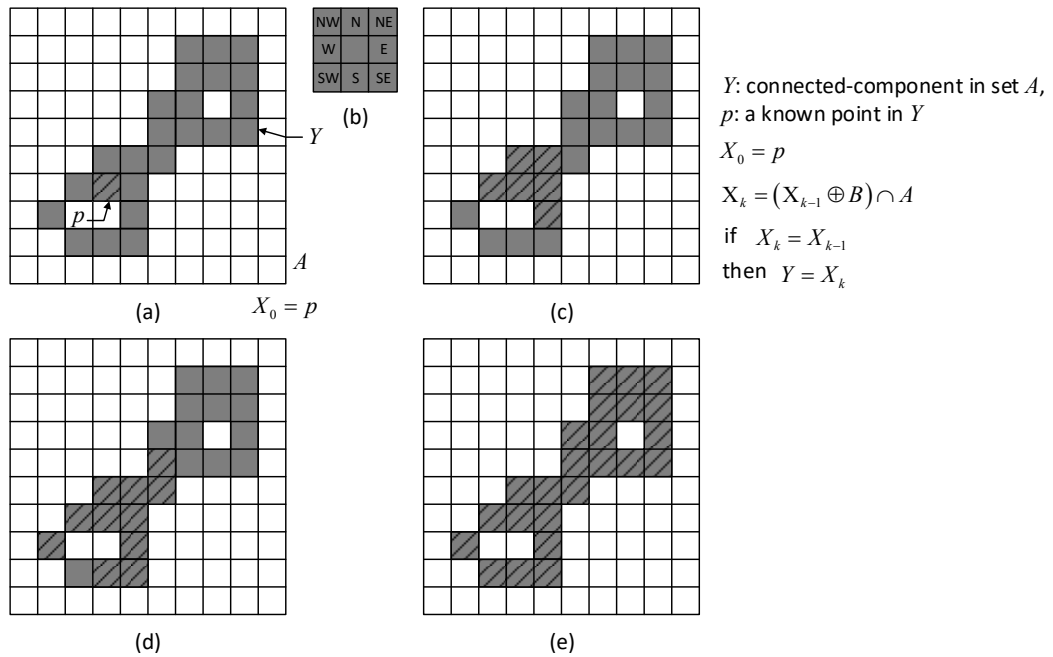
Figure 4.9 Connected-component labelling: (a) Sets A, X_0 composed by initial point p (denoted with the single shaded pixel, all grey pixels but not shades denote the elements of A that are equal to 1, but not yet labelled as connected-components), (b) basic structuring element, (c) result of first iterative step, (d) result of second step and (e) final result (all connected-components have been labelled).

So far, the points along the boundaries are classified in groups according to the connected-component they belong to, however, they are not positioned in the correct order. For this purpose, a sorting procedure is applied aiming to capture the proper design with the interpolation scheme. This problem is formulated as a travelling salesman problem. Yet, specific limitations exist for the points of the bitmap image, since they correspond to nodes of the FE mesh. More specifically, as shown in Figure 4.9(b), initiating from an arbitrarily selected centroid point p, the identification process for the next point is limited to the eight neighboring elements' centroids (i.e. the adjacent elements denoted as W, S, N, E, NE, NW, SE, and SW, in Figure 4.9(b)). Then a procedure is

developed, aiming to separate between points that are interpolated using lines and those that splines are used. The first step of this procedure is to calculate the gradients of the lines that connect two adjacent nodes. Then, a limit number of repeated similar gradients is set that defines which boundaries should be modelled with lines (horizontal or vertical) and the rest boundaries are interpolated with splines. Before applying the interpolation scheme, for the centroids of the second category (i.e. splines) a smoothening phase needs to be implemented in order to avoid sharp edges. This is achieved using weight coefficients (w_i) for modifying the coordinates of the centroids used for deriving the interpolation curves by means of a simple expression:

$$\tilde{P}_j = \frac{1}{2m+1} \sum_{i=-m}^{m} w_i P_{j-1}, \quad j = 3{:}n-2 \tag{4.23}$$

where $2m$ is the number of adjacent centroids (in the current study $m = 4$ and $w_i = 0.2$) whose contribution is considered in Eq. (4.23), $\tilde{P}_j$ denotes the modified coordinates of jth centroid and $n + 1$ the total number of the curve's points. In order to attain a smooth and precise boundary of the geometry, the mathematical model of NURBS is used. NURBS offer great flexibility in 3D-modeling along with the advantages that bring the design through control points, enabling to achieve complex shapes.

A NURBS curve is defined by its order, the set of weighted control points and a knot vector. NURBS curves represent generalizations of both B-splines and Bézier curves and surfaces. The primary difference is the use of weighted control points, which makes NURBS curves more rational (non-rational B-splines are a special case of rational B-splines) [17,85]. NURBS basis function is defined as follows:

$$R_{i,p}(\xi) = \frac{N_{i,p}(\xi)\omega_i}{W(\xi)} = \frac{N_{i,p}(\xi)\omega_i}{\sum_{j=1}^{n} N_{j,p}(\xi)\omega_j} \tag{4.24}$$

where $N_{i,p}(\xi)$ denotes the ith ∈-spline basis function of order p and $\omega_i, (i = 1,2,\cdots,n)$ is the set of n positive weight coefficients. Given a knot vector $\Xi = [\xi_1, \xi_2, \cdots, \xi_{n+p+1}]$, the B-spline basis functions are defined recursively starting with the zero-order basis function ($p = 0$) given by the Cox-de Boor formula, as expressed in the following:

$$N_{i,p}(\xi) = \frac{\xi - \xi_i}{\xi_{i+p} - \xi_i} N_{i,p-1}(\xi) + \frac{\xi_{i+p-1} - \xi}{\xi_{i+p+1} - \xi_{i+1}} N_{i+1,p-1}(\xi) \tag{4.25}$$

The multiplicity of the first and last knots of Ξ is of the $p + 1$ order. A NURBS curve is given by the following expression:

$$C(\xi) = \sum_{I=1}^{n} R_{I,p}(\xi) P_I \tag{4.26}$$

where n denotes the number of basic functions and $P_I \in R^d$ are the control points (where d is the number of spatial directions).

Once the interpolation scheme of the optimized layout is applied, then it is necessary to be translated into a file format able to be imported into a CAD/CAE software. For this purpose, an automatic procedure is developed able to translate the geometry information (coordinates, control points, etc.) into an IGES file format. The IGES file is a vendor-neutral file format that allows the digital exchange of mechanical engineering model data [17] among CAD systems. An IGES file is composed by 80-character American Standard Code for Information Interchange (ASCII) records, divided into 3 columns. The Hollerith format is used to represent text strings and the file is divided into five sections: (i) Start, (ii) Global, (iii) Directory Entry, (iv) Parameter Data, and (v) Terminate, indicated by the characters S, G, DE, PD, and T respectively. The characteristics and geometric information for an entity is split between two sections; one in a two record, fixed-length format (i.e. the directory entry section), the other in a multiple record, comma delimited format (i.e. the parameter data section), as can be seen in a more human-readable representation of the file.

4.7 Numerical examples

Herein, two groups of BF systems are examined and manufacturing constraints are imposed as discussed in section 4.5. The following parameters required to formulate the TOP are used in all cases examined: $nel_x = 80, nel_y = 480$, as suggested the value of p used in Eq. (4.2) is set equal to 3 and density filtering is applied with filter size $r_{min} = 3$.

Figures 4.10 and 4.11 show the optimized layouts achieved for the case of the BF design when using different volume fraction values. The volume fraction used to obtain the domains of Figure 4.10 is set equal to 20%, while for the domains of Figure 4.11 is set equal to 40%. It can be noticed, from these figures that low volume fraction (i.e. 20%) results into truss-like optimized layouts having larger amount of material volume allocated to the bottom half domain. Comparing, the optimized layouts (for example, comparing Figures 4.10(a) and 4.11(a)) it can be observed that although the volume fraction is significantly different, the upper half of the resulted designs is almost the same while the bottom half is totally different, due to high stress concentration at the bottom half.

An observation that worth mentioning also is that the width of the non-optimizable areas ($width_{no}$) has a significant impact on the final design. In the current study, the $width_{no}$ is increased proportionally to the increase of the volume fraction. For the domains of Figures 4.10(b), 4.10(e), 4.11(b) and 4.11(e) the following parameters are considered: (a) $f_{VolFrac} = 20\%$, $width_{no} = 4$ and (b) $f_{VolFrac} = 40\%$, $width_{no} = 8$. For the second case, it can be seen that despite the fact that the width of the non-optimizable areas is
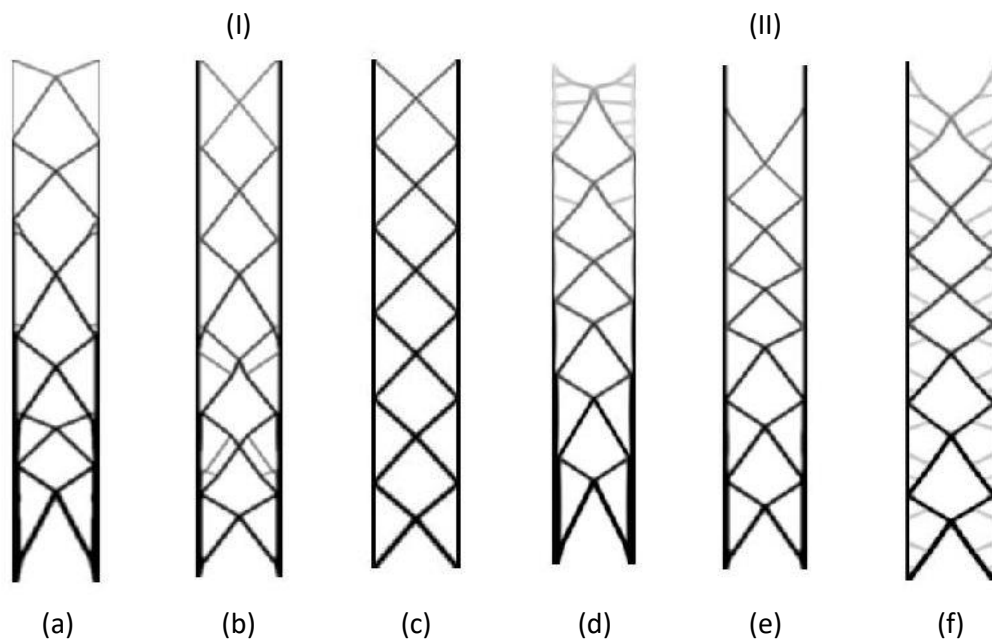
Figure 4.10 BF test example: Optimized layouts ($f_{VolFrac} = 20\%$): I. Concentrated nodal forces: (a) basic case, (b) non-optimizable areas and (c) beam elements. II. Both sides distributed loading: (d) basic case (e) non-optimizable areas and (f) beam elements.
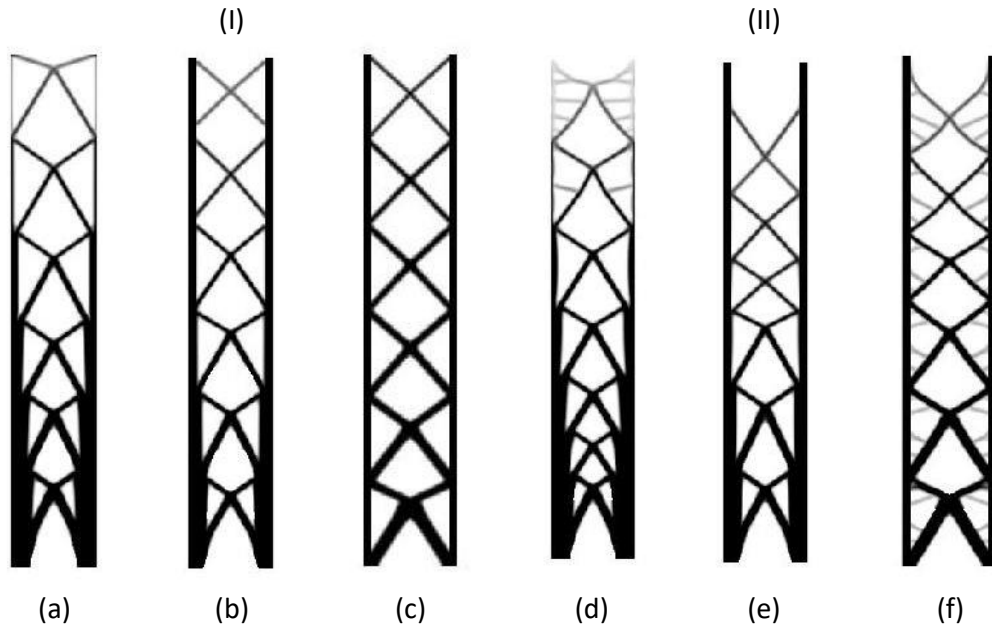
Figure 4.11 BF test example: Optimized layouts ($f_{VolFrac} = 40\%$): I. Concentrated nodal forces: (a) basic case, (b) non-optimizable areas and (c) beam elements. II. Both sides distributed loading: (d) basic case (e) non-optimizable areas and (f) beam elements.

set equal to 8, the width of the vertical structural members of the optimized layout close to the fixed edge, is even larger. In addition, despite the different values of parameter $width_{no}$ that was used for the two $f_{VolFrac}$ values, varying cross-sectional areas are developed in the vertical structural members for both values. In all cases the height of the non-optimizable areas is equal to 480. Worth mentioning that in the above described numerical examples, the elements' properties and the loads' magnitude are taken equal to one, similar to every typical TOP [96].

One issue of major importance for the implementation of the combination of continuum with beam elements case, is that the contribution of the beam elements volume needs to be taken also into account when compared for a specific volume fraction used in the other two cases where Q4 elements are used only. Furthermore, instead of using the parameter that designates the width of the non-optimizable areas ($width_{no}$) corresponding to the Q4 elements, a new one is introduced denoting the width of the non-optimizable beams ($Bwidth_{no}$). In this case, the material properties and the loads have taken real world values (not the imaginary value one mentioned previously), since

the contribution of every FE type is required on the mechanical behaviour of the structural system. Specifically, the Young's modulus of both 4Q elements and beam elements is equal to $E = 200GPa$ (steel ASTM-A36), while the magnitude of the distributed load is $P = 5\frac{kN}{m}$. In addition, the moment of inertia for the beam elements is equal $I = 7.8 \cdot 10^{-5}m^4$ and the values of the cross-sectional area depend on the final volume fraction of the desired design and are defined by the designer. In Figures 4.10, 4.11 (c) and (f) the following parameters are considered: (a) $f_{VolFrac} = 20\%$, $Bwidth_{no} = 4$, $area = 0.021m^2$ and (b) $f_{VolFrac} = 40\%$, $Bwidth_{no} = 8$, $area = 0.05m^2$.

Following the computational investigation and automatic interpretation into a CAD model, which represent major importance tasks for the TO aided conceptual design framework of civil structures presented herein, the IGES files are created. Particularly, in Figure 4.12 the proposed BF systems for $f_{VolFrac} = 40\%$ are illustrated, by importing the IGES files into the commercial software AutoCAD [8]. It is observed that the final layout is very accurate and close to a shape that could have been designed manually.

(a)   (b)   (c)
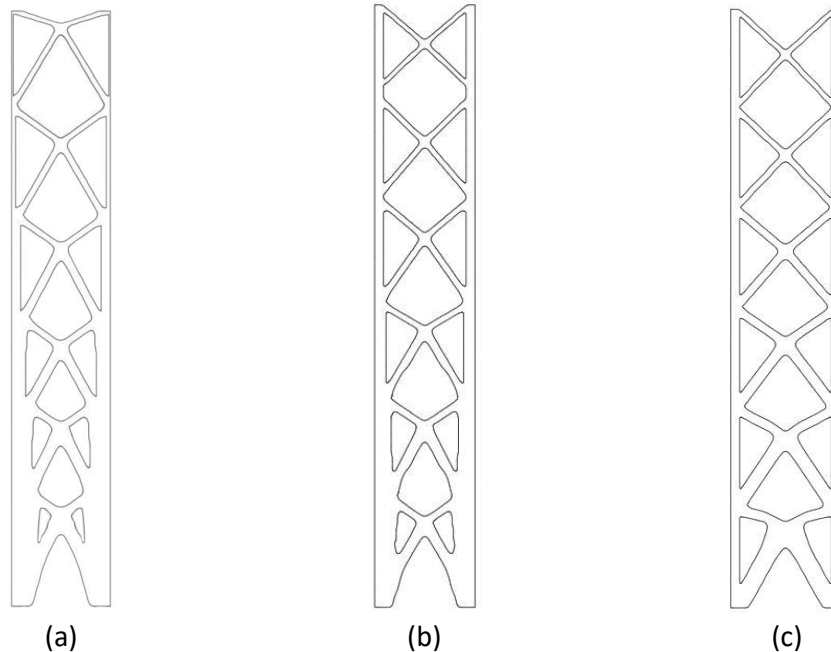
Figure 4.12 Automatic interpretation of the optimized layout ($f_{VolFrac} = 40\%$) for concentrated nodal forces: (a) basic case, (b) non-optimizable areas and (c) beam elements

CHAPTER 5

Conceptual design of structural systems based on topology optimization and prefabricated components

5.1 Introduction

As it is stated in the previous, STO techniques are more difficult to be implemented in the AEC industry as opposed to other industrial applications. This can be justified by the complexity of the architectural conceptual design process and the engineering intuition required to support the outcome of the conceptual process part as well as the design code regulations. The design process for the case of structures (buildings, bridges, hangars, etc.), ranging from the stage of conception of the form to the selection of the structural system and subsequently the design steps, represent a multi-disciplinary process where many disciplines are involved, such as structural engineering, ecological/bioclimatic design, acoustic performance, etc. Parametric design represents an algorithmic thinking-based procedure, where geometry is generated through the expression of parameters and the relations between each other; it allows to discover a range of possible solutions through the variability of the parameters. Well-known architects and engineers have adopted such techniques, e.g. Antonio Gaudi, Frei Otto, Heinz Isler, Pier Luigi Nervi and Heinz Isler [79,2,50] Adriaenssens et al. [3] investigated extensively the history of form finding techniques and optimization from the analogue models in the early 20th century until recently through the wide spread of CAD, Computer-Aided Manufacturing (CAM) and visual programming applications like Grasshopper [41].

In this chapter, aiming to take advantage of the key feature of STO in order to develop structural systems composed by prefabricated units, a novel STO based conceptual design approach is introduced, taking advantage also of the parametric design techniques and tools. The proposed methodology is an alternative, especially in cases where the structural system is composed by multiple components selected out of a discrete set.

113

Additionally, the structural elements of larger scale structural systems can be fabricated using adaptive mechanisms or especially manufactured formworks. Such a procedure ensures that a discrete set of prefabricated specifically shaped units will be generated. The novelty of the proposed methodology focuses on the distribution of a discrete set of specifically shaped units that are inscribed in rectangular FEs. These units are treated as periodic shaped units distributed over the design domain, with reference to the area (2D)/volume (3D) of the predefined shapes. In the sense that a limited size group of units are repeated in the design domain. One part of the proposed methodology, that is referred to the optimization procedure and the Finite Element Analysis (FEA), is developed in MATLAB code, while the parametric design module is developed in Grasshopper environment. Additionally, a 3D hangar structure and a braced tube structural system are produced within the proposed procedure and their fully automated CAD interpretation is highlighted.

5.2 Periodic Shaped Units based Topology Optimization (SUTO)

One of the most significant stages of the TOP formulation is the definition of the manufacturability constraints especially in the framework of architectural conceptual design. In smaller scale type of structures, TO can be integrated well with Additive Manufacturing (AM), making possible the development of complex structural system as a whole, e.g. the frame of a motorbike was 3D printed using aluminum alloy [20]. The application of TO in AEC industry is significantly more complex due to the various limitations imposed in the design process but also due to the larger scale of the corresponding structural systems that cannot be fabricated as a whole by means of AM. In such cases, TO was mainly used as a design tool and the manufacturing process was not included in an explicit manner, e.g. the Akutagawa River Side project where the walls were made of Reinforced Concrete (RC) using custom made formworks [52]. In case that parametric design was combined with density-based TO for designing structural systems, where the result of the conventional TOP formulation of Eq. (4.1) was translated into structures composed by shaped units, there is a major disadvantage; the translation part

requires engineering intervention and personal interpretation. In the current chapter a novel methodology is presented that is based on the idea of replacing the FE of the discretized design domain with periodic shaped units. These units correspond to discrete specifically shaped units manufactured either by means of AM or as prefabricated components using especially manufactured formworks.

5.2.1 The problem formulation

In this chapter, the main objective is to develop structural systems composed of prefabricated structural element using a TOP formulation as the means to optimally distribute material over the design space; with no modification on the proposed methodology 3D printed structural elements can be used as well. More specifically the scope of the study is to optimally distribute specifically shaped structural elements selected from a predefined discrete design set. Thus, instead of distributing material using density values and decide whether a FE exists or not, in the proposed methodology a number of predefined shaped units, representing the components of the discrete design set, are distributed. The shape of the predefined structural components defining the discrete design set is decided first by the designer; a variety of different shaped units can be selected and consequently several candidate designs can be delivered on the basis of the generative design concept. In this manner, interesting architectural forms can be derived that cannot be achieved through conventional methods. Thus, the proposed methodology can be a powerful tool for the architect/engineer in the phase of conceptual design; e.g. when designing a structural system for supporting specific functionalities (like shading). Aesthetic is the criterion adopted in this study for choosing the prefabricated units; if another criterion is used instead, the proposed methodology can also be used for deriving optimal distribution of the selected (by means of any criterion) predefined shaped units. More specifically, modifications on the formulation that is adopted in the current study can be used, for example in order to influence the shading that a shelter or a wall will provide. Additionally, manufacturability preferences can also be implemented

by means of the shaped units selected by the user and possibly other needs that the architect/engineer might desire.

In this part of the study, the fundamental modification on the TOP formulation for the needs of the proposed methodology is presented that originates from its basic concept that is to use the Q4-based (for 2D structural systems) or hexahedral-based (for 3D structural systems) FE mesh discretization and then to assign predefined structural elements to the components of the FE discretization. The mathematical formulation of the periodic shaped unit-based TOP is presented below:

$$\min_{sh_e} C(sh_e) = F^T u(sh_e) = u(sh_e)^T K(sh_e) u(sh_e) \tag{5.1a}$$

$$s.t. $$

$$K(sh_e)u(sh_e) = F \tag{5.1b}$$

$$\frac{V(sh_e)}{V_0} = f_{VolFrac} \tag{5.1c}$$

$$\sum_{e=1}^{N_{ele}} a_e \leq V_0 \tag{5.1d}$$

$$sh_e \in A_{SH} = \{SH_i, i = 1,2,\dots,m\} \tag{5.1e}$$

Without limiting the applicability of the proposed methodology, the compliance of the system $C(sh_e)$ is the objective function of the problem, similar to the SIMP problem formulation, (see Eq. (4.1)). The equality constraint refers to the equilibrium equations and V_0 is the volume of the initial domain. The basic variation of the problem formulation of Eq. (5.1) stems from the design variables. In particular, the design variables refer to the shaped unit sh_e assigned to each element e. They are chosen out of a discrete design set A_{SH} that is composed by m prefabricated shaped units SH_i that correspond to different areas a_i. The design set composed by the predefined shaped units represents the aesthetic intervention of the architect/engineer in the problem formulation of Eq. (5.1). Although single loading cases are presented in the numerical tests section, worth

mentioning also that multiple loading case can easily be treated by the proposed SUTO methodology.

5.2.2 The methodology

The basic algorithmic parts of the proposed methodology are described in detail in this section.

Definition of the discrete design set

The first part of the proposed methodology is the development of the discrete design set. In the current implementation of the methodology specific shaped units are used, without loss of generality, they need to be inscribed into a predefined rectangular of specific size that is selected at the beginning of the implementation; since it is rather straightforward how it can be extended. This is due to the fact that the design domain is discretized with a structured FE mesh, based on a rectangular (or solid) FE of specific size, this size depends on how fine or not the mesh discretization needs to be. The TO procedure will be based on the guiding grid selected initially. The size of the grid is pre-requisite parameter information, since it is defined based on the dimensions of the prefabricated structural elements of the design set A_{SH}. Thus, the units composing the design set need to have 4 nodes at their edges coinciding with the 4-node of the Q4 element for the case of the 2D test examples, as it can be seen in Figure 5.1. For the case of the 3D test examples, hexahedral elements are used, having the same layout with that of the Q4 element. In order to allow using various shaped units, they should be able to be transformed into 4-node equivalent Q4 elements or 8-node solid ones (for the 3D case). In this manner a variety of different structural elements can be derived and satisfy the requirements of the conceptual design. For reasons of manufacturability, the proposed methodology is implemented based on structured FE guiding mesh discretization of the design domain (i.e. rectangular or triangular mesh type).

In the current study the discrete design set is composed by $m = 10$ different star shaped units that will be used in the implementation presented below. A parametric study is

performed in order to derive gradually decreasing areas for the m components of the design set as it is shown in Figure 5.2. More specifically a line is drawn from the middle of each side to the centroid of the rectangle, the midpoint is set as the parameter and it is divided in ten equal segments. The parameter takes such values so that a shaped unit with the minimum area is not an empty shape and the shape with the maximum area will
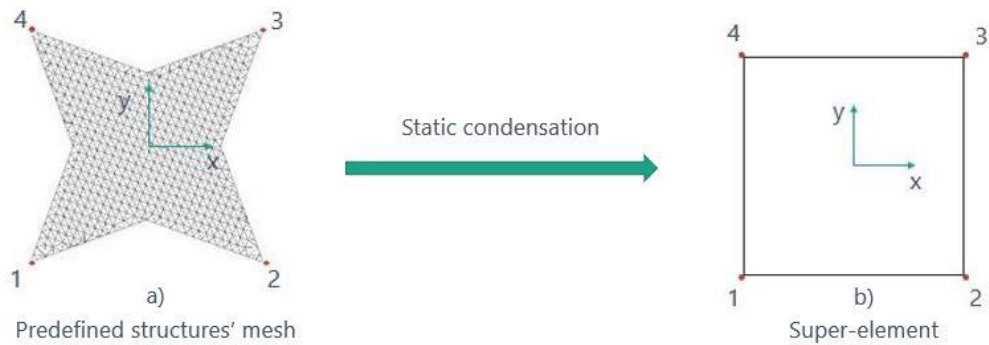
Figure 5.1 Definition of the design set: (a) Predefined FE mesh of a specific predefined periodic shaped units, (b) equivalent quadrilateral FE
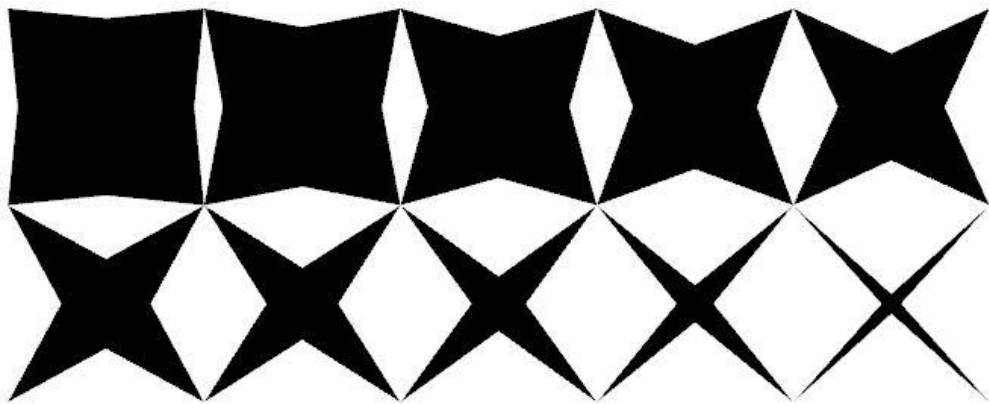
Figure 5.2 Parametric study for ten predefined periodic shaped units.

not be a rectangle. The area of the full rectangle is $a_{rec} = 1$, while the limits of the shaped units' areas are $a_{min} = Area(SH_{m=10}) = 0.1$ and $a_{max} = Area(SH_1) = 0.9$. By definition, the implementation of the proposed methodology described in this study, does not allow regions without any material to be developed. For the specific implementation, generating regions without material would not be either functional or manufacturable. This is without loss of the generality of the proposed methodology, since

the methodology can lead to solutions having regions without material if the problem/formulation requires.

Generation of the equivalent Q4 FEs

Given that the discrete design set was developed, the next part of the methodology is to derive equivalent FE for each component of the design set. The description will be limited, without loss of generality, to 2D structural elements. The implementation of the proposed methodology relies on equivalent rectangular Q4 elements. The stiffness matrix of a Q4 plane stress FE corresponds to a matrix with size 8×8:

$$K_e^{Q4} = \begin{bmatrix} k_{11}^{Q4} & \cdots & k_{18}^{Q4} \\ \vdots & \ddots & \vdots \\ k_{81}^{Q4} & \cdots & k_{88}^{Q4} \end{bmatrix} \tag{5.2}$$

Thus, the predefined specifically shaped units (those shown in Figure 5.2) need to be transformed into equivalent rectangular Q4 elements. The procedure for generating equivalent rectangular Q4 elements initiates with the discretization of each shaped unit of the design set (A_{SH}) using an unstructured mesh generator. For this purpose, three node plane stress triangular elements are used and the global stiffness matrix of each shaped unit, of the design set, is assembled. The number of the DOFs in each predefined specifically shaped unit might be different depending on the quality of the FE mesh discretization. Subsequently, the 8×8 stiffness matrices of the equivalent rectangular Q4 elements are derived by means of the static condensation method. In various studies, reduced model technics were implemented that rely on static condensation [88,81]. Assume that the DOFs that are to be eliminated are denoted as *e* and the remaining ones denoted as *c* are those to be condensed. According to this notation the equilibrium equations for each predefined specifically shaped unit, can be written using partitioned matrices as follows:

$$\begin{Bmatrix} F_e \\ F_c \end{Bmatrix} = \begin{bmatrix} K_{ee} & K_{ec} \\ K_{ce} & K_{cc} \end{bmatrix} \begin{Bmatrix} u_e \\ u_c \end{Bmatrix} \tag{5.3}$$

Multiplying the system in Eq. (5.3) yields the following equations:

$$K_{ee}u_e + K_{ec}u_c = F_e \tag{5.4}$$

and

$$K_{ce}u_e + K_{cc}u_c = F_c \tag{5.5}$$

Solving Eq. (5.4) for the vector u_e and substituting it in Eq. (5.5) leads to the following:

$$u_e = K_{ee}^{-1}(F_e - K_{ec}u_c) \tag{5.6}$$

and

$$(F_c - K_{ce}K_{ee}^{-1}F_e) = (K_{cc} - K_{ce}K_{ee}^{-1}K_{ec})u_c \tag{5.7}$$

Eq. (5.7) can be re-written in compact form as:

$$\bar{F}_c = \bar{K}u_c \tag{5.8}$$

where

$$\bar{K} = K_{cc} - K_{ce}K_{ee}^{-1}K_{ec} \tag{5.9}$$

The condensed stiffness matrix $\bar{K}$ of Eq. (5.9) corresponds to the stiffness matrix of an equivalent rectangular Q4 element. The nodes of the resulting equivalent rectangular Q4 elements, coincide with the condensed 4 nodes of the discretized predefined specifically shaped units.

$$K_{sh}^i = \begin{bmatrix} k_{11}^i & \cdots & k_{1n}^i \\ \vdots & \ddots & \vdots \\ k_{n1}^i & \cdots & k_{nn}^i \end{bmatrix} \rightarrow \bar{K}_{sh}^i = \begin{bmatrix} \bar{k}_{11}^i & \cdots & \bar{k}_{18}^i \\ \vdots & \ddots & \vdots \\ \bar{k}_{81}^i & \cdots & \bar{k}_{88}^i \end{bmatrix} \tag{5.10}$$

$$n = depending\ on\ mesh\ quality, \quad i = 1,2,\dots,m$$

Eq. (5.10) shows the procedure of transforming the global stiffness matrix K_{sh}^i of the discretized shaped unit having n DOFs in total, to that of its equivalent rectangular Q4 element $\bar{K}_{sh}^i$, for each one of the m components of the discrete design set. Thus, the proposed TO procedure can rely on the equivalent rectangular Q4 elements derived based on the structured FE mesh discretization of the design domain initially generated.

Solution of the TOP based on regression analysis

The solution of the TOP requires assembling the global stiffness matrix that corresponds to the form of the design domain resulted, with respect to the values of the design variables for each step of the SIMP approach. Thus, the area values are generated during the steps of the SIMP approach of the equivalent Q4 elements of the FE mesh discretization adopted for the design domain need to be associated to the predefined specifically shaped units out of the discrete design set. Therefore, the area values (in the range a_{min} to a_{max}) generated by the mathematical algorithm (i.e. OC or MMA) need to be translated into discrete prefabricated shapes out of the design set. The first part of this process is to perform regression analysis. For this purpose, a polynomial curve is fitted and in particular a 4-degree polynomial is implemented, as it shown in the following equation:

$$f_{ij}^e(a_e) = a_{ij}a_e^4 + b_{ij}a_e^3 + c_{ij}a_e^2 + d_{ij}a_e + e_{ij} \qquad (5.11)$$

$$\tilde{k}_{ij}^e = f_{ij}^e(a_e) \qquad (5.12)$$

where a_{ij}, b_{ij}, c_{ij}, d_{ij}, e_{ij} are the coefficients of the polynomial curve, representing the unknown variables, and a_e is the area of the eth element. More specifically, regression analysis is performed for every independent coefficient of the stiffness matrix taking advantage of its symmetry. As it is indicatively shown in Figure 5.3 for the case of the $\tilde{k}_{11}^e$ stiffness coefficient, the abscissa (*X*-axis) of the diagram corresponds to the area and the ordinate (*Y*-axis) denotes the value of $\tilde{k}_{11}^e$ stiffness coefficient. As it is shown in Figure 5.3, through regression analysis a 4-degree polynomial was fitted to the values of the $\tilde{k}_{11}^e$ stiffness coefficients corresponding to the equivalent rectangular Q4 elements of the $m = 10$ prefabricated shapes out of the design set. Without loss of generality for the examples presented herein, rectangular Q4 elements were chosen, thus the size of the stiffness matrices is 8×8 and the procedure is repeated for every independent coefficient of the

Figure 5.3 Regression analysis for the stiffness index $\tilde{k}_{11}^e$ and schematic representation of the stiffness coefficient assignment.

stiffness matrix, taking advantage of the symmetry of the stiffness matrix and the identical components of the stiffness matrix. Thus, all the coefficients of the equivalent element's stiffness matrix can be calculated, for every element of the design domain's mesh.

$$\widetilde{K}_e^{sh} = \begin{bmatrix} \tilde{k}_{11}(a_e) & \cdots & \tilde{k}_{18}(a_e) \\ \vdots & \ddots & \vdots \\ \tilde{k}_{81}(a_e) & \cdots & \tilde{k}_{88}(a_e) \end{bmatrix} =$$

$$= \begin{bmatrix} \tilde{k}_1(a_e) & & & & & & & \\ \tilde{k}_2(a_e) & \tilde{k}_3(a_e) & & & & SYM & & \\ \tilde{k}_4(a_e) & \tilde{k}_5(a_e) & \tilde{k}_1(a_e) & & & & & \\ -\tilde{k}_5(a_e) & \tilde{k}_6(a_e) & -\tilde{k}_2(a_e) & \tilde{k}_3(a_e) & & & & \\ -\tilde{k}_1(a_e)/2 & -\tilde{k}_2(a_e) & \tilde{k}_7(a_e) & \tilde{k}_5(a_e) & \tilde{k}_1(a_e) & & & \\ -\tilde{k}_2(a_e) & -\tilde{k}_3(a_e)/2 & -\tilde{k}_5(a_e) & \tilde{k}_8(a_e) & \tilde{k}_2(a_e) & \tilde{k}_3(a_e) & & \\ \tilde{k}_7(a_e) & -\tilde{k}_5(a_e) & -\tilde{k}_1(a_e)/2 & \tilde{k}_2(a_e) & \tilde{k}_4(a_e) & \tilde{k}_5(a_e) & \tilde{k}_1(a_e) & \\ \tilde{k}_5(a_e) & \tilde{k}_8(a_e) & \tilde{k}_2(a_e) & -\tilde{k}_3(a_e)/2 & -\tilde{k}_5(a_e) & \tilde{k}_6(a_e) & -\tilde{k}_2(a_e) & \tilde{k}_3(a_e) \end{bmatrix} \quad (5.13)$$

$$a_e \in A, \qquad A = [a_{min}, a_{max}]$$

where $\tilde{k}_{ij}^e \equiv \tilde{k}_{ij}(a_e)$ denote the stiffness coefficients, derived through the regression curve of Eq. (5.11), while 8 are the independent terms of the stiffness matrix shown in Eq.

(5.13). Furthermore, the derivative of the equivalent element's stiffness matrix, which is required for the sensitivity analysis, is evaluated through the following equation:

$$\frac{d\tilde{k}_{ij}^e}{da_e} = \frac{df_{ij}(a_e)}{da_e} = 4a_{ij}a_e^3 + 3b_{ij}a_e^2 + 2c_{ij}a_e + d_{ij} \qquad (5.14)$$

3D type of structures - solid FEs

The Q4-based FE mesh discretization of the design domain and its equivalent Q4 elements, are used in order to present the proposed methodology described previously. Deriving interesting and innovating hangar-type structural systems such as plates, roofs and domes was the main motivation to develop the proposed methodology. For this reason, the methodology is also enriched with structural elements to be used in hangar-type of structures. For this purpose, similar to the 2D case, the design domain is discretized with a structured FE mesh based on cubic FE of specific dimensions, that depend on how fine or not the mesh discretization needs to be. In particular 3D solid FE having three translational DOFs in each node are used. One layer of elements is generated along the *Z*-axis (perpendicular to the plan view) for discretizing the design domain for the hangar-type of structures; depending on the use of the structure the width of this direction is relatively small or very-small comparing with the other two dimensions. The plan views of the predefined shaped units are those shown in Figure 5.2, having a small thickness equal to $0.01m^2$ and the dimensions of the inscribed hexahedron's plan view is 1×1 dimensionless unit length.

For reasons of manufacturability, the initial guiding mesh discretization of the case of the 3D problems is also structured and an 8-node hexahedron FE is used as the reference element. The procedure is similar to that described for the 2D case. Each shaped unit is discretized using 6-node pentahedron FEs generated using an unstructured mesh generator and the global stiffness matrix for every shaped unit is assembled. Subsequently the stiffness matrix is condensed and 8 nodes are derived through static condensation, corresponding to the nodes of the solid element chosen. Thus, the size of the stiffness matrix for the equivalent hexahedron elements is equal to 24×24. Although

the ultimate goal was to develop by means of the proposed methodology dome structure, its applicability is tested first into 3D plates. If single curvature shallow hangars are examined, they can be simulated using flat FEs as well. Without loss of generality this is the case that is examined in the current study.

5.2.3 Implementation of the methodology in MATLAB

The proposed methodology was developed based on a home-made MATLAB source code. In particular, all aforementioned procedures are included in the function $[K_e, dK_e] = Fshapes(a_e)$, that was written in order to be integrated with the SIMP method as the material interpolation scheme in the classical TOP formulation. The input argument of the function is the area parameter (a_e) for the eth element and the output argument is the local stiffness matrix (K_e) of each equivalent Q4 or hexahedron FE along with its derivative (dK_e). The global stiffness matrix of the design domain is assembled in the same way as that it is performed in the case of the typical rectangle mesh. Subsequently, the procedure is implemented in the same fashion that is used for the case of the conventional TOP. More specifically, the elasticity problem is solved, the objective function is evaluated, the sensitivity analysis is performed and finally the OC method (or the MMA one) defines new values for the design variables of the problem towards the optimum area of the elements of the FE discretization. In order to allow the algorithm (OC or MMA) to develop its exploration capabilities, $\widetilde{K}_e^{sh}$ is used during the steps of the algorithm instead one of the $\overline{K}_{sh}^i, i = 1,2, \ldots, m$. Therefore, after the convergence of the problem, the values of design variables corresponding to the optimized design will not match to any of the m predefined star shaped units of design set (A_{SH}). However, the optimized structural system needs to be composed as a combination of the predefined shaped units. This is performed after convergence; according to the following expression it is chosen which shaped unit out of the design set (A_{SH}) will be assigned to element e:

$$sh_e = SH_j : dist_j = min(dist = |a_e - a_i|), \qquad i = 1,2, \ldots m \qquad (5.15)$$

Thus, the FEs are assigned to the closest defined predefined star shaped unit; i.e. it is imposed that the design variable instead of being continuous, to take discrete values as it is shown:

$$a_e \in A, \qquad A \equiv A_{cont} = [a_{min}, a_{max}] \Rightarrow A \equiv A_{disc} = \{a_1, a_2, \dots, a_m\} \qquad (5.16)$$

where A_{cont} and A_{disc} denote the continuous and discrete variant of the design set for the area A. In the representation of the structure in MATLAB, different colors for each star shaped unit are used, as it is shown in Figure 5.4. The smallest shape corresponds to yellow color, while the largest on to blue. Furthermore, in Figure 5.5 the flowchart of the proposed methodology along with the conventional one is represented. The red color indicates the procedures that were added in the case of SUTO and the green, the procedures that remain the same. Three new functions are developed that are used before entering the main loop. First, a function in which the design set of the predefined shaped units is defined and the mesh discretization of the units is generated. Second, a function in which static condensation is performed and the third refers to $Fshapes$ function that associates the values of the areas (a_e) with the corresponding stiffness matrix by means of regression analysis. The main loop remains the same as a typical TOP, the crucial difference stems from the part where the elements' stiffness matrix is derived that in the proposed methodology by means of the $Fshapes$ function.
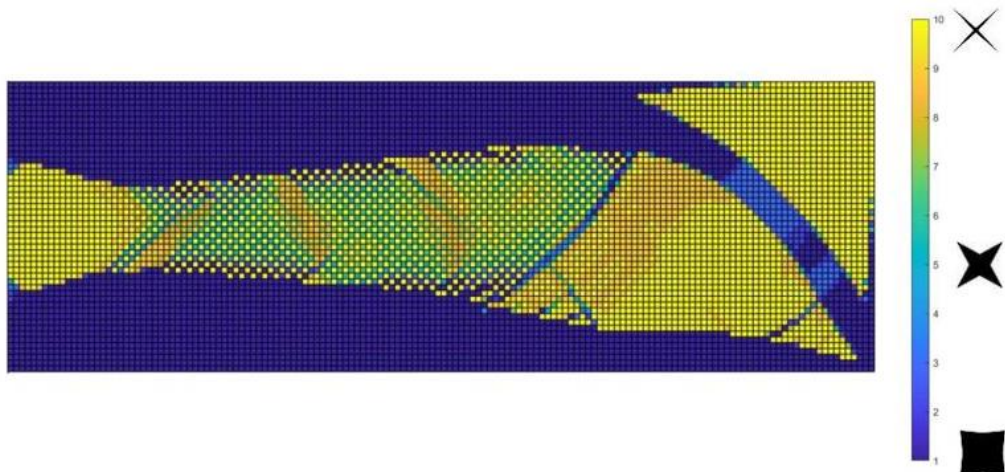
Figure 5.4 Interpretation in MATLAB. Yellow is the smallest shape and blue the biggest.
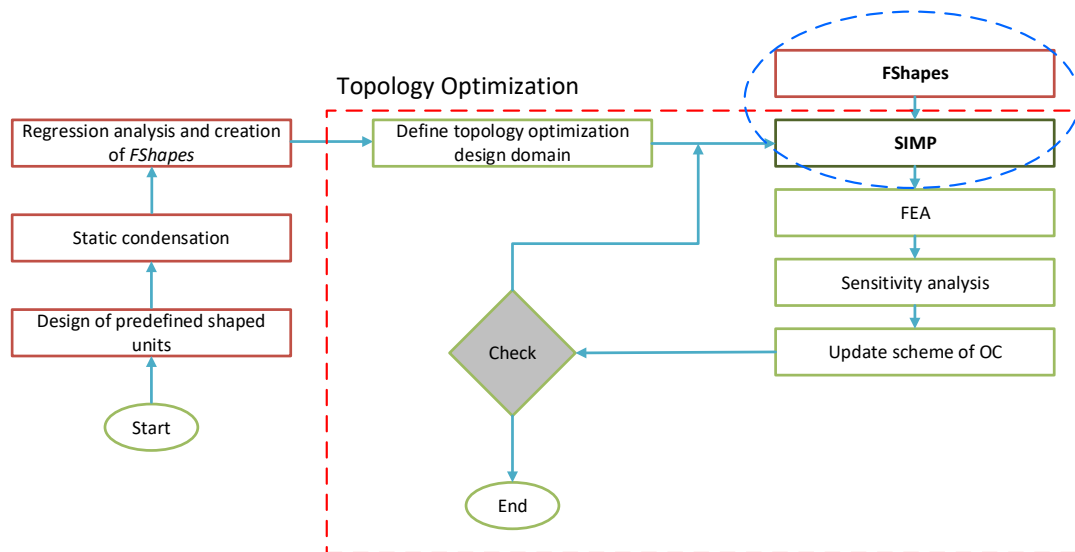
Figure 5.5 Flowchart of both SUTO and SIMP

5.3 CAD interpretation of optimized structural systems

The interpretation phase applied to the design resulted through the optimization procedure, represents a major issue in TO. CAE software solutions that can be used in the interpretation phase are rather few. Furthermore, their capabilities to interact with the TOP formulation or add new constraints are very limited. For this reason, all the new procedures and ideas developed in the framework of the proposed methodology, are integrated using C# programming code with Grasshopper. More specifically, in order to establish the proposed methodology, parametric design technics are combined with TO procedure, relying on the well-known parametric design tool Grasshopper. Tedeschi [121] used Grasshopper in order to present several parametric strategies in the conceptual design stage.

5.3.1 Grasshopper

Grasshopper [41] algorithmic modelling, among others, represents a graphical programming language and provides an environment that is integrated with Rhino3D software [90]. Procedures can be developed by dragging components to the program's canvas. The output of these components is then connected to the inputs of the

subsequent components. Grasshopper was initially used for setting up generative algorithms, such as for generative art. However, due to its capabilities, it is widely applied in parametric modelling for structural engineering, architecture and fabrication problems. The last years an increased number of practitioners (engineers and architects) that are involved in the field of computational mechanics and geometry, not only use the Grasshopper but also develop new plug-ins leading to a huge number of tools that can be applied great variety of problems. For example, *Millipede* [67] focuses on structural analysis and optimization and performs TO using the SIMP approach in order to solve density-based TOP; however, *Millipede* cannot support the needs of the proposed methodology. In this chapter, Grasshopper was used only for defining geometry and generating mesh discretization required along with the interpretation of the optimized structural system. All computations were performed by means of the MATLAB code described before, while the interaction with Grasshopper was implemented with a C# code.

5.3.2 Details on the integration with Grasshopper

The integration of the proposed methodology with Grasshopper is described in this section below, the components of this interaction are shown in Figure 5.6.
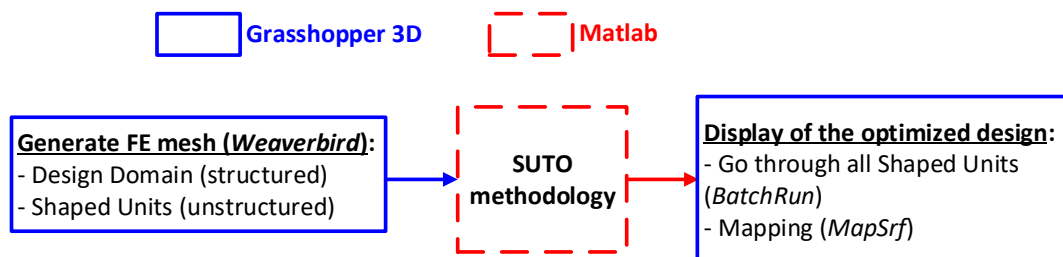
Figure 5.6 Interaction of SUTO methodology with Grasshopper.

The components that need to be combined in order to generate the predefined shaped units, are shown in Figure 5.7(a). In particular a rectangle is created by using the *Point* and *Line* components and the middle points of the edges are set as parameters with the aid of *Series* component. Afterwards the shaped units are created with the *Join* component and the pool composed of the prefabricated units is defined. In this stage, the designer

can change the form of the shaped units and choose the desired ones. Afterwards an unstructured mesh discretization is generated by means of the *Weaverbird* [124] plug-in of Grasshopper, that is used in order to generate triangular elements only, using its *wbTriangles* component. The *Custom Mesh Settings* and *DeMesh* components are also used in order to achieve acceptable mesh quality and decompose it so as to retrieve the node and connectivity information. As it can be seen in Figure 5.7(b) a component is also used to save the coordinates of the nodes and their connectivity into a *txt* file. Subsequently, these data are used to compute the local stiffness matrices and then to assemble the global one of the shaped units of the design set. The specific file format was chosen because it facilitates neutral file exchange and easy to import to MATLAB.

The next step refers to generate the mesh discretization of the design domain. In Figure 5.7(c) it can be seen how a mesh discretization is created for the case of a single curvature shell. More specifically the *Loft* command is used and the surface is generated among the curves we have selected. The mesh generation procedure is similar with the aforementioned one. All above mentioned information concerning the geometry is generated and saved in *txt* files, then it is imported in MATLAB to be used by the source code implementing the proposed methodology. The output of the proposed methodology is also saved into a *txt* file composed of the indexes denoting the optimized distribution of the shaped units into the grid of the design domain.

The next step is also performed using Grasshopper by means of a C# source code and refers to the discretization of the design domain into rectangles as it shown in Figure 5.8(a). In this way, every index of the mesh is identified so every rectangle can be substituted with the optimally selected predefined shaped units. The optimized results that are retrieved from MATLAB, are imported by using the *Read File* component and the *Subset* and *Branch* components are used in order to handle the list of the predefined units. Figure 5.8(b) shows the two basic loops of the program. *BatchRun* component is applied to run through all the predefined shapes and the guiding mesh. When the algorithm identifies the index that must perform the replacement, the *MapSrf* component is mapping the optimized surface in the equivalent rectangle.
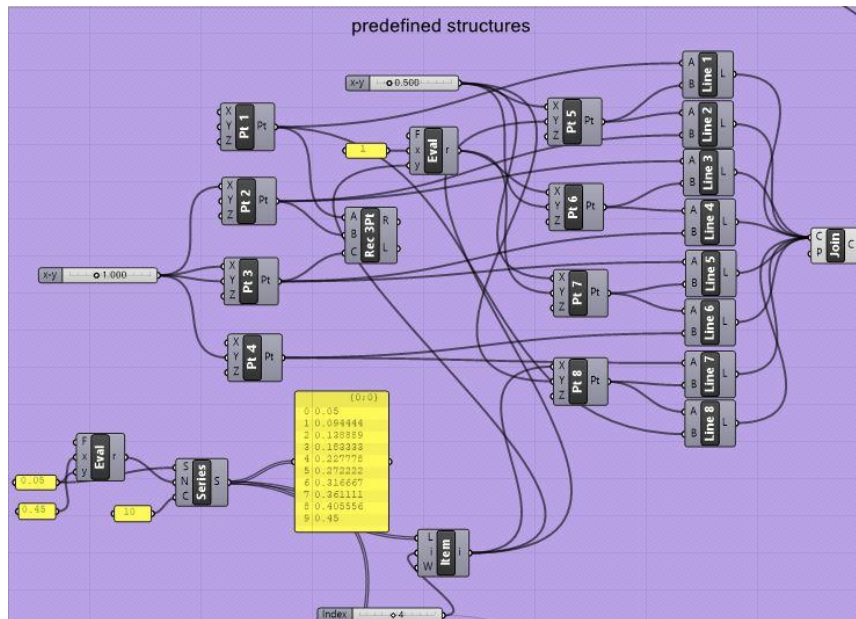
(a)
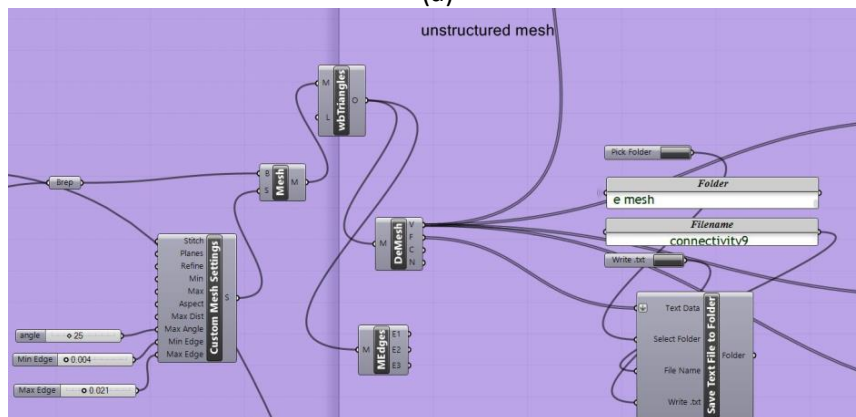
(b)
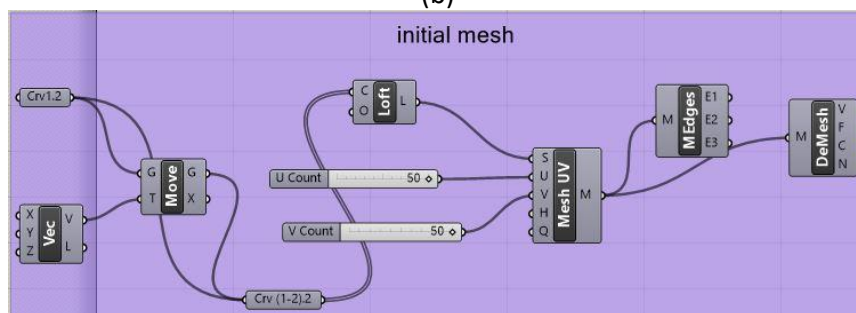
(c)

Figure 5.7 (a) Draw the predefined shaped units, (b) generation of unstructured mesh discretization of the shaped units and (c) generation of structured mesh discretization of the design domain.

129
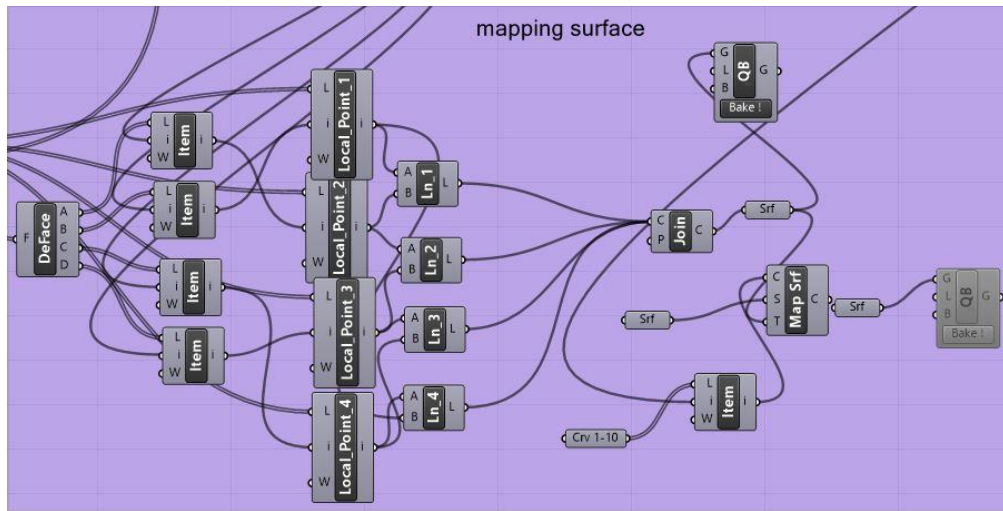
(a)
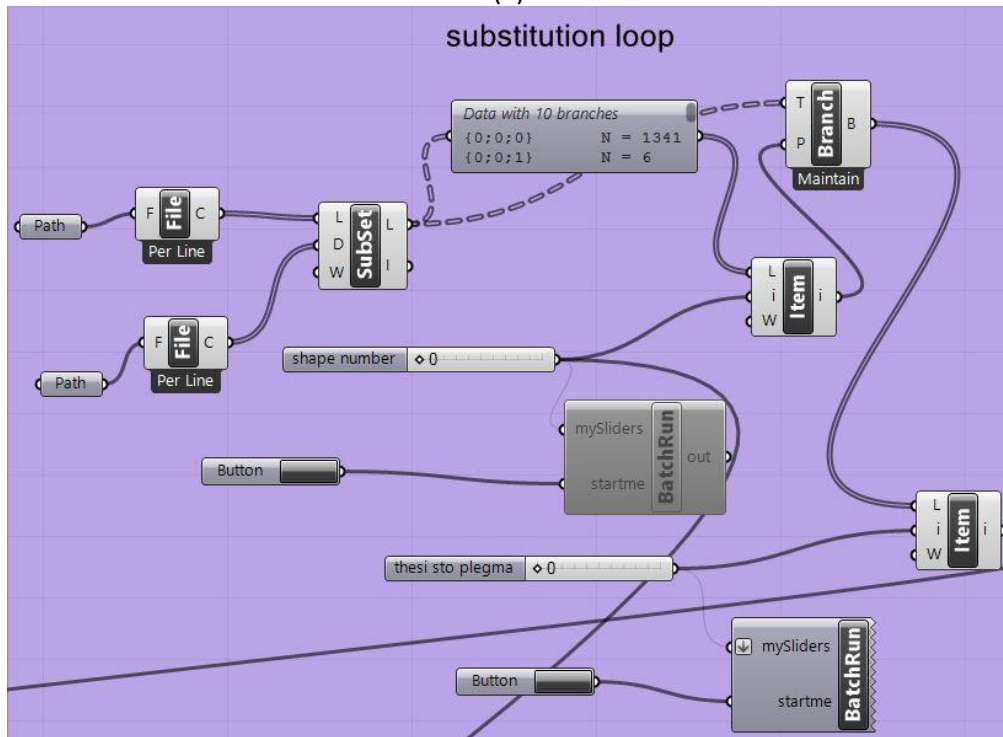
(b)

Figure 5.8 (a) Mapping surfaces and (b) substitution loop (batch run).

5.4 Numerical examples

In this section several 2D and 3D test examples are presented, aiming to show the advantages of the proposed methodology.

2D test examples

In this section two typical TO test examples are considered. The first one refers to the cantilever beam problem shown in Figure 5.9 and is labelled as "*BBeam test example*". The guiding mesh discretization used along the *X* axis is equal to 150 elements times 50 elements along the *Y* axis. The loading conditions refer to a single concentrated unit load along the *Y* axis at the right bottom corner of the design domain and the boundary conditions refer to fixed support along the *Y* axis at the left edge of the design domain (see Figure 5.9(a)). The second test example shown in Figure 5.10 is labelled as "*Simple beam test example*". The guiding mesh discretization along the *X* axis is equal to 200 elements times 50 elements along the *Y* axis. The loading conditions refer to a single concentrated unit load along the *Y* axis at the middle of the top edge of the design domain and the boundary conditions refer to pin supports at the left and right bottom corners of the design domain (see Figure 5.10(a)). The volume fraction selected for both test examples is equal to 50% of the initial domain ($f_{VolFrac} = 50\%$) and no filters were used for the implementation.

In order to assess the results of the proposed methodology, they are compared with those of the conventional GSO procedure. The results obtained by the conventional procedure can be seen in Figures 5.9(b) and 5.10(b), where a penalty parameter equal to 3.0 was used, where the results after applying the proposed SUTO methodology can be seen in Figures 5.9(c) and 5.10(c) for the two test examples, respectively. As it was stated previously, the implementation of the proposed SUTO methodology does not allow regions without material to be developed, thus the optimized domains obtained by the conventional procedure (Figure 5.9(b)) and that of SUTO (Figure 5.9(c)) are totally different. It is important to note that no filtering techniques were implemented so far and that is why the checker boarder problem is observed. Similar to the result of the conventional procedure, in Figure 5.9(c) two horizontal members in the design domain are observed (up and down) and a diagonal in the right part of the design domain. However, in the rest part of the design domain instead of creating diagonals, SUTO methodology distributed a variety of different shaped units. Therefore, the corresponding

check boarder problem is not an issue for the SUTO methodology since all elements of the guiding mesh discretization of the design domain correspond to predefined shaped units out of the design set. In the case of the "*Simple beam test example*" the optimized domains of the two procedures (i.e. Figure 5.10(b) and Figure 5.10(c)) look more alike. As it is observed in Figure 5.10(c), the optimized domain of the proposed methodology generates the same number of main members and along the same direction.
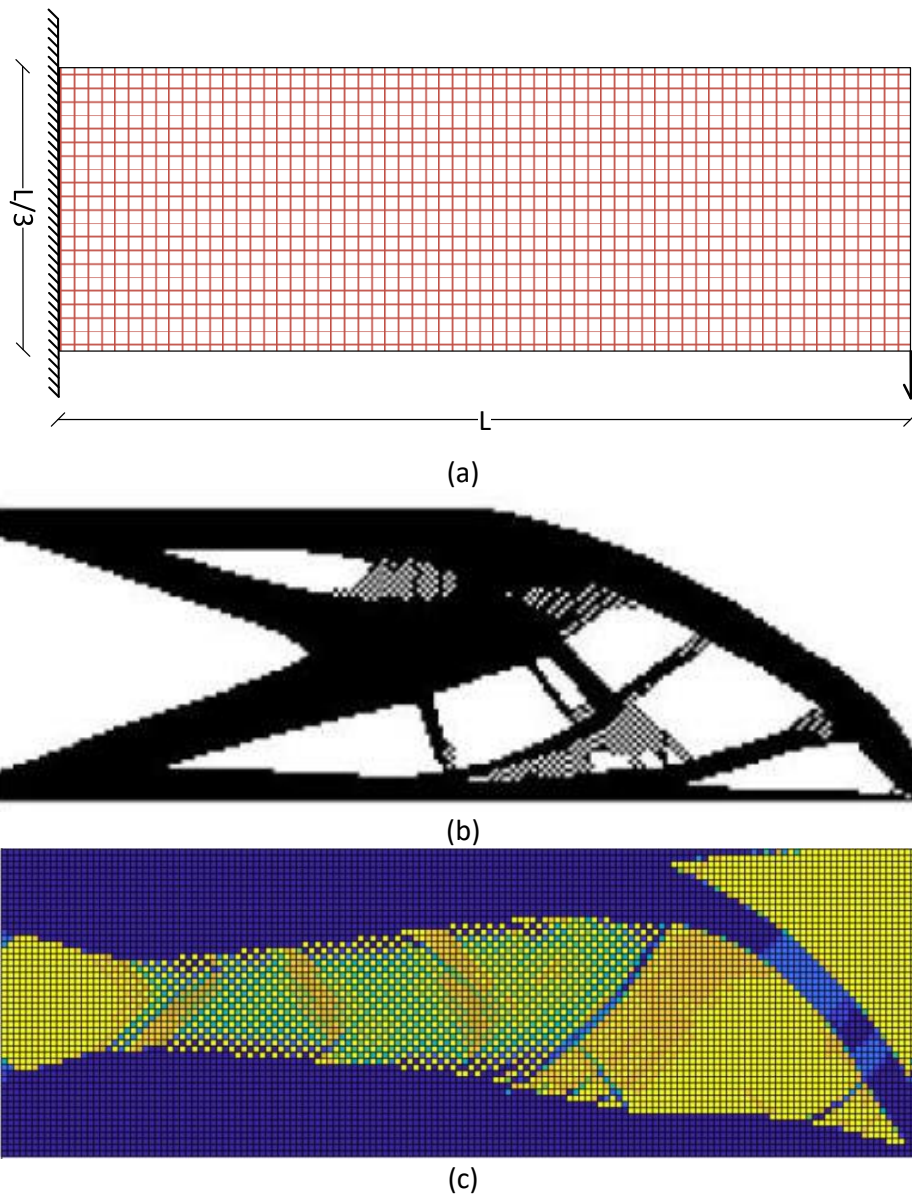
(a)

(b)

(c)

Figure 5.9 BBeam test example: (a) initial design domain, (b) optimized domain by means of SIMP, (c) optimized domain by means of SUTO methodology.

(a)

(b)

(c)
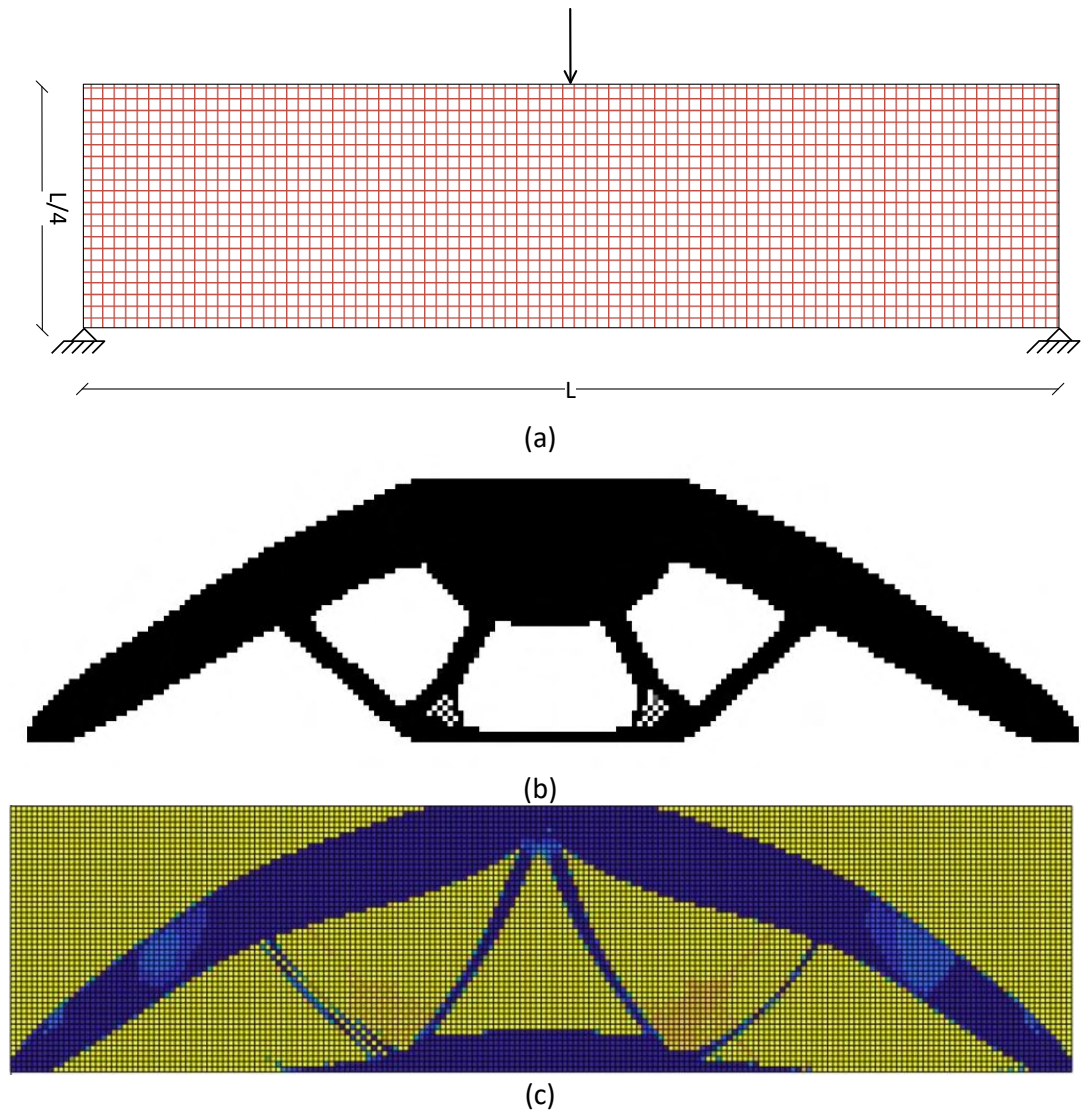
Figure 5.10 Simple beam test example: (a) initial design domain, (b) optimized domain by means of SIMP, (c) optimized domain by means of SUTO methodology.

3D plate test examples

In this section two 3D plate test cases are presented, the first one is labelled as "*Plate test example 1*", while the guiding mesh discretization along the *X* and *Y* axis is equal to 200 elements respectively. The loading conditions refer to a single concentrated unit load along the *Z* axis in the middle of the plate (see Figure 5.11(a)) and the boundary conditions refer to fixed support in the all four edges of the design domain. The second one is labelled as "*Plate test example 2*"; the mesh discretization as well as the boundary

conditions are the same with those of the first test case. The loading conditions refer to five concentrated unit loads, close the middle of the *X* and *Y* axis (see Figure 5.12(a)). The volume fraction is equal to 50% of the initial domain ($f_{VolFrac} = 50\%$) for both test cases. Comparing the results shown in Figures 5.11(b) and 5.12(b) it can be observed that the form of the loading conditions has large effect on the form of the optimized domain. In Figure 5.11(b) it can be seen that the pattern of the optimized domain is composed mainly by four members, two diagonals, one horizontal and one vertical brace. On the other hand, the pattern of the optimized domain of Figure 5.12(b) looks more attractive from architectural design point of view. It can be stated that the pattern of the optimized domain for the "*Plate test example 2*", reminds us forms that can be found in nature, as its shape resembles a butterfly. This test case is more inspiring for creating an innovating shell structure as it is shown in the next section.

(a)   (b)
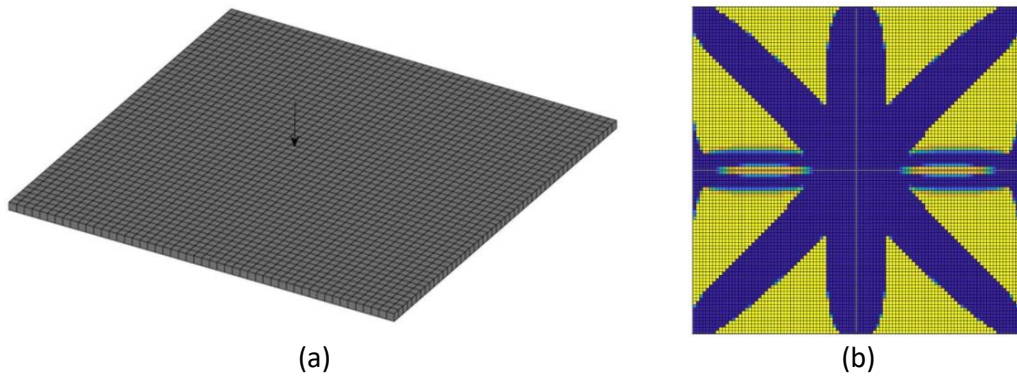
Figure 5.11 Plate test example 1: (a) initial design domain and (b) optimized domain by means of SUTO methodology.

(a)   (b)
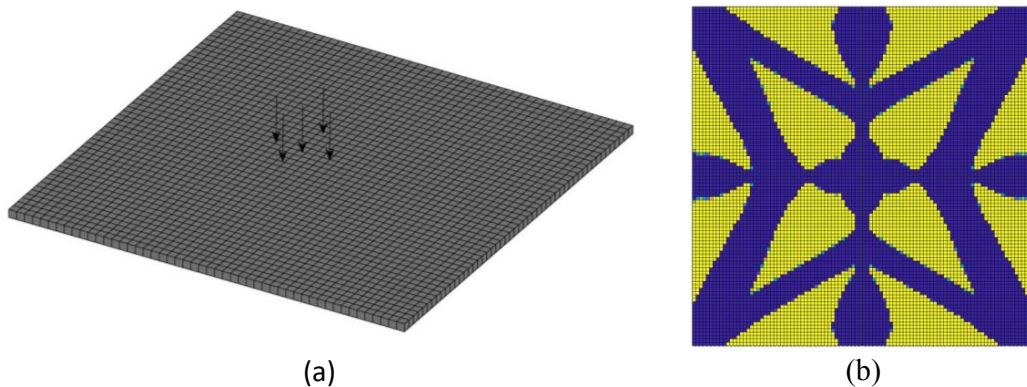
Figure 5.12 Plate test example 2: (a) initial design domain and (b) optimized domain by means of SUTO methodology.

Hangar test example and Grasshopper based interpretation

In this part of the numerical tests, two examples were chosen out of those presented previously in order to be interpreted via Rhino3D, through the C# source code developed for Grasshopper. The first one refers to the "*BBeam test example*", Figure 5.13(a) depicts the optimized structural system, as it is interpreted in Rhino3D while a more detailed view of a specific part of the optimized structural system is shown in Figure 5.13(b). The second test example is similar to "*Plate test example 2*" in terms of loading and boundary conditions with the difference that instead of a plate, a single curvature shell is dealt with the SUTO methodology. It is known that the mesh discretization of the shells that are curved with respect to one of the axes and have small curvature, can be simulated with plane elements. Thus, the proposed SUTO methodology is applied in such a shell structure and the example is labelled as "*Hangar test example*". The results of the SUTO methodology can be seen in Figure 5.14. Top, front and side views of the hangar test example can be seen in Figure 5.14 along with a perspective view. The optimized result is quite interesting corresponding to an innovating shell structure that is inspiring for developing a pavilion or similar type of structural systems.
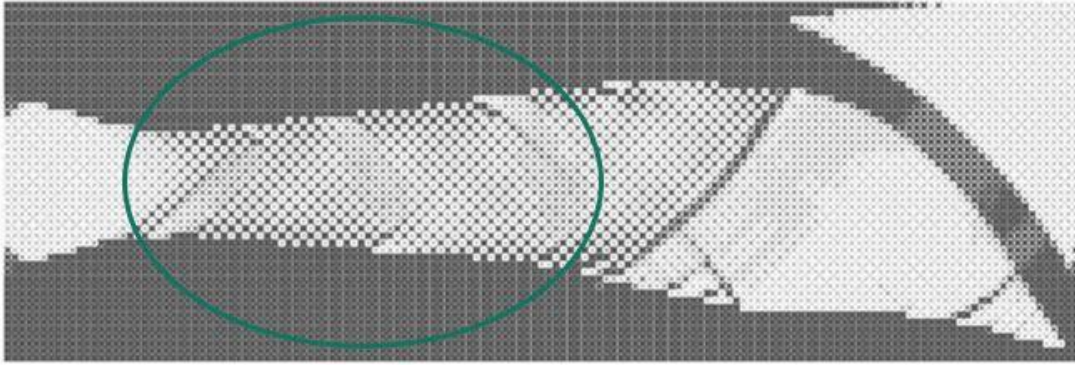
(a)
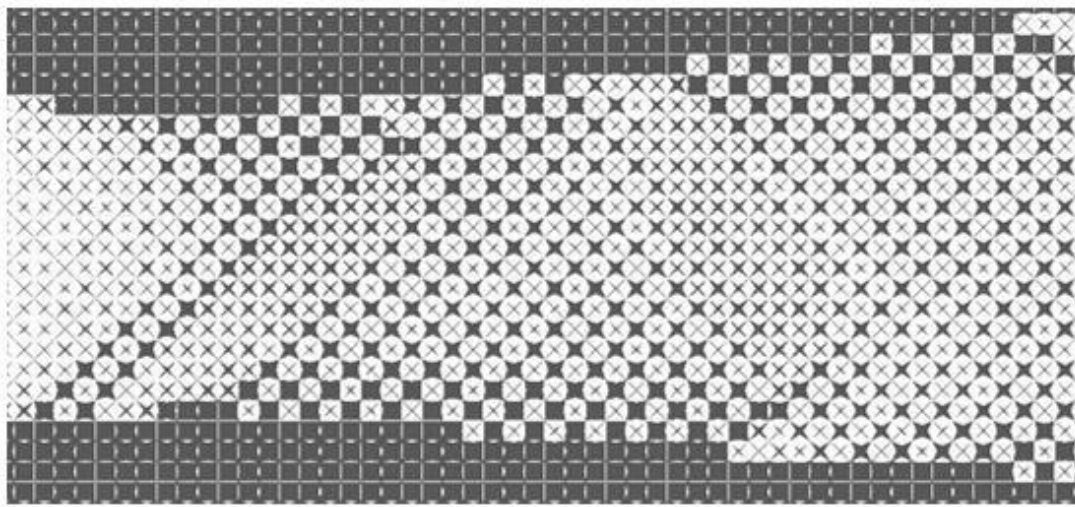
(b)

Figure 5.13 BBeam test example: (a) interpretation in Rhino3D, (b) zoomed area.

(a)

(b)

(c)

(d)
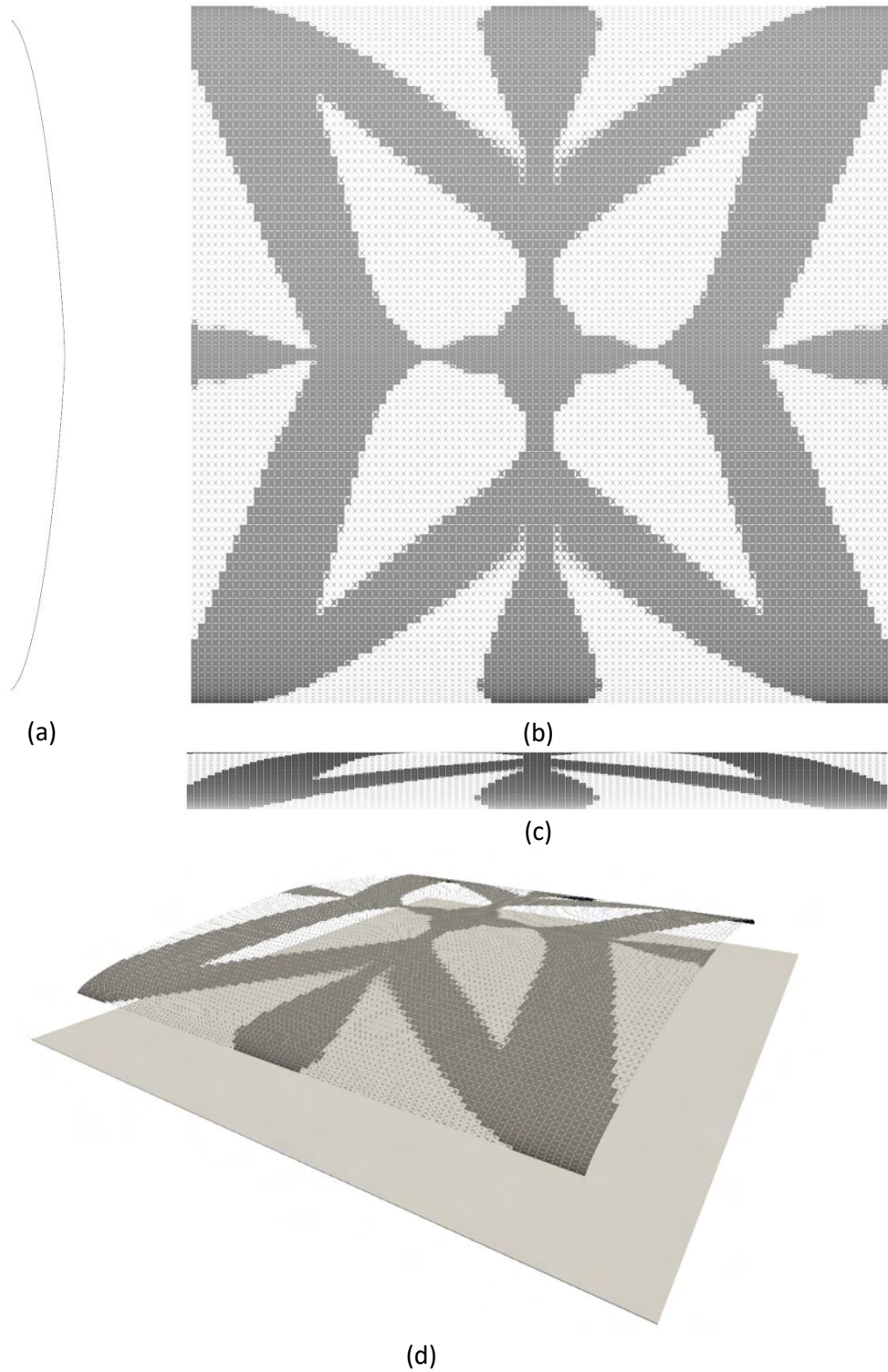
Figure 5.14 Hangar test example: (a) front, (b) top, (c) side and (d) perspective views.

137

In this section a more realistic test case is presented that is labelled as "*Braced Tube RC building test example*"; in particular an RC building is studied belonging to the class of "*Braced Tube*" structural system. The specific structural system is used not only in steel but also in RC buildings structures. In the case of RC buildings instead of using mega diagonal steel braces, shear walls are arranged between the columns in the perimeter of the building, in this study the prefabricated shaped units are arranged in the perimeter of the building. They are located into a diagonal pattern and they transfer the gravity loads, operating as inclined columns. Except for carrying vertical loads, these elements participate in the lateral load resistance, taking advantage of their increased stiffness. Their location in both directions of building's perimeter, contributes the building against lateral loading.

For the braced tube RC building test example considered the following geometry characteristics are adopted: $225m^2$ floor plan, $60m$ height and 20 stories, plan and side views are shown in Figure 5.15. A quadrangular plan view was considered for the floor plan of the building, while the configuration of floor plan view's shape was considered as symmetrical in both directions. Given that the prefabricate shaped units selected are inscribed into squares of size $1.5×1.5m^2$, the guiding mesh discretization used along the *X* axis is equal to 10 elements times 40 elements along the *Y* axis. The loading conditions refer to a single load vector along the *Y* axis concentrated at the middle of the upper side of the domain (see Figure 5.15(a)). The two bottom edge corners are pinned and the volume fraction selected is equal to 40% of the initial domain ($f_{VolFrac} = 40\%$). The results obtained by the SUTO methodology are shown in Figure 5.16(a), interpreted in MATLAB. In Figure 5.16(b), the interpretation of this layout in Rhino3D is depicted. The exoskeleton (braced tube) of the RC building developed, is shown in Figure 5.17 and the optimized structure is automatically interpreted in Rhino3D, through the C# code that was developed for Grasshopper.
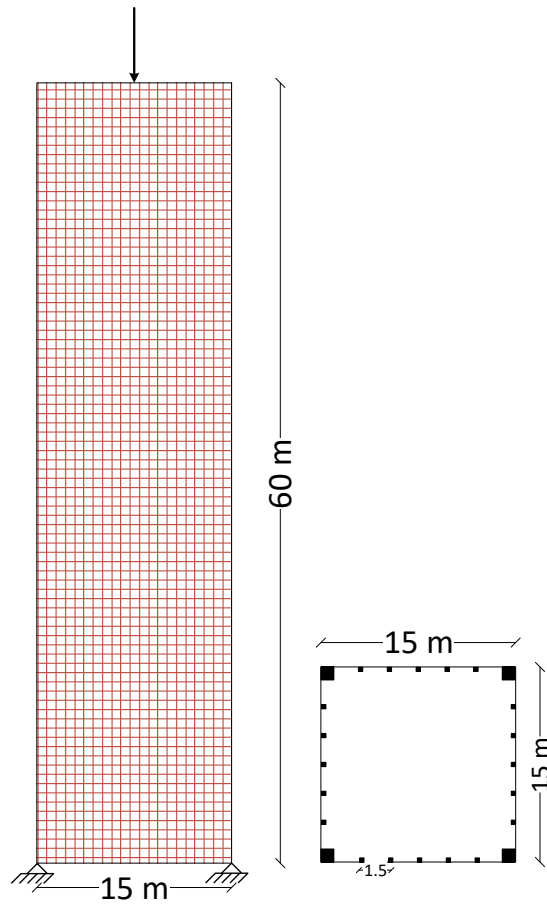
Figure 5.15 Braced tube RC building test example: (a) side and (b) plan views.

(a)   (b)
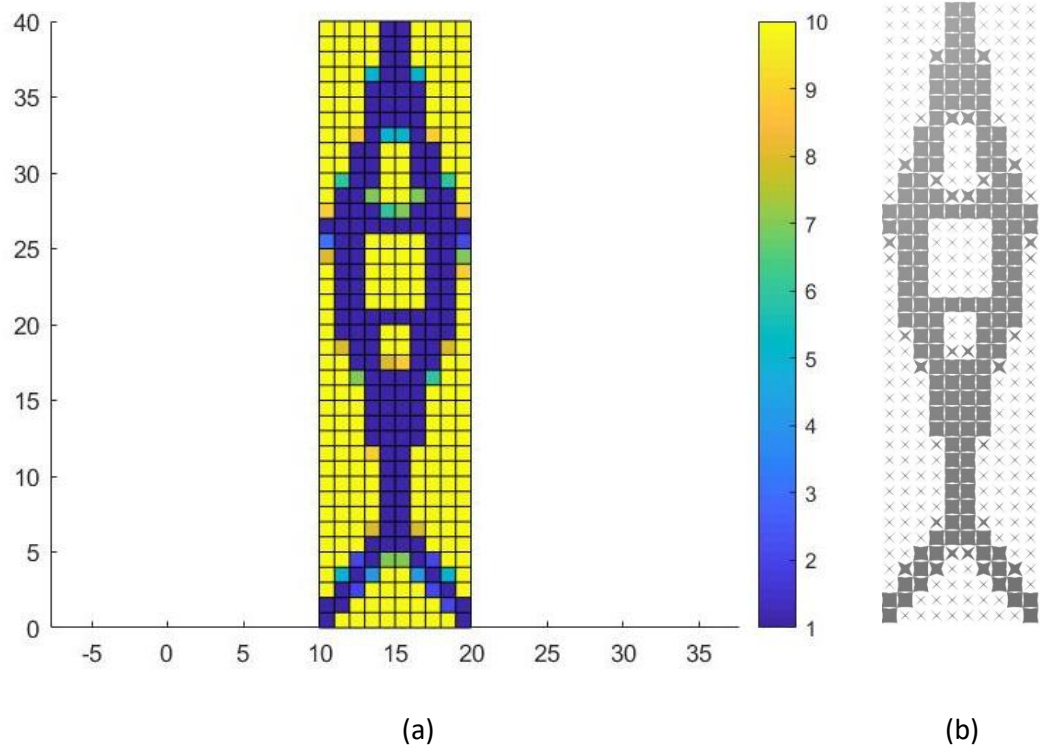
Figure 5.16 Braced tube RC building test example by means of SUTO methodology: (a) optimized domain in MATLAB representation and (b) interpretation in Rhino3D.
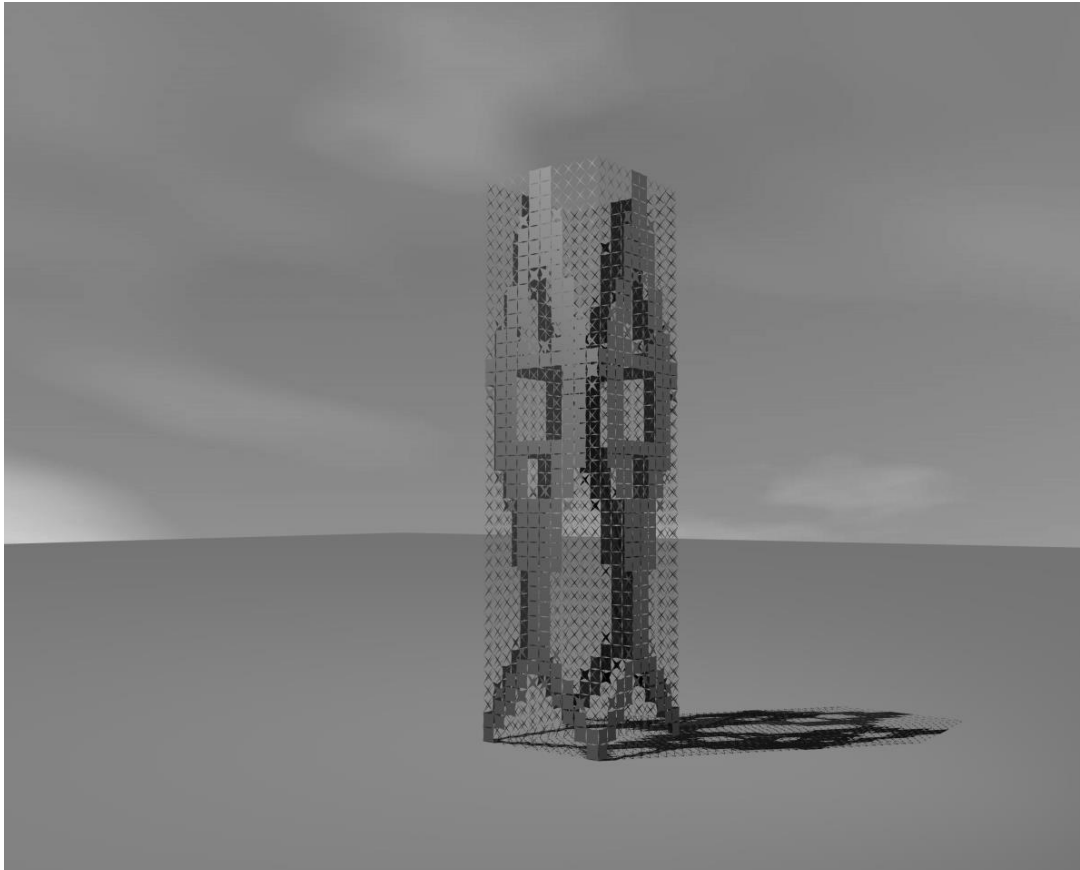
Figure 5.17 Braced tube RC building test example: perspective view.

CHAPTER 6

Compliance-based frame structural topology optimization integrated in SAP2000

6.1 Introduction

So far, the proposed methodologies for the generation of structural systems in civil engineering applications, are implemented based on the GSO approach. In this chapter, the FSTO problem, which is a subfield of LO, is introduced. In the literature, most of the papers that deal with LO problems use Truss Structural Topology Optimization (TSTO) formulations, considering members that develop only axial stresses. However, the consideration of members with both flexural and axial stiffness is an intriguing aspect in the field of STO. The articles in the literature that deal with FSTO problems are quite few and their applications are mainly theoretical, without practical implementation in the field of civil engineering. Fredicson *et al.* [38] presented a method for TO of framed structures with flexible joints that is applied in both 2D and 3D problems. Richardson *et al.* [91] demonstrated a novel two-stage method, applicable to the preliminary design phase of gridshell structures; the objective was to minimize material cost and improve structural performance. Changizi and Jalalpour [25] presented a compliance and stress-based TO approach for framed structures that can handle global and individual member instabilities. Changizi *et al.* [26], examined the interesting topic of the uncertainties encountered in real-world conditions, and proposed an algorithm for solving the probabilistic TO problem of framed structures.

In this chapter, the conventional compliance-based FSTO formulation is presented and GS generation techniques are discussed. Particularly, two applications for the generation of the GS are presented; the first is developed in the Grasshopper [41] environment while the second is applied via MATLAB code. For the implementation of the optimization

procedure, an in-house software tool, that works as an extension of the High-Performance Topology Optimization Computing Platform (HP-TOCP) [105], is developed in C# programming language. In this work, the capability of HP-TOCP to integrate with commercial CAE software is used. Particularly, the implementation of the FSTO in SAP2000 [95] is discussed thoroughly and a wide range of numerical test cases are presented.

6.2 Ground structure generation

The generation of the initial design domain represents one of the most important components of the solution process in LO problems. As it can be noticed from the literature survey that follows, the GS approach appears to be the most often used method for generating the initial design domain in the case of LO problems. The GS method was initially introduced for the Michell structure by Dorn et al. [30], who applied a linear programming method to optimize truss structures. In their approach, the optimized structure is a subset of the set of bars defined before solving the problem. Sokol [100] presented a code written in Mathematica that implemented TO of truss structures consisting of fixed GS. Zegard and Paulino [131,132] presented MATLAB codes for generating GS of arbitrary non-orthogonal domains for 2D and 3D spaces. However, the common characteristic of the aforementioned works, is that the initial structures are created in programming code, leaving the structural designer without too much freedom. In the following subsections, a proposed methodology for generating a GS in CAD environment is presented and some constructability aspects are discussed in a typical MATLAB programming code.

6.2.1 Grasshopper application

In this subsection, the GS generation with the aid of the Grasshopper is presented. As it is stated before, Grasshopper is a parametric design plugin that integrates with the CAD program Rhino3D and is widely used by many architects as a free form design tool. In this way, more complex initial geometries can be applied and more freedom for intervention

is provided to the architect or the engineer. In Figure 6.1 a simple example of the GS generation is shown. At first, the desired initial domain is created inside the Grasshopper environment by developing the proper visual script, Figure 6.1(a), and then the result is illustrated in the Rhino3D program, Figure 6.1(b). Particularly, in the specific example, the *Cross Reference* component is used in order to create a full-level connectivity GS. The advantage of this implementation, is that the initial design domain can be a simple 2D and 3D geometry but also a more complex double curvature gridshell, as it is shown in the following test cases. Regarding the complexity of the initial connectivity of the elements, it can vary from a simple-level connectivity where members are generated between all neighbouring nodes, to a full-level connectivity where each node is connected to all other nodes. Depending on the complexity of the initial geometry and also the designer's demands, any intermediate level of connectivity can be generated using additional Grasshopper's tools. After creating the GS, the geometry must be transferred to the software where the FSTO will be implemented. In this dissertation, two frameworks are used for FSTO. In the first, the problem is implemented in HP-TOCP, using SAP2000 for the structure's analysis while in the second the entire procedure of frame STO is performed using an in-house MATLAB code. For both options, an additional program written in C# was developed, to transfer the initial geometry in the equivalent analysis software and formulate the optimization problem.

(a)

144
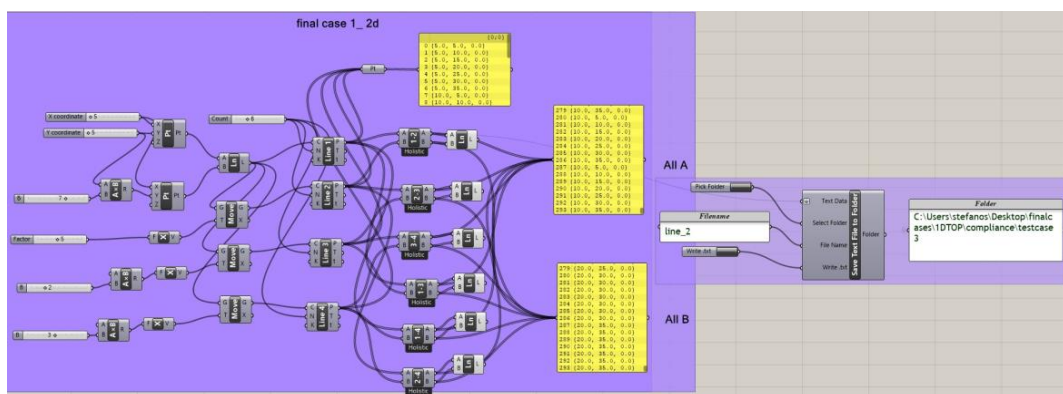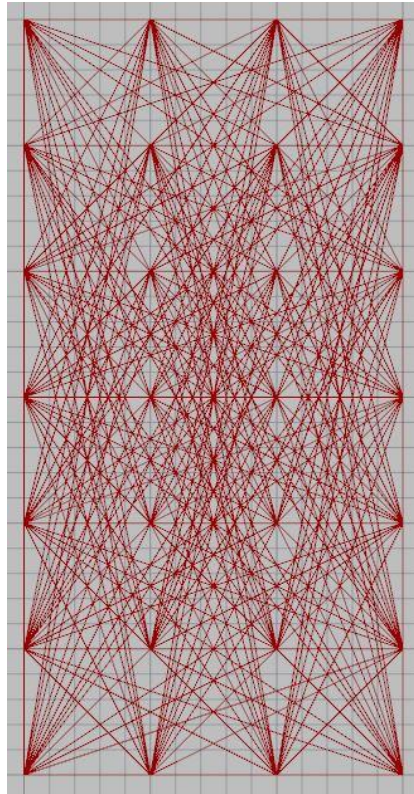
(b)

Figure 6.1 Full-level connectivity GS generation of cantilever beam in (a) Grasshopper's environment and (b) visualization in Rhino3D

6.2.2 MATLAB application

As it is stated above, the main benefit of the GS generation in Grasshopper is that more complex initial geometries can be designed with convenience and then the FSTO procedure can be performed. However, when it comes to simple 2D domains, if some extra manufacturing constraints must be applied, generating the GS through programming code is a simpler choice. Thus, for the support of the proposed methodologies in the current thesis, a personal MATLAB code is developed and specific functionalities are discussed.

The level of connectivity between nodes of the initial design domain represents an important parameter of the procedure that is to be decided. The denser the connectivity for the design domain is chosen, more DOFs are provided to the optimization procedure, possibly leading to lighter optimized designs with better structural performance. Herein,

a projection scheme is applied where the designers defines their preferences with respect to the maximum length of the structural elements (designated through the radius r) and the GS is generated based on this radius. Figure 6.2 illustrates three different GSs depending on the freedom that the designer prefers, designated by the radius, the larger r is, more DOFs are provided in the optimization procedure.

(a)	(b)	(c)	(d)
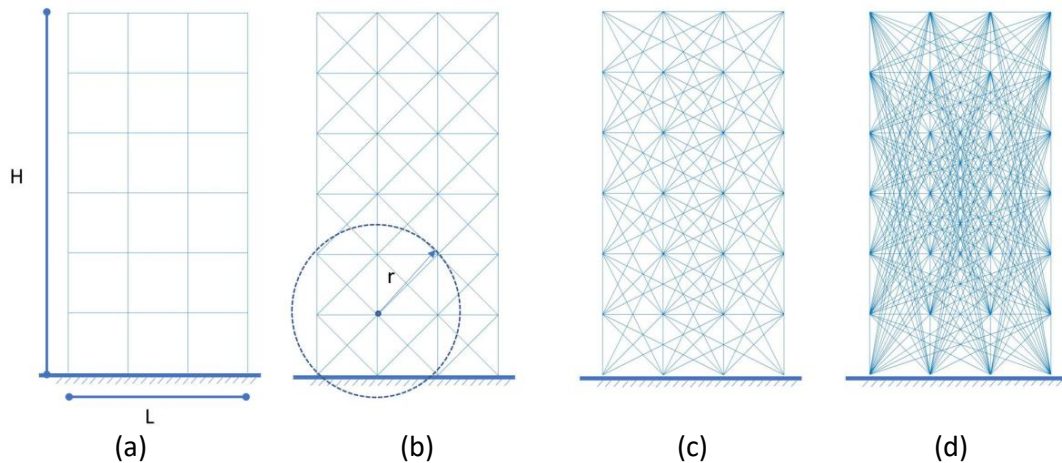
Figure 6.2 (a) Column-beam structure for $L = 3m$, $H = 6m$ and different GS for (b) $r = 1.41m$, (c) $r = 3.0m$ and (d) $r = 6.71m$

Based on the frame structure of Figure 6.2(a) with dimensions $L = 3m$ and $H = 6m$, three GSs are generated for three different values of the radius r. More specifically, $r = 1.41m$ (simple-level connectivity, see Figure 6.2(b)), $r = 3m$ (mid-level connectivity, see Figure 6.2(c)) and $r = 6.71m$ (full-level connectivity, see Figure 6.2(d)), representing the initial design domains for the FSTO problem. Worth noticing some issues that need to be taken into consideration when generating the initial design domain, e.g. in case of real-world tall building structures, if a full-level connectivity GS is chosen the number of the brace elements will be extremely large, increasing the computational demands for the FEA and the optimization procedure (more iterations to convergence). For the needs of the current thesis, two additional functionalities are used, the first one is related to the symmetry that is imposed, the second one refers to cases that nodes are linked with a single FE that is not acceptable. Both functionalities are implemented at the optimized design obtained by the solution of the FSTO. Another issue that needs attention is when

collinear frame elements are generated; for this reason, an additional component is developed that recognizes these elements and replaces them with a single frame FE.

6.3 Mathematical formulation

The general formulation of the performance-based FSTO problem, that deals with the problem of distributing specific material volume in the design domain discretized with frame FE, while optimizing (minimizing or maximizing) a performance-based objective, is defined as follows:

$$\min_a C(a) = F^T d(a) \tag{6.1a}$$

$$s.t. $$

$$K(a)d(a) = F \tag{6.1b}$$

$$a^T \cdot L \leq V_{lim} \tag{6.1c}$$

$$a_{min,e} \leq a_e \leq a_{max,e}, \quad e = 1,2,\ldots,N_{ele} \tag{6.1d}$$

The term *performance-based* stands for the criterion (objective function) adopted to be optimized that is related to the structural performance; in particular, C denotes the compliance that is to be minimized in the formulation presented above (see Eq. (6.1a)). F and d refer to the load and displacement vectors, respectively; K is the global stiffness matrix of the structural system, L is the vector of the frame FEs' length and V_{lim} denotes the material volume of the optimized structure.

The cross-sectional area of the profiles assigned to the frame FE used to discretize the design domain represents the design variables of the problem, denoted with the vector a. In the mathematical formulation, (see Eq. (6.1d)) a_{min} represents a rather small cross-sectional area value denoting the lower allowable value, adopted in order to avoid singularity of the stiffness matrix and a_{max} is the maximum allowable cross-sectional area. Contrary to the GSO, the design variable cannot always get out of the stiffness

matrix as a common factor and perform the sensitivity analysis. The local matrix of the linear 2D frame element is:

$$K_e = \frac{E}{L_e^3} \begin{bmatrix} a_e L_e^2 & 0 & 0 & -a_e L_e^2 & 0 & 0 \\ 0 & 12I_y & 6I_y L_e & 0 & -12I_y & 6I_y L_e \\ 0 & 6I_y L_e & 4I_y L_e^2 & 0 & -6I_y L_e & 2I_y L_e^2 \\ -a_e L_e^2 & 0 & 0 & a_e L_e^2 & 0 & 0 \\ 0 & -12I_y & -6I_y L_e & 0 & 12I_y & -6I_y L_e \\ 0 & 6I_y L_e & 2I_y L_e^2 & 0 & -6I_y L_e & 4I_y L_e^2 \end{bmatrix} \qquad (6.2)$$

where I_y is the moment of inertia. In order to differentiate the above matrix with respect to the design variable, the moment of inertia must be expressed in terms of the cross-sectional area. For cross-sections with simple geometry, the analytical expression of the relationship between $(a_e - I_y)$ is available, e.g. square $\left(I_y = \frac{1}{12} \cdot a_e^2\right)$ and circular $\left(I_y = \frac{\pi}{4} \cdot a_e^2\right)$. However, when it comes to real world structures, more complicated shape sections are required. For those section such expressions don't exist and regression analysis methods must be implemented, as it is shown in the next chapter.

6.4 Sensitivity analysis

Similar with the GSO approach, the sensitivity of the objective function can be evaluated as follows:

$$\frac{\partial C}{\partial a_e} = \frac{\partial (F^T d)}{\partial a_e} = \frac{\partial \left(F^T d - d^T (Kd - F)\right)}{\partial a_e} = \qquad (6.3a)$$

$$= F^T \frac{\partial d}{\partial a_e} - \frac{\partial d^T}{\partial a_e}(Kd - F) - d^T \frac{\partial K}{\partial a_e} d - d^T K \frac{\partial d}{\partial a_e} = \qquad (6.3b)$$

$$= -d^T \frac{\partial K}{\partial a_e} d \qquad (6.3c)$$

Considering the FEA, the derivative of the global stiffness matrix with respect to the design variable can be expressed as follows:

$$\frac{\partial K}{\partial a_e} = \frac{\partial}{\partial a_e}\left(\sum_{e=1}^{N_{ele}} K_e\right) \qquad (6.4)$$

Substituting Eq. (6.4) in Eq. (6.3), yields to:

$$\frac{\partial C}{\partial a_e} = -d_e^T \frac{\partial K_e}{\partial a_e} d_e \qquad (6.5)$$

where d_e are the displacement of each element in the local system.

6.5 Implementation of the methodology in HP-TOCP & SAP2000

In this subsection, the implementation of the aforementioned formulation in HP-TOCP and SAP2000 is described. HP-TOCP is the TO module of High-Performance Optimization Computing Platform (HP-OCP) [104] which focuses on civil engineering problems. HP-OCP is a software developed by the ISAAR-NTUA, that provides a holistic optimization approach for civil engineering structures and has the ability to be integrated with any CAE software that provides Open Application Programming Interface (OAPI), Extensible Markup Language (XML) or any other type of data exchange format. Considering the GS generation, the Grasshopper solution described above is selected, SAP2000 is used for the static analysis of the structures and MATLAB code for performing the sensitivity analysis and applying the optimization algorithm.

To integrate the above independent procedures into a unified process that is executed in the framework of HP-TOCP, an additional module written in C# is developed. The implementation in HP-TOCP is divided in two basic stages. The first is the preprocessing and the second is the iterative procedure. In both parts there are two independent procedures that are performed. Firstly, all the necessary information from the FEA program, herein the SAP2000, must be retrieved. This is achieved by creating some proper delegate functions. In this way, only the useful information from the static program are retrieved. These functions remain the same no matter what the program is, so any other CAE program similar with SAP2000 can be used. In the second part, the computational core of HP-TOCP performs all the necessary computations.

Regarding the structural system that is under examination, after importing the GS in SAP2000, the desired boundary and load conditions must be defined. A critical point in the next step of the implementation, is the selection of the proper frames' cross-sectional shape. As it stated previously, the design variable of the optimization problem is the area of the cross-section. However, when a section property is defined in SAP2000, (and in any commercial software) the exact dimensions of the section must be provided. In this application, simple cross-sectional geometries (circular and rectangular) can be used, in which the dimensions can be evaluated directly by just knowing the areas of the members. Moving forward, the first step of the developed module is to retrieve all the geometrical information from the static analysis software. Some dictionaries are created that collect all the names of the FE, the name and coordinates of the nodes and the name of the load combinations. The next step, is the integration of the design variable vector with the SAP2000 model. For this purpose, as many section properties as the number of the frames are created. In this way each member is independent and can take values all over the range of the design variables bounds.

In the iterative part, the first thing that must be done is to update the structural model with the new dimensions that the mathematical algorithm provides. This is succeeded with the update function that assigns the new dimensions from the optimized cross-sectional area. Afterwards, the structural analysis is performed by the static program. Considering that the objective function of the optimization problem is the structure's compliance, the forces and the displacements of each node of the elements are retrieved using the delegates functions. After collecting these information, the compliance and the volume of the structure can be evaluated. Regarding the optimization algorithm, the *fmincon* function of MATLAB's Optimization Toolbox is used and the interior point method is applied. For the evaluation of the sensitivity analysis, the stiffness matrix of the frame element is needed, as it is shown in Eq. 6.3. Considering that typical 2D frame elements are used, the term $\frac{\partial K_e}{\partial a_e}$ is evaluated directly from the derivation of Eq. 6.2. As it already stated, in this implementation simple cross-sectional geometries, i.e. circular and rectangular, are used, so the analytical expression of the relationship between $a_e - I_y$ is

150

available. For the part of the procedure that is developed in MATLAB, a wrapper is created in order to call all the appropriate functions, so the optimization is performed without even opening MATLAB. After algorithm convergence, the design variable will have values from a_{min} to a_{max}. However, as it stated before, it is considered that a_{min} is a very small number just to avoid numerical instabilities. Thus, an extra threshold for the minimum allowable area must be defined to consider that any frame with cross-sectional area below this limit, actually doesn't exist. A final function recognizes and deletes all the elements below that threshold and finally the optimized structure is displayed. In the flowchart of Figure 6.3, the aforementioned procedure is illustrated in detail.
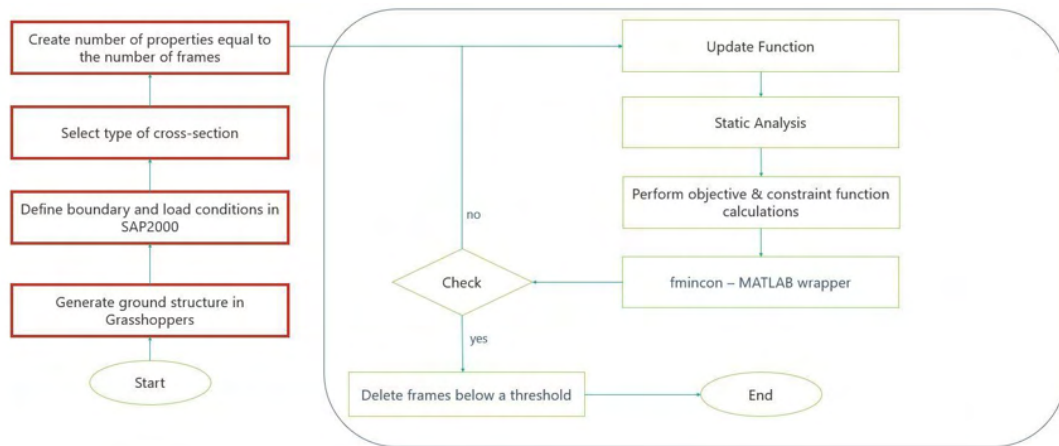
Figure 6.3 Flowchart of FSTO integrated with HP-TOCP

6.6 Numerical examples

In the following, a wide range of applications are conducted in order to determine the applicability of the proposed framework in FSTO. At first, two cantilever structures are examined considering two types of initial connectivity, the simple-level connectivity and the full-level connectivity GS. Additionally, two cross-sectional types, (square and circular) are applied and two different volume limits are studied in each case. Afterwards, a bridge structure for a specific volume limit is studied, using only circular cross-sections and two possible layouts are proposed considering the same types of GSs as before. Finally, a double curvature gridshell under two different loading conditions, considering a simple-level connectivity GS, is examined. In this example, the advantages of the proposed

framework's integration with Grasshopper are highlighted. The modulus of elasticity is considered in all cases equal to $E = 200GPa$. Regarding the bounds of the design variable, the upper and lower limits are considered as: $a_{max} = 4 \cdot 10^{-2}m^2$ and $a_{min} = 2 \cdot 10^{-4}m^2$.

Cantilever structure 1

In the first example, the cantilever structure under a point load applied at the top left corner and the bottom side restrained is presented and subsequently is denoted as CS1. The frame width and height are $L = 3m$ and $H = 6m$ respectively and the value of the force is chosen as $P = 4MN$. Herein, simple-level and full-level connectivity GSs are implemented, considering square and circular cross-sections. In the following, the simple-level connectivity GS is labeled as CS1S#, where # denotes the cross-sectional type (S (square), C (circle)). Similarly, the full-level connectivity GS is labeled as CS1F#. In Figure 6.4 the two GSs that are used for the CS1 test case are illustrated. These four test cases are examined under two different volume constraints, $V_{lim} = 0.4m^3$ and $V_{lim} = 0.8m^3$. In Figure 6.5 the optimized layouts of CS1SS and CS1FS test cases considering $V_{lim} = 0.4m^3$ are illustrated. In Figure 6.6 the optimized structures of CS1SC and CS1FC test cases for the same V_{lim} are depicted. Comparing CS1SS with CS1SC and CS1FS with CS1FC, it is observed that the major frames of the optimized structures are the same but in the case of CS1#C structures, layouts with some extra frames, with low cross-sectional areas, are produced. As shown in the numerical results in Table 6.1, these additional frames reduce slightly the value of the objective function, a bit less than 1%, in both CS1S# and CS1F# test cases. Comparing CS1SS with CS1FS and CS1SC with CS1FC, it is clear that the reduction of the objective function, when using the full-level connectivity GS, is remarkable. Particularly, in CS1#S test cases the compliance is reduced by 10.10% while in CS1#C test cases the objective function is decreased by 9.74%.

In Figures 6.7 and 6.8, the CS1#S and CS1#C test cases for $V_{lim} = 0.8m^3$ are presented, respectively. Comparing CS1SS with CS1SC, it is observed that the number of the frames in the final structures is the same, but their topologies differ a little. However, this small difference in the frames' distribution, leads to 4.3% objective function's reduction for the

case of CS1SC structure in comparison with the CS1SS test case. As it is shown in Table 6.1, in the CS1FC test case, two more frames are developed in comparison with the CS1FS test case but the value of the objective function is very close with each other. Regarding the optimized structures for same cross-sectional type but different GS, the effectiveness of the initial structure's freedom is even bigger than in the previous volume constraint. More specifically, in the CS1#S test cases the compliance's reduction is 17.47% while in the CS1#C test cases the objective function's decrease is 14.44%.

$*(\times 10^4)$

CS1	Simple-level connectivity GS		Full-level connectivity GS		
$V_{lim} = 0.4m^3$	C*(Nm)	N_e	C*(Nm)	N_e	Reduction of C (%)
Square Section	10.961	18	9.854	21	10.10
Circular Section	10.876	26	9.817	33	9.74
$V_{lim} = 0.8m^3$					
Square Section	5.311	42	4.383	39	17.47
Circular Section	5.083	42	4.349	41	14.44

Table 6.1 CS1: Numerical results of the compliance and the number of frames (N_e) in the optimized structure considering simple-level and full-level connectivity GS

(a)   (b)
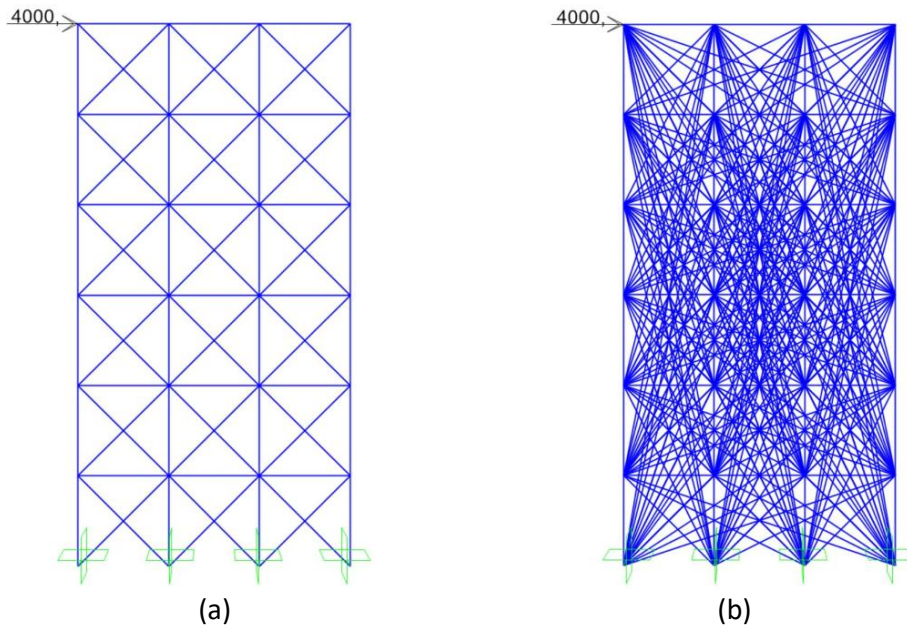
Figure 6.4 CS1: Initial design domain for (a) simple-level (CS1S#) and (b) full-level (CS1F#) connectivity GS

(a)   (b)
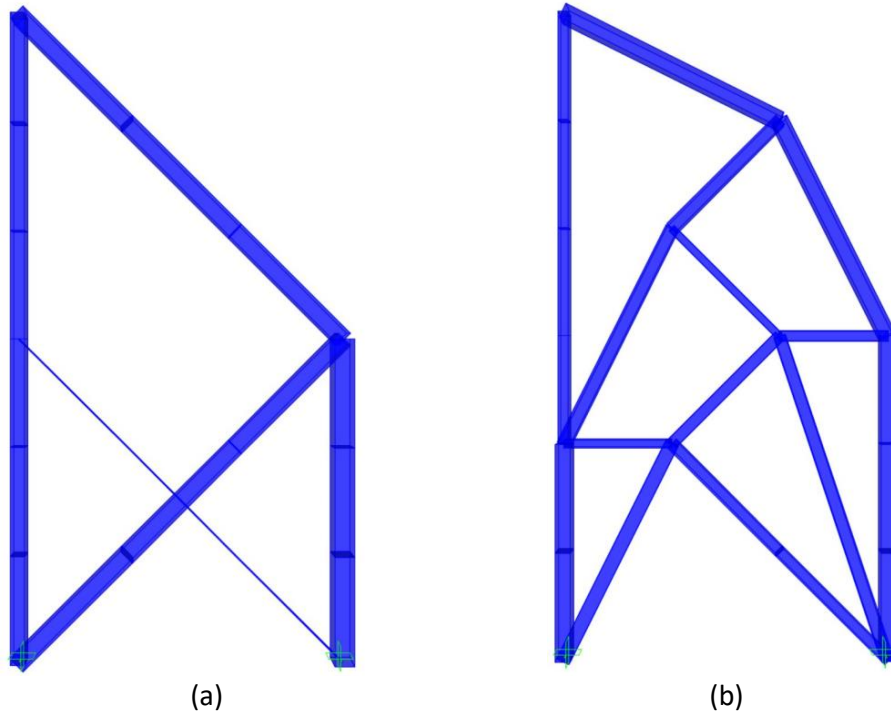
Figure 6.5 CS1: Optimized results for $V_{lim} = 0.4m^3$ considering square cross-section for (a) simple-level (CS1SS) and (b) full-level (CS1FS) connectivity GS

(a)   (b)
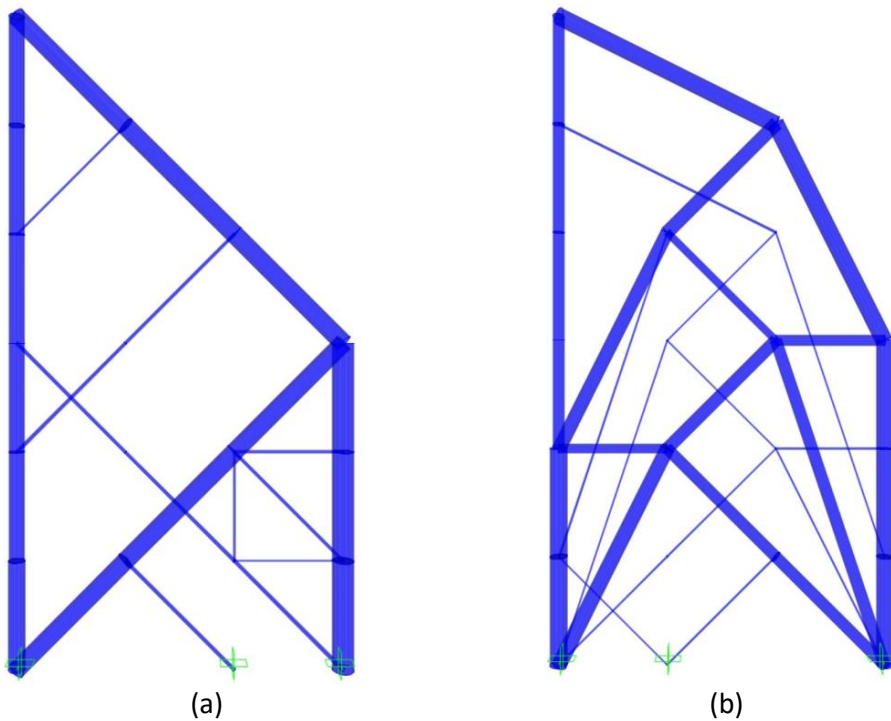
Figure 6.6 CS1: Optimized results for $V_{lim} = 0.4m^3$ considering circular cross-section for (a) simple-level (CS1SC) and (b) full-level (CS1FC) connectivity GS

(a)　　　　　　　　　　　　　　　(b)
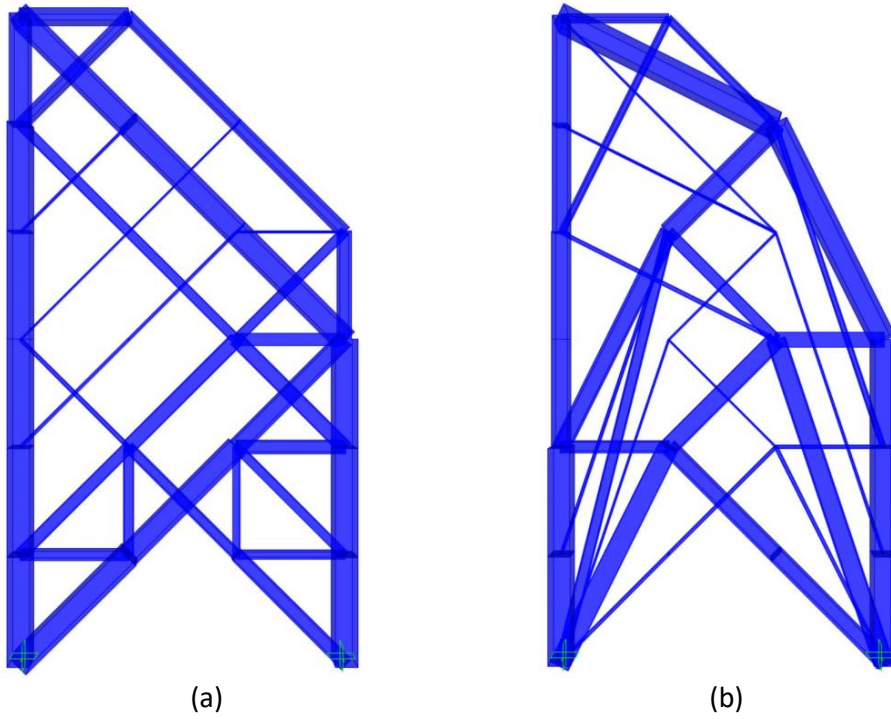
Figure 6.7 CS1: Optimized results for $V_{lim} = 0.8m^3$ considering square cross-section for (a) simple-level (CS1SS) and (b) full-level (CS1FS) connectivity GS

(a)　　　　　　　　　　　　　　　(b)
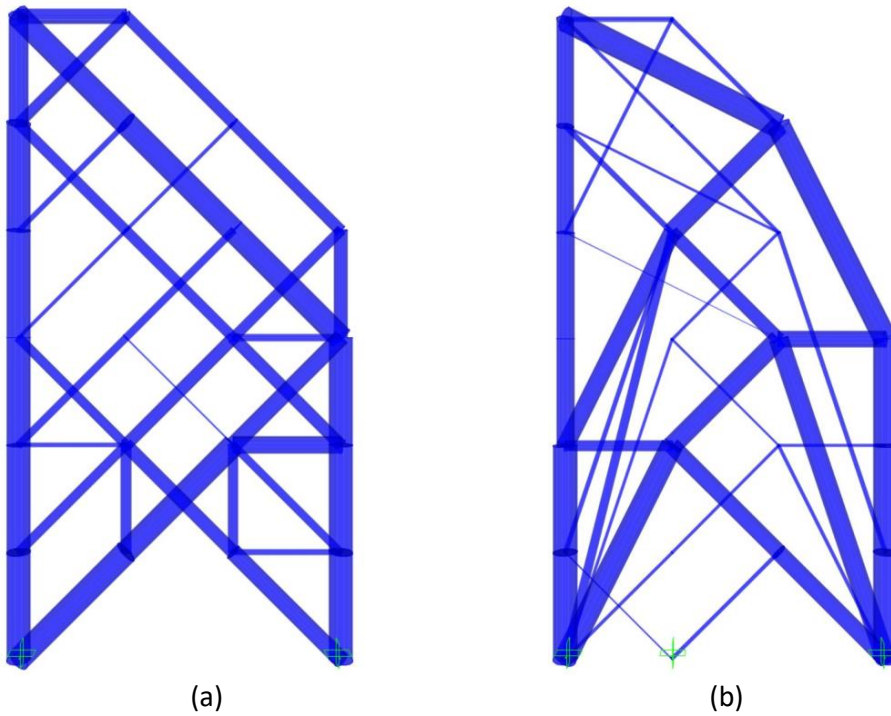
Figure 6.8 CS1: Optimized results for $V_{lim} = 0.8m^3$ considering circular cross-section for (a) simple-level (CS1SC) and (b) full-level (CS1FC) connectivity GS

Cantilever structure 2

In the next example, the cantilever structure under a central load in the top edge and supported in the bottom side is examined and subsequently is denoted as CS2. The frame width and height are $L = 4m$ and $H = 6m$ respectively and the force is selected as $P = 4MN$. In the following, the simple-level connectivity GS is labeled as CS2S#, where # denotes the cross-sectional type (# stand for S (square), C (circle)). Similarly, the full-level connectivity GS is labeled as CS2F#. In Figure 6.9 the two GSs that are used for the CS2 test case are illustrated. These four test cases are examined under two different volume constraints, $V_{lim} = 0.4m^3$ and $V_{lim} = 0.8m^3$. In Figure 6.10 the optimized structures of CS2SS and CS2FS test cases, considering $V_{lim} = 0.4m^3$, are illustrated. In Figure 6.11 the optimized layouts of CS2SC and CS2FC test cases for the same V_{lim} are presented. In the CS2S# test cases, it is observed that the optimized structure of the CS2SC test case contains some additional frames, with small cross-sectional areas, in comparison with the CS2SS test case. In the case that the optimization procedure starts from the full-level connectivity GS, the optimized layout is exactly the same in both section type cases. In the numerical results in Table 6.2, it is shown that, for the same GS, in CS2#C test cases the value of the compliance is slightly lower than in CS2#S test cases. Furthermore, comparing CS2SS with CS2FS and CS2SC with CS2FC, it is observed that for both cross-sectional types, the decrease of the compliance when the full GS is considered, is notable. More precisely, in the CS2#S test cases, the reduction of the objective function is 13.48*%* while in the CS2#C test cases the decrease is 13.20*%*.

In Figures 6.12 and 6.13, the optimized results of the CS2#S and CS2#C test cases for constraint equal to $V_{lim} = 0.8m^3$ are presented, respectively. Comparing CS2#S with CS2#C test cases, it is observed that, for both GS, the final layouts of the CS2#C test cases have additional frames comparing with the structures of the CS2#S test cases. Similar with the previous examples, for the same GS, the compliance of the CS2#C test cases is approximately 1*%* lower than the compliance of the CS2#S test cases. Finally, as it is shown in Table 6.2, the initial bigger freedom of the design domain led to structures with 13.28*%* less compliance in the CS2#S test cases, and 12.58*%* in the CS2#C test cases.

Observing the results of the CS1 and CS2 test cases, it can be stated that the FSTO problem for structures that consist of circular cross-sections, have better convergence than structures that have square cross-sections. Thus, in the next applications circular cross-sections are selected to continue the survey.

$*(\times 10^4)$

CS2	Simple-level connectivity GS		Full-level connectivity GS		
$V_{lim} = 0.4m^3$	C*(Nm)	N_e	C*(Nm)	N_e	Reduction of C (%)
Square Section	7.614	20	6.588	8	13.48
Circular Section	7.571	28	6.572	8	13.20
$V_{lim} = 0.8m^3$					
Square Section	3.804	24	3.299	34	13.28
Circular Section	3.761	30	3.288	38	12.58

Table 6.2 CS2: Numerical results of the compliance and the number of frames (N_e) in the optimized structure considering simple-level and full-level connectivity GS

(a)   (b)
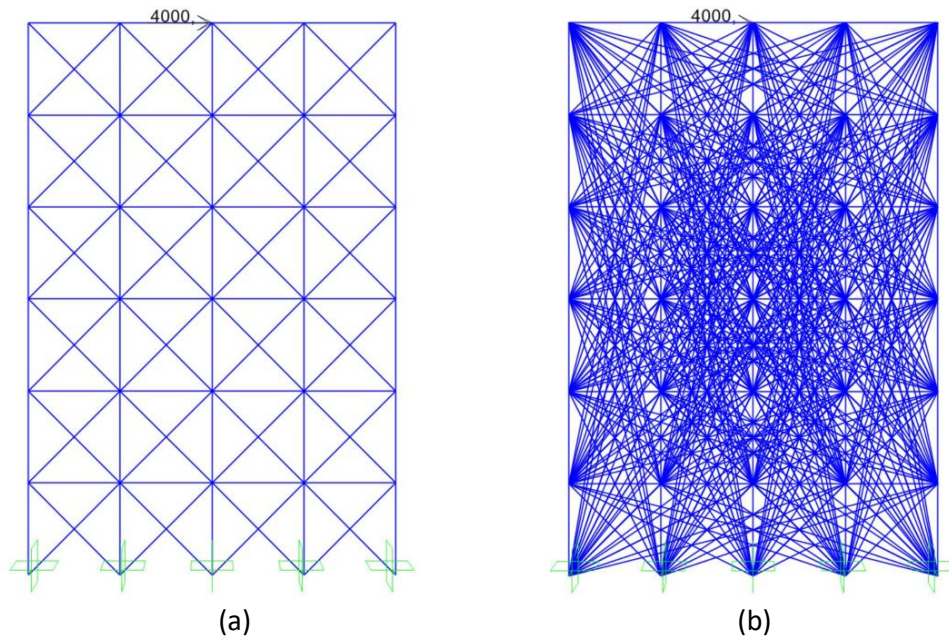
Figure 6.9 CS2: Initial design domain for (a) simple-level (CS1S#) and (b) full-level (CS1F#) connectivity GS
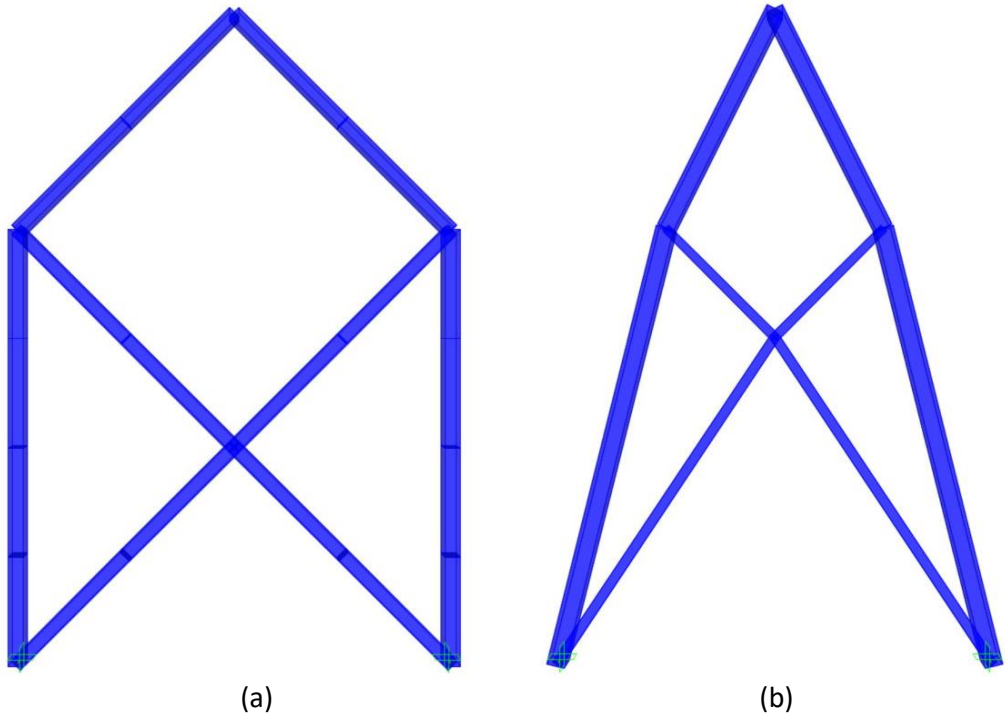
Figure 6.10 CS2: Optimized results for $V_{lim} = 0.4m^3$ considering square cross-section for (a) simple-level (CS2SS) and (b) full-level (CS2FS) connectivity GS
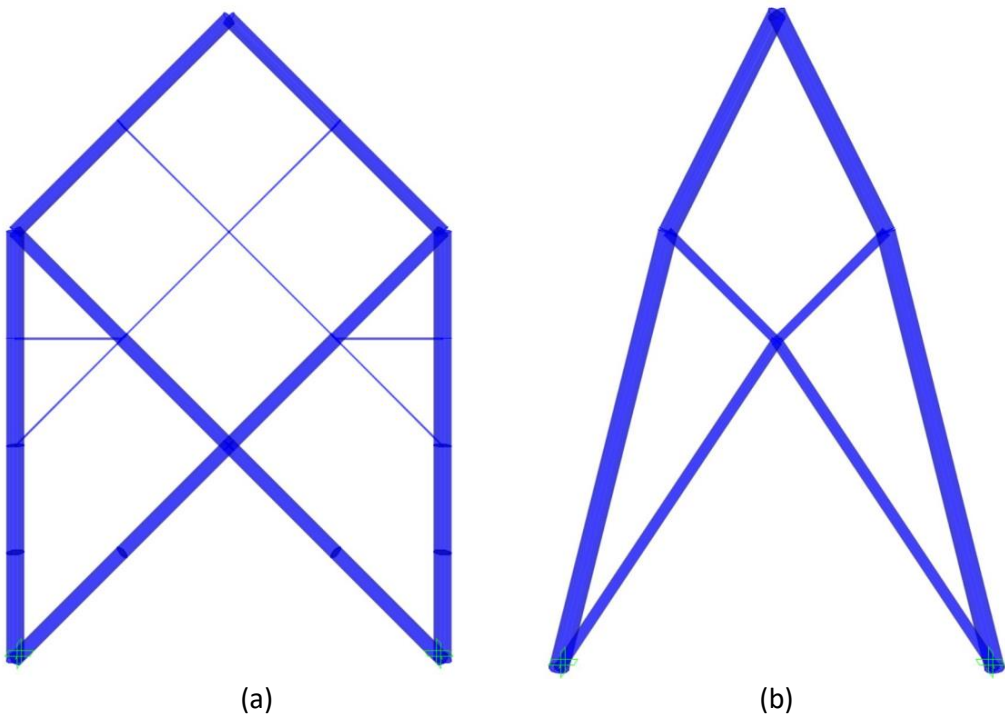
Figure 6.11 CS1: Optimized results for $V_{lim} = 0.4m^3$ considering circular cross-section for (a) simple-level (CS2SC) and (b) full-level (CS2FC) connectivity GS

(a)   (b)
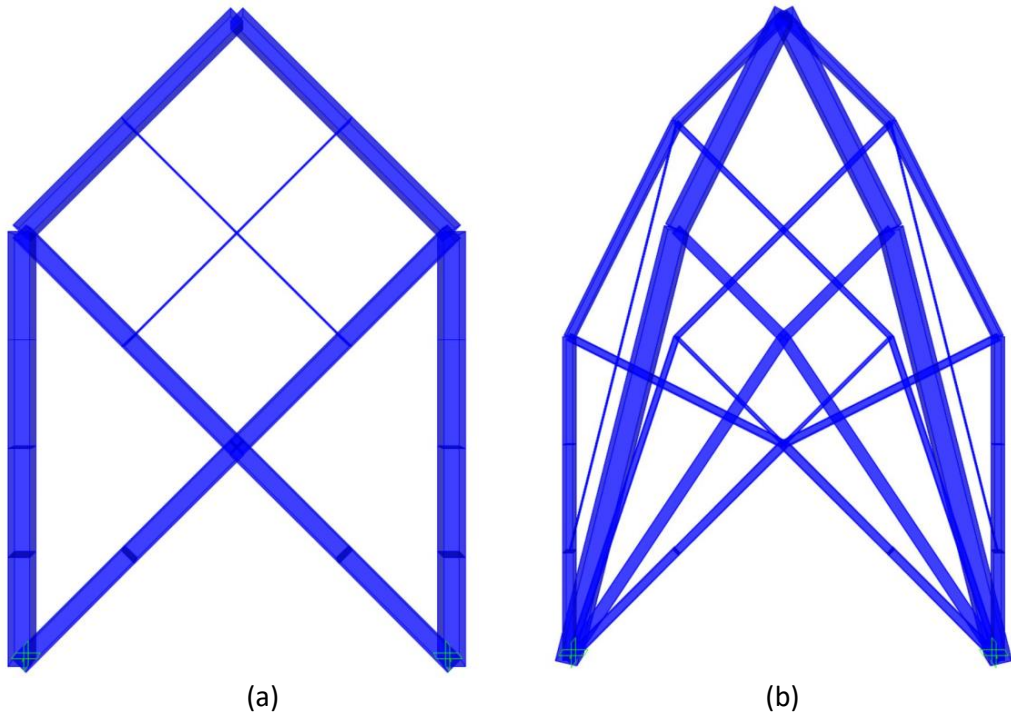
Figure 6.12 CS1: Optimized results for $V_{lim} = 0.8m^3$ considering square cross-section for (a) simple-level (CS2SS) and (b) full-level (CS2FS) connectivity GS

(a)   (b)
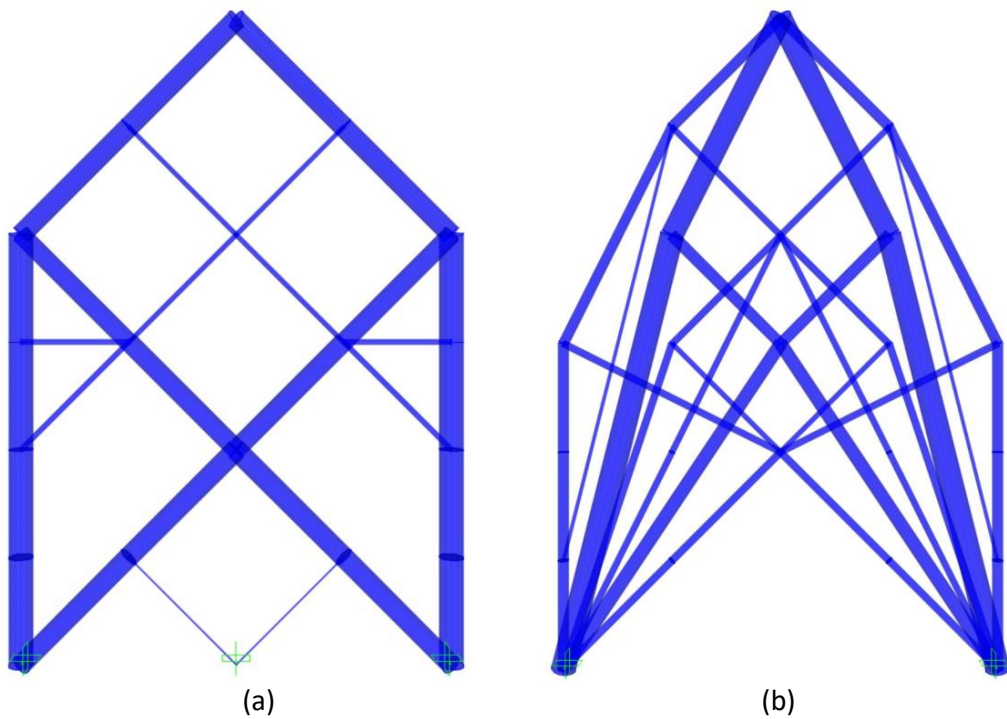
Figure 6.13 CS1: Optimized results for $V_{lim} = 0.8m^3$ considering circular cross-section for (a) simple-level (CS2SC) and (b) full-level (CS2FC) connectivity GS

Bridge structure

Herein, a test case that is closer to a real civil engineering application is conducted. Particularly, a bridge structure under distributed loads in the bottom edge and supports at the left and right bottom edges is presented. The length of the bridge is equal to $L = 24m$ and the height is $H = 6m$, while in each node at the bottom edge, point loads equal to $P = 100KN$ are assigned. As it is stated before, the circle cross-section is selected for the frames' profiles and two GSs are studied (see Figure 6.14), similar with the previous examples. In this test case the constraint of the volume is set as $V_{lim} = 1.2m^3$. In Figure 6.15, the optimized results for the simple-level and the full-level connectivity GS are illustrated. It is observed that in the case that full-level connectivity GS is applied, the final layout is very close to a real bridge structure. Furthermore, in the structure that started from a simple-level connectivity GS, the optimized compliance is equal to $C = 1.31 \cdot 10^3 Nm$ and the number of the frame elements $N_e = 78$, while the same results for the full-level connectivity GS are $C = 1.06 \cdot 10^3 Nm$ and $N_e = 63$. These results, highlight the importance of the freedom of the initial design domain, as far as in the second case the reduction of the objective function is 19.1%, despite fewer frame elements are used.

(a)

(b)
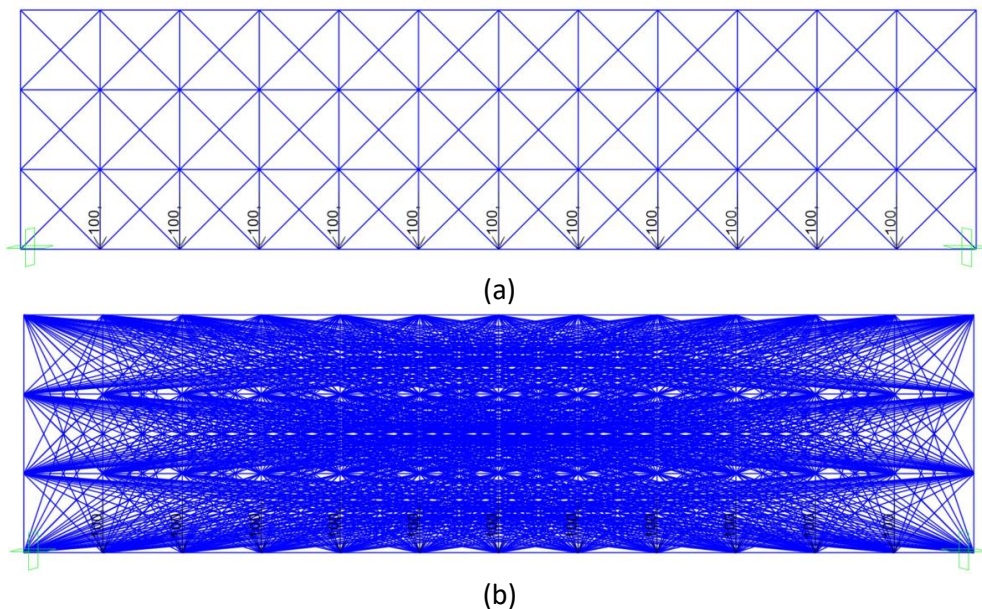
Figure 6.14 Initial design domain for bridge structure with (a) simple-level and (b) full-level connectivity GS

(a)

(b)
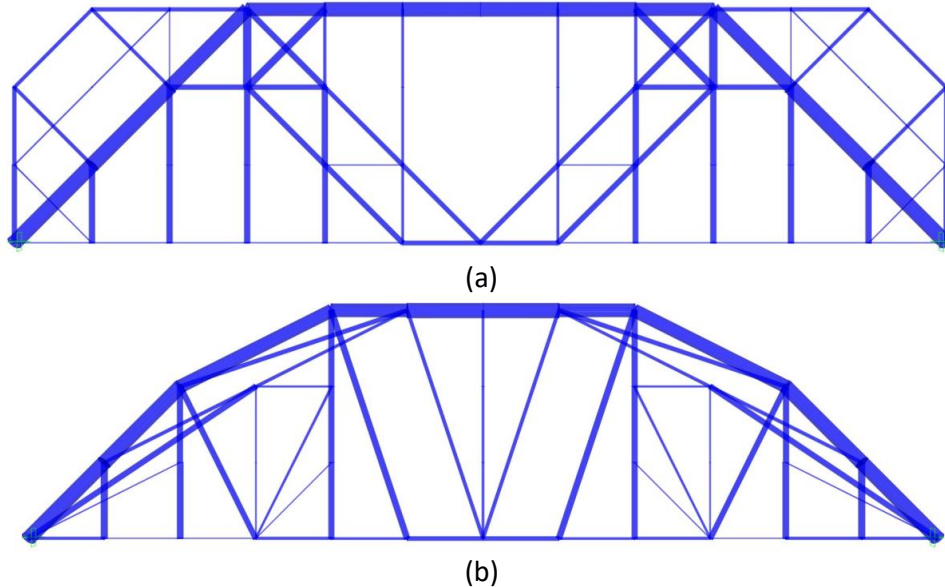
Figure 6.15 Bridge: Optimized results for $V_{lim} = 1.2m^3$ considering circular cross-section for (a) simple-level and (b) full-level connectivity GS

Gridshell structures

In the following examples, a gridshell structure is examined and the importance of implementing the GS generation in Grasshopper is highlighted. In Figure 4.16(a), a double curvature gridshell is shown that is supported in the four corners of its edges. The projection of the structure is a square with length equal to $L_x = L_y = 20m$ and the maximum height is equal to $H = 10m$. Due to the complexity of the initial geometry, only simple-level connectivity GS is considered here and 3D frame elements are used for the simulation of the structure. Additionally, two different load cases are studied. In the first case study, one point-load equal to $P = 4MN$ in the center of the structure is applied, subsequently is denoted as GS1, and in the second case study, four additional loads, are assigned in the middle of the diagonals that connect the node in the center of the shell with the four supports, in the following denoted as GS2. In GS2 the magnitude of all the loads are equal to $P = 0.8MN$. In Figure 4.16, the iso and the top view of the optimized results for the GS1 case for $V_{lim} = 60m^3$ is illustrated. The compliance of the final structure is equal to $C = 4.08 \cdot 10^5 Nm$ and the number of the frame elements is $N_e = 634$. In Figure 4.17, the iso and the top view of the optimized layouts for the GS2 case for

$V_{lim} = 80m^3$ is presented. The compliance of the optimized structure is equal to $C = 1.38 \cdot 10^4 Nm$ and the number of the frame elements is $N_e = 534$. In both gridshell structures, it is observed that FSTO can be used as a powerful tool for the conceptual design procedure as far as innovative structure can be produced. In Figures 4.16 and 4.17, the proposed layouts can be used in the conceptual design phase of producing a shell structure e.g. a shelter or a pavilion.

(a)

(b)   (c)
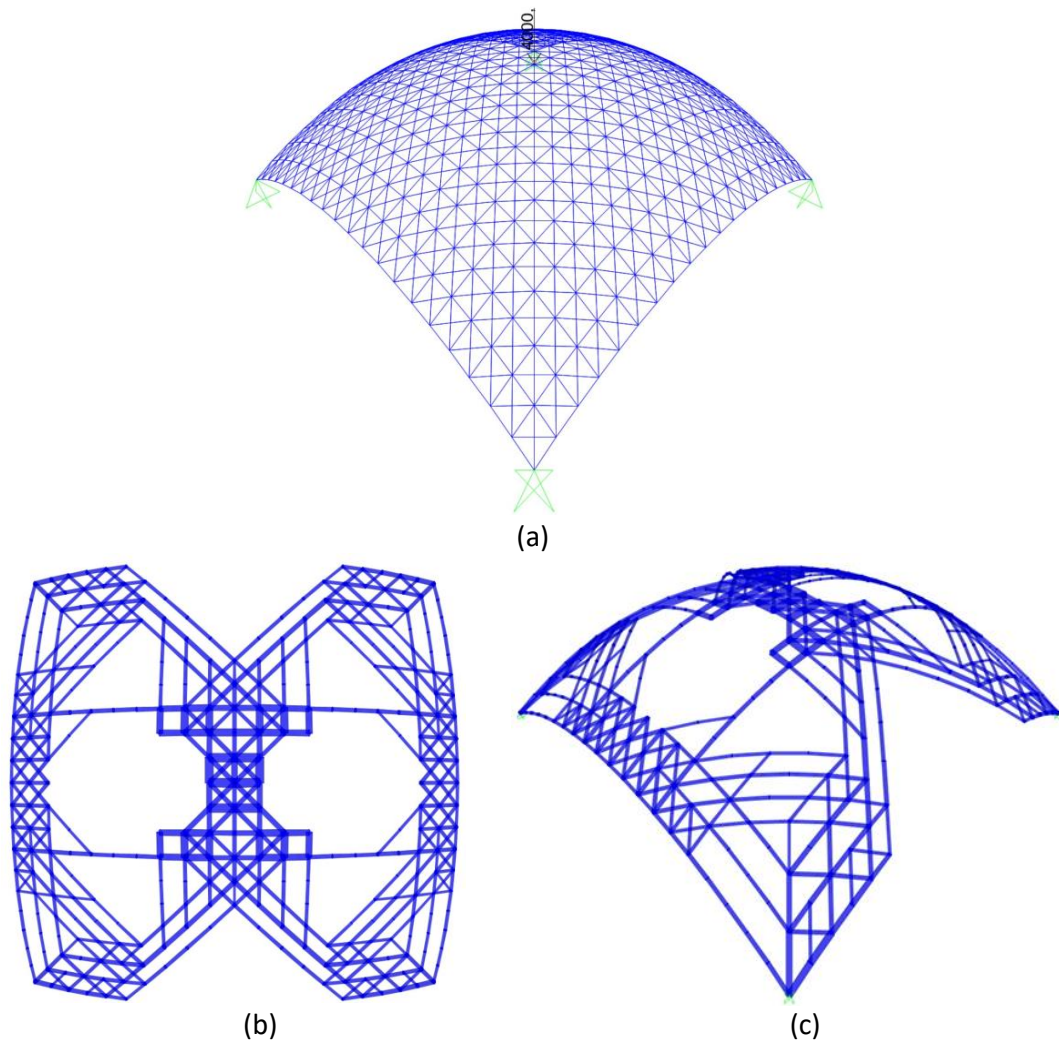
Figure 6.16 GS1: (a) Initial design domain for simple-level connectivity GS, (b) top view and (c) iso view of the optimized structure for $V_{lim} = 60m^3$

(a)

(b)

(c)
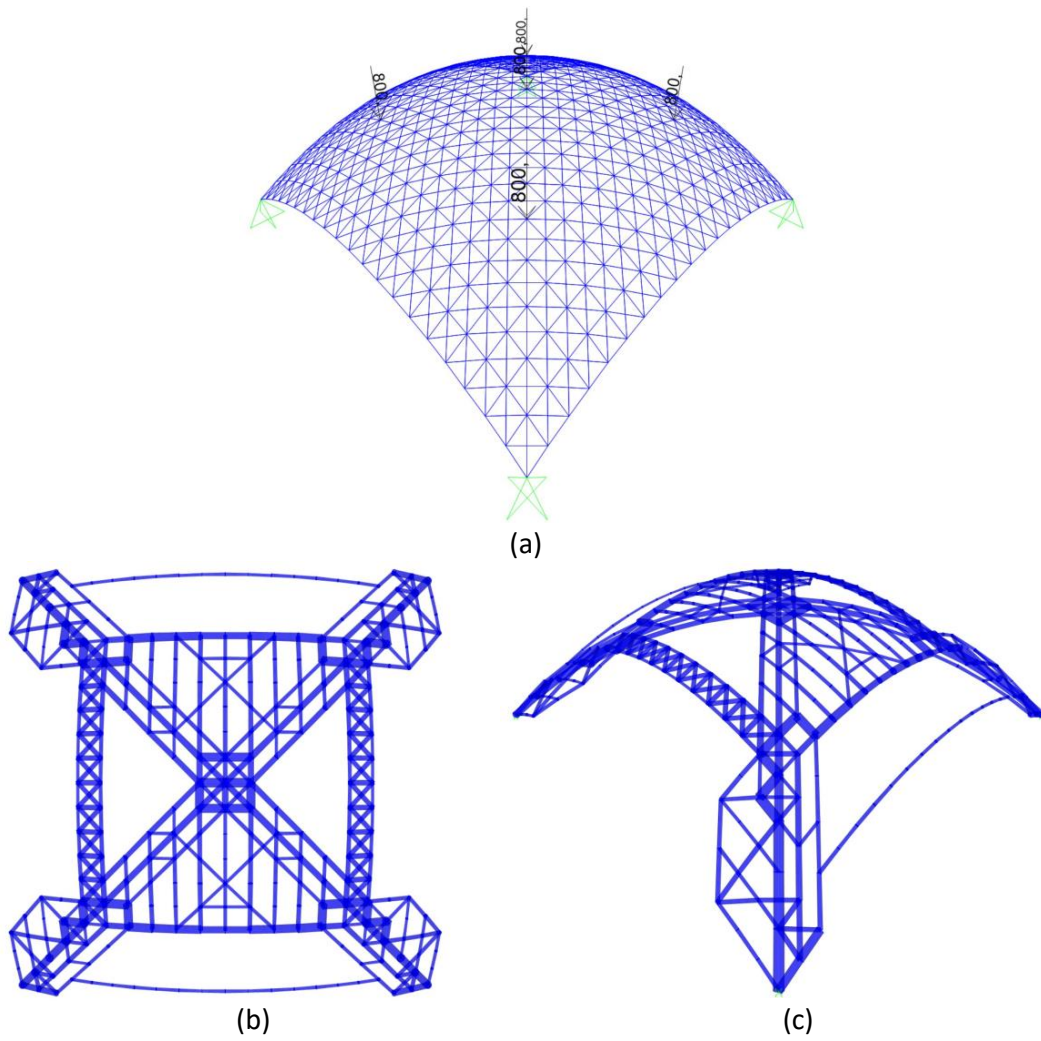
Figure 6.17 GS2: (a) Initial design domain for simple-level connectivity GS, (b) top view and (c) iso view of the optimized structure for $V_{lim} = 80m^3$

CHAPTER 7

A two stages structural optimization-based design procedure of structural systems

7.1 Introduction

In the conventional formulations of the STO problems, the objective function is usually a performance-based criterion, that is related to the structural performance, and one of the constraints is the final volume of the structure. However, in the civil engineering industry, an optimization formulation that is reducing the material cost subjected to specific quantities, related to the structural analysis, is a far more interesting topic. A limited number of studies can be found in the literature dealing with TSTO or FSTO problems, where the material volume is the objective function to be minimized. Ohsaki and Swan [77] presented a branch and bound approach for solving the minimum material volume problem subjected to member stresses constraints, however, limited to small scale benchmark tests. Yamada and Kanno [126], proposed an algorithm that solves a sequence of relaxation problems to obtain a local optimal solution, where the TOP is formulated as a minimum material volume problem subjected to frequency constraints. In the work by Changizi and Jalalpour [24], among others, a minimum volume test case was examined subjected to compliance and stresses constraint functions; where limit bound values for the constraints were obtained from the solution of the dual problem.

In this chapter, two different SO problems are combined in order to support engineers not only in the conceptual design phase but also in the final design one; in particular topology and sizing SO problems are formulated and solved into a sequential manner. For implementation purposes of the two problems' solution process, regression analysis techniques are applied and the two problems are formulated as minimum material volume problems subjected to design code restrictions. Additionally, real-world design characteristics (loading conditions, material properties etc.) and standardized cross-sectional properties are considered, while in the second stage of the methodology the

Eurocode design regulations are applied, thus, resulting into more realistic structures. More specifically, the way that serviceability and ultimate limit states of the Eurocode are applied in the proposed methodology is discussed and the mathematical formulation of the problem is presented. Finally, two groups of numerical test cases are examined in order to present the capabilities of the methodology, not only in the preliminary but also in the final design phase.

7.2 Implementation of standardized cross-sectional profiles

The structural elements of real-world framed structures consist of more than one section profile types. More specifically, in case of steel building structures an often-used allocation of section profile types is: "H" steel section profiles are used for the columns, "I" steel section profiles are adopted for the horizontal beams while hollow steel section profiles, rectangular or circle ones, are implemented for the braces. In this chapter, FSTO problems are formulated for conceptual design purposes of structural systems in case of real-world tall building structures, followed by the final design phase implemented by means of a sizing structural design optimization approach. For the test examples considered, Eurocode 3 (EC3) [87] design code is used for the design requirements; therefore, the European HEA, IPE and CHS section profiles are assigned to the corresponding structural elements. The relationships of the cross-sectional area vector (a) with other cross-sectional properties, required during the FEA and design phases for assessing candidate optimal designs, are derived by means of regression analysis in order to be integrated in the solution process of the optimization problems formulated herein. This is due to the fact that for some cases, FSTO and SSO problems are formulated as a continuous optimization problem (subsequently labelled as continuous approach), while for the cases that the SSO problem is dealt with the HP-OCP [104] the corresponding problems are formulated as discrete ones (labelled as discrete approach).

Selecting the regression relationships that will be used to approximate the required cross-sectional properties with respect to the cross-sectional area (a_e) (see Eq. (6.1d)) is one of the most critical components of the solution process for the FSTO problems. The approximation of the cross-sectional properties is needed during the assessment of the

designs derived by the optimization procedure i.e. performing FEA and design evaluation together with the gradient calculations also required by the derivative-based optimization procedures. Upon convergence of the solution processes for both FSTO and SSO problems, the section properties of the optimized designs achieved are transformed into standardized steel profiles. In the last part of this investigation, where a commercial software is used for the analysis and design, SSO problem is dealt with as a discrete problem, therefore only standardized steel profiles are used. In addition to the differentiability of the regression relationship, the minimum requirement for the expression adopted, is that a positive value should be approximated for every cross-sectional property, e.g. the moment of inertia. Although, a simple polynomial expression can be used for obtaining good approximations of the cross-sectional properties, for certain values of the cross-sectional area (a_e) (much smaller than the minimum of the corresponding list of standardized sections), the cross-sectional property approximated has negative value that is not acceptable. Perhaps, the absolute value of the approximated cross-sectional property can be used because the specific value of the cross-sectional area (a_e) is very small and such section property actually doesn't exist. The result of this approximation was found to be very good, the difference between the solution with the continuous variable and the solution with the discrete value was relatively small; however, the approach was not stable.

Therefore, the following expression that always returns positive value is applied:

$$f_{CSP}(a) = (b_1 a^3 + b_2 a^2 + b_3 a)^2 \qquad (7.1)$$

where $f_{CSP}(a)$ is the regression function for a specific cross-sectional property (*CSP*) of the specific profile and b_i are the coefficients of the expression. Figure 7.1 illustrates the approximation capabilities of Eq. (7.1) for the moment of inertia (I_y), for HEA, IPE and CHS section profiles. It can be observed that a very good approximation of the proposed expression is achieved for all sections of the Eurocode tables.
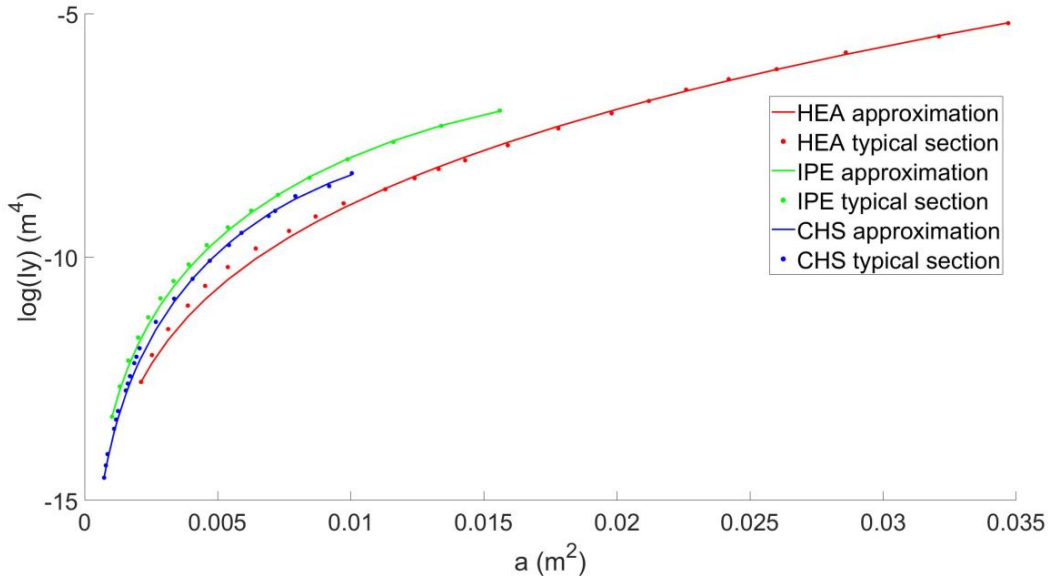
Figure 7.1 Curve fitting after regression analysis for moment of the inertia (I_y) for HEA, IPE and CHS standardized sections

A continuous and differentiable function over the design space $[a_{min}, a_{max}]$ (see Eq. (6.1d)), are the basic requirements of the expression used to derive the regression functions. Thus, the derivatives of the local stiffness matrices of the frame FE that are necessary for evaluating the derivative of the compliance can be defined as follows:

$$\frac{dK_e(a_e)}{da_e} = \frac{E}{L_e}\begin{bmatrix} 1 & 0 & 0 & -1 & 0 & 0 \\ 0 & \dfrac{12\dfrac{df_I(a_e)}{da_e}}{L_e^2} & \dfrac{6\dfrac{df_I(a_e)}{da_e}}{L_e} & 0 & -\dfrac{12\dfrac{df_I(a_e)}{da_e}}{L_e^2} & \dfrac{6\dfrac{df_I(a_e)}{da_e}}{L_e} \\ 0 & \dfrac{6\dfrac{df_I(a_e)}{da_e}}{L_e} & 4\dfrac{df_I(a_e)}{da_e} & 0 & -\dfrac{6\dfrac{df_I(a_e)}{da_e}}{L_e} & 2\dfrac{df_I(a_e)}{da_e} \\ -1 & 0 & 0 & 1 & 0 & 0 \\ 0 & -\dfrac{12\dfrac{df_I(a_e)}{da_e}}{L_e^2} & -\dfrac{6\dfrac{df_I(a_e)}{da_e}}{L_e} & 0 & \dfrac{12\dfrac{df_I(a_e)}{da_e}}{L_e^2} & -\dfrac{6\dfrac{df_I(a_e)}{da_e}}{L_e} \\ 0 & \dfrac{6\dfrac{df_I(a_e)}{da_e}}{L_e} & 2\dfrac{df_I(a_e)}{da_e} & 0 & -\dfrac{6\dfrac{df_I(a_e)}{da_e}}{L_e} & 4\dfrac{df_I(a_e)}{da_e} \end{bmatrix} \quad (7.2)$$

where the derivative of $f_I(a_e)$ is analytically defined based on its expression (see Eq. (7.1)). Through a parametric investigation it was observed that for very small values of a_e, (smaller than the minimum of the corresponding list of standardized sections) the

167

approximated values of I_y are rather overestimated. As a result, for cases of structural elements assigned to cross-sectional area values lower than the minimum of the corresponding list of standardized sections, quite small errors are introduced with respect to the stiffness coefficients and structure's compliance value when section properties are translated to the standardized ones. Furthermore, it is worth noticing that an additional threshold value a_{crit} for the minimum allowable area needs to be defined, so to consider that any frame element with section area below this limit must be eliminated. In this work, the European HEA steel profile list is composed by 24 profiles (i.e. HE 100 A to HE 1000 A) in accordance with Euronorm 53-62 [36]. So, for the list of HEA section profiles, $a_{min} = 0.0021 \ m^2$ and $a_{crit} = 0.001 \ m^2$ while the a_{max} is the maximum cross-sectional area of the HEA section list.

7.3 Design phase

According to Eurocode, the maximum horizontal deflection allowed for the case of one-story buildings is $d_{allow} = \frac{H}{150}$, where H is the height of the building structure, while multi-story buildings are not covered by the Eurocode, therefore, there is no any specific limitation for the horizontal deflection. Smith [99] presented an extended survey on serviceability criteria for the case of tall buildings, pointing out that there is very limited guidance on deflection limits by the international design codes, leading to arbitrary values. The deflection of most buildings varies from $\frac{H}{200}$ to $\frac{H}{600}$ while the majority of them was set equal to $\frac{H}{400}$. In the current study in most of the test cases the range of this limit is selected between $\frac{H}{200}$ and $\frac{H}{600}$, while aiming to examine the behavior of the methodology when a low limit is used, for one test case the deflection limit was set equal to $\frac{H}{100}$. Furthermore, without loss of the generality, for the elastic or plastic design check of the steel structures the conservative approach of the linear interaction is considered according to the EN 1993-1-1:2005 [87], more specifically the conservative approach of the design check (DC_C) is expressed as follows:

$$DC_c = \frac{N_{Ed}}{N_{Rd}} + \frac{M_{y,Ed}}{M_{y,Rd}} + \frac{M_{z,Ed}}{M_{z,Rd}} \leq 1 \qquad (7.3)$$

$$N_{Rd,t} = \frac{Af_y}{\gamma_{M0}}, N_{Rd,c} = \frac{\chi Af_y}{\gamma_{M1}}, M_{Rd} = \frac{Wf_y}{\gamma_{M0}} \qquad (7.4)$$

where N_{Ed}, M_{Ed} are the internal element forces, N_{Rd} is the design plastic resistance of the cross-section in axial force ($N_{Rd,t}$, $N_{Rd,c}$ for tension and compression respectively), M_{Rd} is the design bending moment resistance, depending on the class of the cross-section (plastic for classes 1 and 2 while elastic for class 3) and DC_C the sum of the linear interaction. In members that are under compression, the reduction factor for buckling χ is evaluated according to the following expressions:

$$\chi = \frac{1}{\Phi + \sqrt{\Phi^2 + \bar{\lambda}^2}}, \chi \leq 1 \qquad (7.5)$$

$$\Phi = 0.5\left[1 + a_{imp}(\bar{\lambda} - 0.2) + \bar{\lambda}^2\right] \qquad (7.6)$$

where $\bar{\lambda}$ is the non-dimensional slenderness and a_{imp} the imperfection coefficient. In order to evaluate the above expressions some additional values need to be approximated through regression. More specifically the elastic and plastic section modulus (W_{el}, W_{pl}) are calculated using the corresponding regression function derived through expression of Eq. (7.1). Additionally, the radius of gyration i needs to be approximated, which is necessary for the factor $\bar{\lambda}$, the simple polynomial of Eq. (7.7) is used:

$$i = b_1 a^2 + b_2 a \qquad (7.7)$$

while for the imperfection factor the critical value of the section's area is found in order to decide which value will be chosen, according to the corresponding table of the Eurocode. In the following test cases, the aforementioned design code checks are performed in order to reach solutions close to the optimum. In the final step, some designs were analyzed and checked by means of the ETABS analysis and design software [35], where all the design regulations of the EC3 are applied.

7.4 Mathematical formulation

In order to satisfy the serviceability criteria, a maximum lateral deflection constraint needs to be applied. However, there is no analytical expression of deflection's derivative required by the search algorithm chosen to solve the optimization problems. For this reason, the compliance of the structure constraint is used instead, for which the analytical expression of the derivative is available, as shown in the Eq. (6.5). Furthermore, since no analytical expression for the DC_C is available, the calculation of its derivative is not straightforward, so it is calculated numerically. Initially the problem formulation restricted both compliance and DC_C constraints to be satisfied concurrently:

$$\min_{a} V(a) = a^T L \tag{7.8a}$$

$$s.t.$$

$$K(a)d(a) = F \tag{7.8b}$$

$$C(a) \leq F^T d(a) \tag{7.8c}$$

$$DC_c(a) \leq 1 \tag{7.8d}$$

$$a_{min,e} \leq a_e \leq a_{max,e}, \quad e = 1,2,\dots,N_{ele} \tag{7.8e}$$

For solving the problem described above, the interior point algorithm was used and the search procedure was initiated using uniform material distribution as an initial guess, i.e. same cross-sectional area (a_e) for all frame structural elements. With respect to the performance of the interior point algorithm, two issues need to be underlined. When the optimized design satisfied the DC_C constraints, the reduction of the material was guided by the compliance constraint. More specifically, the same design was obtained for the formulation where both constrains of Eqs. (7.8c) and (7.8d) were imposed in comparison to the one where only the compliance constraint of Eq. (7.8c) was used. Otherwise, as it was noticed, when the optimized design achieved was violating the DC_C, the layout of the initial GS never changed, resulting to an SSO problem rather than a combined FSTO and SSO stages one. Through the first parametric investigation it can be concluded that the

constraints of Eqs. (7.8c) and (7.8d) are conflicting and the convergence to an optimized solution is not possible. Thus, a two-stages SO problem formulation is examined. In the first stage, an FSTO minimum material volume problem is solved, subjected to the constraints of Eqs. (7.8b), (7.8c), (7.8e) and in the second one, an SSO minimum material volume problem is solved, subjected to the constraints of Eqs. (7.8b), (7.8d) and (7.8e). The value of a_{min} adopted for the FSTO stage corresponds to a relatively small quantity just in order to avoid the singularity problem, while in the SSO stage this value corresponds to the minimum cross-sectional areas taken from the lists of standardized sections. In both stages, a_{max} is the maximum cross-sectional area taken from previously mentioned lists. The interior point was found not to be the proper algorithm for both stages because it didn't give stable solutions. For this reason, the above algorithm is used only for the FSTO stage, that it is proved very consistent, and for the SSO stage the Sequential Quadratic Programming (SQP) method is applied. Regarding the SSO process, it was found that the optimized design was depending on the initial guess of the possible solution, contrary to the FSTO stage where it always converged to the same design, irrespectively to the initial one. For this reason, the Global Search function of MATLAB optimization toolbox is implemented in SSO stage.

7.5 Implementation of the methodology

The mathematical formulation of the FSTO stage, is the dual problem of the formulation that is presented in section 6.3. Due to the high nonlinearity of the constraints in the above formulation, the computational cost of the optimization procedure is much larger comparing with the problem of chapter 6. Thus, this procedure cannot be implemented in a commercial software, since the analysis in this kind of software takes much more time, comparing to an inhouse programming code. Consequently, the FSTO stage in the current chapter is performed in a personal MATLAB code. The procedure of the proposed two-stages SO approach is described below. In the current study two variants of the proposed methodology were tested. According to the first one both, FSTO and SSO solution processes where continuous and standardized sections were assigned to the two

optimized designs achieved, afterward the resulted design will be labelled as modified design. According to the second one, FSTO solution process was also continuous, the SSO however was performed by HP-OCP and it was discrete:

Initialization:

1. Define the initial design domain (i.e. the GS), the boundary and load conditions, material properties and maximum deflection allowed.

2. Select the section types per group of structural elements and perform regression analysis for defining the relation between cross-sectional area vector a with I_y, $W_{el,y}$, $W_{pl,y}$ and i. The grouping of the structural elements and the section profiles assigned to each group, depends on member's type (column, beam or brace).

Stage 1: FSTO

3. The FSTO parameters are defined, an initial guess of the material distribution (projected to initial guess of the cross-sectional areas $a_{TOP}^{Initial}$) is selected and the optimization process is performed by means of the interior point algorithm, the convergence tolerance is set equal to 10^{-12}.

4. In every iteration, the system of the FE equilibrium equations is solved, and compliance and volume are computed together with their derivatives.

5. Update the design variable vector a and the corresponding cross-sectional properties and check if convergence was achieved. If not, go back to step 4, otherwise proceed to step 6.

6. Identify which structural elements of the initial design domain are to be removed, i.e. those having cross-sectional area less than the critical limit a_{crit}. Note: nodes not connected with any frame element should also be removed, accordingly loads and boundary conditions needs to be automatically updated. The optimized design achieved ($\alpha_{Conceptual}^*$) refers to the outcome of the conceptual design phase.

Stage 2: SSO

7. The optimization parameters of the SSO are defined. As it was noted earlier SQP algorithm in combination with the MATLAB's Global Search solver are

implemented; therefore, the search process will not significantly be affected by the initial design vector (i.e. the initial guess of the cross-sectional areas $\alpha_{SIZE}^{Initial}$).

8. Similar to stage 1, in every iteration, the system of the FE equilibrium equations is solved, followed by the computation of compliance and volume and then the design checks are performed.

9. The design variable vector a is updated together with the values of the cross-sectional properties (i.e. I_y, $W_{el,y}$, $W_{pl,y}$ and i) check if convergence was achieved. If not, go back to step 8, otherwise stop.

Subsequently the following terminology is used: optimized design stands for the best design achieved through the FSTO and SSO continuous optimization problems, modified design stands for one resulted when assigning the closest standardized section profiles to the cross-sectional properties of the optimized one, and reference design stands for initial one of the SSO procedure.

7.6 Numerical examples

In this section, in order to assess the performance of the proposed methodology together with the associated formulations, several test cases are examined. The test cases are classified into two groups, the first one is denoted as preliminary design phase group and the second as final design one. In the first group, the design checks performed during the implementation of SSO stage (denoted as stage 2), are limited to those described in the previous section (i.e. deformation and axial and shear forces with bending moments interaction design checks). In the second group of test cases the HP-OCP with its integration with ETABS v18 is used for implementing the sizing structural design optimization stage where all the design checks imposed by the provisions of the design code selected are implemented in detail, relying on a commercial structural analysis and design software, specifically ETABS v18.1.1 is used.

All test cases refer to MRBFs of mid- and high-rise building structures. MRBFs represent assemblages of beams, columns and in case of steel structures is composed by braces as well, while the beams are rigidly connected to the columns. Resistance to lateral loads is

provided primarily by rigid frame action, i.e. by the development of shear forces and bending moments in the frame members and joints together with axial forces at the braces. By virtue of the rigid beam-column connections, a moment frame cannot deform laterally without bending beams or columns depending on the connection's geometry. The bending rigidity and strength of the structural system of the MRBF is therefore the primary source of lateral stiffness and strength for the entire building structure. The 1994 Northridge earthquake revealed a common flaw in the construction and building design codes were revised to strengthen them. In this context, among others, the proposed two stages methodology was developed for deriving alternatives of the typical MRBFs that are composed by beam-column-brace layout. In this direction, the FSTO stage is used as a tool to design increased resistance layouts of MRBFs for specific allowable deflection limits, while the SSO stage is implemented for the final design part of the methodology. The resulted optimized designs are intended to be integrated in the design process of mid- and high-rise buildings. In order to present the integration of FSTO formulations in the conceptual design of civil structures, typical MRBFs of varying dimensions are employed. Particularly, in the first group of tests, labeled as preliminary design phase test cases, two MRBFs for mid-rise buildings are examined, where the same list of cross-sectional profiles is used to be assigned to the groupings of the structural elements. Subsequently, an MRBF of a high-rise building is studied and different lists of cross-sectional profiles are used depending on the structural element type. In the second group of test cases, labeled as final design phase test cases, the MRBFs of the mid-rise buildings are studied and the optimized designs achieved for specific deflection limit and different GSs are compared. Finally, a real-world high-rise building modeled using ETABS v18.1.1 is examined, where the methodology aims to enhance the building's lateral strength. Structural steel of class with nominal yield stress of $f_y = 235\ MPa$ and modulus of elasticity equal to $E = 200\ GPa$ is selected in all of the following test cases.

7.6.1 Preliminary design phase test cases

MRBF1: lateral point load on left corner

In the first group of tests, a mid-rise building with 3 bays and 6 stories is considered. The length of each bay is equal to $3m$ and the height of each story is equal to $3m$; therefore, the total width of the building's MRBF is $L = 9m$ and the total height is $H = 18m$. In Figure 7.2, the MRBF is shown, that is subjected to a point load, with magnitude equal to $P = 4MN$, applied at the top left corner and the bottom side restrained, subsequently denoted as MRBF1. In these test cases, to all groupings of the frame structural elements are assigned cross-sectional properties from the same section type list; in particular, HEA section type list is used herein. Thus, the upper value of the designs variables is set equal to $a_{max} = 347cm^2$, that corresponds to the cross-sectional area of HEA1000 section profile and the critical cross-sectional area is equal to $a_{crit} = 10cm^2$. As it was noted earlier, the minimum bound for the designs variables was set equal to a smaller value than minimum cross-sectional area of the corresponding HEA section type list in order to identify the elements of the GS to be eliminated during the implementation of the FSTO stage. Through the parametric investigation, for some cases it was observed that upon convergence of the FSTO stage, some elements of the optimized design resulted to cross-sectional area value less than HEA100 ($a_{min} = 21cm^2$, the minimum cross-sectional area of the corresponding HEA section type list) but very close to this value. When these members were eliminated and standardized section profiles were assigned to the remaining ones, the corresponding compliance and volume values varied significantly compared to those of the optimized design achieved by the continuous approach. For investigation purposes, three different GSs are generated, i.e. those generated using simple-level (S), mid-level (M) or full-level (F) connectivity for the initial design domain, combined with two allowable deflection limits, i.e. $d_{allow,1} = \frac{H}{200}$ and $d_{allow,2} = \frac{H}{400}$.

Table 7.1 presents the results obtained for stage 1 (i.e. FSTO stage), for the three aforementioned GSs, where the initial design domains are composed by 78, 135 and 251 FEs, respectively. Two problem formulations are examined in each GS, varying on the

allowable deflection limit considered (i.e. $d_{allow,1}$ or $d_{allow,2}$). Therefore, the test cases examined for the corresponding formulations are labeled as MRBF1#d#, where MRBF1# denotes the connectivity level of the GS (# stands for S, M or F) and d# denotes the allowable deflection limit considered in the formulation (# stands for 1 or 2). In each formulation, the compliance and the volume of the MRBF1 are evaluated, firstly by using the regression function for the cross-sectional properties and then by implementing the discrete cross-sectional properties of the HEA section type list that is applied after the convergence of the algorithm. The results collected and are presented to Table 1 refer to the values of compliance (C), material volume (V), number of the remaining frame FEs (N_e) in the optimized design and the error between the continuous and the discrete approach. The optimization results of the continuous approach are presented in the columns of Table 7.1, labeled as continuous approach, since they refer to the case where the cross-sectional properties of the MRBF1 structural system are calculated through approximation functions of Eq. (7.1) derived through regression analyses. The corresponding results of the discrete approach, i.e. for the equivalent standard sections, are presented in the columns of Table 7.1, labeled as standardized cross-sectional properties (HEA). The results of this table, confirmed that accurate approximations of the cross-sectional properties to the real ones are obtained through the approximation functions, since the variation on the compliance values varies from 0.20% to 2.78% and that for the material volume of the optimized designs from 0.04% to 2.36%. Additionally, comparing the results for the same allowable deflection limit, the optimized structural systems that derived from denser GSs, always had less volume than the optimized layouts that were produced from GSs with smaller connectivity level. Figure 7.3 shows the optimized designs for MRBF1 for the three different GSs and $d_{allow,1} = \frac{H}{200}$ and in Figure 7.4 the optimized designs for $d_{allow,2} = \frac{H}{400}$ are illustrated.

Table 7.2 presents the results obtained for MRBF1 in the SSO stage; among others the level of feasibility as denoted by the DC for the optimized design is also presented. It should be noticed that feasibility is presented only for the design where the standardized HEA section properties were assigned, since for the optimization runs performed based

on the regression function estimations, the procedure always converged to a feasible design with respect to the design code checks. Significant observations can be derived from Table 7.2 on the performance of the optimized design with reference to the compliance, material volume and *DC*. More specifically, in MRBF1Sd1 test case, SSO procedure required reducing compliance from 0.360MNm to 0.294MNm in order to achieve a feasible solution. On the other hand, in MRBF1Sd2 test case, compliance of SSO-based optimized design was increased from 0.180MNm to 0.279MNm. Accordingly, in MRBF1Md1 test case, SSO procedure required reducing compliance from 0.360MNm to 0.268MNm in order to achieve a feasible solution, while in the MRBF1Md2, the compliance is increased from 0.180MNm to 0.273MNm. Finally, for the MRBF1Fd1 test case, SSO procedure demanded decreasing compliance from 0.360MNm to 0.286MNm, while in the MRBF1Fd2, the compliance is increased from 0.180MNm to 0.288MNm. From the above, it is observed that, independently of the GS, the compliance needs to be changed after the FSTO stage of the optimization, in order to minimize the volume and satisfy the *DC*. Thus, it can be stated that minimizing the volume of a structure by satisfying both, deflections limits and DC is a contradictory procedure. In the MRBF1 test case, it can be noticed that an optimized design is located between 0.268MNm to 0.294MNm or in terms of deflection in the range of $\frac{H}{268}$ to $\frac{H}{246}$. From Table 4.2, it is observed that the structural system with the minimum volume is developed in the case of MRBF1Fd2, proving in this way the importance of providing the initial design domain with more freedom. Details for the standardized cross-sections for the MRBF1#d2 test cases can be found in Table 7.3.

*($\times 10^5$)

Test case	Continuous approach		Standardized cross-sectional properties (HEA)		Error		Number of frames
	C* (Nm)	V (m^3)	C* (Nm)	V (m^3)	C (%)	V (%)	N_e
MRBF1Sd1		1.0944	3.6656	1.1006	1.82	0.57	18
MRBF1Md1	3.6	0.9924	3.7000	0.9920	2.78	0.04	22
MRBF1Fd1		0.9869	3.6879	0.9636	2.44	2.36	20
MRBF1Sd2		2.3508	1.7964	2.3600	0.20	0.39	39
MRBF1Md2	1.8	1.9830	1.8208	1.9660	1.15	0.86	25
MRBF1Fd2		1.9670	1.8259	1.9415	1.44	1.30	20

Table 7.1 MRBF1#d# test cases-FSTO stage: Comparison between continuous approach and standardized section properties.

*($\times 10^5$)

Test case	Continuous approach		Standardized cross-sectional properties (HEA)			Error	
	C* (Nm)	V (m^3)	C* (Nm)	V (m^3)	DC	C (%)	V (%)
MRBF1Sd1	2.9439	1.5635	2.9344	1.5682	1.003	0.32	0.30
MRBF1Md1	2.6896	1.5202	2.6597	1.5382	1.033	1.11	1.17
MRBF1Fd1	2.8634	1.4120	2.8723	1.4093	1.025	0.31	0.19
MRBF1Sd2	2.7992	1.6203	2.8254	1.6076	1.056	0.94	0.79
MRBF1Md2	2.7310	1,5007	2.7353	1.5037	1.021	0.16	0.20
MRBF1Fd2	2.8877	1,3970	2.8692	1.4060	1.029	0.64	0.64

Table 7.2 MRBF1#d# test cases-SSO stage: Comparison between continuous approach and standardized section properties.

Figure 7.2 MRBF1: Initial design domain for (a) simple-level (MRBF1Sd#), (b) mid-level (MRBF1Md#) and (c) full-level (MRBF1Fd#) connectivity GS.

Figure 7.3 MRBF1#d1: FSTO-based optimized layouts for test cases (a) MRBF1Sd1, (b) MRBF1Md1 and (c) MRBF1Fd1.

Figure 7.4 MRBF1#d2: FSTO-based optimized layouts and frames enumeration for test cases (a) MRBF1Sd2, (b) MRBF1Md2 and (c) MRBF1Fd2.

MRBF1Sd2			MRBF1Md2			MRBF1Fd2		
Frame num	HEA section[1]	HEA section[2]	Frame num	HEA section[1]	HEA section[2]	Frame num	HEA section[1]	HEA section[2]
1	HE 650 A	HE 260 A	1	HE 360 A	HE 260 A	1	HE 360 A	HE 260 A
2	HE 1000 A	HE 450 A	2	HE 360 A	HE 260 A	2	HE 360 A	HE 260 A
3	HE 1000 A	HE 550 A	3	HE 360 A	HE 260 A	3	HE 360 A	HE 260 A
4	HE 1000 A	HE 550 A	4	HE 360 A	HE 260 A	4	HE 360 A	HE 280 A
5	HE 1000 A	HE 450 A	5	HE 1000 A	HE 500 A	5	HE 900 A	HE 500 A
6	HE 1000 A	HE 650 A	6	HE 1000 A	HE 500 A	6	HE 1000 A	HE 550 A
7	HE 200 A	HE 180 A	7	HE 1000 A	HE 900 A	7	HE 800 A	HE 800 A
8	HE 140 A	HE 100 A	8	HE 1000 A	HE 900 A	8	HE 800 A	HE 800 A
9	HE 300 A	HE 700 A	9	HE 1000 A	HE 800 A	9	HE 800 A	HE 800 A
10	HE 1000 A	HE 700 A	10	HE 280 A	HE 200 A	10	HE 260 A	HE 220 A
11	HE 1000 A	HE 800 A	11	HE 120 A	HE 160 A	11	HE 360 A	HE 300 A
12	HE 1000 A	HE 900 A	12	HE 900 A	HE 650 A	12	HE 900 A	HE 550 A
13	HE 300 A	HE 320 A	13	HE 600 A	HE 360 A	13	HE 550 A	HE 360 A
14	HE 100 A	HE 220 A	14	HE 650 A	HE 400 A	14	HE 700 A	HE 450 A
15	HE 140 A	HE 120 A	15	HE 120 A	HE 160 A	15	HE 500 A	HE 340 A
16	HE 300 A	HE 240 A	16	HE 550 A	HE 340 A	16	HE 240 A	HE 180 A
17	HE 140 A	HE 140 A	17	HE 220 A	HE 180 A	17	HE 450 A	HE 320 A
18	HE 1000 A	HE 340 A	18	HE 100 A	HE 140 A	18	HE 400 A	HE 320 A
19	HE 240 A	HE 240 A	19	HE 500 A	HE 340 A	19	HE 900 A	HE 600 A
20	HE 240 A	HE 260 A	20	HE 400 A	HE 300 A	20	HE 450 A	HE 340 A
21	HE 100 A	HE 100 A	21	HE 120 A	HE 340 A			
22	HE 180 A	HE 100 A	22	HE 900 A	HE 650 A			
23	HE 100 A	HE 100 A	23	HE 220 A	HE 280 A			
24	HE 220 A	HE 240 A	24	HE 140 A	HE 180 A			
25	HE 1000 A	HE 600 A	25	HE 550 A	HE 340 A			
26	HE 240 A	HE 240 A						
27	HE 1000 A	HE 360 A						
28	HE 240 A	HE 260 A						
29	HE 100 A	HE 100 A						
30	HE 280 A	HE 260 A						
31	HE 240 A	HE 200 A						
32	HE 1000 A	HE 360 A						
33	HE 240 A	HE 240 A						
34	HE 1000 A	HE 400 A						
35	HE 240 A	HE 240 A						
36	HE 280 A	HE 320 A						
37	HE 650 A	HE 280 A						
38	HE 200 A	HE 160 A						
39	HE 340 A	HE 260 A						

Table 7.3 Standardized cross-sections of MRBF1#d2 test cases

The second group of tests performed, corresponds to an MRBF of a mid-rise building (denoted as MRBF2) that is subjected to a point load applied at the tip and the bottom side restrained (see Figure 7.5). The length of each bay is equal to 4m and the height of each story is equal to 3m; therefore, the total width of MRBF2 is $L = 16m$ and the total height is $H = 24m$, while the value of the point load is equal to $P = 4.5MN$. All parameters corresponding to the cross-sectional properties are the same with those of MRBF1 (i.e. HEA section type was chosen and the corresponding bounds a_{max} and a_{crit}). For investigation purposes, similar to MRBF1, three initial design domains based on different GSs are generated, combined with two allowable deflection limits, $d_{allow,1} = \frac{H}{200}$ and $d_{allow,2} = \frac{H}{600}$.

Table 7.4 presents the results obtained for the FSTO stage, for the three aforementioned GSs, where the initial design domains are composed by 140, 292 and 632 FEs, respectively. Table 7.5 presents the results obtained for MRBF2 in the SSO stage. Observing the results of both tables, it is noticed that the prediction of the standardized cross-sectional properties is very close to the real values, since the error projected to compliance varies from 0.02% to 3.52% and that to the material volume from 0.14% to 3.34%. Similar to the MRBF1 test case, in the FSTO stage, the more design freedom is provided to the initial structural system, the less volume it has. However, in the SSO stage, for $d_{allow,2}$ the mid-level connectivity GS converged to a structural system with less volume than the full-level connectivity GS. This means, that providing the structural system with too much freedom not always lead to better results, cause more complicated layouts are produced, making it more difficult to satisfy the *DC*. Regarding the results of $d_{allow,1}$, it is observed that MRBF2Fd1 has 0.6% more volume than MRBF2Md1 but it has 3.99% less compliance. So, with almost the same material volume, better structural performance is succeeded, in terms of compliance. Figure 7.6 shows the optimized designs for MRBF2 for the three different GSs and $d_{allow,1} = \frac{H}{200}$ and in Figure 7.7 the optimized designs for $d_{allow,1} = \frac{H}{600}$ are illustrated. Finally, it is observed that in order to obtain feasible solutions the

compliance of the optimized designs should vary from 0.27MNm to 0.40MNm or in terms of deflection from $\frac{H}{400} - \frac{H}{270}$.

*$(\times 10^5)$

Test case	Continuous approach		Standardized cross-sectional properties (HEA)		Error		Number of frames
	C* (Nm)	V (m^3)	C* (Nm)	V (m^3)	C (%)	V (%)	N_e
MRBF2Sd1		1.4639	4.8610	1.4693	0.02	0.37	36
MRBF2Md1	4.86	1.1160	5.0313	1.0787	3.52	3.34	24
MRBF2Fd1		1.0718	4.7814	1.0986	1.62	2.50	16
MRBF2Sd2		4.6258	1.6242	4.5923	0.26	0.72	54
MRBF2Md2	1.62	3.3465	1.6245	3.3417	0.28	0.14	42
MRBF2Fd2		3.2239	1.6592	3.2150	2.42	0.28	42

Table 7.4 MRBF2#d# test cases-FSTO stage: Comparison between continuous approach and standardized section properties.

*$(\times 10^5)$

Test case	Continuous approach		Standardized cross-sectional properties (HEA)			Error	
	C* (Nm)	V (m^3)	C* (Nm)	V (m^3)	DC	C (%)	V (%)
MRBF2Sd1	4.0209	1.7795	4.0093	1.7870	1.0609	0.29	0.42
MRBF2Md1	3.3866	1.6163	3.4081	1.6126	1.0189	0.63	0.23
MRBF2Fd1	3.2879	1.6113	3.2721	1.6225	1.0217	0.48	0.69
MRBF2Sd2	3.2240	2.3436	3.2139	2.3487	1.0488	0.31	0.22
MRBF2Md2	3.2217	1.7646	3.2729	1.7452	1.0420	1.59	1.09
MRBF2Fd2	2.6933	2.1861	2.7038	2.1790	1.0984	0.39	0.32

Table 7.5 MRBF2#d# test cases-SSO stage: Comparison between continuous approach and standardized section properties.
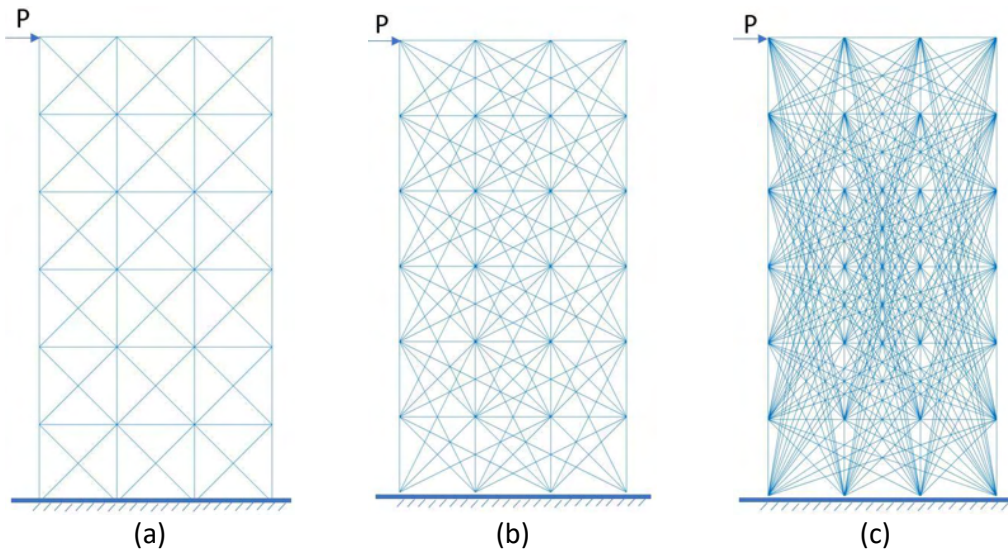
Figure 7.5 MRBF2: Initial design domain for (a) simple-level (MRBF2Sd#), (b) mid-level (MRBF2Md#) and (c) full-level (MRBF2Fd#) connectivity GS.
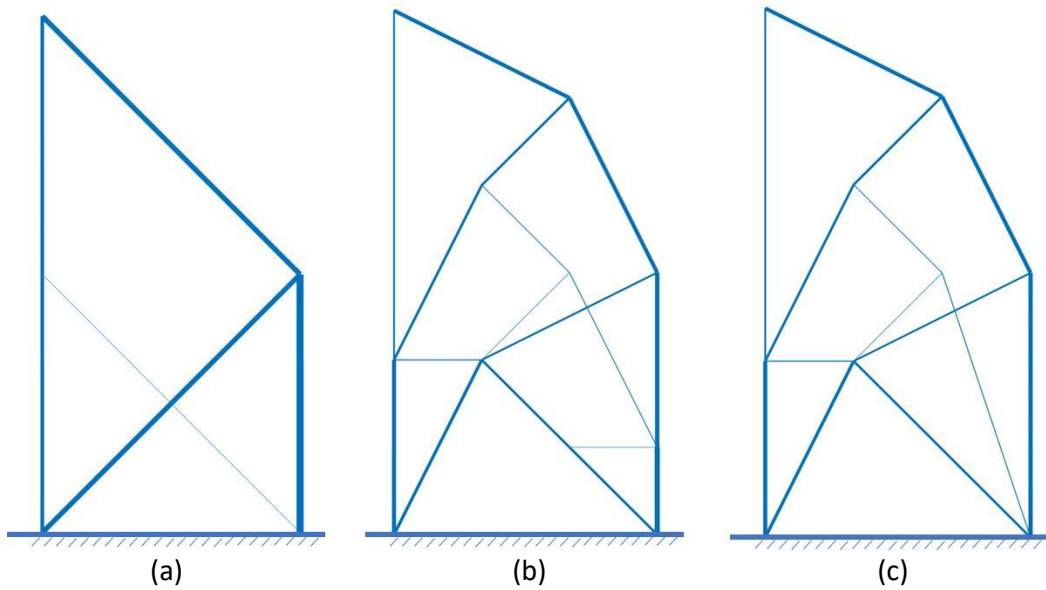

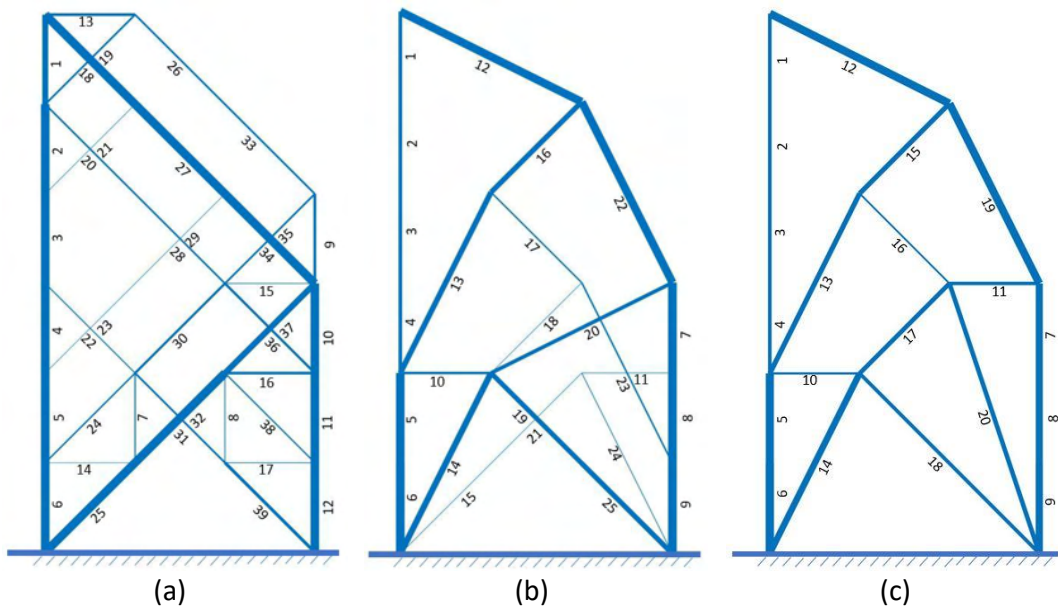Figure 7.6 MRBF2#d1: FSTO-based optimized layouts for test cases (a) MRBF2Sd1, (b) MRBF2Md1 and (c) MRBF2Fd1.

183

Figure 7.7 MRBF2#d2: FSTO-based optimized layouts for test cases (a) MRBF2Sd2, (b) MRBF2Md2 and (c) MRBF2Fd2.

MRBF3: high-rise building

In the following example, the structural system of a high-rise building with 4 bay and 12 stories is considered. The length of each bay is equal to 4m and the height of each story is equal to 3m; therefore, the total width is $L = 16m$ and the total height is $H = 36m$, whereas the value of the point load is equal to $P = 5\ MN$. For the test cases examined for this example, different cross-sectional profile lists are used for the groupings of the frame elements according to the frame type. More specifically, the HEA section profile list is used for the column groupings, the IPE one for the beam groupings and the CHS one for the brace groupings. Additionally, it is considered that frame elements of column and beam type will not be removed during the FSTO stage of the optimization methodology, thus they will remain in the optimized designs of both stages. In order to satisfy this requirement during the minimum volume FSTO stage, the lower bound for the column and beam groupings was set equal to the minimum cross-sectional area of the corresponding section profile lists (i.e. HEA and IPE lists). More specifically, the bounds for the design variables are: $a_{col,max} = 347cm^2$, $a_{beam,max} = 156cm^2$, $a_{brace,max} = 100cm^2$, $a_{col,crit} = 21cm^2$, $a_{beam,crit} = 10cm^2$, $a_{brace,crit} = 7cm^2$. Similar to MRBF1

184

and MRBF2, three initial design domains based on different GSs are generated, combined with three allowable deflection limits: $d_{allow,1} = \frac{H}{100}$, $d_{allow,2} = \frac{H}{200}$ and $d_{allow,3} = \frac{H}{300}$. Figure 7.8 depicts the initial design domains generated for the three different GSs, while in Figures 7.9-7.11 the optimized structural systems for the three allowable deflection limits are presented, respectively. Table 7.6 shows the results of the FSTO stage, where the initial design domains are composed by 204, 296 and 1052 FEs, respectively and in Table 7.7 the results of the SSO stage are presented. From both Tables it is observed that the predictions obtained through regression analyses performed well, since the range of the error in terms of both compliance and volume varies from 0.01% to 5.87%. Similar to MRBF1 and MRBF2 examples, for all tests performed for MRBF3, SSO stage of the methodology converged to feasible designs as indicated by the *DC* index, however slightly infeasible modified designs resulted after assigning standardized cross-sectional properties. In MRBF3Sd# test case, the SSO stage failed to converge for the $d_{allow,1}$ allowable deflection limit, as it can be seen from Table 7.7 the violation with reference to the *DC* index is equal to 44%, much larger to the violation achieved in the previous examples. Thus, the design achieved is not acceptable, for the other two cases the solution process converged normally. Similarly, In MRBF3Md# test case, the SSO stage failed to converge for the $d_{allow,1}$ allowable deflection limit, as it can be seen from Table 7.7 the violation with reference to the DC index is equal to 30%. However, in MRBF3Fd1 test case, contrary to the previous levels of connectivity, the optimized layout derived for $d_{allow,1}$ resulted to a feasible solution. The above observations highlight the importance of the designing freedom, as far as a denser GS is able to reach to feasible solutions even for cases that large deflections are allowed. In MRBF3 test case, it is observed that in order to obtain feasible solutions, the compliance of the optimized designs should vary from 0.55MNm to 0.75MNm (or in terms of deflection from $\frac{H}{327} - \frac{H}{240}$). Regarding all the MRBF test cases, it is noticed that the maximum deflection of the feasible solutions should vary $\frac{H}{400} - \frac{H}{240}$, which is an observation similar with Smith's [99] survey that is presented in the previous section.

($\times 10^6$)

Test case	Continuous approach		Standardized cross-sectional properties (HEA)		Error		Number of frames
	C* (Nm)	V (m^3)	C* (Nm)	V (m^3)	C (%)	V (%)	N_e
MRBF3Sd1		1.8552	1.8678	1.9285	3.63	3.80	150
MRBF3Md1	1.80	1.6028	1.8979	1.6497	5.16	2.84	150
MRBF3Fd1		1.5404	2.1554	1.5638	2.99	1.49	152
MRBF3Sd2		3.4703	0.9221	3.5079	2.40	1.07	154
MRBF3Md2	0.90	2.9640	0.9561	2.9951	5.87	1.04	164
MRBF3Fd2		2.8008	0.9319	2.8750	3.42	2.58	166
MRBF3Sd3		5.9033	0.5978	6.0204	0.37	1.95	198
MRBF3Md3	0.60	4.4444	0.6077	4.5218	1.26	1.71	170
MRBF3Fd3		4.0810	0.6313	4.0571	4.95	0.59	166

Table 7.6 MRBF3#d# test cases-FSTO stage: Comparison between continuous approach and standardized section properties.

($\times 10^6$)

Test case	Continuous approach		Standardized cross-sectional properties (HEA)			Error	
	C* (Nm)	V (m^3)	C* (Nm)	V (m^3)	DC	C (%)	V (%)
MRBF3Sd1	0.9218	6.3012	0.9209	6.3004	1.4415	0.09	0.01
MRBF3Md1	0.7533	7.1541	0.7521	7.1650	1.2967	0.16	0.15
MRBF3Fd1	0.5558	7.6082	0.5522	7.6465	1.0107	0.65	0.50
MRBF3Sd2	0.7228	7.8933	0.7178	7.9147	1.0413	0.69	0.17
MRBF3Md2	0.7071	5.0001	0.7058	5.0084	1.0473	0.18	0.17
MRBF3Fd2	0.6521	4.2166	0.6507	4.2357	1.0248	0.21	0.45
MRBF3Sd3	0.6814	7.3877	0.6828	7.3879	1.0384	0.20	0.00
MRBF3Md3	0.7550	4.4098	0.7568	4.3931	1.0413	0.23	0.38
MRBF3Fd3	0.6635	4.0981	0.6612	4.1177	1.0519	0.35	0.48

Table 7.7 MRBF3#d# test cases-SSO stage: Comparison between continuous approach and standardized section properties.
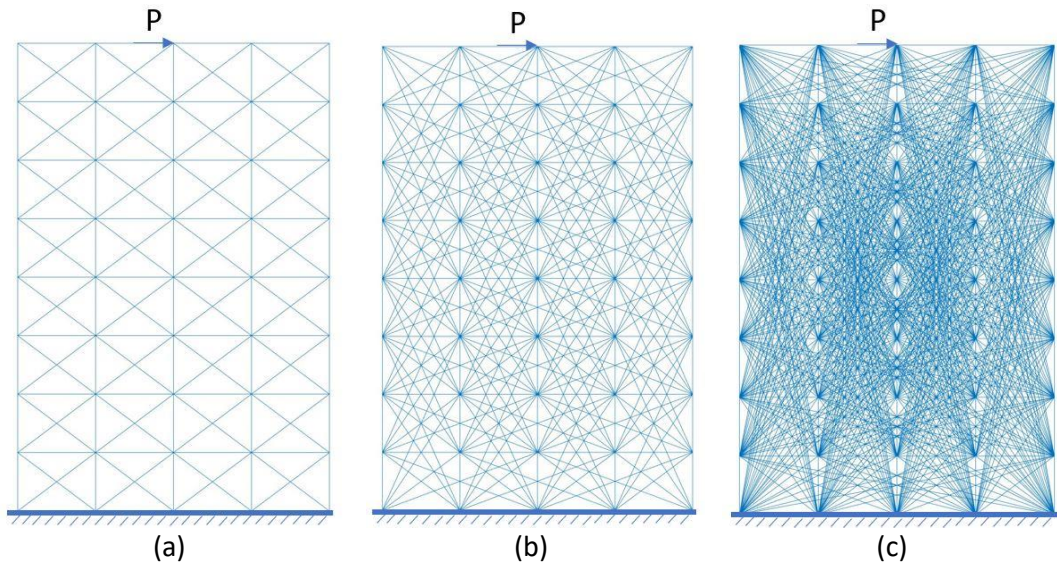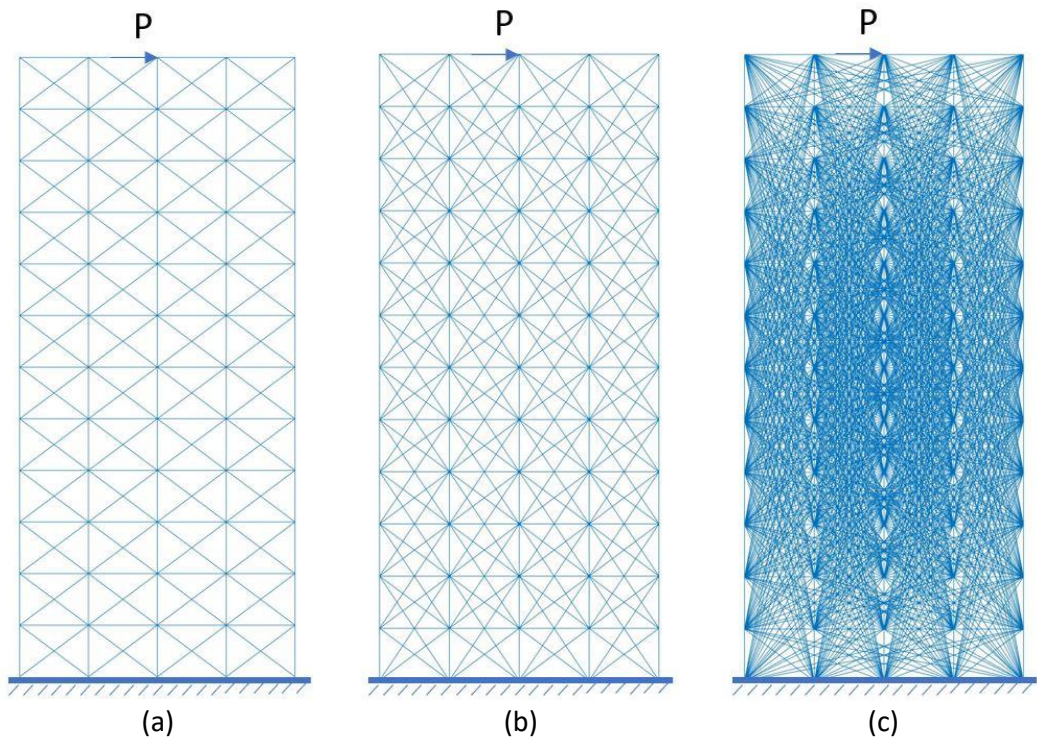
Figure 7.8 MRBF3: Initial design domain for (a) simple-level (MRBF3Sd#), (b) mid-level (MRBF3Md#) and (c) full-level (MRBF3Fd#) connectivity GS.
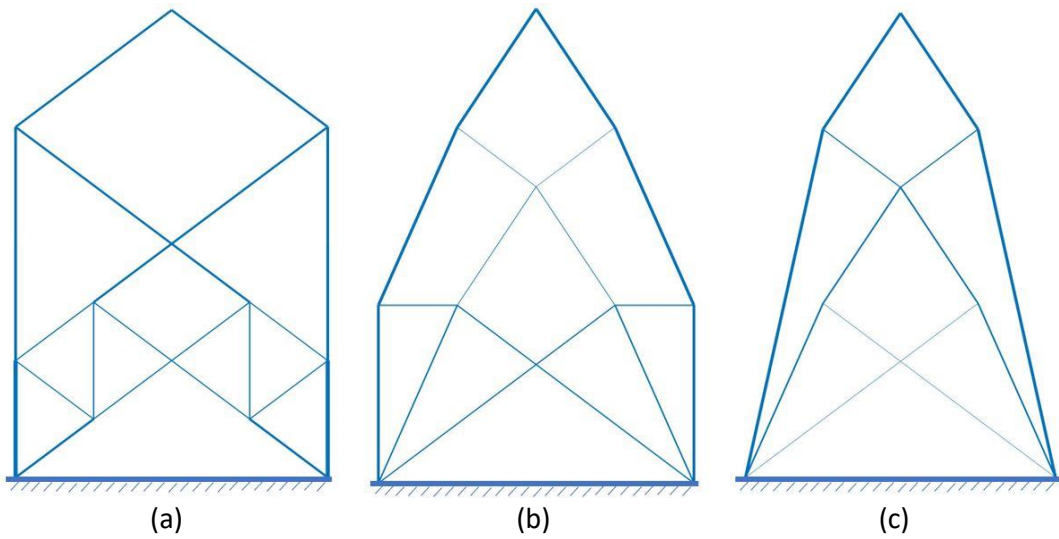

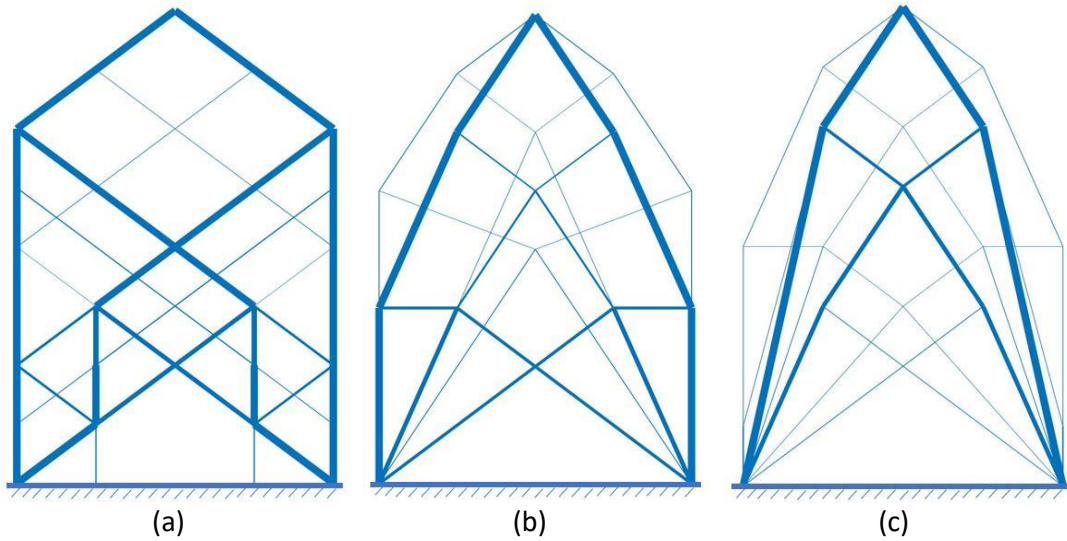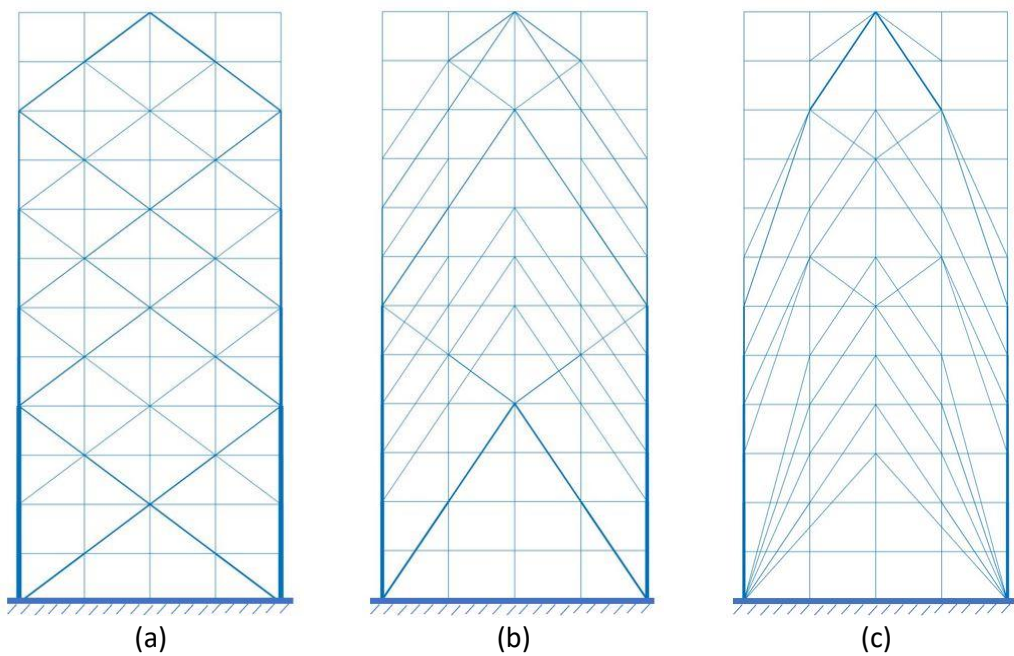*Figure 7.9 MRBF3#d1: FSTO-based optimized layouts for test cases (a) MRBF3Sd1, (b) MRBF3Md1 and (c) MRBF3Fd1.*
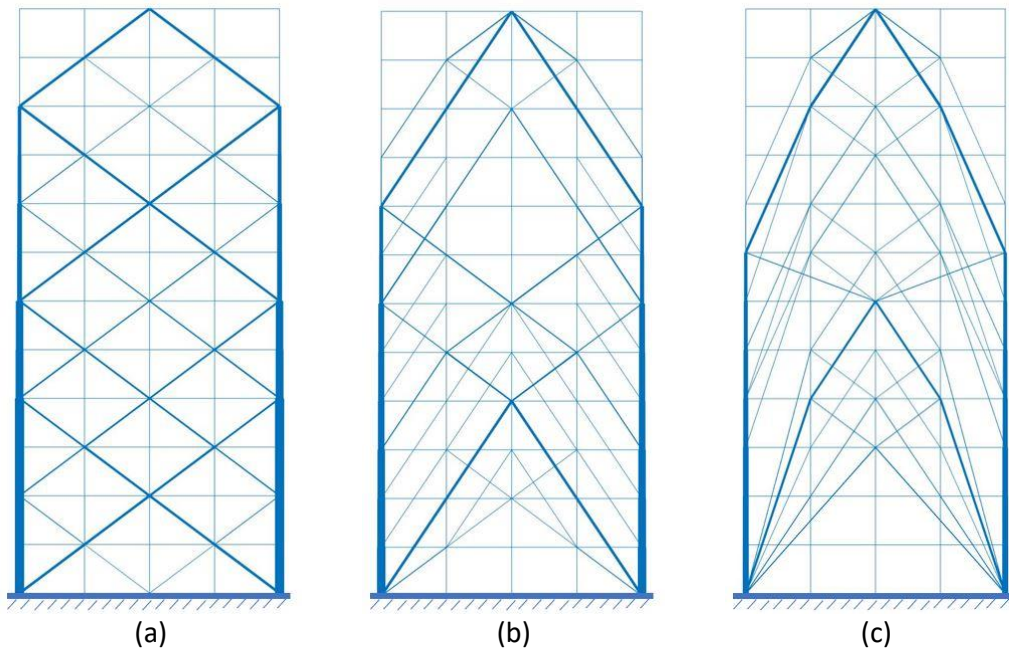
Figure 7.10 MRBF3#d2: FSTO-based optimized layouts for test cases (a) MRBF3Sd2, (b) MRBF3Md2 and (c) MRBF3Fd2.
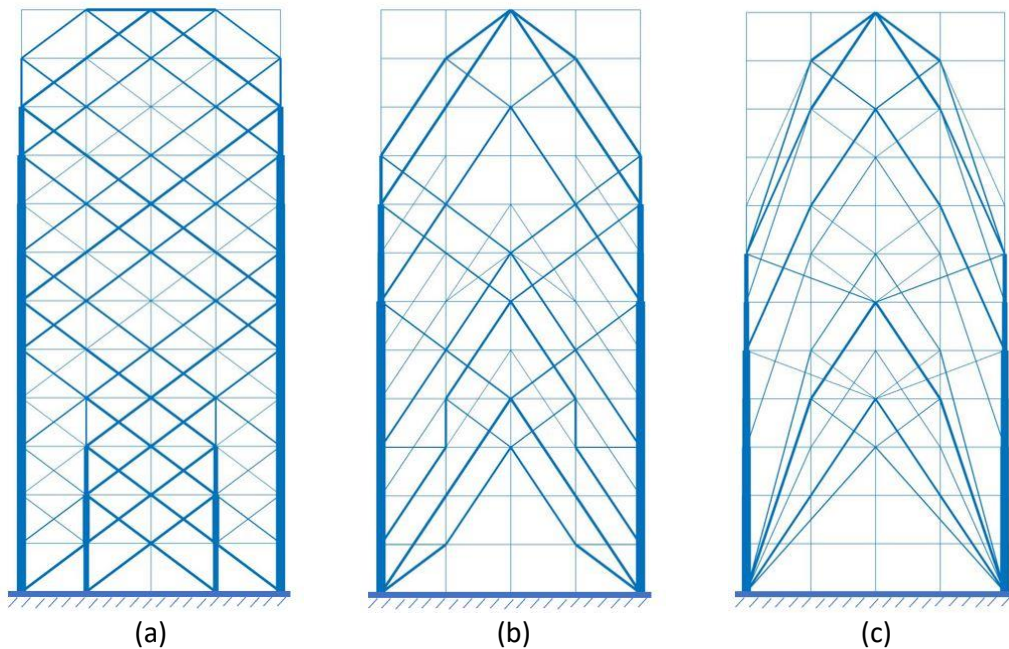
Figure 7.11 MRBF3#d3: FSTO-based optimized layouts for test cases (a) MRBF3Sd3, (b) MRBF3Md3 and (c) MRBF3Fd3.

7.6.2 Final design phase test cases by means of HP-OCP

In the case of the preliminary design phase tests, all FEA and design checks computations along with the optimization algorithms used, are performed using inhouse developed MATLAB codes. The ultimate scope of the proposed work is to integrate the applicability of the proposed methodology to the final design phase as well, integrating the SSO stage into a commercial analysis and design software, providing the opportunity to be implemented in real-world structures. Therefore, in this part of the study the HP-OCP platform is used for performing the SSO stage of the methodology. As it is stated in previous chapter, HP-OCP gives the possibility to be integrated with any commercial analysis and design software. In this study, ETABS v18 of CSI is used.

The solution of the SSO stage for the case of the final design phase is performed by means of the HP-OCP, which is a specially tailored design tool developed to provide optimized design solutions of structural systems. There are some requirements for better performance of HP-OCP, e.g. it is suggested that a feasible reference design is used or slight violating the design check. In the case of the variant of HP-OCP used in the current study, detailed design checks according to EC3 (among others lateral-torsional buckling, effective length method etc.) are performed by ETABS v18.1.1, therefore in all cases the reference design imported in HP-OCP was not feasible. For this reason, a correction process is applied first, more specifically the reference design implemented to HP-OCP relies on the modified design of the previous stage increasing the cross-sectional properties of the latter one, this is done by selecting the first, the second or the third next larger section from the corresponding list of the standardized sections.

Final design phase for MRBF1 and MRBF2

In the following tests the optimization results obtained for the final design phase of MRBF1 and MRBF2 are presented. Boundary and loading conditions together with the cross-sectional properties are the same with those presented in previous section. In order to highlight the importance of integrating the STO problem solving in the design procedure, four structures are compared. A structural system composed of X-braces

allocated in all bays and storeys (simple-level connectivity GS, the corresponding cases are labeled as MRBF1X and MRBF2X), and the structural systems derived for the three GSs described previously (i.e. simple-, mid- and full-level connectivity) while $d_{allow,2} = \frac{H}{400}$ and $d_{allow,1} = \frac{H}{200}$ were used (MRBF1Sd2, MRBF1Md2, MRBF1Fd2 cases together with MRBF2Sd1, MRBF2Md1, MRBF2Fd1 ones). As it can be seen from Table 7.8, HP-OCP managed to reduce the total material volume requirements of the modified design in all cases and to satisfy all the design requirements of the Eurocodes, as implemented by the ETABS software. Figures 7.12(a) to 7.12(d) depict the design check marked for the optimized designs, as it can be seen HP-OCP resulted to designs where the capacity of some of the elements is close to their maximum capacity.

As it was noticed previously, the modified design of the FSTO stage that consists of standardized section properties compared to the reference designs used as the initial one for the SSO stage vary by one, two or three section profiles taken from the list of the standardized profiles than those that are derived from the preliminary design phase. In Table 7.8 two values for the material volume are provided for each test case of the reference design, in parentheses the material volumes of the modified designs achieved for the preliminary design phase are shown and the values outside parentheses denote the material volume of the reference design. It is important to notice the reduction achieved on the material volume requirements for the case of different GSs when HP-OCP is used for performing the SSO stage. Comparing the optimized designs from Table 7.8 it can be seen that reduction of at least 13.54% is achieved when a GS is used for the definition of the initial design domain for the FSTO problems compared to the optimized design of MRBF1X. This can be justified by the observation that many redundant frame elements, that do not contribute to the MRBF1's strength are eliminated for the cases of the different GSs. Comparing the design achieved of the case of MRBF1Sd2 with that of MRBF1Md2 an additional 10.32% reduction on the structural steel requirements is achieved. Therefore, it is noticed that if connectivity freedom is provided, remarkable reduction on the material requirements is attained. Finally, comparing the optimized design achieved of the case of MRBF1Md2 with that of MRBF1Fd2 further reduction of

1.98% is noticed. An observation that worth mentioning is that although double number of frame FEs were available for MRBF1Fd2 compared to the number of frame elements available for MRBF1Md2, the improvement was not proportional to that. Therefore, for larger structural systems it is not always necessary to choose full-level connectivity GSs requiring increased computational effort.

Accordingly, Figures 7.13(a) to 7.13(d) depict optimized designs along with the design checks marked for each design, as it can be seen HP-OCP resulted to designs where the capacity of some of the elements is close to their maximum capacity the result of the SSO. As shown in Table 7.9, the observations related to the structural steel savings achieved with the implementation of HP-OCP are similar with those of MRBF1. More specifically, the optimized layout for the case of MRBF2Sd1 resulted to 30.64% reduced material volume requirements compared with MRBF2X case. While, if the design freedom is increased to a mid-level connectivity GS (MRBF2Md1), additional 10.62% reduction material volume is achieved compared to MRBF2Sd1. Whereas, when the topologically optimized layout achieved for the MRBF2Fd1 case is used, the HP-OCP based optimization procedure resulted to further 1.71% material volume reduction.

Note: [1]MRBF1Sd2 vs MRBF1X, [2]MRBF1Md2 vs MRBF1Sd2, [3]MRBF1Fd2 vs MRBF1Md2.

Test case	Reference (Modified) Design		Optimized Design		Volume Reduction (%)	
	V (m^3)	DC	V (m^3)	DC	by HP-OCP	by test case
MRBF1X	2.3057	0.978	2.2587	0.982	2.04	-
MRBF1Sd2	2.0015(1.6076)	0.967	1.9528	0.974	2.43	13.54[1]
MRBF1Md2	1.7721(1.5037)	0.972	1.7512	0.984	1.18	10.32[2]
MRBF1Fd2	1.7314(1.4060)	0.977	1.7165	0.987	0.86	1.98[3]

Table 7.8 HP-OCP implementation and comparison of different GS for MRBF1

Test case	Reference (Modified) Design		Optimized Design		Volume Reduction (%)	
	V (m^3)	DC	V (m^3)	DC	by HP-OCP	by test case
MRBF2X	3.5419	0.984	3.4943	0.991	1.34	-
MRBF2Sd1	2.4748(1.7870)	0.986	2.4236	0.993	2.07	30.64[1]
MRBF2Md1	2.1894(1.6126)	0.967	2.1662	0.975	1.06	10.62[2]
MRBF2Fd1	2.1489(1.6225)	0.956	2.1292	0.964	0.92	1.71[3]

Table 7.9 HP-OCP implementation and comparison of different GS for MRBF2

(a)   (b)

Figure 7.12 Design check for (a) X-braced structure, (b) MRBF1Sd2, (c) MRBF1Md2 and (d) MRBF1Fd2

193

| (c) | (d) |

Figure 7.13 Design check for (a) X-braced structure, (b) MRBF2Sd1, (c) MRBF2Md1 and (d) MRBF2Fd1

<u>*The cantilever MRBF-RC: composite high-rise building*</u>

In the last part of the investigation the building structure of Figure 7.14(a) is considered, where the proposed methodology will be used to develop the final design of the MRBF-RC structural system that will be used to improve the lateral resistance of the RC building of Figure 7.14 (a). In particular, Figure 7.14 (a) shows a high-rise building (according to the classification of building structures provided by HAZUS [46]) with 4 bay and 12 stories. The length of each bay is equal to 4m and the height of each story is equal to 3m; resulting to a plan view of 16×16m^2 of 36m height, Figure 7.14 (a) shows the 3D view of the building's structural model developed in ETABS v18.1.1.

The thickness of the slabs is equal to 20cm and the dimensions of the section BEAM assigned to all beams are 35×45cm^2. Regarding the columns, three sections are used with dimensions: 55×55cm^2 (COLUMN1), 65×65cm^2 (COLUMN2) and 75×75cm^2 (COLUMN3); the later one is assigned to the columns of the first four storeys of the building structure, for the next four storeys COLUMN2 section is used and for the top four storeys COLUMN1

194

section is assigned to all columns. Subsequently, the loading conditions are defined: dead, live, wind and seismic along both *X* and *Y* directions. For the case of wind and seismic loads an auto lateral load is added according to the EUROCODE1 2005 [86] and EUROCODE8 2004 [33], respectively. After performing analysis and design of the above described design of the RC building many beams failed in shear strength since the interaction of shear force and torsion exceeded maximum capacity. In order to enhance the lateral strength of the RC building, it was decided to use steel braces along all four side views of the building that together with the concrete beams and columns compose an MRBF, labeled as MRBF-RC, the structural system of which will be designed by means of the proposed two stages methodology.

(a)   (b)   (c)   (d)
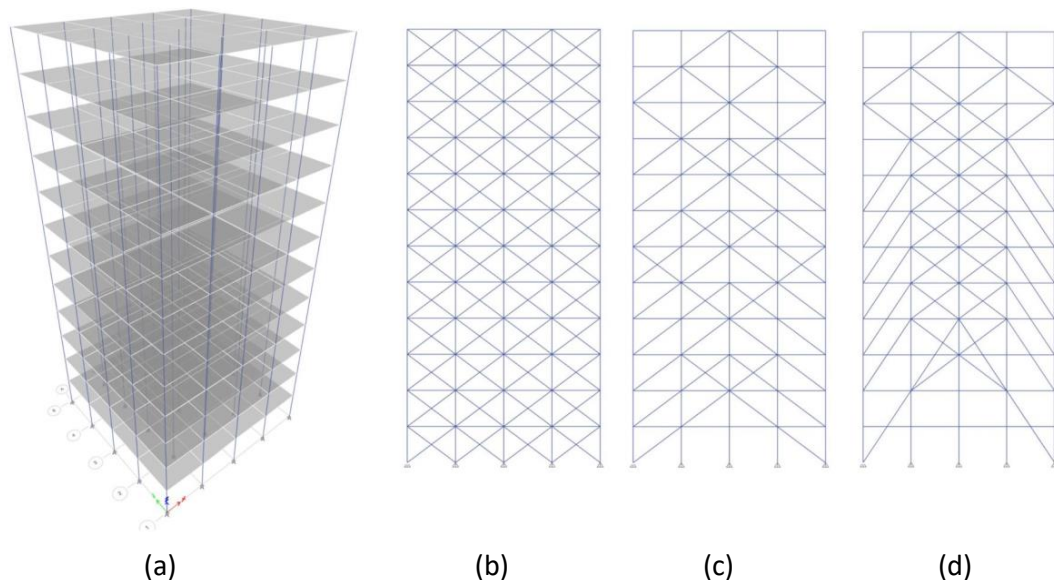
Figure 7.14 a) 3D perspective view of the building's numerical model developed in ETABS 18.1.1, b) X-braces structure (MRBF1), c) layout of FSTO for simple GS (MRBF2), d) layout of FSTO for $r = 8m$ (MRBF3).

In order to develop the concrete-steel MRBF-RC the same boundaries conditions, loads and steel strength with those of MRBF3 described previously are used. The basic difference of MRBF-RC test example with MRBF3 is that its columns and beams are of rectangular cross-section made of reinforced concrete and only its braces are made of steel. Therefore, it was decided that during the optimization procedure, columns and beams will be non-optimizable elements, only braces are considered as design variable.

The three variants of MRBF-RC, shown in Figures 7.14(b) to 7.14(d) are implemented; in particular the one composed by X-braces denoted as MRBF-RCX (i.e. the layout of the simple-level connectivity GS, see Figure 7.14(b)) and those layouts generated by means of the GS with $r = 5$ (denoted as MRBF-RC5m, see Figure 7.14(c)) and $r = 8$ (denoted as MRBF-RC8m, see Figure 7.14(d)) with deflection limit equal to $\frac{H}{200}$. It is important to notice that proposed methodology will be implemented only to the latter two cases, while for the MRBF-RCX case only the sizing design optimization problem is solved in order to define the basis of comparison with the optimized designs derived for the other two cases. The SSO part of the methodology is performed by HP-OCP, while the grouping of the braces was defined through a survey performed for all three test cases with the support of the auto-select functionality of ETABS resulting into 12 groups of brace elements having the same section properties.

During the sizing design optimization procedure of HP-OCP, in addition to the material volume of the braces that defines the problem's objective function, the material volume and cost of the entire building are recorded for being used as performance indices for the following assessment of the optimized designs. Based on the indices related to the material used and structural performance ones some interesting observations can be noticed: (i) The material volume of the braces for MRBF-RCX case is equal to 4.85m^3, for MRBF-RC5m is equal to 3.58 m^3 and for MRBF-RC8m is equal to 3.93 m^3. Both MRBFs derived through the solution of FSTO problems (i.e. MRBF-RC5m and MRBF-RC8m) resulted to significant reduction of structural steel material requirements (up to 26*%*) for the braces with reference to MRBF-RCX. The optimized design resulted for the test case where more DOFs were offered for the FSTO problem formulation (i.e. MRBF-RC8m) led to a structural system requiring almost 10*%* more material volume compared to MRBF-RC5m. A possible justification for this observation is that due to a more complicated layout and larger length of braces, some of them required sections having increased dimensions. An interesting observation related to the RC beams and columns of the MRBFs is that depending on its layout, the steel reinforcement required for the beams and columns varies. The material cost of the aforementioned buildings, excluding

concrete (52,258€) that remains the same for all three test cases, is equal to 108,000€, 105,076€ and 105,789€ for the case of MRBF-RCX, MRBF-RC5m and MRBF-RC8m, respectively. The unit cost values that are considered for calculating the material cost are: 70€/m^3 for the concrete, 0.7€/*Kg* for steel rebar reinforcement and 0.9€/*Kg* for structural steel.

It is worth noticing also, that although the material volume of the steel braces for MRBF-RC5m is 26*%* less than that required for MRBF-RCX, due to reduction of the steel reinforcement needs for the case of MRBF-RCX, the difference between the two designs with respect to the structural plus reinforcement steel cost is equal to 3*%*. (ii) Some interesting observations can be noticed with reference to the structural performance of the building. Comparing the optimized designs obtained for the MRBF-RC5m and MRBF-RC8m cases, it can be noticed that although the cost of the two designs is almost the same (MRBF-RC8m is more expensive by less than 0.5*%*), the maximum deflection developed along the *X* and *Y* directions for the design of the MRBF-RC8m case is by 3*%* less and along the *Z* direction is by 10*%* less compared to that of MRBF-RC5m design. Accordingly, comparing the optimized designs obtained for the MRBF-RCX and MRBF-RC8m cases, it can be noticed that the maximum deflection calculated for the design of the MRBF-RCX case along the *X* and *Y* directions is 3*%* less compared to that of MRBF-RC8m, however, the corresponding maximum deflection calculated for the MRBF-RCX case along the *Z* direction is 29*%* more than that of the MRBF-RC8m case. Figures 7.15(a) to 7.15(c) depict the DC marked for the three optimized designs, as it can be seen for the case of the optimized designs obtained for MRBF-RC5m and MRBF-RC8m, the capacity of the braces is much closer to their maximum capacity compared to the braces of MRBF-RCX design. All aforementioned observations lead to the conclusion that by means of the proposed two stage methodology where both frame STO and SSO problems are dealt with sequentially, improved structural designs are obtained, not only with respect to the material requirements but also with reference to the structural performance of the optimized design.
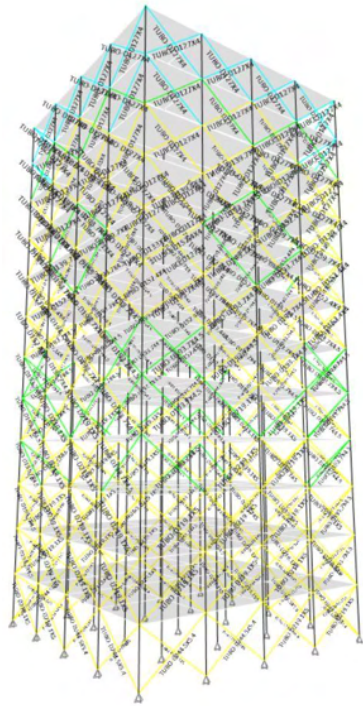
(a)
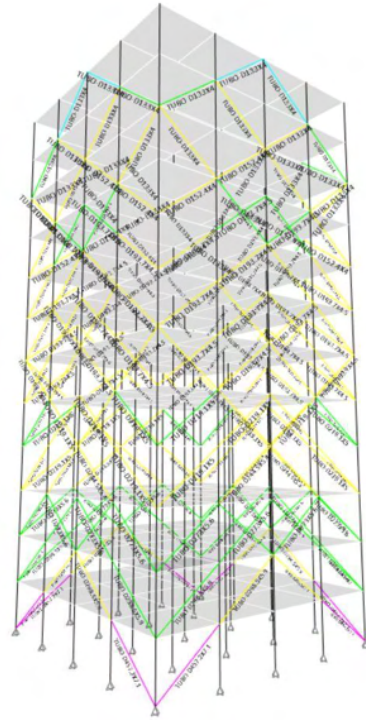
(b)
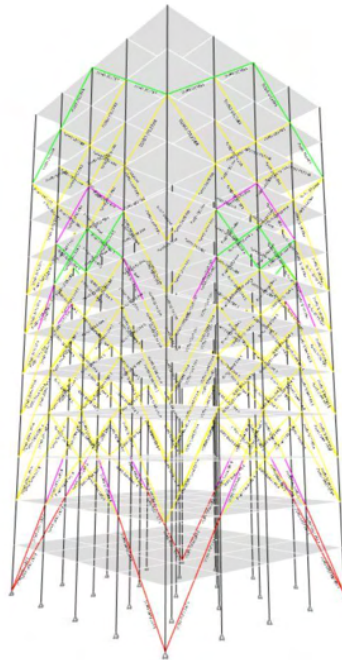
(c)

Figure 7.15 Design check after HP-OCP optimization for a) MRBF-RCX, b) MRBF-RC5m) and c) MRBF-RC8m

CHAPTER 8

Dynamic structural topology optimization for frame structures

8.1 Introduction

The vast majority of the STO research is focused on cases where the loading conditions are static and deterministic. However, taking into account the dynamic response of the structure is far more challenging and, in many cases, closer to the reality. In the case of dynamic STO problems, the approaches adopted concern the free or forced vibration problem using either direct time integration or mode superposition approaches and the Response Spectrum Modal Analysis (RSMA) method.

In the case of the free vibration based STO problems, the first studies were focused on the maximization of a single or multiple eigenfrequencies [61,62,63,82]. In recent studies, additional objective functions were used, such as maximizing building performance to a specific eigenfrequency [83] or maximizing the variance between two consecutive eigenfrequencies [32]. Regarding STO problems that relied on direct time history analyses, Jog [53] employed the dynamic compliance as the objective function to be minimized in order to optimize the structural response. Particularly, periodic cosinusoidal forces were applied to plate type of structures and it was observed that when the driving frequencies were remarkable low, the optimized layout was similar with that obtained for the static compliance optimization problem. Behrou and Guest [11] presented three dynamic TO formulations for structures under time-depended loading cases where the strain energy of the system in different time periods was used as the objective function. More specifically, the goal in the first expression was to minimize the sum of the strain energy during the entire vibration time history, in the second one the objective was to minimize the maximum strain energy that is developed also in the entire time history while according to the last formulation the strain energy was minimized for specific time interval. Bendsoe and Sigmund [15] proposed the minimization of the square of the

compliance in order to avoid numerical implementation issues that needs to be dealt with when minimizing the dynamic compliance.

The disadvantage of direct time integration analyses is the increased computational cost, especially when integrated into SO procedures [58,59,70], STO problems included, where the dynamic equilibrium problem needs to be solved in every iteration of the search process. Yoon [128] presented an extended investigation where model reduction schemes are used in order to reduce the computational demand for dynamic STO problems. Particularly, mode superposition, Ritz vector and quasi-static Ritz vector were applied, reducing the size of the dynamic stiffness matrix and the dynamic response of topology optimized structures were evaluated in the frequency domain. Zhao and Wang [133] examined the efficiency of the mode displacement and mode acceleration methods in STO problems that were solved in the time-domain and they compared the results with those obtained using time history analyses. In particular, three objective functions were used in order to study the effect of the dynamic response of the structures in the STO problem, the mean dynamic compliance, strain energy and squared displacement. Filipov et al. [37] used polygonal FEs with high density resolution to deal with dynamic STO problems, including eigenfrequency optimization and dynamic compliance-based optimization of structures under forced vibration. Martin and Deielrein [65] investigated the dynamic response of tall buildings for STO problems under seismic excitation; particularly, response spectrum analyses were used aiming to minimize the structural vibration.

It should be noticed that the above-mentioned studies, are dealing with STO problems using material interpolation schemes, i.e. 2D and 3D STO problems were studied. Contrary to the GSO problems, the literature that is referring to dynamic TSTO or FSTO problems is even more limited. Indicatively, Nakamura and Ohsaki [72] introduced a method for finding optimized topologies of truss structures for specific eigenfrequencies. Ohsaki et al. [76] extended their work and presented a study on the dynamic STO problem of truss structures when subjected to multiple eigenvalue constraints. Noilublao and Bureerat [75] presented an SO procedure, dealing also with STO problem formulations,

for a truss tower using evolutionary algorithms. The eigenfrequencies and the frequency response function were the objective functions used for defining the dynamic SO problem. Yamada and Kanno [126] proposed an algorithm for solving a sequence of relaxation problems aiming to find local optimal solutions for STO problem of frame structures subjected to frequency constraints.

The main objective of this chapter is to find optimized layouts of the structural system for tall buildings, more specifically for lateral bracing systems, considering the dynamic response of the structures. Initially, free vibration conditions are considered and the maximization of specific eigenfrequencies of the structural systems is the objective function of the FSTO problem. In the following, the dynamic loading problem, considering harmonic loading and earthquake ground motion excitation, is addressed using time history analyses. The dynamic compliance and the Square Root of the Sum of the Squares (SRSS) displacements are the objective functions for the cases of dynamic loading. Finally, the RSMA is applied in order to reduce the computational cost of the dynamic equation and the seismic loading is considered according to the EC8 [33]. In the latter case, the sum of the modal compliances is considered as the objective function.

8.2 The equations of motion and the mass matrix

The equations of motion of a multi-DOF system subjected to time dependent loading can be written in the form:

$$M(a)\ddot{u}_t + C(a)\dot{u}_t + K(a)u_t = R_t \qquad (8.1)$$

that represents a system of coupled homogeneous differential equations, where $M(a)$, $C(a)$ and $K(a)$ are the mass, damping and stiffness matrices defined as functions of the design vector a; R_t is the external load vector, while u, $\dot{u}$ and $\ddot{u}$ are the displacement, velocity and acceleration vectors of the FE assemblage, respectively.

The solution methods of direct integration of equations of motion and of RSMA, which is based on the mode superposition approach, will be considered in the following sections. In these solution methods the mass matrix of the structural system needs to be defined.

Subsequently, the dynamic behavior of MRBFs of tall buildings is examined in the framework of the FSTO problems studied, where the global mass matrix consists of the contribution of both structural and the non-structural mass. The structural mass contribution refers to the mass of the GS, therefore the mass matrix of the frame elements needs to be considered. Specifically, the consistent-mass matrix (M_e^d) of the frame elements is used for the case of 2D FEs, that is defined as follows:

$$
M_e^d = \frac{\rho a_e L_e}{6}
\begin{bmatrix}
2 & 0 & 0 & 1 & 0 & 0 \\
0 & 0 & 0 & 0 & 0 & 0 \\
0 & 0 & 0 & 0 & 0 & 0 \\
1 & 0 & 0 & 2 & 0 & 0 \\
0 & 0 & 0 & 0 & 0 & 0 \\
0 & 0 & 0 & 0 & 0 & 0
\end{bmatrix}
+ \frac{\rho a_e L_e}{420}
\begin{bmatrix}
0 & 0 & 0 & 0 & 0 & 0 \\
0 & 156 & 22L_e & 0 & 54 & -13L_e \\
0 & 22L_e & 4L_e^2 & 0 & 13L_e & -3L_e^2 \\
0 & 0 & 0 & 0 & 0 & 0 \\
0 & 54 & 13L_e & 0 & 156 & -22L_e \\
0 & -13L_e & -3L_e^2 & 0 & -22L_e & 4L_e^2
\end{bmatrix}
\tag{8.2}
$$

where ρ is the material density, a_e is the area of the cross-section and L_e is the length of the eth frame element. As it is observed, M_e^d depends on the design variable value and its derivation by a_e is straightforward. However, in each storey the contribution of the non-structural mass needs to be considered together with that of the structural elements contribution. Non-structural mass stands for the floors, walls, gravity framing etc. In the following, a concentrated mass in the center of each storey is considered for the non-structural mass contribution and the lumped-mass matrix (M^l) is created:

$$
M^l =
\begin{bmatrix}
m_1 & \cdots & 0 \\
\vdots & \ddots & \vdots \\
0 & \cdots & m_{N_f}
\end{bmatrix}
\tag{8.3}
$$

where, m_i is the storey mass and N_f is the total number of storeys. Despite the total mass of the bracing system, that is defined with the global consistent-mass matrix M_g^d (defined by adding the contribution of every frame element M_e^d), is comparatively smaller than that of the non-structural mass, it would be inaccurate to ignore it. Additionally, the lumped-mass matrix of the non-structural elements is independent of the design variable vector $(\nabla_a M^l = 0)$, therefore, if M_g^d is ignored then the derivative of the mass matrix will be a zero matrix, causing numerical instability issues in the sensitivity analysis, when the gradient based algorithm is applied. After transforming the lumped-mass matrix to the

global coordination system, the design dependent global mass matrix of the structural system, is defined as follows:

$$M(a) = M_g^l + M_g^d(a) \tag{8.4}$$

8.3 Free vibration based FSTO

8.3.1 The free vibration problem of a structural system

In the case of free vibration, the equations of motion of Eq. (8.1) can be written as follows:

$$M(a)\ddot{u}_t + K(a)u_t = 0 \tag{8.5}$$

where dumping is ignored and the generalized eigenvalue problem is formulated as:

$$\left(K(a) - \lambda_k(a)M(a)\right)\phi_k(a) = 0, \ \lambda_k = \omega_k^2, \ k = 1, \dots, N_{DOF} \tag{8.6}$$

where $\lambda_k(a)$ and $\omega_k(a)$ are the kth eigenvalue and eigenfrequency respectively, $\phi_k(a)$ is the corresponding eigenvector normalized with reference to the mass matrix and N_{DOF} denotes the total number of DOFs of the structure. $K(a)$ and $M(a)$ are the global stiffness and mass matrices respectively, as functions of the design variable vector.

8.3.2 The FSTO problem for the case of free vibration

The FSTO problem for the case of the free vibration problem, where an eigenvalue is to be maximized, is formulated as:

$$\min_a[-\lambda_k(a)] \tag{8.7a}$$

$$s.t.$$

$$\left(K(a) - \omega_k^2(a)M(a)\right)\phi_k(a) = 0, \quad k = 1, \dots, N_{DOF} \tag{8.7b}$$

$$\phi_j^T(a)M(a)\phi_k(a) = \delta_{jk}, \quad j, k = 1, \dots, N_{DOF} \tag{8.7c}$$

$$a^T \cdot L \leq V_{lim} \tag{8.7d}$$

$$a_{min,e} \leq a_e \leq a_{max,e}, \quad e = 1, 2, \ldots, N_{ele} \tag{8.7e}$$

where L is the vector of the frame elements length, V_{lim} is the final value of the material volume and a is the vector of the frames cross-sectional areas, which are the design variables of the problem.

8.3.3 Sensitivity analysis

For the solution of the above problem, a gradient based algorithm is used, where the following derivative is required:

$$\frac{\partial \lambda_k}{\partial a_e} \in \mathbb{R}^n \tag{8.8}$$

Herein, the adjoint model of the free vibration equations of motion is introduced. Differentiating the generalized eigenvalue system of Eq. (8.6) by a_e is the first step:

$$\frac{\partial(K - \lambda_k M)}{\partial a_e} \phi_k + (K - \lambda_k M) \frac{\partial \phi_k}{\partial a_e} = 0 \tag{8.9}$$

$$\frac{\partial K}{\partial a_e} \phi_k - \frac{\partial \lambda_k}{\partial a_e} M \phi_k - \lambda_k \frac{\partial M}{\partial a_e} \phi_k + (K - \lambda_k M) \frac{\partial \phi_k}{\partial a_e} = 0 \tag{8.10}$$

where for simplifying the presentation of the expressions $K \equiv K(a)$, $M \equiv M(a)$, $\phi_k \equiv \phi_k(a)$ and $\lambda_k \equiv \lambda_k(a)$. By left multiplying the result by ϕ_k^T, the following expression is obtained:

$$\phi_k^T \frac{\partial K}{\partial a_e} \phi_k - \phi_k^T \frac{\partial \lambda_k}{\partial a_e} M \phi_k - \phi_k^T \lambda_k \frac{\partial M}{\partial a_e} \phi_k + \phi_k^T (K - \lambda_k M) \frac{\partial \phi_k}{\partial a_e} = 0 \tag{8.11}$$

Taking into consideration Eq. (8.6), Eq. (8.7c) and the fact that matrices K and M are symmetric the following expression is produced:

$$\phi_k^T \frac{\partial K}{\partial a_e} \phi_k - \frac{\partial \lambda_k}{\partial a_e} - \lambda_k \phi_k^T \frac{\partial M}{\partial a_e} \phi_k = 0 \tag{8.12}$$

Thus,

$$\frac{\partial \lambda_k}{\partial a_e} = \Phi_k^T \left(\frac{\partial K}{\partial a_e} - \lambda_k \frac{\partial M}{\partial a_e} \right) \Phi_k \qquad (8.13)$$

Where the eigenvalue sensitivity of λ_k is directly evaluated through the eigenvector Φ_k, and the gradients of the matrices K and M. The gradient $\frac{\partial K}{\partial a_e}$ is described in details in section 7.2 and $\frac{\partial M}{\partial a_e}$ is easily defined through the derivation of $M_g^d(a)$.

8.4 Time history analysis based FSTO

8.4.1 The linear dynamic problem of a structural system

The equations of motion for the case of forced vibration of a structural system can be written as follows:

$$M\ddot{u}_t + C\dot{u}_t + K u_t = F_t \qquad (8.14)$$

where F_t is the time-dependent applied transient load, that in the case of harmonic excitation takes the following form:

$$F_t = P sin(\omega t) \qquad (8.15)$$

and in the case of ground motion:

$$F_t = -Mr\ddot{u}_g(t) \qquad (8.16)$$

where r is the influence vector, with size equal with the total DOFs, and $\ddot{u}_g(t)$ is the ground acceleration. Where r represents the displacements of the masses resulting from static application of a unit ground displacement, where for a 2D structural system is composed by zero values, except of the DOFs in the direction of the ground motion where the value is equal to one. In the current implementation, Rayleigh damping is used, where the global damping matrix is proportional to the mass and stiffness matrices:

$$C = a_r M + \beta_r K \qquad (8.17)$$

The damping coefficients a_r, β_r depend on the damping ratio and the eigenfrequency. In this work the ratio chosen is equal to $\zeta = 0.05$, a reasonable estimation for steel structures.

The system of Eq. (8.14) can be solved by means of direct time integration numerical procedures. In the current implementation, without loss of the generality, the Newmark Beta integration scheme is used, where the acceleration and velocity vectors are defined as:

$$\ddot{u}_{n+1} = \frac{(u_{n+1} - u_n)}{(\beta \Delta t^2)} - \frac{\dot{u}_n}{\beta \Delta t} - \left(\frac{1}{2\beta} - 1\right)\ddot{u}_n \tag{8.18}$$

$$\dot{u}_{n+1} = \frac{(u_{n+1} - u_n)\gamma}{(\beta \Delta t)} + \dot{u}_n\left(1 - \frac{\gamma}{\beta}\right) + \left(1 - \frac{\gamma}{2\beta}\right)\ddot{u}_n \Delta t \tag{8.19}$$

Subsequently, the expressions of $\ddot{u}_{n+1}$ and $\dot{u}_{n+1}$ are replaced in Eq. (8.14), and the corresponding expression for u_{n+1} is derived:

$$Au_{n+1} = B_n \tag{8.20}$$

Where:

$$A = \frac{M}{\beta \Delta t^2} + \frac{C\gamma}{\beta \Delta t} + K \tag{8.21}$$

$$B_n = F(t+1) + M\left[\frac{u_n}{(\beta \Delta t^2)} + \frac{\dot{u}_n}{\beta \Delta t} + \left(\frac{1}{2\beta} - 1\right)\ddot{u}_n\right] +$$

$$+ C\left[\frac{u_n\gamma}{\beta \Delta t} - \dot{u}_n\left(1 - \frac{\gamma}{\beta}\right) - \left(1 - \frac{\gamma}{2\beta}\right)\ddot{u}_n \Delta t\right] \tag{8.22}$$

The parameters γ and β that are used in the Newmark Beta integration scheme, correspond the two special values that specifies the variation of the acceleration. When $\gamma < 0.5$ the method is unstable while for $\gamma \geq 0.5$ it is conditionally stable. In this work these values are chosen as $\gamma = 0.5$ and $\beta = 0.25$, which means that the acceleration within the time interval t_n and t_{n+1} is constant.

8.4.2 The FSTO problem for the case of dynamic excitations

Ma et. al [62] proposed the dynamic compliance of a structural system defined as the product of the time-dependent loading (F_t) times the displacement vectors (U_t):

$$C_{dyn} = F_t^T U_t \tag{8.23}$$

where C_{dyn} denotes the dynamic compliance; an issue of the expression of Eq. (8.23), is that the dynamic compliance may assume negative values when the vibration frequency is higher than the fundamental frequency of the system, (see reference [62]). One way to tackle with this problem is to minimize the absolute value of C_{dyn} [78]. An alternative to the issue is to choose the square of the dynamic compliance as the objective function [15]. In this work in order to avoid this issue, half-cycle sinusoidal loads are applied [68]. More specifically, the dynamic compliance of the structure is calculated during the time interval, from the initial time t_i to the final time t_N as:

$$f = \int_{t_i}^{t_N} u^T F_t dt \tag{8.24}$$

Therefore, the expression of the dynamic compliance is determined as follows:

$$min\ f = \sum_{j=t_i}^{t_N} \sum_{i=1}^{N_{dof}} u_i^T F_j \Delta t \tag{8.25a}$$

$$s.t.$$

$$M(a)\ddot{u}_t + C(a)\dot{u}_t + K(a)u_t = F_t \tag{8.25b}$$

$$a^T \cdot L \leq V_{lim} \tag{8.25c}$$

$$a_{min,e} \leq a_e \leq a_{max,e}, \quad e = 1,2,\dots,N_{ele} \tag{8.25d}$$

where $t_i = 0$ and Δt is a small time-increment depending on the driving frequency. In the case of time dependent point load, the dynamic compliance is considered a suitable objective function. However, when real earthquake records are used, this objective

function cannot be implemented, since the dynamic compliance might take negative values. For this reason, an alternative objective function is used for the dynamic response of the structural system under seismic excitation. The SRSS displacements, is a general form that captures the amplitude of the displacement vibration in both directions:

$$f = \|l^T u_t\|_2 = \sqrt{\sum_{t=0}^{t_N} (l^T u_t)^2} \qquad (8.26)$$

where l is the location index vector with size equal with the total number of DOFs. The vector is fulfilled with the number one in the DOFs that are under examination and with zero in the rest indexes. A reasonable measurement of dynamic response in mid- and high-rise buildings is the tip deflection.

8.4.3 Sensitivity analysis

In SO, the order of the system of sensitivity analysis's equation is related to the governing system of equilibrium equations of the structure. Herein, the equation of motion refers to a system of coupled second-order differential equations, hence the equation of the displacement sensitivity analysis is also a second-order differential equation. The displacement sensitivity can be calculated by means of the finite difference methods, the Adjoint Variable Method (AVM) or the Direct Differentiation Method (DDM). Both forward and central difference methods provide accurate values for the displacement sensitivity, however with increased computation cost due to the two function evaluations required in each step [42]. Regarding AVM, in static analysis optimization problem is more efficient than DDM, because in the AVM the implicit response sensitivity with respect to the design variable is eliminated, on the contrary with the DDM that the above calculation is required. However, when it comes to dynamic problems the efficiency of the two methods is similar. On the one hand, AVM avoids calculating explicitly the response sensitivities; on the other hand, instead of calculating the adjoint variable λ once (in case of static loading), λ_n is evaluated in each step of the time history analysis. Additionally, λ_n is calculated through a backward procedure, starting from the last iteration making it

a terminal-value problem [130,51]. DDM explicitly evaluates the response sensitivities in every time step, that similar to the equation of motion in Eq. (8.14) corresponds to an initial value problem. Regarding that the computation effort for the AVM is unevenly harder comparing with the DDM, the second method is applied in the current work. Direct differentiation of Eq. (8.14) with respect to design variable a_e, leads to the equation below:

$$M \frac{d^2}{dt^2}\left(\frac{du}{da_e}\right) + C \frac{d}{dt}\left(\frac{du}{da_e}\right) + K \frac{du}{da_e} = \frac{\partial F_t}{\partial a_e} - \frac{\partial M}{\partial a_e}\ddot{u} - \frac{\partial C}{\partial a_e}\dot{u} - \frac{\partial K}{\partial a_e}u \qquad (8.27)$$

The above equation, is a second-order differential equation for $\frac{du}{da_e}$, which is the sensitivity of the displacements [48,110]. Similar to the equation of motion, any numerical method can be performed for solving the above equation. Substituting u_n with $\frac{du_n}{da_e}$ the Eqs. (8.18) to (8.22) remain the same and the sensitivity of the displacement can be evaluated. The only difference appears in Eq. (8.22), where the expression of the force is:

$$F_{der}(t) = \frac{\partial F_t}{\partial a_e} - \frac{\partial M}{\partial a_e}\ddot{u}_t - \frac{\partial C}{\partial a_e}\dot{u}_t - \frac{\partial K}{\partial a_e}u_t \qquad (8.28)$$

More details for the above solution can be found in the work by Yamakawa [127]. After evaluating the derivative of the displacements, the derivative of the objective function needs to be defined. Regarding the dynamic compliance, the sensitivity at time t_n can be written as:

$$\frac{\partial}{\partial a_e}(u_n^T F_n) = \frac{\partial}{\partial a_e}(u_n^T M \ddot{u}_n + u_n^T C \dot{u}_n + u_n^T K u_n) \qquad (8.29)$$

$$\frac{\partial u_n^T}{\partial a_e} M \ddot{u}_n + u_n^T \frac{\partial M}{\partial a_e}\ddot{u}_n + u_n^T M \frac{\partial \ddot{u}_n}{\partial a_e} + \frac{\partial u_n^T}{\partial a_e} C \dot{u}_n + u_n^T \frac{\partial C}{\partial a_e}\dot{u}_n + u_n^T C \frac{\partial \dot{u}_n}{\partial a_e} +$$
$$\frac{\partial u_n^T}{\partial a_e} K u_n + u_n^T \frac{\partial K}{\partial a_e}u_n + u_n^T K \frac{\partial u_n}{\partial a_e} \qquad (8.30)$$

Differentiating the equations of motion at time t_n with respect to the design variable, the acceleration sensitivity term is obtained:

209

$$M \frac{\partial \ddot{u}_n}{\partial a_e} = -\frac{\partial M}{\partial a_e}\ddot{u}_n - \frac{\partial C}{\partial a_e}\dot{u}_n - C\frac{\partial u_n}{\partial a_e} - \frac{\partial K}{\partial a_e}u_n - K\frac{\partial u_n}{\partial a_e} \qquad (8.31)$$

After some algebraic manipulation, the sensitivity of the objective function at time t_n is expressed as:

$$\frac{\partial}{\partial a_e}(u_n^T F_n) = \frac{\partial u_n^T}{\partial a_e}M\ddot{u}_n + \frac{\partial u_n^T}{\partial a_e}C\dot{u}_n + \frac{\partial u_n^T}{\partial a_e}Ku_n \qquad (8.32)$$

For the problem of minimizing the roof displacement over time, the derivative of the SRSS (see Eq. (8.26)) is expressed as follows:

$$\frac{\partial f}{\partial a_e} = 0.5\left(\sum_{t=0}^{t_N}(l^T u_t)^2\right)^{-1/2}\sum_{t=0}^{t_N}2l^T u_t \frac{\partial u_n}{\partial a_e} \qquad (8.33)$$

8.5 Response spectrum modal analysis based FSTO

8.5.1 Response spectrum analysis

The RSMA represents a simplification of the mode superposition approach aiming to avoid using the time history analysis of the dynamic equation. The computational benefits become more significant in the framework of SO problems, FSTO problems included, especially when dealing with large-scale structural systems. In civil engineering applications, when a structure is designed against short and nondeterministic time dependent events, like the ground motion, the RSMA method is often used. Using this method, a very precise estimation of the expected earthquake frequency content is achieved and the dynamic response of the structure is evaluated taking under consideration only a small number of mode shapes. Particularly, the displacements of a structural system can be evaluated as follows:

$$u_t = \sum_{j=1}^{n} \Gamma_j \phi_j SD_j \qquad (8.34)$$

Where n is the maximum number of modes considered, ϕ_j is the mode shape, SD_j is the spectral displacement retrieved from the design response spectrum and Γ_j is the modal participation factor for mode j, that is calculated as follows:

$$\Gamma_j = \frac{\phi_j^T M r}{\phi_j^T M \phi_j}$$ (8.35)

where r is the influence vector. A crucial difference between the forced single driving frequency force and the earthquake, is that in the second case the external forces are arising from the inertia and are design-dependent. In previous section, it is discussed that the biggest part of the global mass matrix consists of the lumped-mass but it is highlighted that in all the formulations so far, the total mass matrix is applied. In the following, only for the evaluation of the external seismic forces, the M_g^l is used, leading in this way to design-dependency relaxation. Consequently, the peak modal displacement vectors U_j are evaluated using static analysis by enforcing equivalent modal loads for each mode j:

$$U_j = K^{-1} F_j$$ (8.36)

$$F_j = \Gamma_j M_g^l \phi_j SA(T_j)$$ (8.37)

where F_j is the earthquake modal force vector of mode j and $SA(T_j)$ is the elastic spectral pseudo-acceleration derived from the design code for period T_j. Additionally, the maximum displacement is evaluated with the SRSS method:

$$U = \sqrt{\sum_{j=1}^{n} U_j^2}$$ (8.38)

For the definition of the maximum mode n that will be considered, the rules of the EC8 are applied. Particularly, according to the Eurocode, the analysis must include a sufficient number of modes to obtain a combined modal mass participation of at least 90% of the actual mass in each orthogonal level. The calculation of the effective modal mass for each eigenmode is as follows:

$$m_{en,i} = \frac{\left(\phi_j^T M r\right)^2}{\phi_j^T M \phi_j} \tag{8.39}$$

8.5.2 The FSTO problem for the case of modal compliances

In the case of the RSMA the objective function of the corresponding FSTO problem is the weighted average of the modal compliances that is to be minimized, aiming to improve the structural performance in terms of vibration. Herein, the FSTO problem is dealt with in a similar way with the weighted average of static compliance for multiple loading case, with the difference that, in the current work, the loads are evaluated from the spectral analysis. The FSTO problem of the sum of the modal compliances [65] is formulated as follows:

$$min\ f = \sum_{j=1}^{n} F_j^T(a) U_j(a) \tag{8.40a}$$

$$s.t.$$

$$\left(K(a) - \omega_j^2 M(a)\right)\phi_j = 0 \tag{8.40b}$$

$$a^T \cdot L \leq V_{lim} \tag{8.40c}$$

$$a_{min,e} \leq a_e \leq a_{max,e}, \quad e = 1,2,\dots,N_{ele} \tag{8.40d}$$

where the values of U_j and F_j are calculated through Eqs. (8.36) and (8.37), respectively.

8.5.3 Sensitivity analysis

In any optimization problem where a gradient-based iterative algorithm is used, sensitivity analysis represents a crucial counterpart for its efficient implementation. For the problem formulation of Eq. (8.40), the derivative of the objective function is calculated by means of the adjoint sensitivity analysis method. The gradient of the sum of modal compliances is:

$$\frac{df}{da_e} = \sum_{j=1}^{n} \frac{df_j}{da_e} \tag{8.41}$$

where f_j is the modal compliance and a_e is the design variable. The derivative of the modal compliance is expressed similarly with the static compliance subjected to loadings that are design variables dependent [39]. More specifically, the gradient of f_j is defined as follows:

$$\frac{df_j}{da_e} = -U_j^T \frac{\partial K}{\partial a_e} U_j + 2U_j^T \frac{\partial F_j}{\partial a_e} \tag{8.42}$$

As it was mentioned before, the modal loads are considered constant in this work, meaning that in each optimization loop the second term of the above equation is becoming equal to zero, since $\frac{\partial F_j}{\partial a_e} = 0$. Therefore, substituting the expression of Eq. (8.42) into Eq. (8.41), the derivative of the objective function becomes:

$$\frac{df}{da_e} = \sum_{j=1}^{n} -U_j^T \frac{\partial K}{\partial a_e} U_j \tag{8.43}$$

8.6 Numerical examples

In order to examine the effect of the vibration on the design of lateral resistance structural systems of tall buildings, several test cases are examined in this section. The test cases are classified into three groups. In the first one, the structural systems are subjected to free vibration, the structural damping is ignored and the objective function of the optimization problem is formulated as the maximization of specific eigenfrequencies. In case of high-rise buildings, the first eigenfrequency is not the critical one; for this reason, in the following examples the first five eigenfrequencies of the structural systems are maximized. In the second group of tests, the time history analysis method is used and two different types of loading are applied, in particular a concentrated harmonic load and ground motion seismic excitation using a real record. In the first case, the objective function of the FSTO formulation is the dynamic compliance for a half-cycle sinusoidal

concentrated load and in the second one is the minimization of the roof deflection calculated using SRSS. Finally, in the third group of the numerical tests, the response spectrum of EC8 [33] is implemented for simulating the seismic load. Particularly, two different hazard zones in Greece are studied and the corresponding solutions obtained are discussed. For all numerical tests, structural steel of class with nominal yield stress of $f_y = 235 MPa$, modulus of elasticity equal to $E = 200 GPa$ and structural density of $\rho = 7,800 \frac{kg}{m^3}$ are considered. Considering the section profiles of the frames, the HEA section profile list is used for the column groupings, the IPE one for the beam groupings and the CHS one for the brace groupings. Additionally, it is considered that frame elements of column and beam type will not be removed during the FSTO procedure, thus they will remain in the optimized designs. The bounds of the design variables are the same with the MRBF3 test case in section 7.6.1.

Figure 8.1 depicts the mass distribution of the initial GSs, where the concentrated floor masses of the non-structural elements are denoted with the blue color and with the red color the nodal mass contribution of the frame elements that joint in each node.
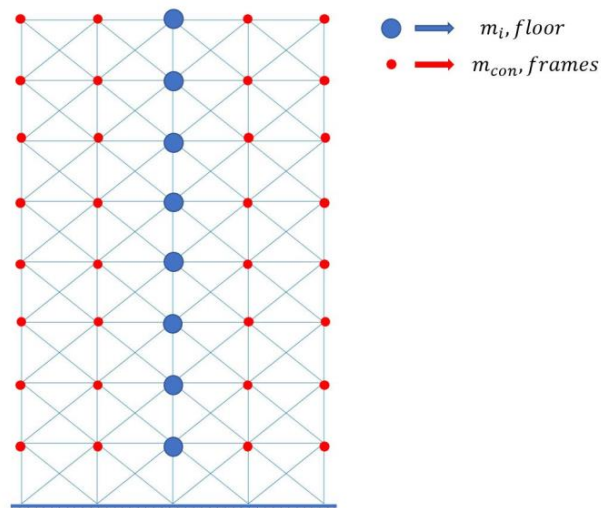

Figure 8.1 Initial structural system mass distribution, with blue colour the floor mass and with red the frame consistent mass

8.6.1 FSTO free vibration test cases

In the first group of numerical tests, an MRBF of a high-rise building (HRB) and a mega-braced frame (MBF) system are examined. More specifically, for each test two different initial GSs are generated, a simple-level and a mid-level connectivity, and the first five eigenfrequencies are maximized independently, resulting into five separate problems. The first structural system refers to a 4-bay, 16-story structure with column spans equal to $5m$ and floor heights equal to $4m$, along stories while each floor mass is equal to $m_i = 10^6 kg$. In the following description the simple-level connectivity GS case will be referred as HRBS and the mid-level one as HRBM. The constraint, which is the lateral bracing system material volume limit, was set equal to $V_{lim} = 3m^3$. The second structural system refers to a 4-bay, 24-story structure with horizontal spans equal to $10m$ and vertical spans equal $8m$ throughout all the building height. Similar as before, the simple-level connectivity initial structural system is referred as MBFS and the mid-level one as MBFM. In this structural system the constraint is equal to $V_{lim} = 9m^3$.

Figures 8.2 and 8.3 depict the optimized layouts obtained for the first five eigenfrequencies of the HRBS and HRBM systems respectively, and Table 8.1 presents the corresponding objective function values, the eigenfrequencies of the optimized layout achieved for the problem, where w_2 is to be maximized are denoted in blue. Accordingly, the rest of the eigenfrequency values refer to optimized designs obtained through the solution of the corresponding problems. Regarding the optimized topologies in each case, the first observation is that maximizing the eigenfrequency of the fundamental mode, leads to similar layouts with those obtained for classic static compliance optimization problem. This is reasonable, since the two formulations have comparable objective

$*(rad/s)$

Eigenfreq.	w_1*		w_2*		w_3*		w_4*		w_5*	
Test Case	HRBS	HRBM	HRBS	HRBM	HRBS	HRBM	HRBS	HRBM	HRBS	HRBM
Opt. w_1	**0.99**	**1.09**	2.86	2.71	4.93	4.27	6.56	4.87	7.77	5.71
Opt. w_2	0.59	0.54	**3.71**	**4.10**	4.53	4.10	7.77	5.99	8.68	6.43
Opt. w_3	0.54	0.55	2.44	2.26	**7.41**	**7.47**	7.41	7.47	8.59	7.81
Opt. w_4	0.54	0.54	2.66	2.00	4.98	4.71	**10.60**	**10.82**	10.60	10.82
Opt. w_5	0.47	0.54	1.56	2.07	4.51	4.73	6.51	6.42	**13.48**	**12.86**

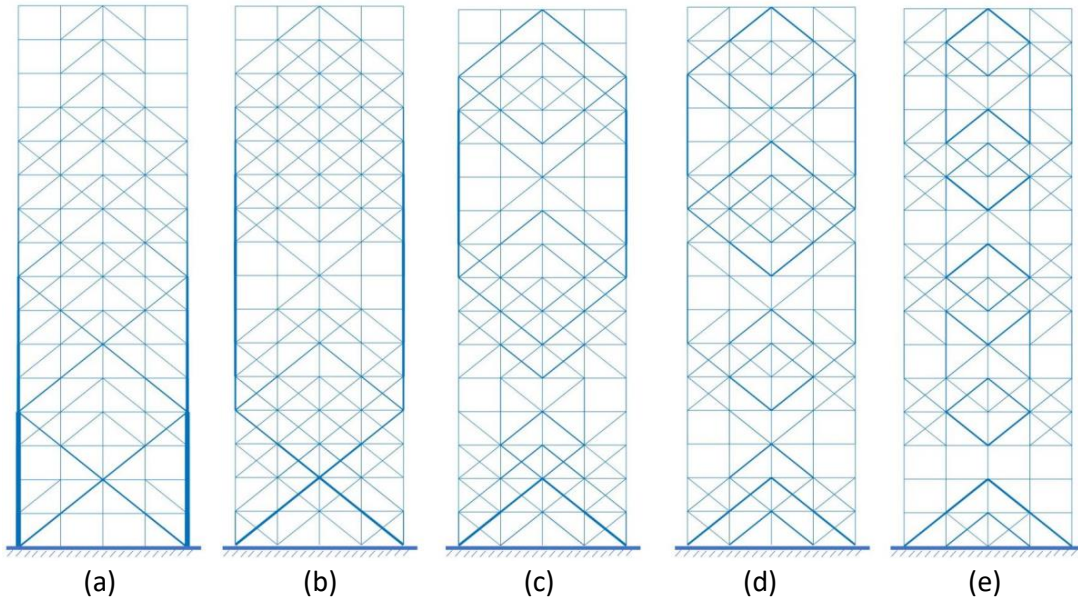*Table 8.1 HRBS and HRBM test cases – maximization of the first five eigenfrequencies*

Figure 8.2 HRBS (64m height), topology optimized structural systems for maximizing the first 5 frequencies (a)-(e)
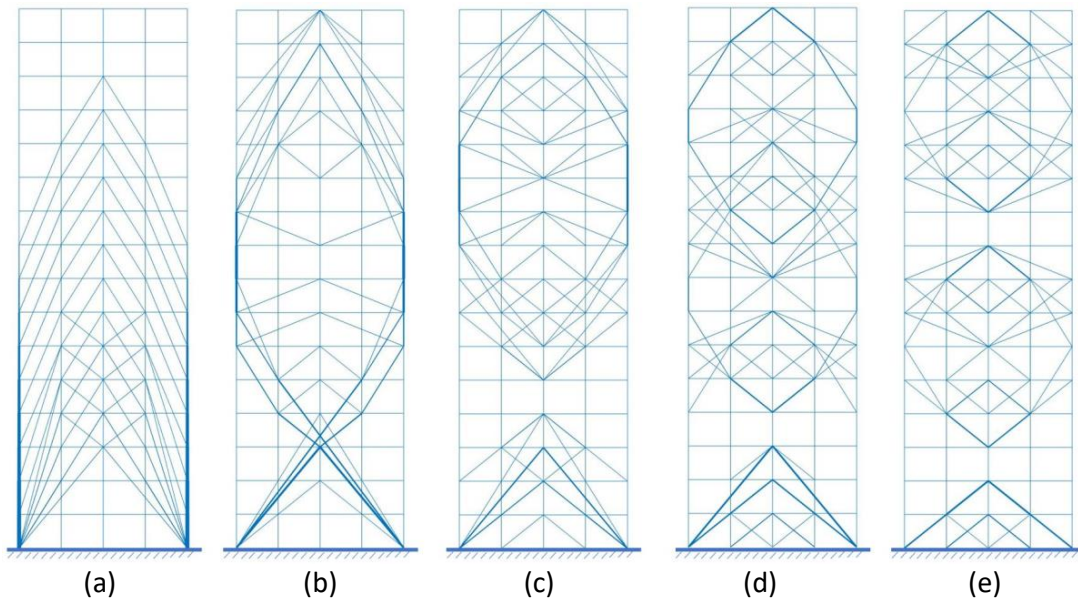

Figure 8.3 HRBM, topology optimized structural systems for maximizing the first 5 frequencies (a)-(e)

functions, both aim to maximize structural stiffness. A second interesting observation through the above Figures, is that the number of zones reinforced with braces that are developed is analogous to the index of the eigenfrequency that is to be maximized; i.e. two zones for the second eigenfrequency, three zones for the third, etc. Additionally, it can be noticed that every layout of the structural system, follows the shape of the eigenmode used for the FSTO problem formulation, i.e. the areas without braces are concentrated in the extremes of the eigenshape areas. Thus, for the problem where the fundamental frequency was maximized, less diagonals are observed in the top of the structural system. Accordingly, for the problem where the second frequency was maximized less braces are developed in the mid height of the system; while for the rest of the problems, the distance between the less-developed areas with braces is equal to $\frac{H}{ID_{freq}}$, where H is the building height and ID_{freq} is the index of eigenmode that is to be maximized.

For the case of the mid-level connectivity GS similar observations are obtained. However, due to larger freedom in the design procedure, the diagonals are located in such way, that ellipsoidal shapes are produced and the number of them is increasing when higher frequencies are to be maximized. Regarding the results of Table 8.1, the first observation is that for the HRBM case, the eigenfrequency that is optimized almost always (except of the fifth eigenfrequency) is larger than in the HRBS. However, at the same time the gap between consecutive eigenfrequencies is smaller. Although the objective function obtained for the HRBM problems is better (larger eigenfrequency), worth mentioning that the rest of the eigenfrequencies slightly vary, denoting a characteristic that is not often preferable for a structural system. Another important observation is that when the second eigenfrequency is optimized, in the HRBM case there is a repeated eigenfrequency for the second and the third mode, while in the HRBS not. Repeated eigenfrequencies are appeared in both cases when higher modes are maximized. In Figure 8.4 and Figure 8.5 the optimized topologies for the MBFS and MBFM are illustrated and in Table 8.2 the numerical results are shown. Regarding the shape, the location of the braces and the emptier areas, the results are similar with the HRB case. Contrary to HRB structural

systems, in MBF lateral systems when the initial GS is denser, not only the eigenfrequency that is maximized is bigger than the simple-level connectivity GS, but also the difference between the rest eigenfrequencies is larger. Because MBF structural system is remarkable higher than the HRB, larger brace member and more complicated layouts are even more efficient than traditional X-braces. All the above results, highlight the challenge of optimizing multiple eigenfrequencies with different GSs and the difficulties that the engineer must deal with.

*(rad/s)

Eigenfreq.	w_1*		w_2*		w_3*		w_4*		w_5*	
Test Case	HRBS	HRBM	HRBS	HRBM	HRBS	HRBM	HRBS	HRBM	HRBS	HRBM
Opt. w_1	**0.52**	**0.56**	1.62	1.57	2.96	2.76	4.21	3.81	5.27	4.48
Opt. w_2	0.31	0.27	**2.12**	**2.37**	2.12	2.37	5.10	4.42	5.30	4.76
Opt. w_3	0.27	0.26	1.28	1.32	**4.53**	**4.92**	4.53	4.92	4.72	5.29
Opt. w_4	0.26	0.26	1.22	1.27	2.87	2.76	**6.89**	**7.16**	6.89	7.16
Opt. w_5	0.26	0.27	1.22	1.26	2.80	2.81	4.64	4.41	**9.21**	**9.16**

Table 8.2 MBFS and MBFM test cases – maximization of the first five eigenfrequencies
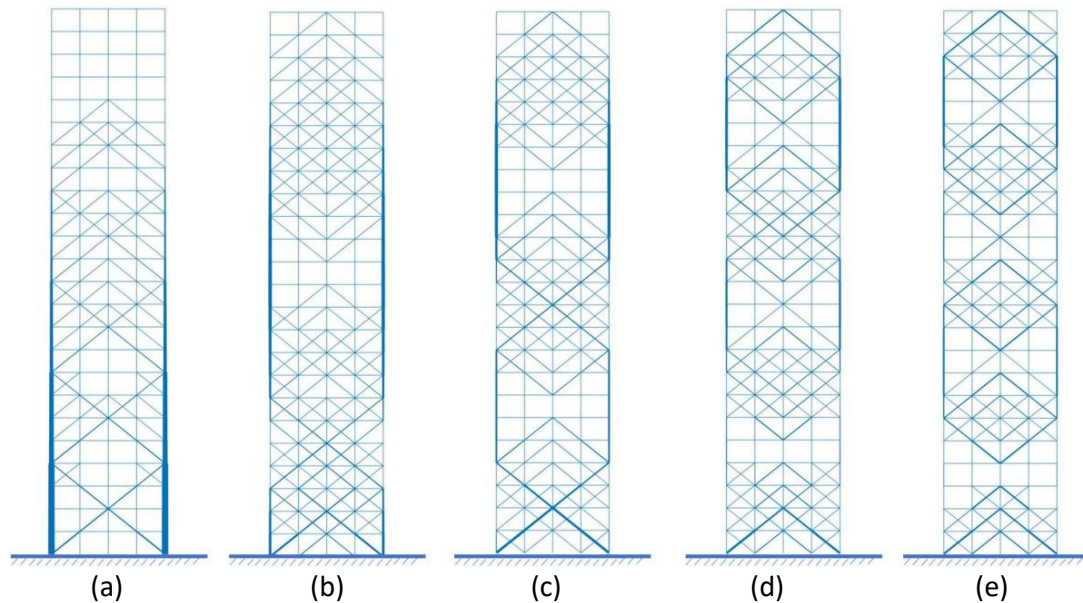

Figure 8.4 MBFS (192m height), topology optimized structural systems for maximizing the first 5 frequencies (a)-(e)
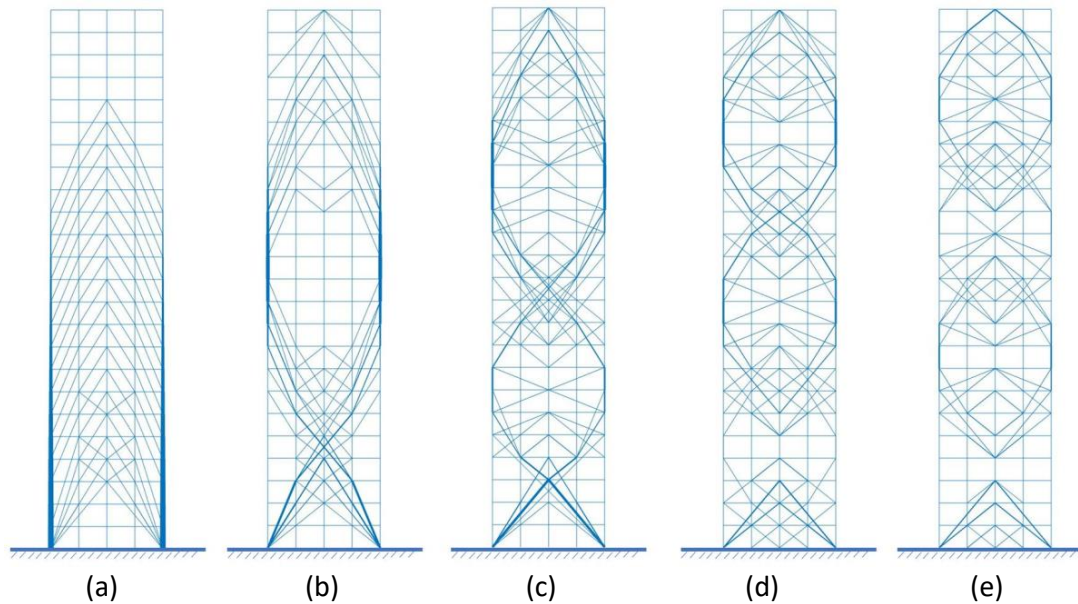
Figure 8.5 MBFM, topology optimized structures for maximizing the first 5 frequencies (a)-(e)

8.6.2 Linear time history test cases

In the second group of tests, due to the time history analyses, the computational cost of the optimization procedure is remarkably higher. For this reason, the structural system of a mid-rise building (MRB), starting from a simple-level and a mid-level connectivity GS (MRBS and MRBM) and the HRB cases are studied. MRB is a 4-bay, 8-story structural system with column span equal to 5m and floor height 4m throughout all stories.

Harmonic Load

Although harmonic load is simple, compared to recorded excitations such as earthquake ground motion or wind vortex shedding, studying the characteristics of the optimized structural systems obtained when subjected to harmonic vibration, provides valuable information regarding the response under similar types of loads. In the following cases examined, the harmonic loading is assumed to be half-cycle sinusoidal excitations, applied at the roof of the structural system. In order to understand better the dynamic performance of the structural systems and the differences with that of the static analysis, in each case study, the results of the static compliance problem are also shown. In the

MRB test cases, the amplitude of all loads is equal to $P = 4MN$, the $V_{lim} = 1.5m^3$ and $m_i = 10^6 kg$. In order to choose the driving frequencies that will be studied, the first three eigenfrequencies of the optimized layouts obtained for the static loading, are evaluated, i.e. $\omega_{n1} = 1.55 \frac{rad}{s}$, $\omega_{n2} = 5.56 \frac{rad}{s}$ and $\omega_{n3} = 7.21 \frac{rad}{s}$. In the following, three sinusoidal loads with different frequencies of the excitation (driving frequencies) equal to $\omega_1 = 1 \frac{rad}{s}$, $\omega_2 = 4 \frac{rad}{s}$ and $\omega_3 = 8 \frac{rad}{s}$ are applied.

Figures 8.6 and 8.8 illustrate the optimized layouts obtained for the MRBS and MRBM optimization problems under static load and the three different dynamic excitations. Regarding the low driving frequency cases, it is observed that the optimal layouts are similar with the results from the static load. This is rational since the frequency of the excitation is sufficient smaller than the fundamental eigenfrequency; therefore, the optimization procedure will lead the structural system to increase its eigenfrequencies by adding stiffness, similar to the static analysis design optimization process. Regarding the second frequency ω_2 of the excitation, in both MRBS and MRBM cases, different material distribution is observed. Particularly, more X-braces and diagonals are added in the core of the structural system while more material distribution is required in the upper part of the structural system, compared to the optimized designs obtained for the lower frequency excitation. This is reasonable since the frequency of the excitation lies between the second and third eigenfrequencies, therefore different distribution of the stress over the structural elements of the system is expected. Finally, in the case that the driving frequency of the excitation is even higher than the third eigenfrequency, the optimized layout corresponds to a totally different topology. In both MRBS and MRBM structural systems, braces are developed only in the upper half part and the larger fragment of the material is concentrated in this part of the design domain, ending up in a practically complete damping of the vibrations at this area. These optimized layouts are similar with those of the topology optimized structural systems achieved when solving the forced vibration dynamic problem with the continuum mechanics approach and the SIMP method [15]. As it was described previously, half-cycle sinusoidal point loads are considered; therefore, for different driving frequency ω_i, different time periods and Δt

are used for the integration. In order to have a common reference point, after the end of the STO procedure, the final structural systems are enforced to 10 seconds vibration and the tip deflection during the time is studied.

Figures 8.7 and 8.9 illustrate the time histories of the roof displacements for the optimized layouts obtained for MRBS and MRBM cases. In order to implement 50 time-steps for the half-cycle sinusoidal point load, the proper value of Δt is selected for every driving frequency case. Table 8.3 shows the dynamic compliance and the maximum absolute roof displacement of optimized MRB structural systems. As it can be observed, for all driving frequencies implemented, the structural systems optimized based on the mid-level connectivity GS, develop lower values of the tip deflection compared to the corresponding designs based on the simple-level connectivity GS. Another observation, is related to the maximum roof displacement that its value is not necessarily increased when the driving frequency is increased, due to the resonance effect.

(a) (b) (c) (d)

Figure 8.6 MRBS Optimized structural system for (a) static load, (b) $\omega_1 = 1\ rad/s$, (c) $\omega_2 = 4\ rad/s$ and (d) $\omega_3 = 8\ rad/s$

(a) (b) (c)

Figure 8.7 Tip deflection for MRBS under 10 seconds vibration for (a) $\omega_1 = 1\ rad/s$, (b) $\omega_2 = 4\ rad/s$ and (c) $\omega_3 = 8\ rad/s$

(a)	(b)	(c)	(d)

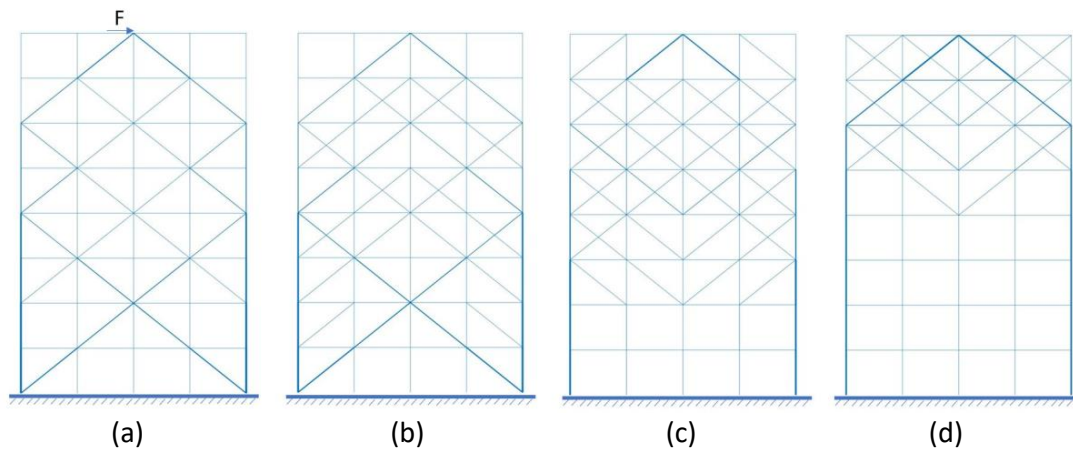*Figure 8.8 MRBM Optimized structural system for (a) static load, (b) $\omega_1 = 1\ rad/s$, (c) $\omega_2 = 4\ rad/s$ and (d) $\omega_3 = 8\ rad/s$*

(a)	(b)	(c)

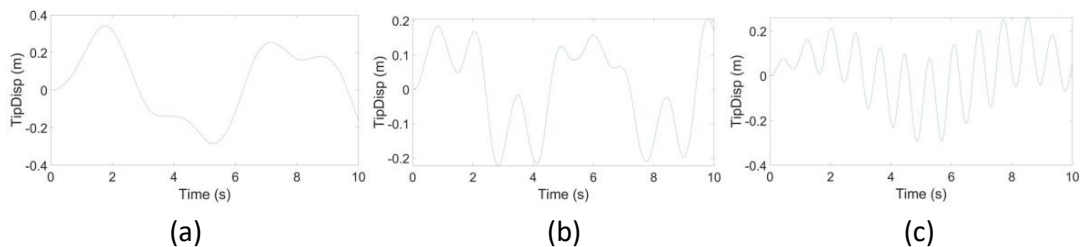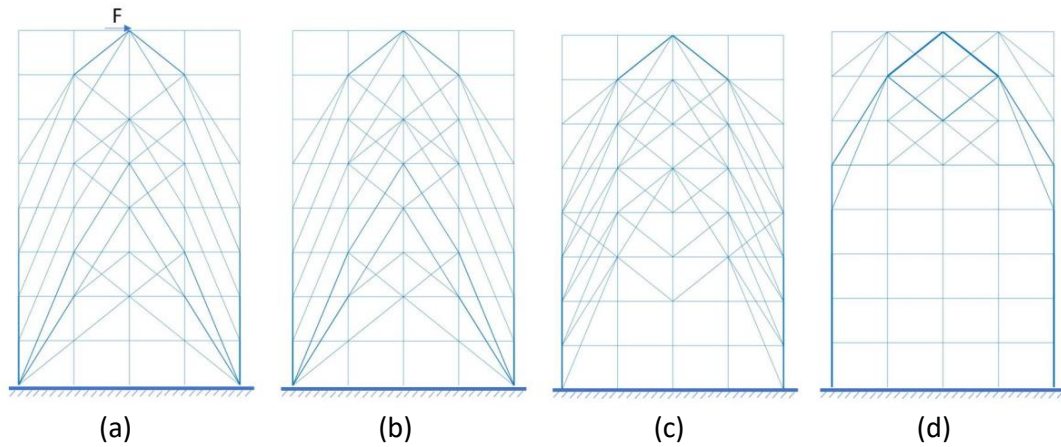*Figure 8.9 Tip deflection for MRBM under 10 seconds vibration for (a) $\omega_1 = 1\ rad/s$, (b) $\omega_2 = 4\ rad/s$ and (c) $\omega_3 = 8\ rad/s$*

$*(\times 10^6)$

Test case	MRBS		MRBM	
	C* (Nm)	D (m)	C* (Nm)	D (m)
$\omega_1 = 1$	4.880	0.341	3.894	0.258
$\omega_2 = 4$	3.013	0.223	2.197	0.197
$\omega_3 = 8$	2.861	0.294	1.817	0.148

Table 8.3 MRBS and MRBM test cases – dynamic compliance (C) and maximum tip deflection (D) through 10 second vibration

Figures 8.10 and 8.12 present the optimized layouts obtained for the HRBS and HRBM optimization problems when subjected to static load and three sinusoidal excitations. In the HRB cases, the amplitude of the sinusoidal excitations is equal to $P = 2MN$, the $V_{lim} = 3m^3$ and $m_i = 0.5 * 10^6 kg$. The first three eigenfrequencies of the optimized structural system obtained for the static loading are equal to $\omega_{n1} = 0.94\frac{rad}{s}$, $\omega_{n2} = 3.34\frac{rad}{s}$ and $\omega_{n3} = 4.62\frac{rad}{s}$, respectively. Consequently, the following frequencies of

the excitation are used: $\omega_1 = 0.5 \frac{rad}{s}$, $\omega_2 = 3 \frac{rad}{s}$ and $\omega_3 = 6 \frac{rad}{s}$. With respect to the HRBS case, for the lower frequency of the excitation a larger number of X-braces is developed compared to the design obtained for static load case. On the other hand, for the HRBM case, due to the increased design freedom the optimized design of the static case achieved a layout of high stiffness, thus, fewer differences between the static load case and the ω_1 case are observed. Another important observation is that in the HRBM case more chevron bracing type members are created comparing to the HRBS where more X-braces are developed, leading to the fact that the use of chevron connections generate stiffer structural systems. Regarding the ω_2 frequency, in both HRBS and HRBM structural systems the most material is distributed in the upper half of the structural system and more X- braces are produced in HRBM. For the case of the largest driving frequency, most of the material is concentrated in the upper half of the structural system. It is observed that instead of chevron braces more V-bracing members are developed. Generally, it can be stated that when dynamic loading is considered, the best type of braces connection depends on the frequency of the excitation.

Figure 8.10 HRBS Optimized structural system for (a) static load, (b) $\omega_1 = 0.5\ rad/s$, (c) $\omega_2 = 3\ rad/s$ and (d) $\omega_3 = 6\ rad/s$

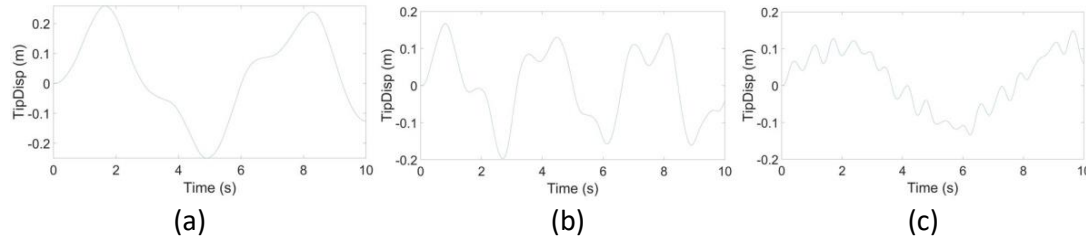*Figure 8.11 Tip deflection for HRBS under 10 seconds vibration for (a) $\omega_1 = 0.5\ rad/s$, (b) $\omega_2 = 3\ rad/s$ and (c) $\omega_3 = 6\ rad/s$*

Figures 8.11 and 8.13 illustrate the time histories of the roof displacements for the optimized layouts obtained for HRBS and HRBM cases. Table 8.4 shows the dynamic compliance and the maximum absolute tip displacement of HRB structural systems. Regarding the response of the structural system for the different GSs, similar results with the MRB cases are produced.

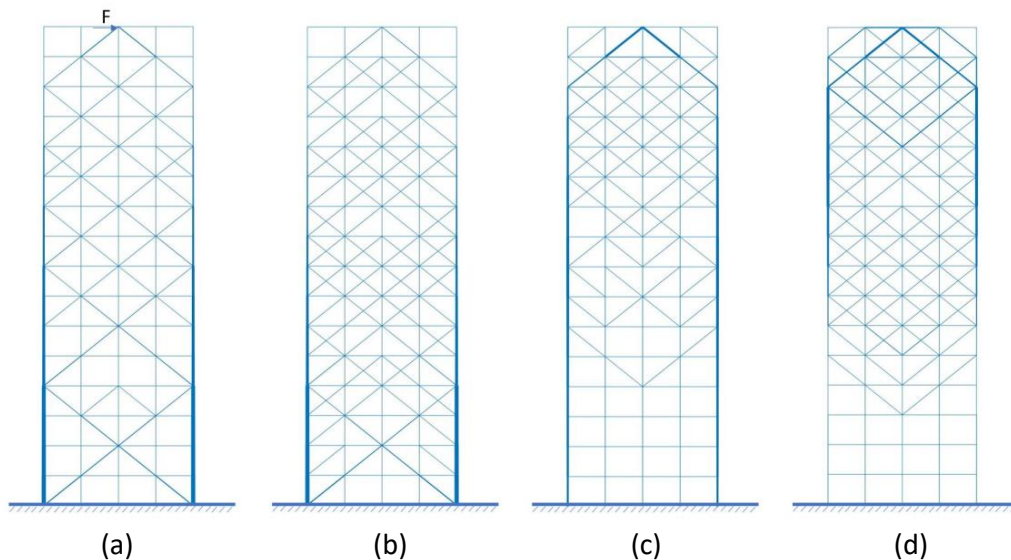*Figure 8.12 HRBM Optimized structural system for (a) static load, (b) $\omega_1 = 0.5\ rad/s$, (c) $\omega_2 = 3\ rad/s$ and (d) $\omega_3 = 6\ rad/s$*
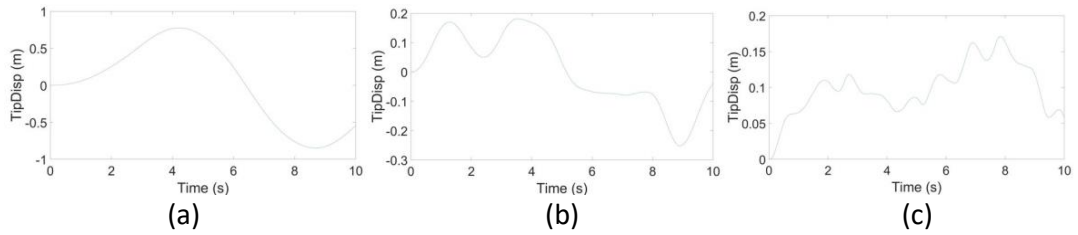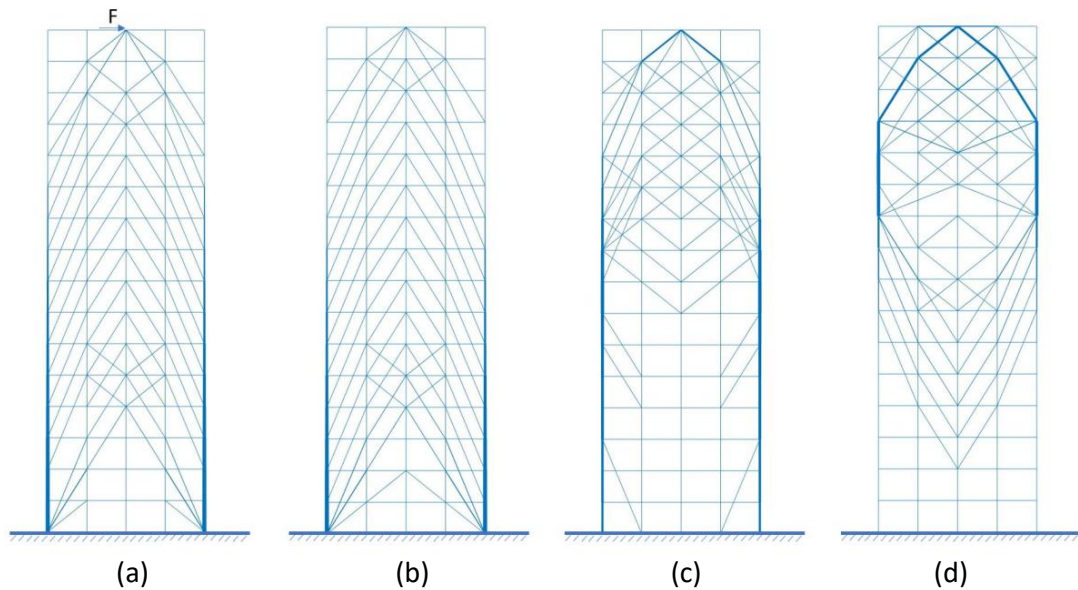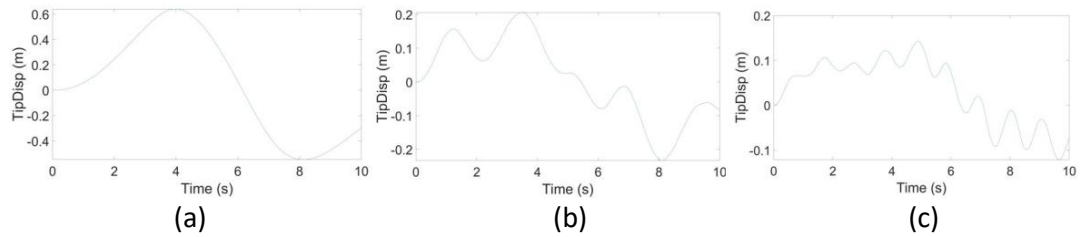
Figure 8.13 Tip deflection for HRBM under 10 seconds vibration for (a) $\omega_1 = 0.5\ rad/s$, (b) $\omega_2 = 3\ rad/s$ and (c) $\omega_3 = 6\ rad/s$

$* \times 10^6$

Test case	MRBS		MRBM	
	C* (*Nm*)	D (*m*)	C* (*Nm*)	D (*m*)
$\omega_1 = 0.5$	7.450	0.848	5.516	0.639
$\omega_2 = 3$	1.370	0.252	1.264	0.233
$\omega_3 = 6$	1.263	0.171	0.915	0.143

Table 8.4 HRB# test cases – dynamic compliance (C) and maximum tip deflection (D) through 10 second vibration

Recorded Ground Motion-Athens 7 Sept. 1999 Earthquake

In the following investigation, a recorded earthquake data of the ground motion time history is used to simulate the seismic excitations for the structural dynamic optimum design, aiming to improve the structural design in high seismic active areas. The earthquake that it is studied, is the disastrous earthquake ($M_w = 6.0$) that struck Athens, the capital of Greece, on 7 September 1999. Despite that the magnitude was moderate and the area was belonging to a low seismic hazard, the damages were severe. Over a hundred of people were killed, thousands were injured or left homeless and a great number of buildings collapsed or sustained considerable damage [80]. Figure 8.14(a) depicts the epicenter and the ground acceleration time history of the main event is illustrated in Figure 8.14(b).

In the following investigation the MRB and HRB structural systems having the same properties as before are studied when subjected to the seismic excitation of Athens seismic event. As it was mentioned in previous section, the proper objective function for the optimization problem when the seismic excitation is used, refers to the minimization of SRSS displacement. Figure 8.15 shows the optimized MRBS and MRBM structural

225

(a)   (b)
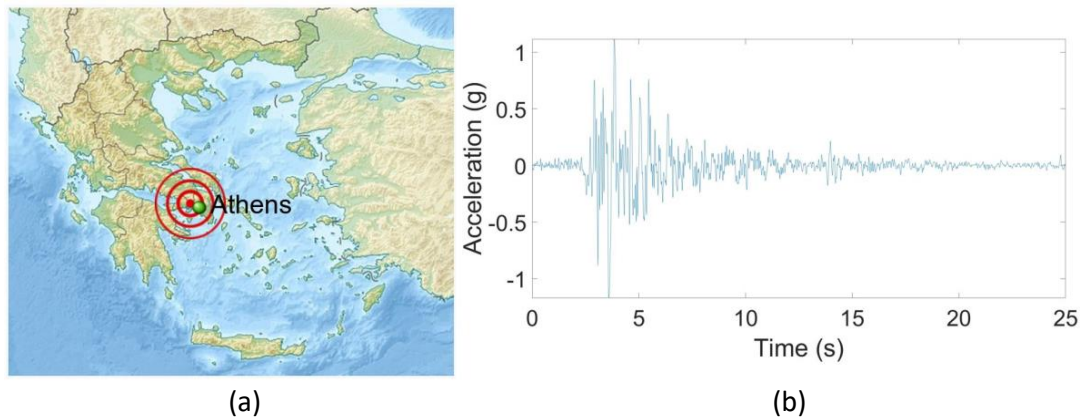
Figure 8.14 (a) Location of 1999 Athens earthquake (Wikipedia (2021)) and (b) ground acceleration time history for 25 seconds

systems, along with the roof displacement time history for each one. Regarding the initial connectivity of the GS, it is noticed that a denser one, led to remarkably smaller maximum of the absolute roof displacement. As it is shown in Figure 8.15(c), the maximum roof displacement of MRBS case is equal to $TipDisp = 0.394\,m$ and for the MRBM case is equal to $TipDisp = 0.228\,m$. Therefore, it can be said that providing more freedom in the design procedure of the bracing system, the performance of the structural system is improved where the corresponding maximum roof displacement is decreased by 42%.

Accordingly, Figure 8.16 illustrates the optimized layouts for HRBS and HRBM lateral systems and the corresponding roof displacement time history. The maximum absolute roof displacement for the HRBS structural system is equal to $TipDisp = 0.658\,m$ while for the HRBM system is equal to $TipDisp = 0.301\,m$. Consequently, it is observed that when more design freedom is allowed during the optimization design process the roof displacement shows remarkable decrease, specifically by more than 50%. Regarding the bracing type, it is noticed that a combination of chevron type and X-braces is more effective than using X-braces only.

226
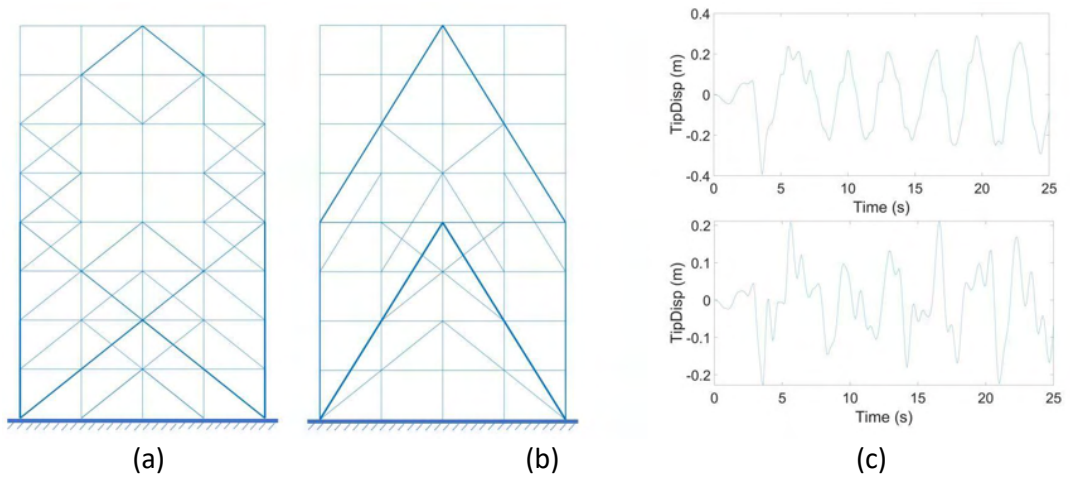
Figure 8.15 Optimized structural system for (a) MRBS, (b) MRBM, (c) tip displacement for MRBS (upper) and MRBM (down)
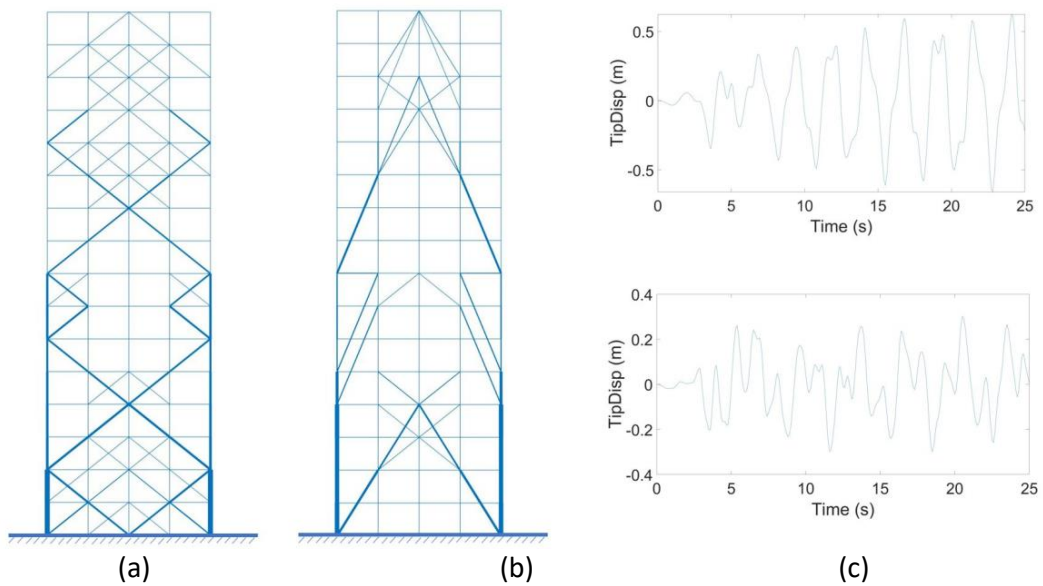
Figure 8.16 Optimized structural system for (a) HRBS, (b) HRBM, (c) tip displacement for HRBS (upper) and HRBM (down)

8.6.3 EC8 response spectrum test cases

In the following, the MRBM and HRBM lateral bracing systems are studied under seismic action and the Eurocode standards are applied. The number of the important eigenmodes that will be considered for evaluating the dynamic response is defined first. In the structural systems studied, the requirement of the 90% of the total system mass,

227

according to the Eq. (8.41), is satisfied when at least the first two eigenmodes are considered. For better understanding of the proposed methodology in each of the next test cases, three different layouts are generated considering either the sum of the first two, or those of the first three and first four eigenmodes, respectively. Regarding the seismic load, the EC8 design response spectrum is considered. More precisely, the shape of the response spectrum used corresponds to Type 1, that refers to the typical high seismicity hazard. The building important factor is selected $\gamma_I = 1$, assuming typical structures of average importance. The ground type is defined as type B, deposits of very dense sand, gravel, or very stiff clay, at least several tens of meters in thickness, characterized by a gradual increase of mechanical properties with depth. The viscous damping ratio of the structures is considered as $\zeta = 5\%$ and the soil factor is $S = 1.2$. The critical value for defining the hazard of a possible earthquake is the value of the reference peak ground acceleration on type A ground, a_{gR}. In the Greek National Annex, the a_{gR} for each seismic zone is equivalent with the period T_{NCR} of the earthquake excitation when requiring that a building will not collapse or equally with the possibility of exceedance in 50 years. In the following, two different hazard zones in Greece are selected and the equivalent results are discussed. Within this procedure, different layouts for different seismic zones are shown and solutions are proposed for improving the structural systems performance. In Figure 8.17 the two elastic pseudo-acceleration response spectra are shown, for seismic hazard Zone II ($a_g = 0.24$) and III ($a_g = 0.36$) in Greece.
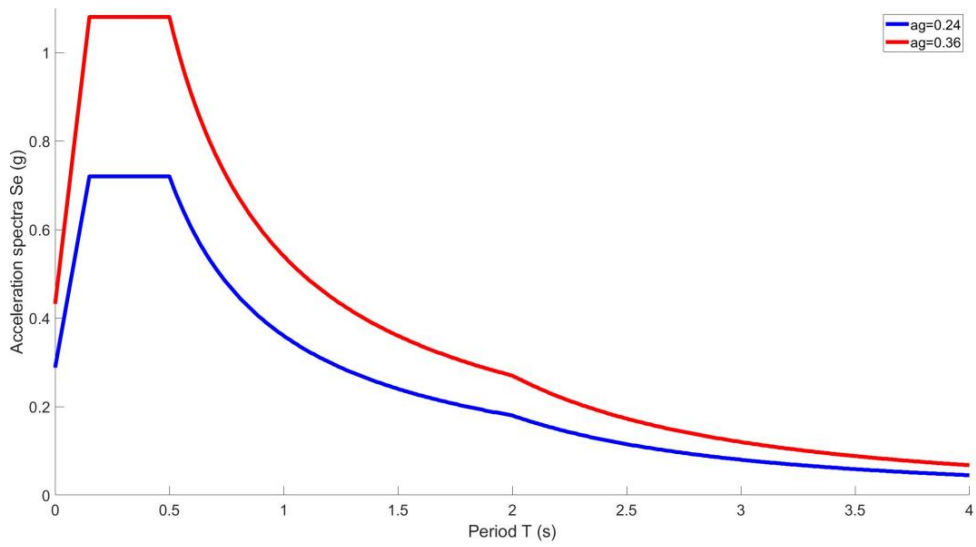
Figure 8.17 Earthquake elastic pseudo-acceleration spectra Se for Greek hazard Zones II $\left(a_g = 0.24\right)$ *and III* $\left(a_g = 0.36\right)$
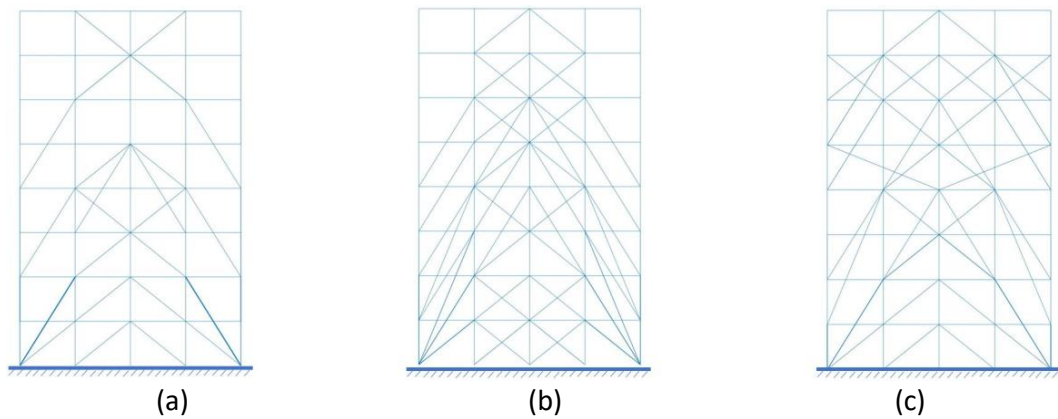
Figure 8.18 MRBM: Optimized structural system for hazard zone II $\left(a_g = 0.24\right)$ *using the first (a) two, (b) three and (c) four eigenmodes*

(a)   (b)   (c)
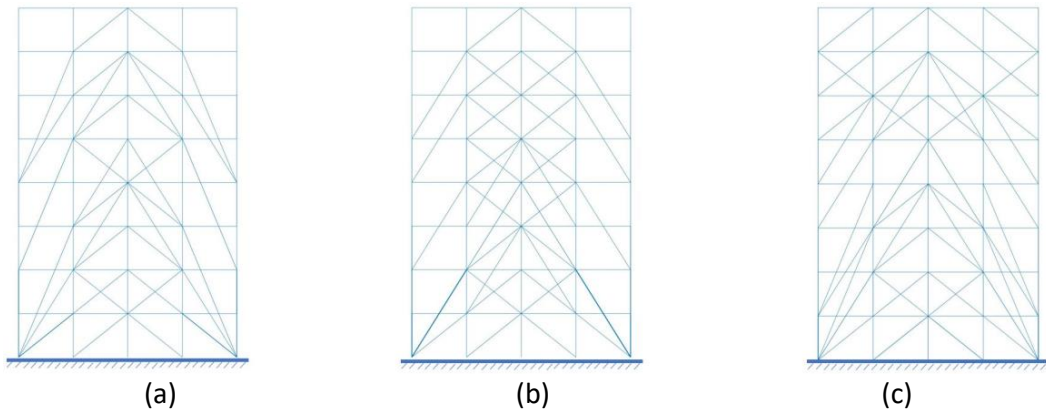
Figure 8.19 MRBM: Optimized structural system for hazard zone III $\left(a_g = 0.36\right)$ using the first (a) two, (b) three and (c) four eigenmodes

(a)   (b)   (c)
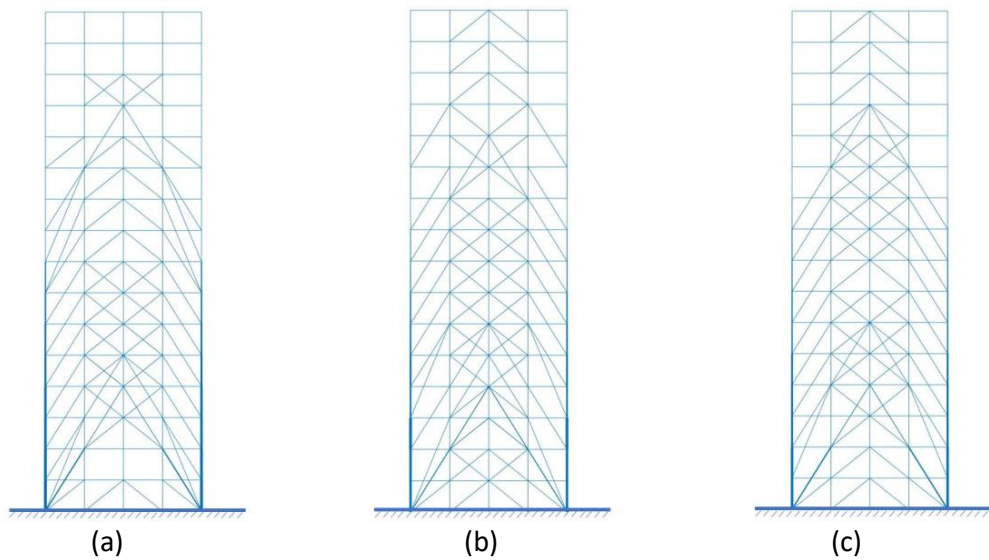
Figure 8.20 HRBM: Optimized structural system for hazard zone II $\left(a_g = 0.24\right)$ using the first (a) two, (b) three and (c) four eigenmodes
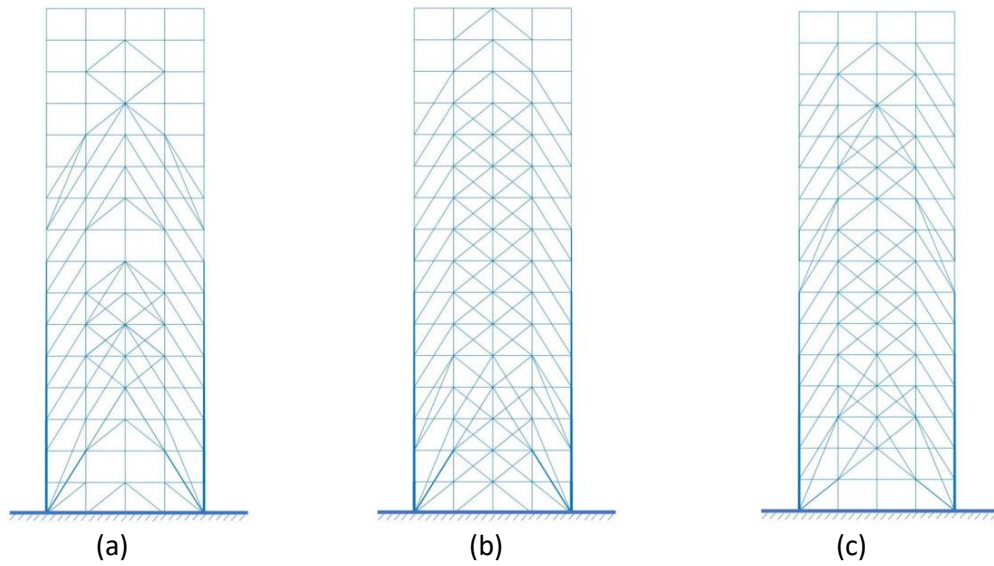
Figure 8.21 HRBM: Optimized structural system for hazard zone III $(a_g = 0.36)$ using the first (a) two, (b) three and (c) four eigenmodes

In Figure 8.18 and Figure 8.19, the results of the MRBM structural system for hazard Zones II and III are presented. In both cases it is observed that when the first two eigenmodes are considered fewer braces are developed and mostly in the lower half of the structural systems, compared with the results where more modes are considered. For the hazard Zone II the maximum displacement is equal to $U_{M2,II} = 0.162\ m$ and for hazard Zone III $U_{M2,III} = 0.292\ m$. When it comes to the first three eigenmodes, more X-braces and chevron braces are developed in the core of the structural system, while the maximum displacements using the SRSS method are equal to $U_{M3,II} = 0.139\ m$ and $U_{M3,III} = 0.258\ m$. Therefore, although one additional eigenmode is considered the optimization procedure converged to structural systems with smaller displacements. Lastly, when the first four eigenmodes are considered, more braces are developed in the upper half of the MRBF compared with the previous cases and the max displacements are equal to $U_{M4,II} = 0.166\ m$ and $U_{M4,III} = 0.253\ m$. In the Zone II, it is clear that when the first three eigenmodes are considered the final structural system is stiffer while in the Zone III the first three and the first four eigenmodes lead to solution with almost similar performance, regarding the displacements.

In Figure 8.20 and Figure 8.21 the corresponding layouts obtained for the HRBM lateral system are presented for the two hazard zones considered. In both cases, when the first three eigenmodes are considered more braces are developed in the core of the structural system compared with the results obtained when only the first two eigenmodes are considered. Similar to the MRBF, regarding the maximum displacements the case with the three eigenmodes lead to structural systems with smaller displacements. Particularly, for the case of two modes evaluation the maximum displacements are equal to $U_{H2,II} = 0.348\ m$, $U_{H2,III} = 0.495\ m$ while for the case of three modes are equal to $U_{H3,II} = 0.335\ m$, $U_{H3,III} = 0.473\ m$. Comparing the case that three eigenmodes are considered with the case where four eigenmodes are considered, the layouts obtained are similar with each other. In the latter case, the maximum displacements are equal to $U_{H4,II} = 0.337\ m$, $U_{H4,III} = 0.498\ m$. Through the investigation described above, it is observed that the layouts obtained when using the sum compliance of the first three eigenmodes show the best behaviour, in terms of maximum roof displacement, subjected to seismic loading according to EC8.

CHAPTER 9

Conclusion and future research

9.1 Contributions

This dissertation proposed novel STO methodologies, aiming to support architects and engineers in the conceptual and final design phase of structural systems. It contributes to the fields of GSO and FSTO, while civil engineering applications on these fields were presented. Regarding the GSO, the first contribution of the thesis comprises the imposition of manufacturing and aesthetic constraints in the mathematical formulation of the problem, leading to the development of innovative structural systems that cannot be achieved through conventional approaches. Particularly, a framework for the generation of BF systems for tall buildings was developed, while the proposed structural systems were symmetrical and composed by distinctive structural members. Additionally, a novel methodology, that can assist conceptual design of larger scale structural systems using prefabricated structural elements, was introduced. Through this method, an impressive single curvature shell structure was generated, while a structural system for the support of a high-rise building was examined too. The second contribution of the dissertation that is related to the GSO, is the automatic interpretation of the optimized structural systems in CAD environment. In the case that the optimized layout was a binary image, the structure's boundaries were extracted using image processing techniques, NURBS were employed for the generation of the shape while an IGES translator was developed for the automatic integration with CAD software. For the interpretation of the structural systems that were composed by prefabricated structural elements, parametric design techniques were applied, using the well-known design tool Grasshopper.

In the field of FSTO, the contributions of the current dissertation rely on the generation of structural systems considering real-world static and dynamic loading conditions. The first contribution in this field, is the development of a framework for implementing the

233

conventional compliance-based FSTO in commercial CAD and CAE software. High-level complexity GSs were generated using Grasshopper while the analyses of the structural systems were performed by SAP2000. Through this framework, innovative double curvature gridshell structures were generated, supporting in this way the conceptual design phase of producing a shelter or a pavilion.

The second contribution in FSTO, was the development of a combined topology-sizing optimization-based methodology, for supporting the design phases of structural systems, from the conceptual design phase to the final one. Standardized section properties of Euronorm were applied, where regression analysis was performed for deriving the cross-sectional properties required in order to use gradient-based search algorithms. The highlight of this methodology is that the constraints were imposed by the serviceability and ultimate limit states of the Eurocode design provisions, while the objective function of the problem was the minimization of the volume. Various MRBFs were generated using this procedure, while a basic remark was that the compliance and the design regulations are conflicted constraints. The proposed framework, managed to achieve optimized structural systems considering both of these constraints. Additionally, this methodology was integrated with the commercial software ETABS v18.1.1 and part of the proposed MRBFs was tested with real world design conditions. In all of the examined MRBFs, increased design freedom led always to lighter structural systems.

The third contribution in the field of FSTO, comprise the consideration of the structural systems' dynamic response in the optimization procedure. An extended survey of different mathematical formulations of FSTO problems was performed and applications in the generation of MRBFs for tall buildings were presented. At first, the free vibration problem is considered, where the objective function of the STO problem is the maximization of a specific eigenvalue subjected to the constraint of the material volume. An important observation in this case, is that giving more freedom to the initial GS, leads to larger objective functions, but for some MRBFs the gap between consecutive eigenfrequencies is smaller. Consequently, the forced vibration case is considered and the FSTO problem based on time history analysis is developed. For the case of the harmonic

loading, half-cycle sinusoidal loads are applied and the dynamic compliance is chosen as the objective function. It is observed that when the driving frequency is close to an eigenfrequency, more braces are developed to prevent a resonance effect. In the case where a real earthquake is applied, the objective function of the STO problem is the minimization of the SRSS. An interesting observation in this case is that, in the optimized structural systems that derived from denser GSs, more types of braces are produced, leading to MRBF with much smaller tip deflections. Finally, in order to implement the EC8 design response spectrum in the FSTO problem, the sum of the modal compliances is introduced. By studying two different MRBFs in two Greek hazard Zones, it is observed that for the specific structural systems, if the first three eigenmodes are used for the evaluation of the sum of compliance, the optimized MRBF has the best structural response, in terms of maximum roof displacement. This dissertation succeeded to proposed methodologies for reducing the material of structural systems but also to increase their performance. The material reduction has big economic and societal impact, by reducing the cost of the structures but also by making them more eco-friendly, conserving natural resources.

9.2 Future work

The developed frameworks that were presented in the current dissertation, were applied in specific conditions and structural systems. Herein, some limitations of the proposed methodologies are discussed along with suggestions for further research. Regarding the proposed methodology where prefabricated structural elements were used for assembling the structural systems, predefined star shaped units are used that are enclosed in a square which is part of structured mesh. An interesting investigation could be the implementation of different shape units in unstructured mesh, without the limitation of the square. Additionally, due to the form of the proposed structural systems, stress concentration is expected in the nodes where the different components are connected. For this reason, an additional design procedure needs to be carried out both for the structural elements and the joints that allows to attach each other safely.

Furthermore, in the presented structural systems, linear static analyses were performed considering unit loads and Young modulus. Thus, if the proposed shaped units-based topology optimization methodology is to be applied to real world problems, the proposed methodology should be accompanied by a design procedure considering instability, buckling and other types of failure checks. Furthermore, an extension of the proposed framework in order to be applicable to double curvature shell structures would be an interesting challenge.

The two stages topology-sizing optimization-based methodology was applied on MRBFs. Implementing the proposed approach to other civil engineering structural systems would be an interesting extension. The intriguing aspect of this methodology, is the consideration of members with both flexural and axial stiffness, since most of the previous work in the literature employ members that develop only axial stresses. An extended survey that compares structural systems under the same conditions but different types of members i.e., truss and frames, would highlight the significance of the flexural stiffness in the optimization procedure. Furthermore, the proposed work was successfully tested for generating 2D structures. However, it can easily be extended to 3D frame structures. Interesting field for further research, is to implement the proposed methodology to structures that consist of 3D frame FEs or different type of 1D structures like gridshells.

Regarding the dynamic FSTO, an interesting extension concerning the structural system's eigenvalues, is instead of maximizing a specific eigenfrequency, to maximize the gap between consecutive eigenfrequencies. Additionally, in the survey that dynamic conditions were considered, in all of the mathematical formulations the basic constraint was the final volume of the structural system. As it is stated, engineers are more interested in saving the cost following the design codes. The study of the dual mathematical formulation would be very challenging, as far as the computational cost in this case is increasing a lot, making it difficult for simulating large-scale structures. Combining dynamic analysis with reduced order models and machine learning techniques would be an intriguing challenge.

References

1. Aage N., Amir O., Clausen A., Hadar L., Maier D., Søndergaard A., (2014) Advanced Topology Optimization Methods for Conceptual Architectural Design. In: Block P., Knippers J., Mitra N., Wang W. (eds), Advances in Architectural Geometry, Springer, Cham, 159-179

2. Abruzzese D., Tursi A., (2003) Form finding research: development between empirical and numerical methods, In: F. Bontempi (Ed.), System-Based Vision for Strategic and Creative Design, Balkema Publishers, 569-578

3. Adriaenssens S., Block P., Veenendaal D., Williams C., (2014) Shell Structures for Architecture, Form Finding and Optimization, Routledge

4. Allaire G., Jouve F., Toader A.M., (2002) A level-set method for shape optimization, C R Math, 334(12) 1125–1130.

5. Allaire G., Jouve F., Toader A.M., (2004) Structural optimization using sensitivity analysis and a level-set method. J Comput Phys, 194(1) 363–393

6. Amir O., Bogomolny M., (2012) Conceptual design of reinforced concrete structures using topology optimization with elastoplastic material modeling, International Journal for Numerical Methods in Engineering, 90 1578-1597

7. Andreassen E., Clausen A., Schevenels M., Lazarov B.S., Sigmund O., (2011) Efficient topology optimization in Matlab using 88 line of code, Structural and Multidisciplinary Optimization, 43:1-16

8. AutoCAD software, https://www.autodesk.com/products/autocad/overview?term=1-YEAR (last accessed April 2021).

9. Bathe K.J., (1996) Finite Element Procedures, Prentice Hall

10. Beghini L.L., Beghini A., Katz N., Baker W.F., Paulino G.H., (2014) Connecting architecture and engineering through structural topology optimization, Engineering Structures, 59: 716-726

11. Behrou R., Guest J.K., (2017) Topology optimization for transient response of structures subjected to dynamic loads, 18th AIAA/ISSMO Multidisciplinary Analysis and Optimization Conference, Denver, 5-9 June 2017

12. Bendsøe M.P., (1989) Optimal shape design as a material distribution problem, Structural Optimization, 1 193–202

13. Bendsoe M.P., Kikuchi N., (1988) Generating optimal topologies in structural design using a homogenization method, Computer Methods in Applied Mechanics and Engineering, 71(2), 197-224

14. Bendsøe M.P., Sigmund O., (1999) Material interpolation schemes in topology optimization, Arch Appl Mech 69 (9–10) 635–654

15. Bendsøe M.P., Sigmund O., (2003) Topology Optimization-Theory, Methods and Applications, Springer Verlag, Berlin Heidelberg

16. Besserud K., Katz N., Beghini A., (2013) Structural Emergence: Architectural and Structural Design Collaboration at SOM Architectural Design, 83 48-55

17. Bloor M.S., Owen J., (1991) CAD/CAM product-data exchange: the next step, Computer-Aided Design, 23(4): 237-243

18. Bourdin B., (2001) Filters in topology optimization. International Journal for Numerical Methods in Engineering, 50(9) 2143-2158.

19. Branke J., Deb K., Miettinen K., Slowiński R., (2008) Multiobjective Optimization: Interactive and Evolutionary Approaches, Springer, Berlin.

20. Bromberger M., (2016) Altair is making headlines with the light rider motorbike, Digital Engineering Magazin, 7

21. Bruns T.E., Tortorelli D.A., (2001) Topology optimization of non-linear elastic structures and compliant mechanisms, Computer Methods in Applied Mechanics and Engineering, 190 (26-27) 3443-3459.

22. Cassinello P., Schlaich M., Torroja J., (2010) Félix Candela. En memoria (1910-1997). Del cascarón de hormigón a las estructuras ligeras del s. XXI, Informes de la Construccion 62(519) 5-19

23. Chacon J.M., Bellido J.C., Donoso A., (2014) Integration of topology optimized designs into CAD/CAM via an IGES translator, Structural and Multidisciplinary Optimization, 50:1115-1125

24. Changizi N., Jalalpour M., (2017) Stress-based topology optimization of steel-frame structures using members with standard cross sections: gradient-based approach, Journal of Structural Engineering, 143(8)

25. Changizi N., Jalalpour M., (2018) Topology optimization of steel frame structures with constraints on overall and individual member instabilities, Finite Elements in Analysis and Design, 141 119-134.

26. Changizi N., Kaboodanian H., Jalalpour M., (2017) Stress-based topology optimization of frame structures under geometric uncertainty, Computer Methods in Applied Mechanics and Engineering, 315 121-140.

27. Christensen P.W., Klarbring A., (2009) An introduction to Structural Optimization, Springer, Netherlands.

28. Dapogny C., Faure A., Michailidis G., Allaire G., Couvelas A., Estevez R., (2017) Geometric constraints for shape and topology optimization in architectural design, Computational Mechanics, 59: 933-965

29. Dombernowsky P., Sondergaard A., (2009) Three-dimensional topology optimization in architectural and structural design of concrete structures, International Association for Shell and Spatial Structures (IASS) Symposium 2009, Valencia.

30. Dorn W., Gomory R., Greenberg H., (1964) Automatic design of optimal structures, Mecanique, 3(1) 25–52.

31. Douthe C., Baverel O., Caron J. F., (2006) Form-finding of a grid shell in composite materials, Journal of the International Association for Shell and Spatial Structures, 47(150) 53. 14

32. Du J., Olhoff N., (2007) Topological design of freely vibrating continuum structures for maximum values of simple and multiple eigenfrequencies and frequency gaps, Struct Multidisc Optim, 34 91–110

33. ENV 1998 (1994) EUROCODE 8: Design of structures for earthquake resistance -Part 1: General rules, seismic actions and rules for buildings, CEN Brussels, April 2004.

34. Eschenauer H.A., Olhoff N., (2001) Topology optimization of continuum structures, Applied Mechanics Reviews, 54(4) 331-390

35. ETABS v18 software, https://www.csiamerica.com/products/etabs (last accessed April 2021).

36. Euronorm 53-62, Poutrelles à larges ailes à faces parallèles, Publications Office of the EU, CB-00-53-062-FR-C, July 1962.

37. Filipov E.T., Chun J., Paulino G.H., Song J., (2016) Polygonal multiresolution topology optimization (PolyMTOP) for structural dynamics, Struct Multidisc Optim 53 673–94

38. Fredricson H., Johansen T., Klarbring A., Petersson J., (2003) Topology optimization of frame structures with flexible joints, Structural and Multidisciplinary Optimization, 25 199-214.

39. Gao T., Zhang W.H., Zhu J.H., Xu Y.J., Bassir D.H., (2008) Topology optimization of heat conduction problem involving design-dependent heat load effect, Finite Elements in Analysis and Design, 44 (14), 805-813

40. Gonzalez R.C., Woods R.E., (1992) Digital image processing, Addison-Wesley Publishing Company, New York, USA

41. Grasshopper 3D, https://www.grasshopper3d.com (last accessed April 2021).

42. Greene W.H., Haftka R.T., (1991) Computational aspects of sensitivity calculations in linear transient structural analysis, Struct Optim, 3 176–201

43. Halis Gunel M., Emre Ilgin H., (2006) A proposal for the classification of structural systems of tall buildings. Building and Environment, 42(7) 2667-2675.

44. Hassani B., Hinton E., (1998) A review of homogenization and topology optimization II — Analytical and numerical solution of homogenization equations, Computers & Structures, 69(6) 719-738

45. Hassani B., Hinton E., (1999) Homogenization and Structural Topology Optimization, Springer, London

46. HAZUS-MH 2.1 Earthquake Model Technical Manual, FEMA, 2013.

47. Ho G.W.M., (2016) The Evolution of Outrigger System in Tall Buildings, International Journal of High-Rise Buildings, 5(1) 21-30

48. Hsieh C.C., Arora J.S., (1984) Design sensitivity analysis and optimization of dynamic response, Comput Methods Appl Mech Eng, 43 195-219

49. https://taxonomy.openquake.org/terms/moment-frame-lfm

50. Isler H., (1961) New shapes for shells. Bulletin of the International Association, 8 123-130

51. James K.A., Waisman H., (2015) Topology optimization of viscoelastic structures using a time-dependent adjoint method, Comput Methods Appl Mech Eng, 285 166-187

52. Januszkiewicz K., Banachowicz M., (2017) Nonlinear shaping architecture designed with using evolutionary structural optimization tools, IOP Conference Series: Materials Science and Engineering, 245 082042

53. Jog C.S., (2002) Topology design of structures subjected to periodic loading, J Sound Vib 253 687-709

54. Kazakis G., Kanellopoulos I., Sotiropoulos S., Lagaros N.D., (2017) "Topology optimization aided structural design: Interpretation, computational aspects and 3D printing", Heliyon 3(10)

55. Kirsch U., (1989) Optimal topologies of structures, Applied Mechanics Reviews, 42(8) 223-239.

56. Kirsch U., (1993) Structural Optimization—Fundamentals and Applications, Springer, Berlin.

57. Labanda S.R., Stolpe M., (2015) Automatic penalty continuation in structural topology optimization, Structural and Multidisciplinary Optimization, 52 1205-1221.

58. Lagaros N.D., Fragiadakis M., Papadrakakis M. and Tsompanakis Y., (2006) Structural optimization: a tool for evaluating seismic design procedures, Eng Struct, 28 1623–1633.

59. Lagaros N.D., Papadrakakis M., (2007) Robust seismic design optimization of steel structures, Struct Multidisc Optim, 33 457–469.

60. Lin C.Y., Chao L.S., (2000) Automated image interpretation for integrated topology and shape optimization, Structural and Multidisciplinary Optimization, 20:125-137

61. Ma Z.D., Cheng H.C., Kikuchi N., (1994) Structural design for obtaining desired eigenfrequencies by using the topology and shape optimization method, Comput Syst Eng, 5 77–89

62. Ma Z.D., Kikuchi N., Cheng H.C., (1995) Topological design for vibrating structures, Comput Methods Appl Mech Eng, 121 259–280

63. Ma Z.D., Kikuchi N., Hagiwara I., (1993) Structural topology and shape optimization for a frequency response problem, Comput Mech, 13 157–174

64. Malek S., (2012) The effect of geometry and topology on the mechanics of grid shells, Ph.D. thesis, Massachusetts Institute of Technology, Dept. of Civil and Environmental Engineering, http://hdl.handle.net/1721.1/74425

65. Martin P., Deielrein G.G., (2020) Structural topology optimization of tall buildings for dynamic seismic excitation using modal decomposition, Eng Struct, 216 110717.

66. Mattheck C., Burkhardt S., (1990) A new method of structural shape optimization based on biological growth, Int J Fatigue, 12(3) 185–190

67. Millipede, Created by Panagiotis Michalatos, https://www.grasshopper3d.com/group/millipede (last accessed April 2021).

68. Min S., Kikuchi N., Y.C. Park, S. Kim, S. Chang, Optimal topology design of structure under dynamic loads, Struct Optim, Springer, 17 (1999) 208–218

69. Mitropoulou Ch., Kazakis G., Sotiropoulos S., Lagaros N.D., (2020) "Structural Optimization Computing Platform (SOCP) and SCIA Software", Procedia Manufacturing, 44

70. Mitropoulou C.C, Lagaros N.D., (2016) Critical incident angle for the minimum cost design of low, mid and high-rise steel and reinforced concrete-composite buildings, International Journal of Optimization in Civil Engineering, 6 135–158.

71. Mlejnek H.P., (1992) Some aspects of the genesis of structures, Structural Optimization 5 64–69

72. Nakamura T., Ohsaki M., (1992) A natural generator of optimum topology of plane trusses for specified fundamental frequency, Comput Methods Appl Mech Eng, 94 113-129

73. Nguyen V.P., Kerfriden P., Bordas S., Rabczukc T., (2014) Isogeometric analysis suitable tri-variate NURBS representation of composite panels with a new offset algorithm, Computer Aided Design, 55: 49-63

74. Nocedal J., Wright S.J., (2006) Numerical Optimization, Springer Series in Operations Research and Financial Engineering, Springer, New York

75. Noilublao N., Bureerat S., (2011) Simultaneous topology, shape and sizing optimization of a three-dimensional slender truss tower using multi-objective evolutionary algorithms, Computers and Structures, 89 2531-2538

76. Ohsaki M., Fujisawa K., Katoh N., Kanno Y., (1999) Semi-definite programming for topology optimization of trusses under multiple eigenvalue constraints, Comput Methods Appl Mech Eng, 180 203-217

77. Ohsaki M., Swan C.C., (2002) Topology and geometry optimization of trusses and frames, Recent Advances in Optimal Structural Design, 46.

78. Olhoff N., Du J., (2016) Generalized incremental frequency method for topological design of continuum structures for minimum dynamic compliance subject to forced vibration at a prescribed low or high value of the excitation frequency, Struct Multidisc Optim, 54 1113-1141

79. Otto F., Rasch B., (1996) Finding Form: Towards an Architecture of the Minimal, Stuttgart: Edition Axel Menges

80. Papadimitriou P., Voulgaris N., Kassaras I., Kaviris G., Delibasis N., Makropoulos K., (2002) The Mw = 6.0, 7 September 1999 Athens Earthquake, Natural Hazards, 27 15-33.

81. Paz M., Leigh W., (2001) Integrated Matrix Analysis of Structures: Theory and Computation, Springer-Verlag London Limited

82. Pedersen N.L., (2000) Maximization of eigenvalues using topology optimization, Struct Multidisc Optim, 20 2–11

83. Pedersen N.L., Nielsen A.K., (2003) Optimization of practical trusses with constraints on eigenfrequencies, displacements, stresses, and buckling, Struct Multidisc Optim, 25 436–445

84. Pederson P., (1993) Topology Optimization of Three-Dimensional Trusses. In: Bendsøe M.P., Soares C.A.M. (eds) Topology Design of Structures. NATO ASI Series (Series E: Applied Sciences), vol 227. 19-30 Springer, Dordrecht.

85. Piegl L.A., Tiller W., (1995) The NURBS book, Springer, Berlin, Germany

86. prEN 1991-1-4, EUROCODE 1: Actions on structures - Part 1-4: General actions - Wind actions, CEN Brussels, December 2003.

87. prEN 1993-1-1, EUROCODE 3: Design of steel structures, Part 1-1: General rules and rules for buildings, CEN Brussels, November 2003

88. Qu Z.Q., (2004) Model Order Reduction Techniques: with Applications in Finite Element Analysis, Springer-Verlag London Limited

89. Razak S.M., Kong T.C., Zainol N.Z., Adnan A., Azimi M., (2018) A Review of Influence of Various Types of Structural Bracing to the Structural Performance of Buildings, E3S Web of Conferences 34, 01010

90. Rhino3D software, https://www.rhino3d.com/ (last accessed April 2021).

91. Richardson J. N., Adriaenssens S., Coelho R. F., Bouillard P., (2013) Coupled form-finding and grid optimization approach for single layer grid shells, Engineering Structures, 52 230-239.

92. Rozvany G., Lewinski T., (2014) Topology Optimization in Structural and Continuum Mechanics, Springer, London

93. Rozvany G.I.N., (1997) Topology Optimization in Structural Mechanics, Springer, Wien

94. Rozvany G.I.N., (2009) A critical review of established methods of structural topology optimization, Struct Multidisc Optim, 37 217–237.

95. SAP2000 software: https://www.csiamerica.com/products/sap2000, (last accessed April 2021).

96. Sigmund O., (2001) A 99 line topology optimization code written in MATLAB, Structural and Multidisciplinary Optimization, 21: 120-127

97. Sigmund O., (2011) On the usefulness of non-gradient approaches in topology optimization, Struct Multidisc Optim 43, 589–596

98. Sigmund O., Maute K., (2013) Topology optimization approaches, Struct Multidisc Optim 48, 1031–1055

99. Smith R., Deflection limits in tall buildings – Are they useful?, Structures Congress 2011, April 14-16, 2011 | Las Vegas, Nevada, United States.

100. Sokol T., (2011) A 99-line code for discretized Michell truss optimization written in Mathematica, Structural and Multidisciplinary Optimization, 43 181-190.

101. Sotiropoulos S., Kazakis G., Lagaros N.D., (2020) "Conceptual design of structural systems based on topology optimization and prefabricated components", Computer & Structures, 226, 106136

102. Sotiropoulos S., Kazakis G., Lagaros N.D., "Conceptual design by means of topology optimization", Thirteenth International Conference on Computational Structures Technology 2018, Sitges, Spain, September 4-6, 2018.

103. Sotiropoulos S., Kazakis G., Lagaros N.D., "High performance topology optimization computing platform", 1st International Conference on Optimization-Driven Architectural Design (OPTARCH 2019), Aman, Jordan, November 5-7, 2019.

104. Sotiropoulos S., Kazakis G., Kallioras N., Xynogalas S., Mitropoulou C., Chatzieleftheriou S., Damikoukas S., Tsakalis P. and Lagaros N.D., (2021) High Performance Optimization Computing Platform, in: WCCM-ECCOMAS2020.

105. Sotiropoulos S., Kazakis G., Lagaros N.D., (2020) High performance topology optimization computing platform, Procedia Manufacturing, 44: 441-448

106. Sotiropoulos S., Lagaros N.D., (2020) "Topology Optimization of Framed Structures using SAP2000", Procedia Manufacturing, 44

107. Sotiropoulos S., Lagaros N.D., "Topology Optimization of Framed Structures using SAP2000", 1st International Conference on Optimization-Driven Architectural Design (OPTARCH 2019) Aman, Jordan, November 5-7, 2019.

108. Sotiropoulos S., Lagaros N.D., "A two stages structural optimization-based design procedure of structural systems", (under review)

109. Sotiropoulos S., Lagaros N.D., "Topology optimization of braced frames subjected to dynamic loadings", (under review)

110. Sousa L.G., Cardoso J.B., Valido A.J., (1997) Optimal cross-section and configuration design of elastic–plastic structures subject to dynamic cyclic loading, Struct Optim 13 112–118

111. Spunt L., (1971) Optimum Structural Design, Prentice-Hall, Englewood Cliffs, New Jersey, USA

112. Stolpe M., Svanberg K., (2001) An alternative interpolation scheme for minimum compliance topology optimization, Struct Multidisc Optim 22, 116–124

113. Stromberg L.L., Beghini A., Baker W.F., Paulino G.H., (2011) Application of layout and topology optimization using pattern gradation for conceptual design of buildings, Structural Multidisciplinary Optimization, 43, 165-180

114. Stromberg L.L., Beghini A., Baker W.F., Paulino G.H., (2012) Topology optimization for braced frames: Combining continuum and beam/column elements, Engineering Structures, 37: 106-124

115. Suzuki K., Kikuchi N., (1991) A homogenization method for shape and topology optimization, Computer Methods in Applied Mechanics and Engineering, 93(3) 291-318

116. Svanberg K., (1987) The method of moving asymptotes - a new method for structural optimization, International Journal for Numerical Methods in Engineering, 24(2) 359-373.

117. Svensson S., Castlen Rist V., (2016) Methodology for preliminary design of high-rise buildings, Master thesis, TVSM-5000 VSM820 20161, http://lup.lub.lu.se/student-papers/record/8884631

118. Tang G., (2015) An overview of historical and contemporary concrete shells, their construction and factors in their general disappearance, International Journal of Space Structures, 30(1) 1-12.

119. Tang P.S., Chang K.H., (2001) Integration of design and manufacturing for structural shape optimization, Advances in Engineering Software, 32:555-567

120. Taranath B.S., (2010) Reinforced concrete design of tall buildings, CRC Press

121. Tedeschi A., (2014) AAD Algorithms-Aided Design. Parametric strategies using Grasshopper, Le Penseur Publisher

122. Topping B.H.V. (1992) Mathematical Programming Techniques for Shape Optimization of Skeletal Structures. In: Rozvany G.I.N. (eds) Shape and Layout Optimization of Structural Systems and Optimality Criteria Methods. International Centre for Mechanical Sciences (Courses and Lectures), vol 325. 379-375, Springer, Vienna

123. Wang M., Wang X., Guo D., (2003) A level set method for structural topology optimization. Comput Methods Appl Mech Eng, 192(1–2) 227–246

124. Weaverbird: Topological Mesh Editor, developed by Giulio Piacentino, https://www.grasshopper3d.com/group/weaverbird (last accessed April 2021).

125. Xie Y.M., Steven G.P. (1993) A simple evolutionary procedure for structural optimization, Comput Struct 49 885–896

126. Yamada S., Kanno Y., (2016) Relaxation approach to topology optimization of frame structure under frequency constraint, Struct Multidisc Optim 53 731–744

127. Yamakawa H., (1984) Optimum structural designs for dynamic response, In: E. Atrek et al. (eds) New directions in optimum structural design, Wiley, New York, 249–266

128. Yoon G.H. (2010), Structural topology optimization for frequency response problem using model reduction schemes, Comput Methods Appl Mech Eng, 199 1744-1763

129. Young V., Querin O.M., Steven G.P., Xie Y.M. (1999) 3D and multiple load case bi-directional evolutionary structural optimization (BESO), Struct Optim, 18 (2–3) 183–192

130. Yun K.S., Youn S.K., (2017) Design sensitivity analysis for transient response of non-viscously damped dynamic systems, Struct Multidisc Optim, 55 2197-2210

131. Zegard T., Paulino G.H., (2014) Ground structure-based topology optimization for arbitrary 2D domains using MATLAB, Structural and Multidisciplinary Optimization, 50 861-882.

132. Zegard T., Paulino G.H., (2015) Ground structure-based topology optimization for arbitrary 3D domains using MATLAB, Structural and Multidisciplinary Optimization, 52 1161-1184.

133. Zhao J., Wang C., (2016) Dynamic response topology optimization in the time domain using model reduction method, Struct Multidisc Optim, 53 101–114.

134. Zhou M., Rozvany G.I.N., (1991) The COC algorithm, part II: topological, geometry and generalized shape optimization, Comput Methods Appl Mech Eng, 89(1–3) 309–336.

135. Zhou M., Rozvany G.I.N., (2001) On the validity of ESO type methods in topology optimization, Structural and Multidisciplinary Optimization, 21(1) 80-83.

136. Ziewnkiewicz O.C., Taylor R.L., (2000) The Finite Element Method. Volume 1: The Basis, Butterworth Heinemann.